DRAFT REPORT FOR CONSULTATION

ICRP ref 4819-7515-1888
2012 July 03

Annals of the ICRP

ICRP Publication XXX

Assessment of Radiation Exposure of Astronauts in Space

Editor
C.H. CLEMENT

Assistant Editor
M. SASAKI

Authors
G. Dietze, D.T. Bartlett, F.A. Cucinotta, M. Pelliccioni, T. Sato, V. Petrov, G. Reitz, I.R. McAulay, J. Xianghong, D.A. Cool

PUBLISHED FOR

The International Commission on Radiological Protection

CONTENTS

PREFACE

Space flight is one of the occupational exposures from natural sources already listed in ICRP Publication 60 (1991), but the number of persons involved in space flights was small and hence no guidelines have been developed by ICRP to date.

The present report is the first publication of the International Commission on Radiological Protection (ICRP) dealing with the topic of radiation exposures of astronauts in space. The following terms of reference were given to the Task Group preparing this report:

- Analyze the radiation fields in space with special attention to the high-LET components and solar particle events,
- Investigate the application of dose quantities used in radiological protection ,
- Describe devices for measurement of particle fluences and doses in space environment,
- Describe procedures of the assessment of doses to astronauts performed by measurements and calculations, and
- Present some data of fluence-to-dose conversion coefficients for heavy ions.

The report was prepared by a Task Group on "Radiation Protection in Space" of ICRP Committee 2. The membership of the Task Group was:

G. Dietze (Chairman)	D.T. Bartlett	F.A. Cucinotta
M. Pelliccioni	V. Petrov	G. Reitz
T. Sato		

Corresponding members were:

I.R. McAulay	D.A. Cool	J. Cooper
J. Xianghong		

The membership of Committee 2 during the preparation of this report was:

(2005-2009)

H.G Menzel. (Chairman)	W. Bolch	M. Balonov
V. Berkovski	A. Bouville	G. Dietze
K. Eckerman	N. Ishigure	J. Harrison
N. Ishigure	J. Lipsztein	F. Paquet
H. Paretzke	A. Pradhan	J. Stather
Ch. Streffer (Chairman until 2007)		Z. Yongzeng

(since 2009)

H.G Menzel. (Chairman)	W. Bolch	M. Balonov
D. Bartlett	V. Berkovski	R. Cox
G. Dietze	K. Eckerman	A. Endo
J. Harrison	Jinzeng Ma	N. Ishigure
R. Leggett	J. Lipsztein	F. Paquet
N. Petoussi-Henss	A. Pradhan	

MAIN POINTS

- The radiation field astronauts are exposed to in space is very complex. It contains electrons, protons, alpha particles and heavier ions up to very high energies from galactic cosmic radiation, protons and electrons emitted from the Sun, protons and electrons trapped in belts by the magnetic field of the Earth, and various secondary radiations created in interactions of the primary radiation with materials of the spacecraft. Depending on the time present in space, mission doses to astronauts may become much higher than 100 mSv. Only external radiation exposure to astronauts needs to be considered.
- Due to the specifics of the radiation field in space not all concepts of quantities defined for radiological protection applications on Earth are appropriate for applications in space missions, especially when risk assessment is an important task. A radiation weighting factor $w_R = 20$ for all types and energies of heavy ions in the definition of equivalent dose is not justified. For heavy ions the ratio of w_R and mean quality factors averaged over the human body is up to a factor of 10 depending on the type and energy of the ion.
- No specific operational dose quantity is recommended for area monitoring in space. Quantities to be measured are radiation fluence rates and energy distributions of different types of particles, and LET-distributions. For individual monitoring, measurement of absorbed dose at the surface of the body in combination with LET-distributions may be appropriate for an assessment of effective dose equivalent or organ dose equivalent.
- Radiation transport calculations are important tools for information about radiation exposure of astronauts. Based on data about the primary radiation fields transport calculations are able to calculate radiation fields inside spacecrafts, fields on the body of astronauts and in organs or tissues of anthropomorphic phantoms.
- Generally, two different procedures may be applied for the assessment of doses in the astronaut´s body by calculations. One may either assess the radiation field parameters near to an astronaut and then apply fluence-to-dose conversion coefficients for all types of particles involved for the assessment of organ doses or one may calculate organ doses in a body using the radiation field data outside of the spacecraft and a code which combines radiation transport in the spacecraft and in the human body. Measurements with individual dosemeters near to the body of an astronaut in combination with calculations may be directly correlated to doses in the human body.
- The report presents conversion coefficients for mean absorbed doses in organs and tissues of the body for heavy ions up to Z = 28. The calculations are based on the reference voxel phantoms following the 2007 Recommendations of the Commission. Data are given for isotropic (ISO) exposure of the body. Also mean quality factors, Q_T, for the specified organs and tissues of the body are presented. Q_T-values vary between about 2 and 25.
- Information and data are also presented for the quality factor concept derived from the track structure of charged particles in tissue as proposed by NASA... This results in a different distribution of Q in terms of LET with a stronger decrease of Q with increasing LET.

EXECUTIVE SUMMARY

a) Astronauts are living and working in low Earth orbits for extended periods of time, especially during the operation and maintenance of the International Space Station (ISS) and scientific investigations. Furthermore, plans are already discussed for outer space missions of astronauts.

b) . In ICRP 103 it is stated that "in exceptional cases of cosmic radiation exposures, such as exposure in space travel, where doses may be significant and some type of control warranted, should be dealt with separately from the conventional approach of occupational exposure". Therefore, although astronauts are exposed to ionizing radiation during their occupational activities they are usually not classified as being occupationally exposed in the sense of the ICRP system for radiation protection.

c) The report contains 7 Chapters. The first one is an introduction describing the specific situation of astronauts in space and the differences of the radiation field in space compared to fields on Earth, thereby showing areas where approaches applied in radiological protection measures on Earth need to be modified.

d) In Chapter 2 the radiation fields in space are described in detail. The solar system with the Sun at its centre is embedded in a complex mixture of galactic cosmic radiation (GCR) - protons, α-particles and heavy ions - which continuously enters the heliosphere from all directions. Inside the heliosphere, the GCR fluence rate and particle energy distributions are modulated by the interplanetary magnetic field produced by the charged particles continuously emitted by the Sun, the so-called solar wind. In addition to the solar wind, the Sun occasionally emits unusually large pulses of energetic particles – mostly protons and electrons – called solar-particle events (SPEs). Celestial bodies equipped with a magnetic moment like the Earth are surrounded by toroidal belts of particulate radiation. Such radiation belts constitute an important third primary exposure source. Fluence rates of cosmic radiation are not constant; they vary between two extremes which correspond in time with the maximum and minimum solar activity. Solar activity and cosmic radiation fluence rates are inversely correlated. In Sections 2.2 to 2.5 the various components of the radiation field in space are presented and the influence of the Earth´s magnetic field is described.

e) Chapter 3 is dealing with the quantities used in radiological protection. In the first part the system of dose quantities as given in Publication 103 (2007) is described and secondly the relative biological effectiveness (RBE) is discussed especially with respect to the large contribution of heavy ions and the very high energies. A single w_R-value of 20 for all heavy ions of all energies is not appropriate for space radiation fields. Hence, for space applications the concept of a quality factor, $Q(L)$, is applied also to the protection quantities. In Section 3.3 the approach for applications in space is described in detail.

f) In Chapter 4 the methods of fluence and dose measurements in space are described. This includes instrumentation for fluence measurements, radiation spectrometry, area dosimetry, and individual monitoring. Passive and active devices are mentioned and also the use of biomarkers for the assessment of mission doses is described. Some advice for quality control and the assessment of uncertainties is also given in this Chapter.

g) In Chapter 5 the methods of determining quantities describing the radiation fields within a spacecraft are given. Radiation transport calculations are the most important tool for an assessment of radiation fields inside a spacecraft starting from the radiation field in free space and considering the walls and further equipment of the spacecraft. In this chapter some

physical data used in radiation transport codes are presented and the various codes used for calculations in high-energy radiation fields as in space described. Results of calculations of radiation fields in spacecrafts are given. A discussion of shielding possibilities is included in this Chapter, too.

h) Chapter 6 is dealing with methods of determining mean absorbed doses and dose equivalent s in organs and tissues of the human body. Calculated conversion coefficients of fluence to mean absorbed dose in an organ or tissue are given for heavy ions up to Z=58 for energies from 10 MeV/u to 100 GeV/u. For the same set of ions and ion energies mean quality factors in organs and tissues are presented using on the one hand the $Q(L)$ function defined in Publication 60 of the Commission and on the other hand a $Q(Z,E)$ function proposed by NASA. In Sections 6.4 assessment of doses in the body by measurements are described and results are compared with calculations. In Section 6.5 biodosimetric measurements for the assessment of mission doses are presented.

i) In Chapter 7 operational measures with regard to the assessment of the exposure of astronauts during space missions. This includes pre-flight mission design, area and individual monitoring during flights in space and dose recording. The importance of considering uncertainties in dose assessment is also mentioned.

j) In an Annex numerical data of conversion coefficients and mean quality factors for protons, neutrons, alpha particles and heavy ions ($2 < Z \leq 28$) are given.

GLOSSARY

Absorbed dose, *D*

The absorbed dose is the quotient of $\mathrm{d}\bar{\varepsilon}$ by d*m*:

$$D = \frac{\mathrm{d}\bar{\varepsilon}}{\mathrm{d}m}$$

where $\mathrm{d}\bar{\varepsilon}$ is the mean energy imparted by ionising radiation to matter of mass d*m*. The unit of absorbed dose is joule per kilogram (J/kg), and its special name is gray (Gy).

Ambient dose equivalent, *H**(10)

The dose equivalent at a point in a radiation field that would be produced by the corresponding expanded and aligned field in the ICRU sphere at depth of 10 mm on the radius vector opposing the direction of the aligned field. The unit of ambient dose equivalent is joule per kilogram (J/kg), and its special name is sievert (Sv).

Biomarker

A traceable substance indicating changes in a cell or an organ caused by environmental actions, e.g. by ionising radiation.

Charged Particle Equilibrium

Charged particles equilibrium in a volume of interest means that the energies, numbers and directions of the charged particles are constant throughout this volume. This is equivalent to saying that the distribution of charged particle energy radiance does not vary within the volume. In particular, it follows that the sums of the energies (excluding rest energies) of the charged particle entering and leaving the volume are equal

Cross section, σ

The cross section of a target entity for a particular interaction produced by incident charged or uncharged particles of a given type and energy is given by:

$$\sigma = \frac{N}{\Phi}$$

where *N* is the mean number of such interactions per target entity subjected to the particle fluence, Φ. The unit of cross section is m^2. A special unit often used for the cross section is the barn where 1 barn (b) = 10^{-28} m^2. A full description of an interaction process requires, *inter alia*, the knowledge of the distributions of cross sections in terms of energy and direction of all emergent particles from the interaction. Such distributions, sometimes called 'differential cross sections', are obtained by differentiations of σ with respect to energy and solid angle.

Deterministic effect

See 'Tissue reaction'.

Detriment

The total harm to health experienced by an exposed group and its descendants as a result of the group's exposure to a radiation source. Detriment is a multi-dimensional concept; its

principal components are the stochastic quantities probability of attributable fatal cancer, weighted probability of attributable non-fatal cancer, weighted probability of severe heritable effects, and length of life lost if the harm occurs.

Directional dose equivalent, $H'(d,\Omega)$

The dose equivalent at a point in a radiation field that would be produced by the corresponding expanded field in the ICRU sphere at a depth, d, on a radius in a specified direction, Ω. The unit of directional dose equivalent is joule per kilogram (J/kg) and its special name is sievert (Sv).

Dose conversion coefficient

A coefficient relating a dose quantity to a physical quantity, both for internal and external radiation exposure. In internal dosimetry this term is also called a 'dose coefficient'.

Dose equivalent, H

The dose equivalent at a point in tissue is given by:

$$H = Q\,D$$

where D is the absorbed dose and Q is the quality factor at that point. The unit of dose equivalent is joule per kilogram (J/kg), and its special name is sievert (Sv).

Dose equivalent in an organ or tissue, $H_{T,Q}$

The product of the mean quality factor, Q_T, and the mean absorbed dose, D_T, in an organ or tissue T: $H_{T,Q} = Q_T\,D_T$.

A quantity introduced by ICRP in Publication 26 and replaced by equivalent dose in an organ or tissue in Publication 60.

Dose limit

Recommended value of a dose to an individual that shall not be exceeded in planned exposure situations.

Effective charge number, Z*

The charge number Z of a nuclei reduced by a factor depending on the relative velocity β (velocity of the nuclei relative to the velocity of light) which takes account of the fact that at low velocities the nuclei is not completely ionised. It is

$$Z^* = Z\,(1-\exp(-125\,\beta\,Z^{2/3}))$$

Effective dose, E

The tissue-weighted sum of equivalent dose in an organ or tissue from all specified organs and tissues of the body, given by the expression:

$$E = \sum_{T} w_T \sum_{R} w_R D_{T,R} = \sum_{T} w_T H_T$$

where H_T is the equivalent dose in an organ or tissue T, $D_{T,R}$ is the mean absorbed dose in an organ or tissue T from radiation of type R, and w_T is the tissue weighting factor. The sum is performed over organs and tissues considered to be sensitive to the induction of stochastic

effects. The unit of effective dose is joule per kilogram (J/kg), and its special name is sievert (Sv).

Effective dose equivalent, H_E

The tissue-weighted sum of dose equivalent in an organ or tissue from all specified organs and tissues of the body, given by the expression:

$$H_E = \sum_T w_T H_{T,Q}$$

where $H_{T,Q}$ is the dose equivalent in an organ or tissue T. The unit of effective dose equivalent is joule per kilogram (J/kg), and its special name is sievert (Sv).
A quantity introduced by ICRP in Publication 26 and replaced by effective dose in Publication 60.

Equivalent dose in an organ or tissue, H_T

The equivalent dose in an organ or tissue is given by:

$$H_T = \sum_R w_R D_{T,R}$$

where $D_{T,R}$ is the mean absorbed dose from radiation of type R in the specified organ or tissue T, and w_R is the radiation weighting factor. The unit of equivalent dose is joule per kilogram (J/kg) and its special name is sievert (Sv).

Fluence, Φ

The quotient of dN by da, where dN is the number of particles incident on a sphere of cross-sectional area da, thus:

$$\Phi = \frac{dN}{da}$$

The unit of fluence is m^{-2}.

Galactic cosmic radiation (GCR)

Charged particle radiation which continuously enters the heliosphere from outer space from all directions. The radiation contains electrons (about 2%) and a broad range of charged particles from protons up to high-Z particles with high energies up to several hundreds of GeV and even higher. The fluence rate of the GCR in the heliosphere is inversely correlated with the solar activity. It is caused by the solar magnetic field, which is coupled to the solar wind.

Geomagnetic cut-off rigidity

See “rigidity threshold”.

Heavy ion

Ions of elements heavier than He.

Heliosphere

The space formed by the Sun and its planets.

ICRU 4-element tissue

ICRU 4-element tissue has a density of 1 g/cm^3, and a mass composition of 76.2 % oxygen, 11.1 % carbon, 10.1 % hydrogen, and 2.6 % nitrogen.

ICRU sphere

A hypothetical sphere, 30 cm in diameter, of tissue-equivalent material (ICRU 4-element tissue) with a density of 1 g cm^{-3} and a mass composition of 76.2 % oxygen, 11.1 % carbon, 10.1 % hydrogen and 2.6 % nitrogen.

K-, Kp-index

Index quantifying disturbances in the horizontal component of Earth's magnetic field with a number in the range 0-9 with 1 being calm and 5 or more indicating a geomagnetic storm. The K-index is derived from the maximum fluctuations of horizontal components observed on a magnetometer during a three-hour interval. The official planetary Kp-index is derived by calculating a weighted average of K-indices from a network of geomagnetic observatories.

Kerma, K

Quantity for ionising uncharged particles, defined by the quotient of dE_{tr} by dm, where dE_{tr} is the mean sum of the initial kinetic energies of all the charged particles liberated in a mass dm of a material by the uncharged particles incident on dm, thus:

$$K = \frac{\mathrm{d}E_{\mathrm{tr}}}{\mathrm{d}m}$$

The unit of kerma is joule per kilogram (J/kg) and its special name is gray (Gy).

Kerma approximation

Kerma is sometimes used as an approximation to absorbed dose. The numerical value of the kerma approaches that of the absorbed dose to the degree that charged-particle equilibrium exists, that radiative losses are negligible, and that the kinetic energies of the uncharged particles are large compared to the binding energies of the liberated charged particles.

Lineal energy

The quotient of ε_{i} by $\bar{l}$ **,** where ε_{i} is the energy imparted to the matter in a given volume by a single energy-deposition event i and $\bar{l}$ is the mean chord length of that volume, thus

$$y = \frac{\varepsilon_i}{\bar{l}}.$$

The unit of lineal energy is joule per meter (J/m)

Linear energy transfer/unrestricted linear energy transfer, L or LET

The quotient of dE by dl, where dE is the mean energy lost by the charged particle due to electronic interactions in traversing a distance dl thus:

$$L = \frac{\mathrm{d}E}{\mathrm{d}l}$$

The unit of linear energy transfer is joule per metre (J/m), often given in keV/µm.

Linear-non-threshold (LNT) model

A dose-response model which is based on the concept that, in the low dose range, radiation doses greater than zero will increase the risk of excess cancer and/or heritable disease in a simple proportionate manner.

Low Earth Orbit (LEO)

Orbit in space near to the Earth where astronauts are protected against parts of particles of galactic and solar origin by the Earth magnetic field. The shielding depends on the inclination of the spacecraft. On the other hand the Earth magnetic field is responsible for the formation of the trapped radiation belts where mainly protons and electrons from galactic and solar origin are stored.

Magnetosphere

The Earth magnetic dipole field which extends over a distance from Earth up to about 75 000 km around the geomagnetic equator. Charged particles in a specific energy range are trapped in the magnetic field. They move in spirals along the geomagnetic field lines, are reflected back between the magnetic poles acting as mirrors and form radiation belts. These belts were discovered by van Allen.

Mean absorbed dose in an organ or tissue, D_T

The mean absorbed dose in a specified organ or tissue T, is given by

$$D_T = \frac{1}{m_T} \int D \mathrm{d}m \quad ,$$

where m_T is the mass of the organ or tissue T, and D is the absorbed dose in the mass element dm. The unit of mean absorbed dose is joule per kilogram (J/kg), and its special name is gray (Gy).

Nuclear track detectors (NTD)

Detectors where the tracks of passing charged particles can afterwards be made visible by suitable chemical treatment and microscopically viewed. These passive detectors are either plastic nuclear etched track detectors (PNTD) where the tracks are made visible by chemical etching or nuclear emulsions. Etched track detectors are generally insensitive for radiation with an LET in water below about 10 keV μm^{-1}.

Occupational exposure

The radiation exposure of workers incurred as a result of their work. The Commission limits its use of ‘occupational exposures’ to radiation exposures incurred at work as a result of situations that can reasonably be regarded as being the responsibility of the operating management.

Operational quantities

Quantities used in practical applications for monitoring and investigating situations involving external exposure and intakes of radionuclides. They are defined for measurements and assessment of doses in the body.

Organ absorbed dose

Short phrase for “mean absorbed dose in an organ or tissue”.

Organ dose equivalent

Short phrase for “dose equivalent in an organ or tissue”.

Organ equivalent dose

Short phrase for “equivalent dose in an organ or tissue”.

Optically stimulated luminescence dosemeters (OSLD)

Detectors where the energy stored by particles in the detector material (glasses) is release as luminescence light by optical laser stimulation. The amount of emitted light is proportional to the absorbed dose.

Personal dose equivalent, $H_p(d)$

The dose equivalent in soft tissue at an appropriate depth, d, below a specified point on the human body. The soft tissue is ICRU 4-element tissue. The unit of personal dose equivalent is joule per kilogram (J/kg) and its special name is sievert (Sv). The specified point is usually given by the position where the individual dosemeter is worn. For the assessment of effective dose, a depth of 10 mm is recommended, and for the assessment of equivalent dose to the skin and the lens of the eye, depths of 0.07 mm and 3 mm, respectively, are recommended.

Protection quantities

Dose quantities related to the human body used for setting exposure limits and in the context of optimisation. They have been developed by the Commission for radiological protection to allow quantification of the detriment to people from exposure of the human body to ionising radiation from both whole and partial body external irradiation and from intakes of radionuclides.

Quality factor, Q

A dimensionless factor defined to reflect the relative biological effectiveness of high-LET radiations compared to low-LET radiation at low exposure levels.

Q is usually given by a function $Q(L)$, where L is the unrestricted linear energy transfer in water.

The quality factor at a point in tissue, is given by

$$Q = \frac{1}{D} \int_{L=0}^{\infty} Q(L) D_L \mathrm{d}L$$

where D is the absorbed dose at that point, D_L is the distribution of D in unrestricted linear energy transfer L at the point of interest, and $Q(L)$ is the quality factor as a function of L. The integration is to be performed over D_L, due to all charged particles, excluding their secondary electrons.

Radiation belt

See “Magnetosphere”.

Radiation weighting factor, w_R

A dimensionless factor by which the mean absorbed dose in an organ or tissue, D_T, is multiplied to reflect the relative biological effectiveness of high-LET radiations compared

with low-LET radiations. The product of w_R and D_T is the equivalent dose in the organ or tissue T.

Reference male and reference female (reference individual)

An idealised male or female with characteristics defined by the Commission for the purpose of radiological protection, and with the anatomical and physiological characteristics defined in Publication 89 (ICRP, 2002).

Reference person

An idealised person for whom the equivalent doses in organs and tissues are calculated by averaging the corresponding doses of Reference Male and Reference Female. The equivalent doses of the Reference person are used for the calculation of the effective dose.

Reference phantom

The computational phantom of the human body (male or female voxel phantom based on medical imaging data) defined in Publication 110 (ICRP, 2009) with the anatomical and physiological characteristics defined in Publication 89 (ICRP, 2002).

Reference value

Value of a quantity recommended by the Commission for use in dosimetric applications or biokinetic models. Reference values are fixed and specified with no uncertainty, independently of the fact that the basis of these values may include many uncertainties.

Relative biological effectiveness (RBE)

The ratio of absorbed dose of a low-LET reference radiation to absorbed dose of the radiation considered that gives an identical biological effect. RBE values vary with absorbed dose, absorbed dose rate and the biological endpoint considered. In radiological protection the RBE at low and very low doses (RBE_M) is especially of interest.

Rigidity, R

The magnetic rigidity of an ion given by its momentum (often given in units of GeV/c) divided by its charge. Parameter used for characterizing the movement of a high-energy charged particle in the magnetic field in space.

Rigidity threshold (geomagnetic cut-off rigidity), R_c

For each point inside the Earth´s magnetosphere and each direction from that point there exist a rigidity threshold below which the cosmic particles are not able to reach this point. This rigidity is called the geomagnetic cut-off rigidity, R_c.

Solar cosmic radiation (SCR)

Radiation emitted from the Sun. The radiation includes continuously emitted electrons and protons (solar wind) and also high energy particles (mainly electrons and protons) emitted during solar particle events (SPE).

Solar cycle

Variation of the solar activity between two extremes with a cycle time of about 11 years. The solar activity can be described by the number of observed sunspots.

Solar particle event (SPE)

An eruption at the Sun surface that releases a large number of particles (mostly electrons and protons with few helium ions and heavy charged particles) over the course of hours or days.

Solar wind

Mostly low-energy electrons and protons continuously emitted from the Sun into the heliosphere and producing the interplanetary magnetic field. The intensity of the solar wind depends on solar activity and varies with the solar cycle.

South Atlantic anomaly (SAA)

An area where the radiation belt, and hence the trapped protons, comes closer to the Earth surface due to a displacement of the magnetic dipole axes from the Earth's centre.

Stochastic effect

Effects resulting from damage in a single cell, such as cancer and heritable effects. The frequency of the event, but not its severity, increases with an increase in the dose. For protection purposes it is assumed that there is no threshold dose.

Thermoluminescence detector (TLD)

Small sintered chips or pellets of crystals which show luminescence during heating after exposure to ionising radiation. By fast controlled heating of the crystal, the stored energy is released through light emission. The function between the actual temperature and the intensity of the emitted light (glow curve) shows various peaks, the heights of which are proportional to absorbed dose. These detectors are often used for personal dosimetry.

Tissue reaction

Injury in populations of cells, characterized by a threshold dose and an increase in the severity of the reaction as the dose is increased further, also termed ‘deterministic effect’. In some cases, these effects are modifiable by post-irradiation procedures including biological response modifiers.

Tissue weighting factor, w_T

The factor by which the equivalent dose in an organ or tissue T is weighted to represent the relative contribution of that organ or tissue to overall radiation detriment from stochastic effects. It is defined such that:

$$\sum_{T} w_T = 1 \ .$$

Trapped particles

Particles trapped in the Earth's magnetic field as a result of the interaction of galactic cosmic radiation and solar cosmic radiation with the Earth´s magnetic field and the atmosphere. Mainly protons and electrons are involved (see also “Magnetosphere”).

Voxel phantom

Computational anthropomorphic phantom based on medical tomographic images in which the anatomy is described by small three-dimensional volume elements (voxels). Collections of these voxels are used to specify the organs and tissues of the human body.

References

ICRP, 2007. The 2007 Recommendations of the International commission on Radiological Protection. ICRP Publication 103. Ann. ICRP 37(2-4).

ICRP, 2012. Conversion Coefficients for Radiological Protection Quantities for External Radiation Exposures. ICRP Publication 116, Annals of the ICRP 40 (1).

ICRU, 2011. Fundamental Quantities and Units for Ionising Radiation (*Revised*). ICRU Report 85a. Journal of ICRU 11 (1a).

1. INTRODUCTION

(1) The radiation field in space is very different from environmental radiation fields on Earth both with respect to the various types of radiation involved and to their intensities. The primary radiation field on the Earth surface is composed of low-LET radiations with small high-LET components including neutrons from cosmic radiation and α-particles emitted from terrestrial radionuclides. In contrast, the primary radiation field in space includes electrons, protons, neutrons, α-particles and heavy ions up to very high energies. Additional secondary radiations (e.g. gamma radiation, electrons, muons, neutrons, pions, and collision and projectile fragments) are produced by interactions within the materials of a spacecraft and its equipment and the astronauts themselves.

(2) The term ”space” generally means the galactic space outside of the aviation altitudes in the lower atmosphere of the Earth. In manned space flight astronauts may experience three different exposure conditions. The first situation is in low Earth orbit (LEO) where they are protected against parts of particles of galactic and solar origin depending on the inclination of the spacecraft by the Earth magnetic field. On the other hand this magnetic field is responsible for the formation of the trapped radiation belts. In addition, through interaction of the solar and galactic particles with the nuclei of the Earth´s atmosphere albedo radiation is created. Secondly, leaving the Earth magnetic field to outer space in interplanetary missions, the radiation exposure due only to particles of solar and galactic origin, which are directly impinge on the spacecraft. In planetary missions, about one hemisphere is shielded by the mass of the planet. If there is no atmosphere, the primary radiation interacts with the nuclei of the soil which leads to the production of secondary particles with a high contribution of high-LET components. If a thin atmosphere is present, as in case of Mars, both interactions in the atmosphere and in the soil contribute to secondary radiation.

(3) Astronauts are living and working in low Earth orbits for extended periods of time and will be involved in outer space missions. They are living under extraordinarily different environmental conditions than ever encountered on Earth. For missions outside the magnetosphere, ionising radiation is recognized as the key factor through its impact on crew health and performance. Obviously the radiation environment is quite different from that on Earth and human exposure in space is much higher than on Earth and cannot be avoided by radiation shielding. The reasons for that are the extreme high energies of particles in space radiation fields and their high penetration depth in matter combined with the release of secondary radiations (e.g. neutrons and photons) in interactions of the primary radiation with that material. The exposure of astronauts in space is a special case of environmental exposure. In long term missions, the exposure of astronauts will be higher than the annual limits recommended for exposure of workers on Earth. In ICRP 103 it is stated that “in exceptional cases of cosmic radiation exposures, such as exposure in space travel, where doses may be significant and some type of control warranted, should be dealt with separately”. Therefore, although astronauts are exposed to ionizing radiation during their occupational activities they are usually not classified as being occupationally exposed in the sense of the ICRP system for radiation protection. Their situation during space missions is similar to special planned exposure situations in emergency exposure situations, in which so-called rescuers may be exposed to radiation levels during their intervention exceeding dose limits for occupationally exposed persons. Thus, for a specific mission planned, reference values for risks or doses may be selected at appropriate levels and no dose limits may be

applied for the given mission.

(4) During the last two decades there was a marked development in the activities in space including an increase of the number of astronauts participating in space missions. Nevertheless, even today, the number of astronauts is small as compared to the large number of occupationally exposed persons on Earth and in civil aviation. However, considering the extraordinary exposure situation of this group, radiological protection concepts need to be well defined and realistically implemented with respect to the specific situation found in the space environment and during long-term space missions.

(5) The basis for any measure in radiological protection should always be the knowledge of the radiation fields involved. Therefore, measurements of the environmental radiation and the assessment of the exposure of astronauts are very important tasks. Since the discovery of cosmic radiation at the start of the last century by V.F. Hess in 1912 (see e. g. Compton, 1936) the study of cosmic radiation and its various components has already been performed for a long time and has become even more important during the last fifty years when activities in space are strongly increasing and frequently include the presence of astronauts. Obviously the basic information regarding cosmic radiations and their various components can only be obtained through measurements and this has been performed for many years. The specific environmental situation in and around a spacecraft can be estimated either by various measurements at different positions in the specific spacecraft or also by radiation transport calculations when the spacecraft design is sufficiently modelled and the specific composition of the external radiation field including its variation in time is well considered within the simulation code applied. Some parts of this report, therefore, deal with the various components of the radiation field in space (Chapter 2) and with the computer codes and calculational approaches used to simulate both radiation shielding possibilities for the various radiation fields incident upon the spacecraft and the resulting tissue absorbed doses imparted to the astronauts within the spacecraft (Chapters 5 and 6).

(6) The specific radiation field in space with its important contribution of heavy ions does not allow simple application of the complete system of dosimetric quantities defined for use in radiological protection on Earth. The radiation weighting factor of 20 defined for all heavy ions of all energies is not appropriate, nor is the concept of the operational dose quantities for external exposure situations applicable to the space situation because very high-energy particles are involved. The concept of operational quantities has been introduced by the ICRU and ICRP mainly looking at electron, photon and neutron radiations of energies up to few tens of MeV and has not considered radiation fields in space which include many other particle types with even higher energies. This topic will be discussed in more detail in Chapter 3.

(7) On Earth, radiological protection of workers and the primary dose limits defined are aimed at limiting the probability of the occurrence of stochastic effects, e.g. risk of cancer or hereditary effects, to a level acceptable when compared to other health risks during human life, while at the same time avoiding detriments in humans by deterministic effects (tissue reactions). For practical reasons the primary limits are defined in terms of doses (effective dose and equivalent dose to the skin, hands, feet and lens of the eye where specific limits have been defined for avoiding deterministic effects) which can be assessed with sufficient precision for applications in radiological protection, and not in terms of radiation risks the value of which depends on many individual factors (e.g. age, sex, individual genetic properties). Especially at low levels of exposure, the knowledge regarding these risks is very limited and combined with high uncertainties. The value of the quantity effective dose is calculated by averaging organ equivalent doses over both sexes and using mean values of

weighting factors obtained from epidemiological data, hence from large groups of exposed and unexposed persons. Effective dose should, therefore, not be used for the assessment of individual risks. In addition to "limitation" of doses and risks the principle of ALARA (As Low As Reasonably Achievable) is generally applied in radiological protection which means that even below exposure limits "optimisation" of radiation protection always needs to be considered and may require further measures.

(8) The situation in space is quite different. An exposure of astronauts by environmental radiation cannot be avoided in space. Prevention by shielding cannot be completely achieved. Nevertheless, optimisation of radiation protection is an important task, especially because in long-term missions doses to astronauts may exceed 100 mSv. The occurrence of deterministic effects can also not generally be excluded. In addition, the knowledge of radiobiological effects of cosmic radiation in particular heavy ions is very limited. The number of persons involved is small and hence individual risk assessment is of much higher interest. As a consequence, values of mean absorbed doses in organs and tissues of the human body play an important role, since the weighting factors used in the definition of effective dose or equivalent dose in an organ or tissue are not appropriate in the radiation field in space. In addition, for many years, the use of organ dose equivalent has been preferred by many space agencies instead of the quantity equivalent dose in an organ (see Chapter 3).

(9) Both radiation monitoring in the spacecraft environment and assessment of doses in the human body of astronauts are important parts of the radiological protection measures in space missions. Due to the complex radiation field and the special requirements for use in space flight radiation monitoring needs specific measurement devices and procedures. Usually, more than a single dosemeter type is needed for this task and often additional calculations are necessary to interpret device response (see Chapters 4 and 6).

(10) Calculation of conversion coefficients which relate values of particle fluence or dose external to the human body to values of absorbed dose and mean quality factors in organs and tissues within the body is an important task and is often used for the assessment of doses in the body from external measurements. While reference data on conversion coefficients related to the reference voxel phantoms defined in ICRP Publication 110 have already been published by the Commission in Publication 116 (ICRP, 2011), data for heavy ions have become available only recently (Sato et al., 2010). In this report data are presented for isotropic exposure of both male and female voxel phantoms. Omni-directional exposure (ISO) is the most realistic exposure situation in space. While shielding effects may result in a more non-isotropic exposure, the movement of the astronauts within the spacecraft balances this situation. Hence, data are presented for ISO exposure only (see Chapter 6 and the Annex). The use of conversion coefficients is, however, not the only method in assessing organ doses in the body. Based on knowledge of the radiation field outside a spacecraft, calculation of organ doses can be performed including the full radiation transport through the walls and the equipment of a spacecraft (see Chapter 6).

(11) While on Earth biological dosimetry is mainly restricted to applications in accidental exposure situations due to the usually low doses of occupationally exposed workers and the difficulty in measuring doses below about 50 mSv by this method with acceptable uncertainty, the situation in space is quite different. Mission doses may be above that "threshold" and biological dosimetry (e.g. study of biological effects on lymphocytes in the human body) allows a very individual assessment, if in advance the individual sensitivity is determined and hence an individual calibration is performed. Methods and measurements are discussed in both Chapters 4 and 6 of the report.

767

2. RADIATION ENVIRONMENT IN SPACE

(12) The radiation environment in space is a complex mixture of particles of solar and galactic origin with a broad range of energies. For radiological protection, the relevant radiation fields are the galactic cosmic radiation (GCR), particles ejected from the Sun during solar energetic particle (SPE) events, and secondary radiation produced through interaction with the planet's atmospheric nuclei. Solar wind particles, even when enhanced due to higher solar activity, do not significantly contribute to the radiation exposure to man due to their relative low energy and hence their absorption in already very thin shielding materials. Nevertheless, the solar wind modulates the fluence rate of galactic cosmic radiation in the energy range below about 1 GeV/u. During phases of higher solar activity, the cosmic radiation fluence rate is decreased by a factor of three to four compared with phases during minimum solar activity.

(13) Presently, there is no measurable contribution to the radiation exposure by primary electromagnetic ionising radiation such as from solar Roentgen flares like that which occurred on November 4th 2003 UTC 19:29 or from conspicuous extreme gamma radiation bursts such as that which occurred on December 27th 2004 UTC 21:30:26.55; hence, they are omitted, although on geological time scale, their impact on the biosphere might have been significant. Secondary electromagnetic radiation of course contributes as bremsstrahlung emitted from charged particles upon penetration though matter and as gamma radiation from the decay of neutral pions π^0 created in the Earth´s atmosphere.

(14) From the point of view of radiological protection, the focus is on the particulate components of space radiation of ions and electrons only. Electrons might become relevant during extravehicular activities (EVAs) or if manned activities in the outer radiation belts become an issue which, however, will not be the case for the foreseeable future.

(15) Through the Earth´s magnetic field and an atmospheric shield with a thickness of about 1000 g cm^{-2}, the exposure to cosmic radiation on the Earth surface is reduced to a negligible level. Leaving Earth, astronauts are shielded by the structure of the spacecraft and its interior by an average of about 20 g cm^{-2}, a shielding close to that of the Martian atmosphere, but when in low Earth orbit, they are still protected by the Earth´s magnetic field which limits even the exposure to solar energetic particles to a level far below the cause of early radiation effects in man.

(16) In the absence of sporadic solar particle events, the radiation exposure in near Earth orbits inside spacecraft is determined by the galactic cosmic radiation (protons and heavier ions) and by the protons inside the South Atlantic Anomaly (SAA), an area where the radiation belt comes closer to the Earth surface due to a displacement of the magnetic dipole axes from the Earth's centre. In addition, there is an albedo source of neutrons produced as interaction products of the primary galactic particles with the nuclei of the Earth atmosphere. Outside the spacecraft, the exposure of astronauts is dominated by the electrons of the horns of the radiation belt located at about 60° latitude in Polar regions.

(17) All these radiations from different sources and their interactions by various mechanisms determine the actual field of ionising radiation at any given time and location within the heliosphere. Its complexity is unrivalled by anything we know from terrestrial experience. The radiation field inside a spacecraft is even more complex through the interaction of the high energy particles with the spacecraft shielding material and the body tissues of the astronauts.

(18) In deep space missions the Earth´s radiation belts will be crossed in a couple of minutes and therefore its contribution to their radiation exposure is quite small. However, the subsequent protection by the Earth´s magnetic field is then lost, leaving only mission planning and shielding measures as a means of exposure reduction. The following sections describe the radiation field in space and the interaction of the charged particles with the magnetic field and shielding materials. Some numbers are given on the radiation exposure in low Earth orbits and in interplanetary missions.

2.1 Primary radiation fields

(19) Three major primary sources of radiation can be specified in space.

- The solar system with the Sun at its centre is embedded in a complex mixture of ionising radiation, galactic cosmic radiation (GCR), which continuously enters the heliosphere from all directions. Inside the heliosphere, the GCR fluence rate and particle energy distributions are modulated by the interplanetary magnetic field produced by the charged particles continuously emitted by the Sun, the so-called solar wind.
- In addition to the solar wind, the Sun occasionally emits unusually large pulses of energetic particles – mostly protons and electrons with a small and variable contribution from helium and heavy ions - ejected in to space by these solar eruptions. The most significant of these solar-particle events (SPEs) are produced by the expulsion of large amounts of material in coronal-mass ejections (CMEs).
- Celestial bodies equipped with a magnetic moment like the Earth are surrounded by toroidal belts of particulate radiation which are constantly replenished by solar particles and secondary particles caused by the interaction of solar and galactic particles with the atmosphere. Such radiation belts constitute an important third primary exposure source.

(20) Figure 2.1 illustrates these three sources of ionising radiation in space, their respective spatial scales and the dominant role the Sun plays in modifying its composition. The highest energies measured for GCR particles (Fig. 2.1) are too large to be compatible with their postulated acceleration and containment by intra-galactic magnetic fields thereby giving rise to speculations about extra-galactic sources for this part and hence extending the spatial scales even further. The corresponding intensities, however, are too low to contribute substantially to radiation exposures.

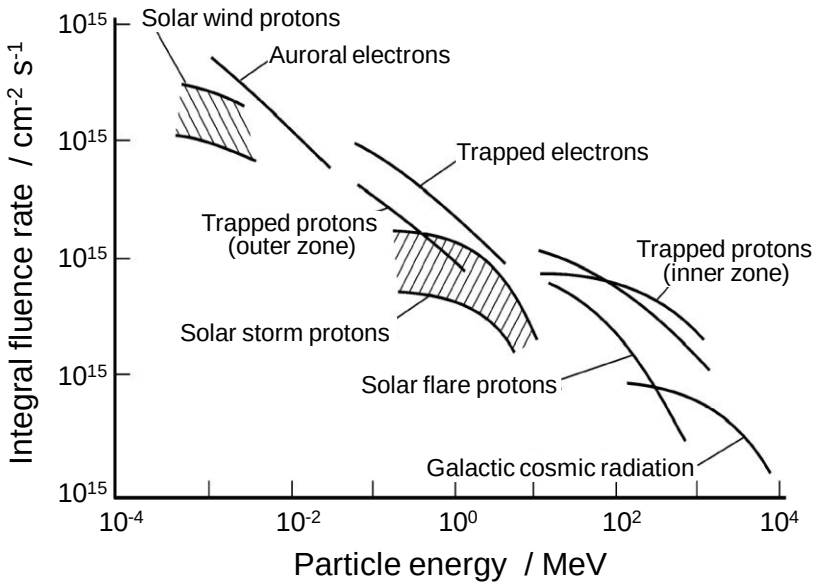

Fig. 2.1. Synoptic view of integral particle fluence rate of space radiation versus upper boundary of particle energy (Wilson, 1978).

(21) In addition to their variation with location in space, the intensity and particulate composition in these fields are subject to temporal variations. As far as space radiation is concerned, two temporal scales of space weather events are relevant. Similar to the annual alternation between summer and winter of ordinary weather on Earth, we have to deal with a nearly regular change of solar activity between phases of maximal ('summer') and minimal ('winter') solar activity. The solar 'year' in this case is the Schwabe cycle, a period of about 11 years the duration of which however (presently) varies due to so far unknown mechanisms between 9 and 13.6 years. One measure of this activity for which a continuous observational record exists since 1755 is the Zürich sunspot number (Hathaway et al., 2002). Apparently, the maximum of solar activity is inversely associated with the length of the cycle. In addition to the field variation during the regular solar cycle, episodes of extreme solar activity characterised by explosive releases of magnetic energy (Chen, 2001) which eject giant masses of charged particles from the Sun´s corona into the interplanetary magnetic field. After further acceleration in this field, particle energies up to several GeV can be attained. The impact of these solar particle events (SPE) on the radiation field in space can last for days to some weeks.

(22) Further observed solar periodicities like the magnetic Hale cycle of 22 years, the Gleisberg cycle of about 88 years or the De Vries- or Suess cycle of about 210 years have not yet been identified to substantially modulate the radiation field, although their impact on the biosphere probably is important as a recent study on glacial climate cycles discloses (Braun et al., 2005).

2.2 Galactic cosmic radiation

(23) Galactic cosmic radiation originates outside the solar system and impinges isotropically on Earth. There is no conclusive proof of the mechanisms accelerating the charged particles and of the astrophysical sites where matter becomes cosmic particle

radiation. There is no information about the directional position of their sources since these particles are scrambled by irregular interstellar magnetic fields on their way towards the Earth. Because of their high energies - up to 10^{20} eV - they most probably originate from supernova explosions, neutron stars, pulsars or other sources where high-energy phenomena are involved. Detected radiation consists of 98% baryons and 2% electrons. The baryonic component is composed of about 85% protons (hydrogen nuclei), with the remainder being alpha particles (about 14%) and heavier nuclei (about 1%). Figure 2.2 shows the abundances of these elements up to tin relative to silicon. The ions heavier than alpha particles are termed HZE-particles (high charge, with charge numbers Z>2 and high energy). Although iron ions are one-tenth as abundant as carbon or oxygen, their contribution to absorbed dose in tissue is substantial, since this dose is proportional to the square of the particle charge. This is indicated in Fig. 2.2 (Cucinotta et al, 2001).

(24) In addition to the galactic cosmic radiation, a so-called anomalous component is observed. It consists of originally neutral particles coming from the interstellar gas which become singly ionised by solar radiation after entering the heliosphere. These particles are then accelerated in collision regions between fast and slow moving streams of the solar wind. They are able to penetrate deeper into the magnetic field than fully ionised cosmic particles. Their energies are around 20 MeV/u and consequently they can only contribute to radiation effects behind thin shielding. However, it has to be considered that they lose all their electrons after penetration of a very small amount of shielding material and thus also deposit energy proportional to the square of their charge number Z.

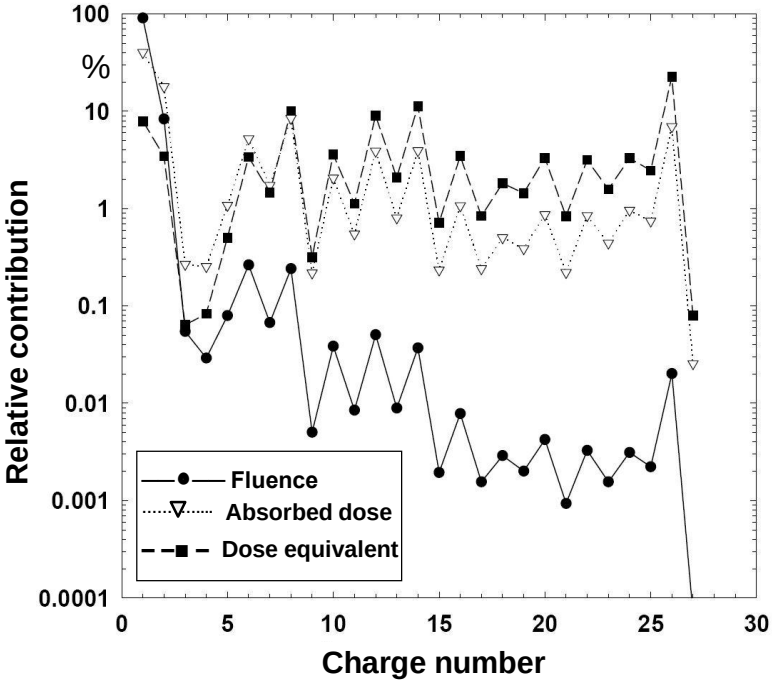

Fig. 2.2. Elemental composition of galactic charged particles and their relative contribution to absorbed dose and dose equivalent in tissue (Cucinotta et al, 2001).

(25) In this report energies of GCR nuclei are always presented as kinetic energy per atomic mass unit (amu or u), *E*. This has the advantage that all nuclei having the same value of energy per amu move with nearly the same velocity regardless their mass. Using this energy scale the energy distributions of the different cosmic ray nuclei are very similar.

Fluence rate distributions in energy for hydrogen, helium, carbon and oxygen, and iron are shown in Fig. 2.3. At energies E above some GeV/u the fluence rate is well represented by a power law $N(E) \sim E^{-\gamma}$ with γ around 2.5. Towards lower energies the distributions get flatter and show a maximum at about some hundred MeV/u.

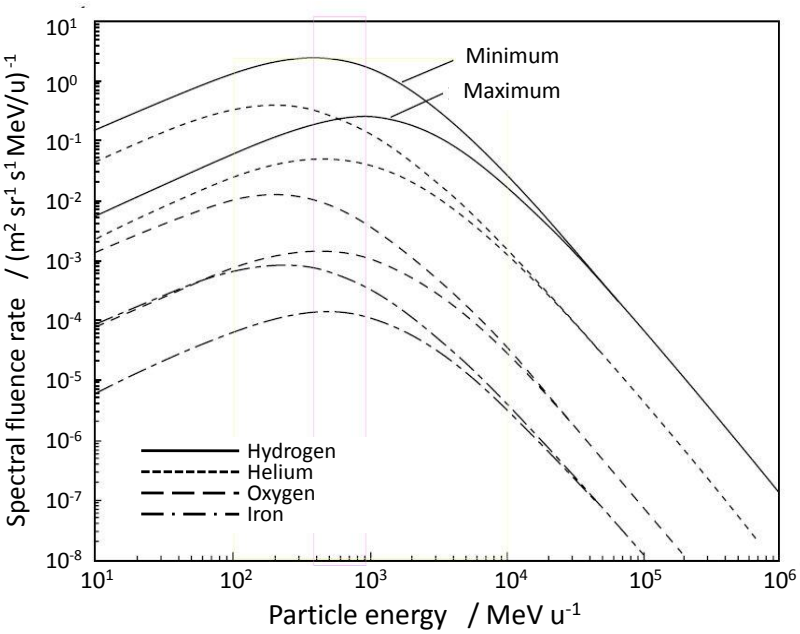

Fig. 2.3. Energy distribution of fluence rate versus particle energy for 4 GCR particles and their modification by solar activity (for solar minimum (1977) and solar maximum (1959)) at 1 AU as relevant for radiological protection (Badhwar, 1997).

(26) Fluence rates of cosmic radiation are not constant; they vary between two extremes which correspond in time with the maximum and minimum solar activity. Solar activity and cosmic radiation fluence rates are inversely correlated. The slope of the energy distribution in Fig. 2.3 for energies below some GeV/u is affected by this modulation of the cosmic radiation fluence rate (Badhwar, 1997). It is caused by the solar magnetic field, which is coupled to the solar wind. The solar wind is a continuous stream of highly-ionised plasma emerging from the Sun. Its intensity depends on solar activity which can be described by the number of observed sunspots. During the minimum of the 11-year solar cycle the solar wind has a minimum strength and its effect on the energy distribution is smaller than at maximum solar activity. Cosmic particles incident on the solar system interact with the solar magnetic field and thus lose energy. This leads to flattened energy spectra at lower energies. With increasing solar activity, the maximum of the fluence rate is shifted to higher particle energies. At 100 MeV/u, the particle fluence rates differ by a factor of about 10 between maximum and minimum solar activity conditions, whereas at about 4 GeV/u only a variation of about 20% is observed.

(27) Monitoring of solar modulation is possible on Earth based on the fluence rate of secondary neutrons produced in the Earth's atmosphere by interactions of galactic cosmic radiation. This fluence rate has been measured over longer periods by different ground based stations using neutron monitors. Figure 2.4 shows an example of data taken over several years with the neutron monitor at Kiel University (NMDB, 2011). It can be seen that details of the modulation seem to be unpredictable statistical fluctuations. However, maxima and minima clearly appear inversely correlated to the 11-year solar cycle with a roughly

sinusoidal form around an average particle fluence rate. However, the magnitude of the extremes again undergoes fluctuations. Predictions for future satellite missions are limited in accuracy within a factor of two or even more based on such unpredictable fluctuations.

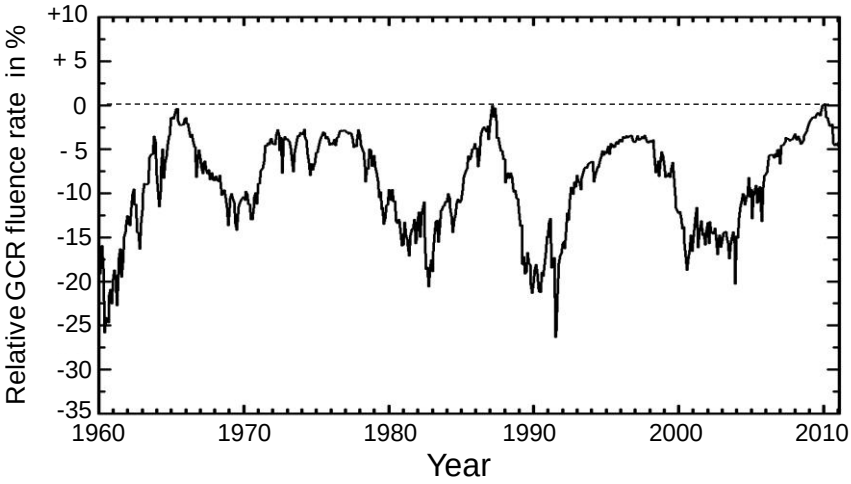

Fig. 2.4. Relative fluence rate variation of cosmic radiation (GCR) with time in the solar cycle of the heliocentric potential measured by the neutron monitor in Kiel (NMDB, 2011).

2.3 Solar cosmic radiation

(28) Besides electromagnetic radiation, the Sun continuously emits particle radiation, mainly consisting of protons and electrons, the solar wind. The intensities of these low energy particles vary by 2 orders of magnitude between about some 10^{10} and 10^{12} particles cm^{-2} s^{-1} sr^{-1}. In terms of velocity, this particle stream is characterised by velocities between about 300 km s^{-1} and 800 km s^{-1} and more. The particle energies, however, are so low (for protons between 100 eV and 3.5 keV), that the particles will be stopped within the first few microns of unshielded skin. They are, therefore, not of concern for radiation effects in man.

(29) Nevertheless, the temporal variation of the solar wind is a major driver which determines radiation exposure from GCR in space, at least within the inner heliosphere. The heliosphere itself can be defined as that domain of the interstellar space which the solar wind can fill out. The magnetic field based on the solar wind provides a similar shielding as the geomagnetic field does. The shielding strength can be simulated in terms of a pseudo-electrostatic heliocentric potential against which the charged particles have to work when entering the heliosphere from the local interstellar medium. This potential modifies the GCR energy spectra to the same degree as the interplanetary magnetic field does.

(30) Occasionally, the surface of the Sun releases large amounts of energy in sudden local outbursts of gamma radiation, hard and soft x-rays and radio waves in a wide frequency band. In these solar particle events (SPEs), large currents and moving magnetic fields in the solar corona accelerate solar matter. Coronal particles with energies up to several GeV escape into the interplanetary space. They spiral around the interplanetary magnetic field lines. Within the ecliptic plane, field lines expand from the Sun into the interplanetary medium like the stream of water from a rotating garden hose. They connect the Earth with a certain spot on the western part of the Sun. The number and energy distribution of particles observed in solar particle events at Earth is different from GCR and depends on this connection. SPEs

show an enormous variability in particle fluence rates and energy distribution and have the potential to expose space crew to high life-threatening doses

(31) An SPE well-connected with high particle fluence rates observed at Earth is an infrequent event which is most likely to be observed during the period of increasing and decreasing maximum solar activity. Therefore, major SPEs are observed at Earth as random events with a low frequency, typically one per month. They last for several hours or days. Events with significant fluence rates of protons with higher energies can be observed as "ground-level events" (GLE) by neutron monitors. Figure 2.5 shows the number of GLEs observed over the last solar cycles. Long gaps with no events can be seen during solar minimum activity. Between the last GLE in cycle 21 and the first one in cycle 22 there was a 65 month quiet period which was followed by a sequence of 11 GLEs within one year with approaching maximum of the present solar cycle.

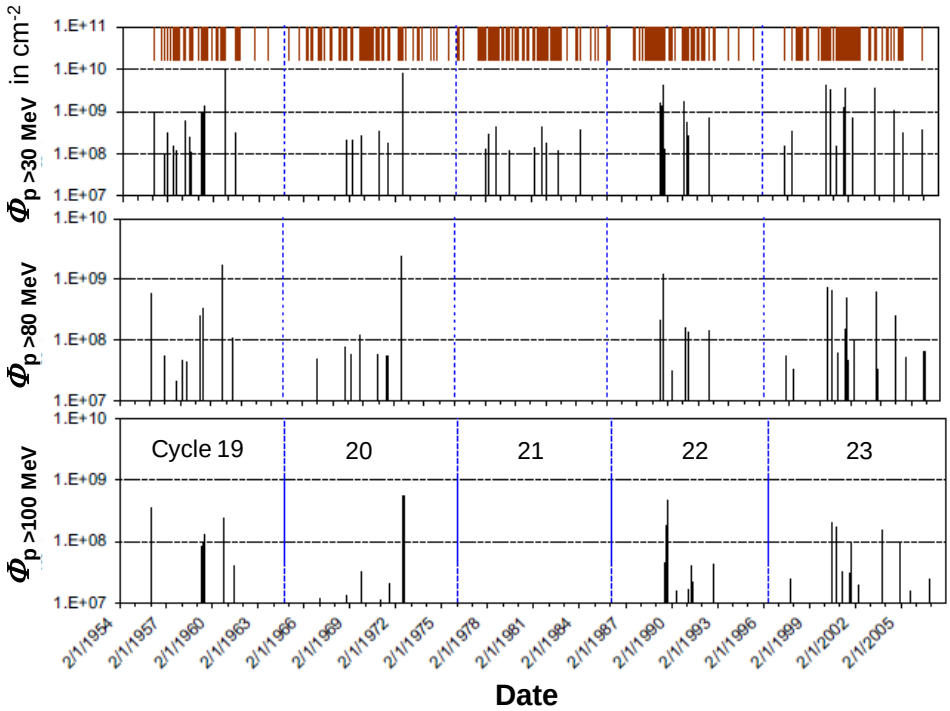

Fig. 2.5. Occurrence of major solar particle events in solar cycles No. 19 to 23 and the integral particle fluence, Φ_p, for protons with energies >30 MeV, >60 MeV, and >100 MeV (Kim et al., 2011).

(32) Since high energetic particles arrive first and are followed by particles of lower energies, the energy distribution of SPE particles observed at Earth depends on time after onset of the event. Above energies of about 10 MeV, SPE particle spectra following approximately the power law $I(E) = I_0\ E^{-\gamma}$. After the onset of the event, the exponent γ decreases with time. This means that the contribution by high-energy particles decreases with time during the event. The constant I_0, describing the absolute number of particles, shows a great deal of structure during the event caused by field irregularities and shock structures in the interplanetary medium.

(33) Such events can induce adverse skin reactions in astronauts if they get caught outside shielding since above about 10 MeV protons can penetrate space suits and reach the skin or the lens of the eye. Depending on the particle intensities they may induce erythema or trigger late radiation cataracts within the lens of the eye. While the latter take several years to

develop and hence pose no threat to a safe mission completion, severe erythema may well induce performance decrements which could compromise mission success.

(34) Since 1955, five SPEs with intensities and energies large enough to jeopardise crew health behind normal or even enhanced spacecraft shielding have so far been observed. For these strong events integral fluence distributions (total number of particles per unit area above an energy *E*) have been measured by satellite instruments (see Fig. 2.6). For a sixth event - that of February 23rd 1956 - the fluence distribution has been inferred from an analysis of the count rates of terrestrial neutron monitors which recorded the induced secondary neutrons. Such enhancements of neutron count rates are monitored in a worldwide net of neutron monitor stations a selected subset of which forms the so called Spaceship Earth. Ground level enhancement (GLE) events indicate that associated SPE protons with energies above about 450 MeV were sufficiently numerous to raise the neutron fluence rate at sea level by at least 5%.

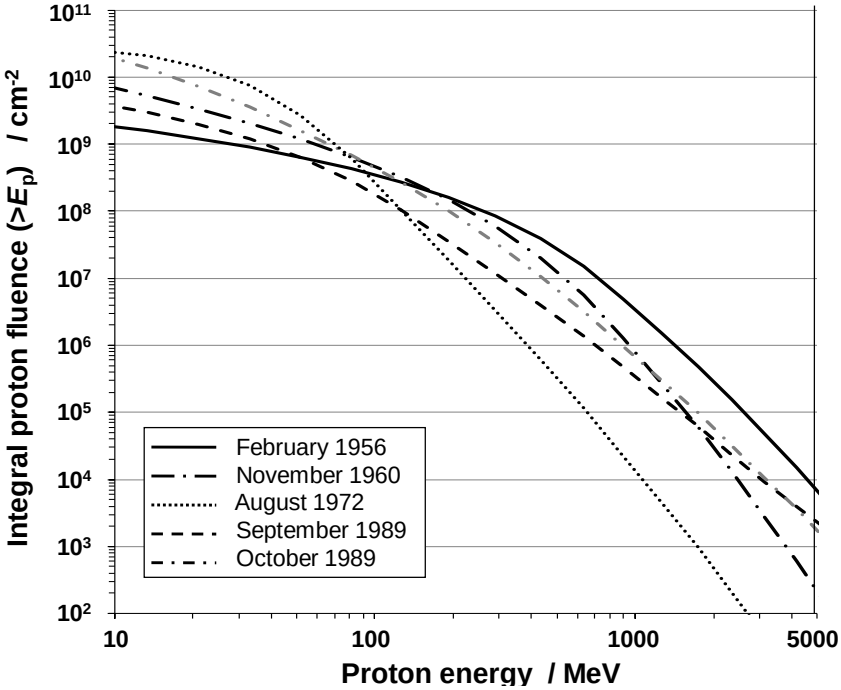

Fig.2.6. Integral fluence spectra of protons from historical 'worst-case' solar particle events (Kim et al., 2010a).

(35) A comprehensive list of GLE´s observed since February 23rd 1956 (GLE No. 5) and July 14th 2000 (GLE No. 59) together with all neutron monitor stations where these events were observed is provided by the Australian Antarctica Data Centre (http://data.aad.gov.au/aadc/gle/events.cfm). Among all these GLEs, the enhancement by GLE No. 5 in Leeds (lat.: 53.83 N, long.: 358.42 E, alt.: 100 m, Pc=2.20 GV) is about 4600% higher than the pre-event count rate, whereas for other SPEs the enhancement very rarely exceeds a 100% increase.

(36) A small fluence rate of solar particles with low energies also reaches the Earth from SPEs at other positions of the Sun which are not fully directed to the Earth. These fluence rates add up to a solar component which dominates over the galactic component at energies below 30 MeV/u. Depending on the conditions of the interplanetary medium, this component undergoes fluctuations which are highly variable and unpredictable. During

periods of maximum solar activity, when the fluence rate of galactic cosmic radiation is depressed and SPEs are more frequent, the contribution of the solar component is more significant.

(37) For long-term mission planning, in addition to the magnitude that a worst case event can attain, the frequency of occurrence of events as well as the proton energy spectrum becomes important too. Fig. 2.7 gives a probability that a particle event with protons of energies above 30 MeV occur, based on the random nature of SPE occurrence and event size and based on the records taken for fluence measurements of the last five solar cycles.

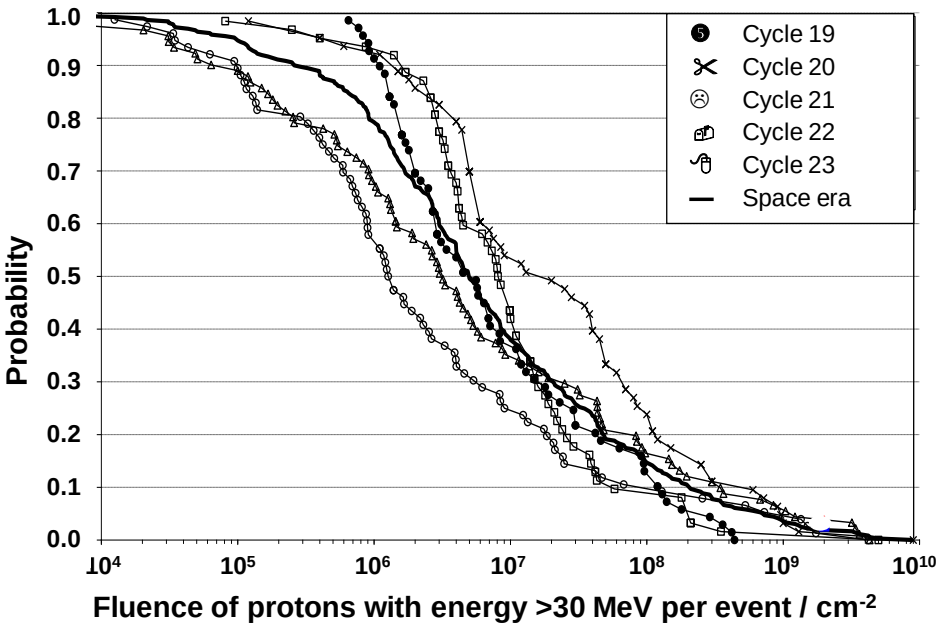

Fig. 2.7. Probability of an SPE event with protons exceeding the energy of 30 MeV versus proton fluence per event for different cycles and for the complete space era (Kim et al., 2011).

2.4 Trapped radiation

(38) The radiation field around the Earth comprises the third radiation source. The particles trapped in the radiation belts discovered by van Allen are a result of the interaction of GCR and SCR with the Earth's magnetic field and the atmosphere. The radiation belts consist of electrons and protons, and some heavier ions. Electrons reach energies of up to 7 MeV and protons up to 700 MeV. The energy of heavy ions is less than 50 MeV/u, and because of their limited penetration capacity, they are of no consequence for satellite electronics or radiological protection of humans. Charged particles with these energies moving into a dipole field can never enter into inner areas of this field. However, if they are put into this field for any reason, they are restricted to certain positions and cannot escape. They move in spirals along the geomagnetic field lines and are reflected back between the magnetic poles, acting as mirror points. Different processes contribute to fill in particles into the radiation belt and two main zones of captured particles are observed. The inner belt is mainly formed by decaying neutrons, coming from the atmosphere in which they are produced in cosmic particle interactions, and producing protons and electrons. The outer belt

consists mainly of trapped solar particles, and is populated largely by electrons. During disturbances of the magnetosphere by magnetic storms related to solar flares, where the geomagnetic cut-off is usually depressed, particles of lower energies can penetrate from outside towards the inner regions and fill them. The radiation belts extend over a distance from Earth from about 200 km to about 75000 km around the geomagnetic equator. Energy loss by cyclotron radiation and by penetration into the upper atmosphere near the geomagnetic mirror points constitutes the major loss mechanisms for the trapped particle population.

(39) Extensive measurements during the recent decade with more advanced and dedicated instrumentation on several satellites in well-coordinated orbits yielded the main quantitative database which then became integrated in the AP-8 TRAPPED PROTON MODEL (Sawyer et al., 1976) and which provides energy spectra of average proton fluence rates during quiet magnetospheric conditions. A major application which these models have been designed for is the assessment of the radiation exposure from trapped radiation during manned low Earth orbit (LEO) missions such as presently on the International Space Station (ISS). The AE-8 TRAPPED ELECTRON MODEL (Vette, 1991) serves the same purpose of prediction radiation doses yet mainly for the radiation environment in geostationary orbits where energetic electrons constitute the dominant source of ionising radiation.

(40) An improved AE-9/AP-9 Model is being developed as part of the Proton Spectrometer Belt Research (PSBR) Program and is planned to be released in near future by a consortium of institutions, such as the National Reconnaissance Office (NRO), Aerospace Cooperation, the Air Force Research Laboratory (AFRL), Los Alamos National Laboratory (NAL) and the Naval Research Laboratory NRL).

(41) There is a strong east-west effect in trapped proton fluence rates. At the bottom of their path around the magnetic field lines, protons are travelling eastwards, whereas those on the top of their path are travelling westwards. The westwards travelling particles have emerged from a region of the atmosphere at lower altitude. Therefore, they encounter a denser atmosphere and are more efficiently removed by interactions with the nuclei of the atmosphere (Lenchek and Singer, 1962).

(42) Figure 2.8 displays the spatial distribution of electron fluence rate for electron energies above 0.5 MeV (right) and of proton fluence rate for proton energies above 34 MeV (left) at which energy the latter are able to penetrate about 1.4 g cm^{-2} Al, the shielding provided by lighter space craft. Proton fluence rates in the inner belt are intense and protons reach sufficient energies to penetrate the shielding provided by walls and equipment of space craft so that primarily their energy distribution as shown in Fig. 2.9 have to be known in order to assess radiation exposures of astronauts. The data in Fig. 2.9 are the results of measurements of the energy distribution of trapped proton fluence rate in the early 1960s (Filius, 1965; Freden et al., 1964). As a natural coordinate system to specify the satellite position within the geomagnetic field, the (B, L) coordinates are used. Here, B denotes the magnetic field strength at a given point and L the altitude in units of Earth radii at which the magnetic field line through this point intersects the plane through geomagnetic equator.

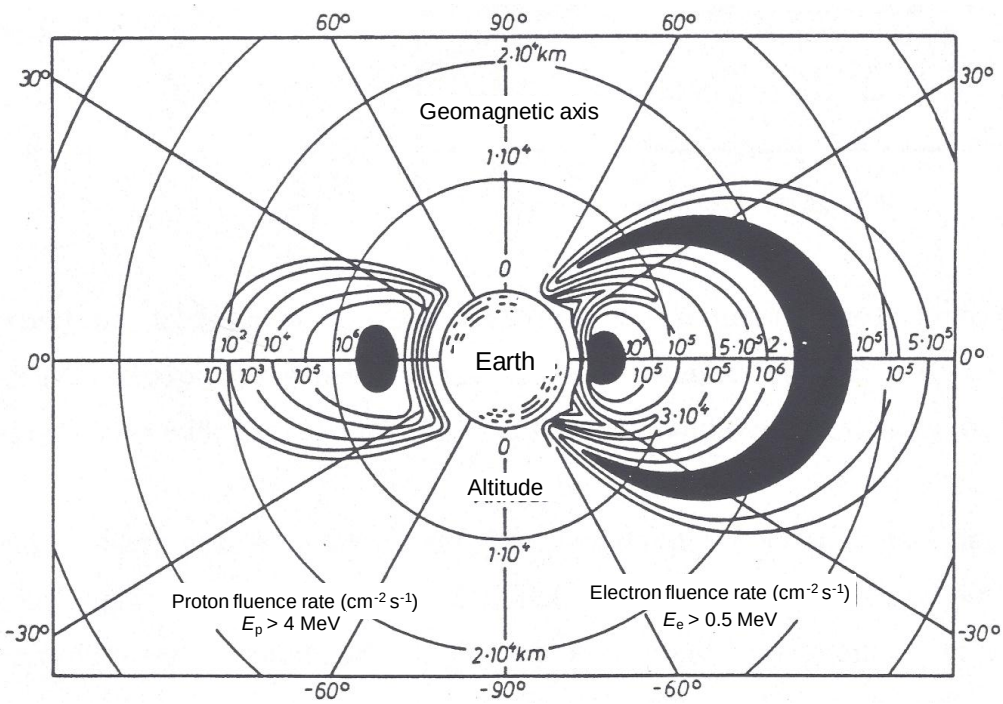

Fig. 2.8. Fluence rates in inner and outer terrestrial radiation belts for trapped protons and electrons in $cm^{-2}\ s^{-1}$ (Allkofer, 1975).

(43) Figure 2.10 shows the fluence rate energy distributions of trapped electrons and protons averaged over the orbit of the Hubble Space Telescope. Electron fluence rates during solar maximum are greater than during solar minimum, pointing to the Sun as the dominant primary source which feeds the trapped electron population. In contrast, the trapped proton fluence rates reflect the (Forbush) modulation of the GCR intensity by the solar wind which results in higher intensities during solar minimum conditions.

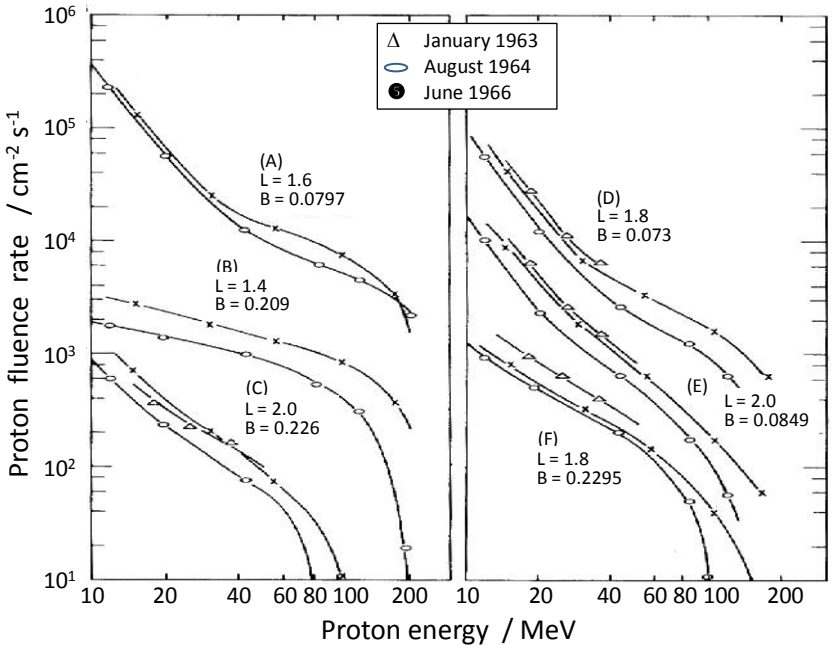

Fig. 2.9. Fluence rate spectra of inner belt protons measured at various locations within the belts as expressed in the *B*,*L*-coordinate system (Filius, 1965; Freden et al., 1964).

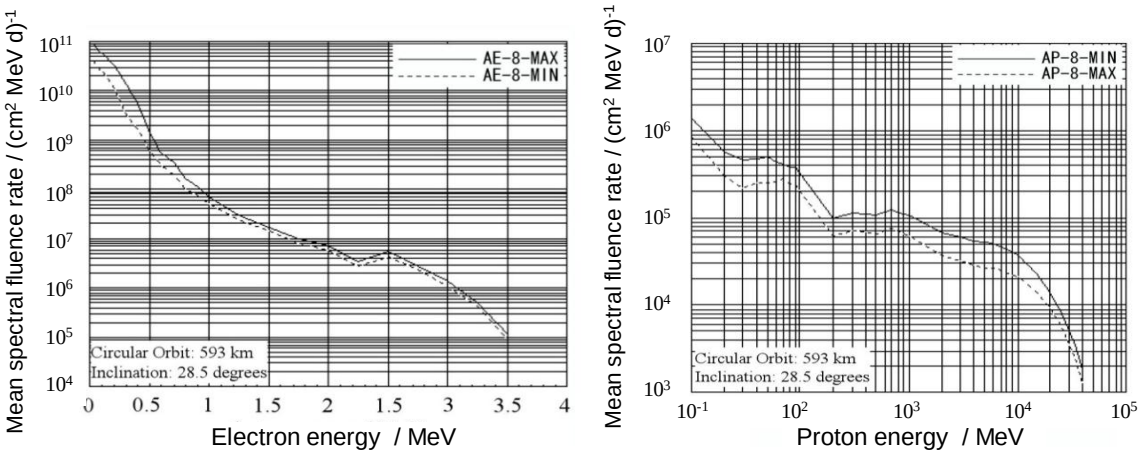

Fig. 2.10. Left: Mean energy distribution of fluence rate of trapped electrons at solar minimum and maximum conditions calculated with the AE-8 model for the position of the Hubble space telescope (Jones, 2000).
Right: Mean energy distribution of fluence rate of trapped protons at solar minimum and maximum conditions calculated with the AP-8 model for the position of the Hubble space telescope (Jones, 2000).

(44) The fluence rates and energy distributions shown pertain to quiet magnetic conditions of the terrestrial and interplanetary magnetic field during the minimum and maximum of solar activity. In addition to the regular solar cycle variation, both magnetic storms and intensive fluence rates from energetic solar particle events (SPE) significantly shift positions and energies of trapped particle populations so that even additional though transient radiation belts can be created.

(45) The trapped radiation is modulated by the solar cycle: with increasing solar activity, proton intensity decreases, while electron intensity increases. Diurnal variations by a factor of between 6 and 16 are observed in the outer electron belt, and short term variations due to magnetic storms may raise the average fluence rate by two or three orders of magnitude. The centre of the inner belt is quite stable, especially with respect to protons. However, at the lower edge of the belt, electron and proton intensities may vary by up to a factor of 5. For the majority of space missions in low Earth orbit (LEO), protons are an important part of the radiation exposure inside spacecrafts. Because of their higher energies and correspondingly longer range, their total dose surpasses that of electrons at shielding thickness above about 0.3 g/cm^2 aluminum. At lower shielding, e.g. in case of extravehicular activities (EVA), the absorbed dose to the skin is dominated by the electron contribution and may reach up to 10 mGy per day.

(46) Of special importance for low Earth orbits is the so called 'South Atlantic Anomaly' (SAA), at the moment a region over the coast of Brazil, where the radiation belt extends down to altitudes of 200 km. This behaviour is due to an 11° inclination of the Earth's geomagnetic dipole axis from its axis of rotation towards northern America and a 500 km displacement of the dipole centre towards the western Pacific, with corresponding significantly reduced field strength values. Radiation received in LEO at low inclinations includes GCR and radiation due to passages through the SAA. At an orbit with 28.5° inclination, six orbital rotations per day pass through the anomaly, while nine per day do not. Although traversing the anomaly takes less than about 15 min and occupies less than 10% of the time in orbit, this region accounts for a significant fraction of total exposure.

(47) In addition to the trapped charged particles in radiation belts, the GCRs are producing secondary neutrons by nuclear reactions in the upper atmosphere of the Earth. Neutrons are produced in practically two energy regions by two processes. Neutrons in the region between 1 and 10 MeV are mostly evaporation products of highly excited nuclei with a fairly isotropic angular distribution. High-energy neutrons originate as knock-on neutrons mainly in peripheral collisions or in charge exchange reactions of high-energy protons. Their energy distribution peaks at about 100 MeV. They leak into the exosphere and contribute also to the exposure in spacecraft. Measured neutron spectra in the Earth atmosphere are shown in Fig. 2.11. Their contribution to the radiation field in LEO is, however, relatively low. A similar neutron field as measured in the atmosphere is of course produced by interactions of the GCR with the spacecraft material and the astronaut’s body. This contribution to the exposure of astronauts is substantial (Bartlett et al., 2006).

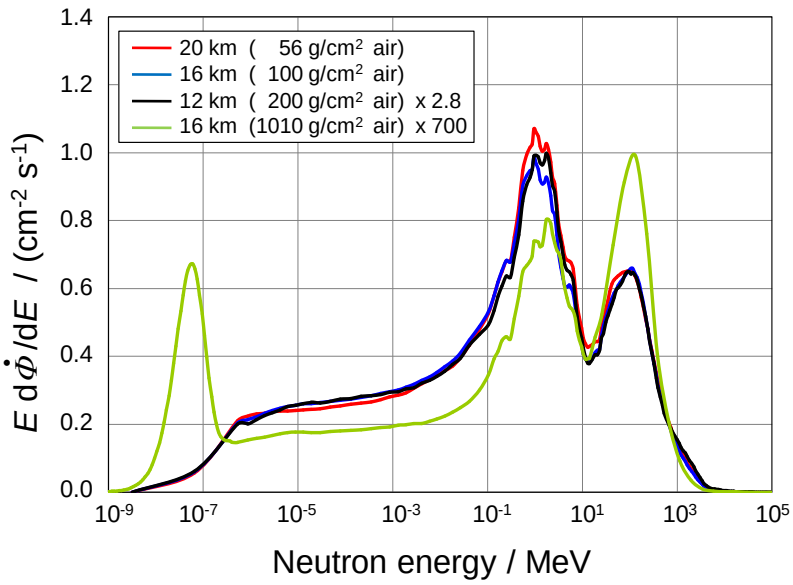

Fig. 2.11. Neutron spectra from cosmic radiation on ground and in different atmospheric depths at air flight altitudes measured with Bonner spheres during the AIR ER 2 flights and on the ground at sea level (Goldhagen et al., 2004).

2.5 Interaction with magnetic fields

(48) To reach spacecraft in low Earth orbits (LEO) a charged particle has to penetrate the Earth's magnetic field. Penetrability is a property related to the ions magnetic rigidity which is given by its momentum divided by its charge. All particles with the same rigidity follow a track with the same curvature in a given magnetic field. For each point inside the magnetosphere and each direction from that point, there exist a rigidity threshold below which the cosmic particles are not able to reach this point. This rigidity is called the geomagnetic cut-off rigidity and is proportional to the magnetic field component perpendicular to the direction of particle motion. For a particle moving towards the centre of Earth, for example, the cut-off rigidity has a maximum value at the equator, since the particle moves perpendicular to the field lines and the cut-off rigidity vanishes at the pole, since the particle moves in the direction of the field lines. Therefore, geomagnetic shielding is less effective for high inclination orbits than for low inclination orbits. This means that in low inclination orbits, only particles of high energy have access. Towards higher inclinations, additional particles of lower energies are observed. For a geomagnetic latitude λ, the vertical cut-off rigidity R_c can be calculated approximately by $R_c = 14.9 \cos^4\lambda/(r/r_e)^2$, where r/r_e is the ratio of the distance r from the dipole centre to the Earth radius, r_e. The rigidity for particles arriving from other directions than vertical is dependent from the angle of incidence. Due to latitude dependent shielding, the number of particles incident in the altitude of orbiting spacecraft increases from lower inclinations towards higher inclinations.

(49) In LEO, as well as in aviation heights, a second shielding mechanism has to be incorporated into the transport of the primary GCR or SPE ions. Whereas the geomagnetic field on the one hand is responsible for the added radiation exposure in LEO from trapped radiation, it also causes a quite substantial reduction of radiation exposure, at least near the geomagnetic equator (which differs from the geographic equator). This stems from the

deflection due to the Lorentz force of charged particles by the geomagnetic field as illustrated in Fig. 2.12.

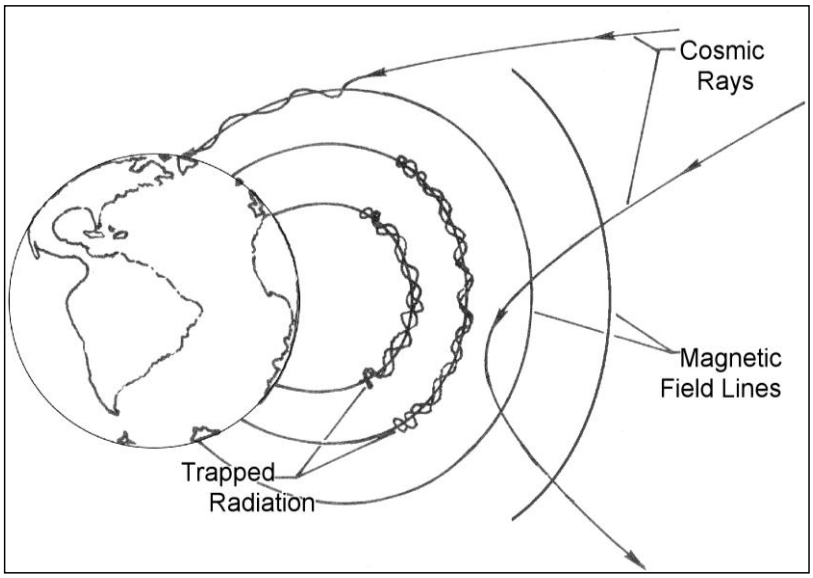

Fig. 2.12. Deflection and trapping of charged particles by the geomagnetic field (Spjeldvik et al., 1983).

(50) Figure 2.13 provides a global map of the vertical cut-off rigidities for the geomagnetic field model of Epoch 2000 (Smart et al., 2008). For a homogeneous dipole field, the iso-rigidity lines would be parallel to the (geomagnetic) equator. The marked asymmetry with a peak above 17 GV of the cut-off rigidity at the Indian Ocean (long. 90E, lat: 10N) reflects the offset from the geographic centre of the magnetic centre by about 450 km in this direction. At the opposite side, in the South Atlantic this offset results in the corresponding subsidence of the lower fringes of the inner proton belt creating thereby the so called South Atlantic Anomaly (SAA). This is the reason for the already mentioned fact that the bulk of radiation exposure in most LEOs is accumulated in this region.

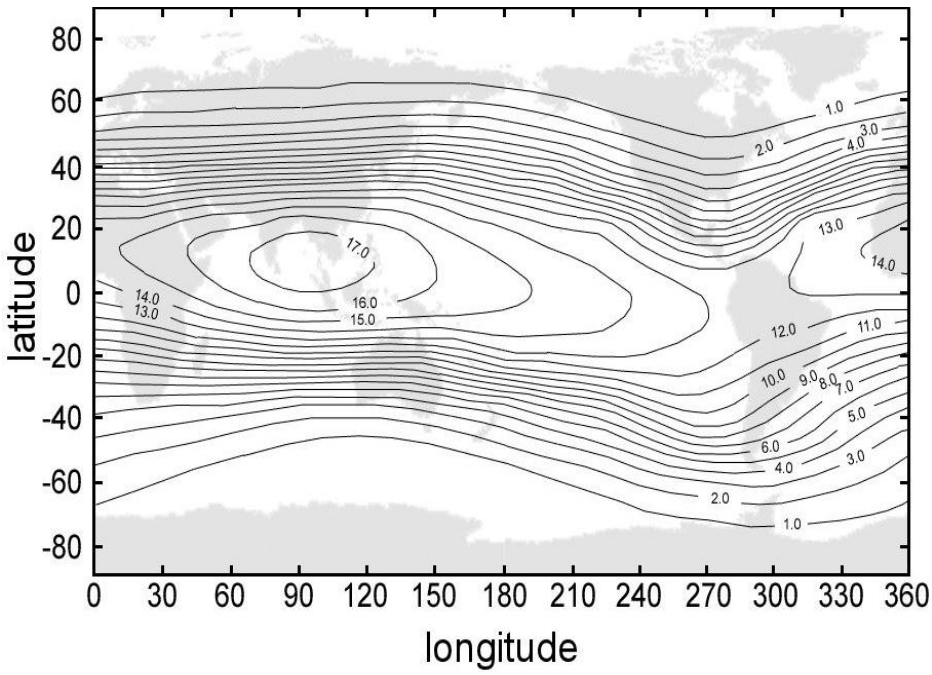

Fig. 2.13. Map of vertical cut-off rigidities in GV for the geomagnetic field model of Epoch 2000 (Smart et al., 2008).

(51) For a given orbit, the shielding due to this effect is expressed by the geomagnetic transmission factor which specifies the fraction of the GCR or solar particle fluence rate of a given particle energy (or momentum given in units of $GeVc^{-1}$) which has access to this orbit or by the cut-off rigidity probability which specifies the probability that a particle with a given rigidity reaches that orbit. Figure 2.14 (a) demonstrates the dependence of the geomagnetic shielding on the orbit inclination for a circular orbit at 223 km altitude. For an orbit of 28.5 degrees inclination which for a large fraction evades the SAA, on the average the GCR with a momentum below about 4.2 GeV c^{-1} do not reach that flight route.

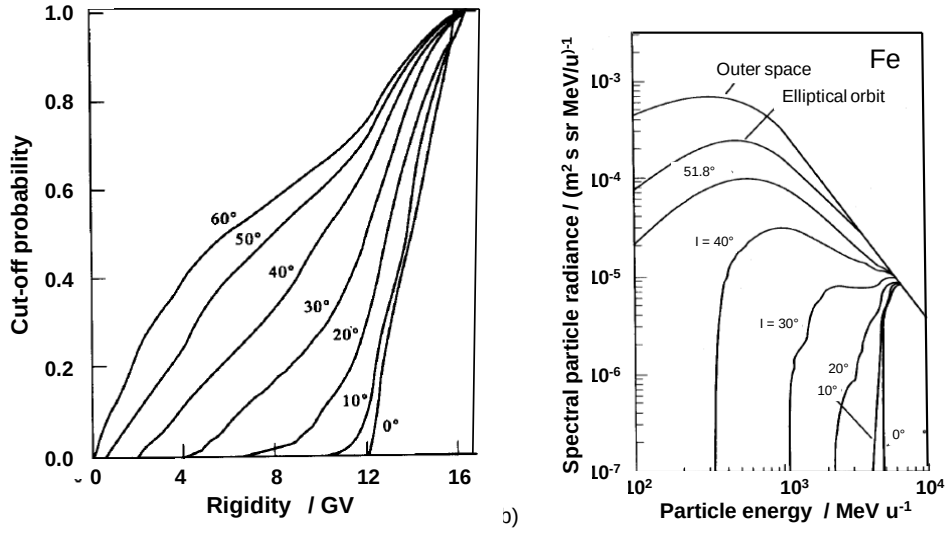

(a) (b)

Fig. 2.14. (a) Cut-off rigidity probability for different inclination for a circular orbit of 223 km (Heinrich et al., 1979).
(b) Energy spectra of iron nuclei for outer space and for orbits in 223 km altitude of different inclinations (Heinrich et al., 1979).

(52) For a 45 degree inclination, this momentum threshold drops to about 1.1 GeV c^{-1}, whereas for polar orbits at least 20% of particles with the lowest energies always have access to this altitude. On the other hand the shielding effect vanishes for ions with a momentum above about 15 GeV c^{-1}, where at any inclination all charged ions reach this orbit. Figure 14 (b) shows the influence of the magnetic shielding on the particle spectra, e.g. for Fe, which varies strongly with the different inclination. The functions in Fig. 2.14 do not, however, include the shadow effect of the Earth itself.

(53) The shadow effect of the Earth for the Hubble Space Telescope (HST) at 28.5 degree inclination reduces the fluence rate of even the most energetic GCR by about 30%. An Earth observation satellite such as e.g. TERRA, on the other hand, must use a near polar orbit and therefore can be accessed by charged particles of all energies. Its higher altitude also slightly reduces the shielding by the Earth shadow. The high inclination of the International Space Station (ISS) of 51.6 degree makes this manned spacecraft accessible to SPE ions of 100 MeV/u or above. This is particularly important, since in case of geomagnetic disturbances which often accompany solar events, this geomagnetic shielding is further reduced. Fig. 2.15 demonstrates this loss of geomagnetic shielding for the ISS for storms as characterized by the *K*p index of global geomagnetic activity (see: http://isgi.cetp.ipsl.fr/des_kp_ind.html) which can vary between 0 and 9. Under conditions of such storms a much larger fraction of SPE ions can reach the orbit of the ISS.

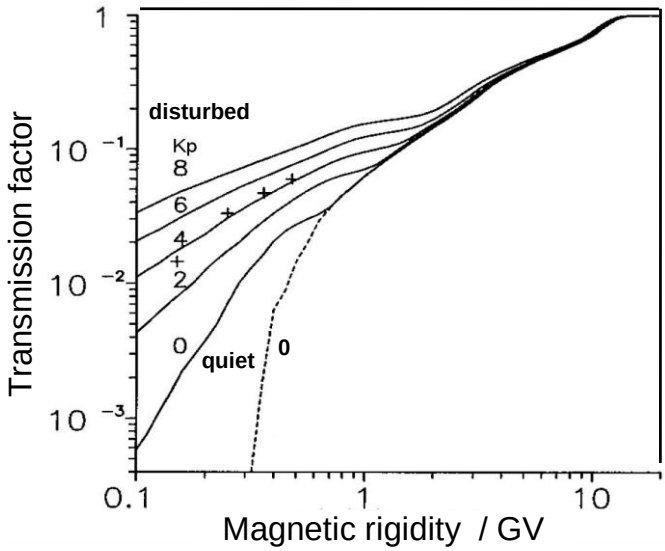

Fig. 2.15. Calculated geomagnetic transmission functions for the ISS orbit versus magnetic rigidity for a quiet time geomagnetic field (dotted line) (IAGA, 1992) and for disturbed geomagnetic conditions (solid lines) as expressed by the *K*p index (Nymmik, 1999). The crosses are the results from Boberg et al. (1993) for *K*p = 5.

3. QUANTITIES USED IN RADIOLOGICAL PROTECTION

(54) The description and quantification of exposure of humans to ionising radiation needs the definition of specific quantities and units. For many years this has been performed by ICRU and ICRP and the actual definitions can be found in their publications (ICRU, 1993; 2011 and ICRP, 2007). Human exposure to ionising radiation can occur from radiation incident on the human body (external exposure) or from radionuclides incorporated in the body (internal exposure). For exposure of astronauts in space, internal exposure is of very little relevance and therefore this chapter concentrates on the concept of quantities relevant for external radiation exposure.

(55) In the past, the definition of the specific quantities for radiological protection has mainly considered occupational and public exposure situations on Earth concentrating on human exposures by photons, electrons and neutrons, and also α-particles in internal exposure. In addition, the protection quantities are defined for application in situations of low dose and low dose rates. Limits are given in terms of these quantities in order to limit the probability of the occurrence of stochastic detriments to humans to an acceptable level and to avoid deterministic effects (tissue reactions).

(56) The exposure situation in space is different from that on Earth mainly due to the strong differences in the radiation fields (see Chapter 2) and to the higher environmental dose rate in space than on Earth whereby the likelihood of stochastic effects are increased and deterministic effects cannot be excluded. The high contribution of heavy ions in GCR and secondary radiation to doses in the human body needs to be considered in particular.

(57) The consequences for the definition of appropriate radiation protection quantities for use in space situations are considered in the following sections. Organizations active in space missions have defined detailed procedures for the assessment of human exposure in space since long time (see e.g. NCRP 2000; 2002). In principle, they are interested not only in the determination of individual doses, but in the assessment of individual radiation risks based on such doses and this has some consequences for the definition of dose quantities. The astronauts can be treated as single persons, or as members of small groups. Information on sex and age can be applied and better information on the astronaut's organ size and shape might be available, and there may be the possibility of applying individual sensitivity factors to the assessed organ doses if specific individual risks need to be determined (Atwell, 1994; Bahadori et al., 2011; Bahadori et al., 2012).

3.1 Dose quantities in radiological protection

(58) In radiological protection, the system of dose quantities defined by ICRP and ICRU (ICRP, 1991; ICRP, 2007; ICRU, 1993) and generally used in situations on Earth and in usual aviation altitudes includes protection quantities and operational quantities. Protection quantities (e.g. equivalent dose in an organ or tissue, effective dose) are based on mean absorbed doses to the organs and tissues of the human body and can be related to the risks of ionising radiation exposure. The ICRP system of protection quantities is shown in Fig. 3.1 (ICRP, 2007).

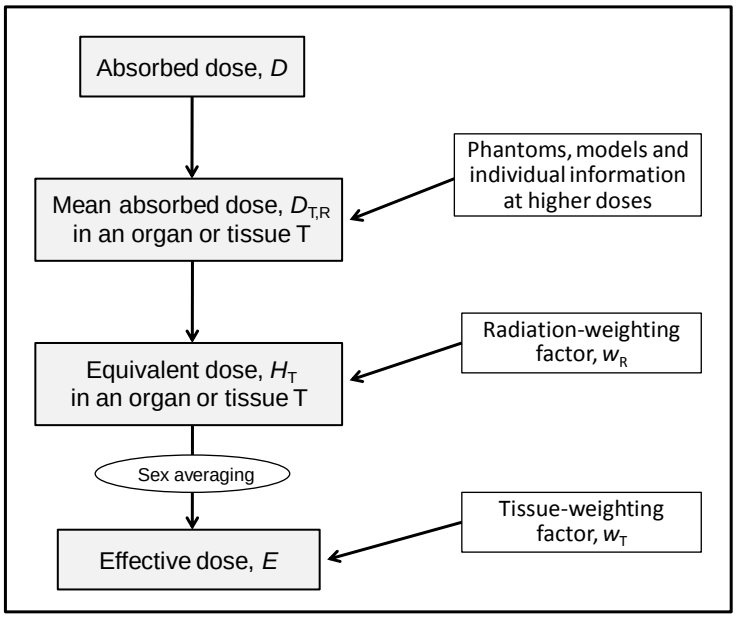

Fig. 3.1. Dose quantities for radiological protection (protection quantities) recommended by the Commission (ICRP, 2007).

(59) Operational quantities (e.g. ambient dose equivalent or personal dose equivalent) are defined for use in measurements which often enable an assessment of effective dose or mean doses in organs or tissues of humans which are generally not measurable.

(60) In radiation biology, clinical radiology, and radiological protection the absorbed dose, D, is the fundamental physical dose quantity. It is used for all types of ionising radiation and any irradiation geometry.

(61) Absorbed dose, D, is defined as the quotient of $\mathrm{d}\bar{\varepsilon}$ by $\mathrm{d}m$, where $\mathrm{d}\bar{\varepsilon}$ is the mean energy, imparted by ionising radiation to matter of mass $\mathrm{d}m$, thus

$$D = \frac{\mathrm{d}\bar{\varepsilon}}{\mathrm{d}m} \quad . \tag{3.1}$$

The SI unit is J kg^{-1} and its special name is gray (Gy). Absorbed dose takes account of the radiation field inside and outside the specified volume of mass $\mathrm{d}m$ and hence of all charged particles which were produced in or enter that volume. Its value is derived from the mean value of the stochastic quantity of energy imparted, ε, and does not reflect the random fluctuations of the interaction events in tissue. Generally, absorbed dose is a measurable quantity and primary standards exist to allow its determination by measurement.

3.1.1 Protection quantities

(62) Generally, radiological protection is concerned with controlling exposures to ionising radiation so that tissue reactions are prevented and the detriment from stochastic effects is limited to accepted levels. The fundamental *protection quantities* are based on absorbed doses imparted to organs and tissues of the human body. These quantities are designed to allow quantification of the exposure to ionising radiation from both whole and partial body irradiation (ICRP, 1991; 2007). The estimated doses can then be compared with

recommended dose limits for e.g. occupationally exposed people or at higher doses mean absorbed doses in organs and tissues may be used for the assessment of risk of cancer or other detriments.

(63) **Mean absorbed dose in an organ or tissue** In radiological protection, the main interest is not directed to the absorbed dose at a point in the human body, but to the absorbed dose averaged over a tissue or organ volume. The mean absorbed dose, $D_{\mathrm{T,R}}$, in an organ or tissue T due to a radiation of type R is the basic quantity for the definition of the protection quantities equivalent dose and effective dose used for describing exposures at low doses and dose rates where stochastic effects are dominant. In a mixed radiation field the mean absorbed dose, D_{T}, in an organ or tissue T is given by

$$D_{\mathrm{T}} = \sum_{\mathrm{R}} D_{\mathrm{T,R}} \quad . \tag{3.2}$$

(64) The mean absorbed dose is not always representative of the local absorbed dose throughout an organ or tissue, e. g. for low-penetrating radiation. For strongly-penetrating radiation, however, the absorbed dose distribution within most organs may be sufficiently homogeneous and thus the mean absorbed dose is mostly a suitable measure of the dose throughout the organ or tissue.

(65) **Equivalent dose in an organ or tissue** The protection quantity *equivalent dose in an organ or tissue*, H_{T}, is defined by

$$H_{\mathrm{T}} = \sum_{\mathrm{R}} w_{\mathrm{R}} D_{\mathrm{T,R}} \tag{3.3}$$

where w_{R} is the radiation weighting factor for radiation R which considers the differences in the radiobiological effectiveness of different radiations (details see Section 3.2.2) and $D_{\mathrm{T,R}}$ the average absorbed dose in the volume of a specified organ or tissue, T, due to the radiation of type R. The radiation R is given by the type and in the case of neutrons the energy of radiation either incident on the body or emitted by radionuclides residing within the body. The sum is performed over all types of radiations involved. The unit of equivalent dose is J kg^{-1} and has the special name sievert (Sv). Equivalent doses, $H_{\mathrm{T}}^{\mathrm{M}}$ and $H_{\mathrm{T}}^{\mathrm{F}}$, are specified in male and female bodies represented by male and female reference voxel phantoms.

(66) **Effective dose** The effective dose, E, introduced in Publication 60 (ICRP, 1991) and again defined in Publication 103 (ICRP, 2007) as:

$$E = \sum_{\mathrm{T}} w_{\mathrm{T}} H_{\mathrm{T}} \tag{3.4}$$

where w_{T} is the tissue weighting factor for organ or tissue T representing the relative contribution of that organ or tissue to the total health detriment resulting from uniform irradiation of the body at low doses and dose rates. It is $\Sigma\, w_{\mathrm{T}} = 1$. The sum is performed over 14 organs and tissues of the human body individually considered in the definition of E and for which specific w_{T} values are given in Table 3.1 and an additional remainder tissue representing a mean value of further tissues (14 tissues, but only 13 tissues for each gender) (see Table 3.1).

(67) The unit of effective dose is J kg^{-1} with the special name sievert (Sv). The same unit is also used for the operational dose quantities. Care must be taken in ensuring that the quantities being used are clearly stated.

(68) In the calculation of effective dose the equivalent doses H_{T} are taken as the mean values averaged over the male and female organs and tissues:

$$H_{\mathrm{T}} = 0.5(H_{\mathrm{T}}^{\mathrm{M}} + H_{\mathrm{T}}^{\mathrm{F}}). \tag{3.5}$$

(69) The concept of tissue weighting factors has been introduced already in 1977 (ICRP, 1977), extended in 1991 (ICRP, 1991) and further modified in 2007 (ICRP, 2007). The values of w_{T} for the specified tissues and organs are based on the detriment due to stochastic effects after radiation exposure and on judgments. They represent mean values for humans averaged over all ages and both sexes.

Table 3.1. Tissue weighting factors, w_{T} (ICRP, 2007)

Organ/Tissue	w_{T}	**Total Contribution**
Lung, Stomach, Colon, Bone marrow, Breast, Remainder	0.12	0.72
Gonads	0.08	0.08
Thyroid, Oesophagus, Bladder, Liver	0.04	0.16
Bone surface, Skin, Brain, Salivary glands	0.01	0.04

Notes:

1. *The w_{T} for gonads is applied to the mean of the doses to testes and ovaries.*
2. *The dose to the colon is taken to be the mass-weighted mean of ULI and LLI doses, as in the Publication 60 formulation. The specified remainder tissues (14 in total, 13 in each sex) are: Adrenals, Extrathoracic tissue (ET), Gall bladder, Heart, Kidneys, Lymphatic nodes, Muscle, Oral mucosa, Pancreas, Prostate(♂), Small intestine (SI), Spleen, Thymus, Uterus/cervix (♀).*

(70) The use of effective dose allows exposures in very different situations (e.g. internal and external exposure by different types of radiation and inhomogeneous exposures of the body) to be combined and results in a single dose value which considerably simplifies the specification of exposure limits. Effective dose, however, is not designed as a quantity considering individual properties of a specific person and should, therefore, not be applied for an assessment of radiations risks of a single person.

3.1.2 Operational dose quantities

(71) The protection quantities defined by mean organ or tissue doses in the human body are not measurable in practice and, therefore, cannot be used as quantities in radiation monitoring. For radiation measurements in situations of external exposure (area or individual monitoring) specific operational dose quantities have been defined by ICRU (ICRU 1985; 1988; 1993; 2001). In monitoring at low doses the values of these quantities are taken as sufficiently accurate assessments of effective dose or skin dose, respectively, if their values are below the recommended limits for occupational exposure.

(72) The basis for the definition of the operational quantities is the quantity dose equivalent, H, defined by

$$H = Q\,D \tag{3.6}$$

where D is the absorbed dose at the point of interest in tissue and Q the corresponding mean quality factor due to the charged particles at that point.

(73) For the different tasks of monitoring of external exposures the following scheme can be used for describing the application of the different operational dose quantities (ICRP, 2007)

Task	Operational dose quantities for	
	area monitoring	**individual monitoring**
Control of effective dose	ambient dose equivalent, $H^*(10)$	personal dose equivalent, $H_p(10)$
Control of doses to the skin, the hands and feet	directional dose equivalent, $H'(0.07, \Omega)$	personal dose equivalent, $H_p(0.07)$
Control of doses to the the lens of the eye	directional dose equivalent, $H'(3, \Omega)$	personal dose equivalent, $H_p(3)$

(74) The operational quantities for area monitoring at a location in a radiation field are defined by the dose equivalent at a point in a simple phantom, the ICRU sphere. It is a sphere of tissue-equivalent material (30 cm in diameter, ICRU (soft) tissue with density: 1 g cm^{-3}, and mass composition: 76.2 % oxygen, 11.1 % carbon, 10.1 % hydrogen and 2.6 % nitrogen). These quantities are defined to be point quantities fulfilling the condition of being additive with respect to the different components of the radiation field at the point of interest. For its definition the terms "*expanded*" and "*aligned*" radiation field are introduced (see Glossary) and the value of the quantity is given by the dose in a point at a fixed depth in the sphere. The sphere is hypothetical, a mathematical construct for the determination of the values of the quantities for area monitoring.

Ambient dose equivalent, $H^*(10)$

(75) For area monitoring the operational quantity for assessing effective dose is the ambient dose equivalent, $H^*(10)$, defined by (ICRU 2001):

> The *ambient dose equivalent*, $H^*(10)$, at a point in a radiation field, is the dose equivalent that would be produced by the corresponding expanded and aligned field in the ICRU sphere at a depth of 10 mm on the radius vector opposing the direction of the aligned field.

(76) In most practical situations on Earth ambient dose equivalent provides a conservative estimate of effective dose a person would receive at that position. This, however, may not be the case for persons in high energy radiation fields, e.g. in cosmic radiation fields (Pelliccioni, 1998).

Directional dose equivalent, $H'(d, \Omega)$

(77) For area monitoring the quantity for assessing the dose to the skin and the extremities (hands, arms, feet) and the dose to the lens of the eye, the operational quantity is the directional dose equivalent, $H'(d, \Omega)$ defined by:

> The *directional dose equivalent*, $H'(d, \Omega)$, at a point in a radiation field, is the dose equivalent that would be produced by the corresponding expanded field in the ICRU sphere at a depth, d, on a radius in a specified direction, Ω.

(78) For assessing the dose to the skin and the extremities $d = 0.07$ mm is used and $H'(d, \Omega)$ is then written $H'(0.07, \Omega)$. In case of monitoring the dose to the lens of the eye the quantity $H'(3, \Omega)$ with $d = 3$ mm was recommended by ICRU.

Personal dose equivalent, $H_p(d)$

(79) Individual monitoring of external exposure is usually performed with personal dosemeters worn on the body and the operational quantity defined for this application takes this situation into account. For individual monitoring the operational quantity is the personal dose equivalent, $H_p(d)$.

The *personal dose equivalent*, $H_p(d)$, is the dose equivalent in ICRU (soft) tissue (see Section 4.3) at an appropriate depth, *d*, below a specified point on the human body.

(80) The specified point is usually given by the position where the personal dosemeter is worn. For the assessment of effective dose a depth d = 10 mm and for assessing equivalent dose to the skin and to the hands and feet a depth d = 0.07 mm is recommended. In special cases of monitoring the dose to the lens of the eye a depth d = 3 mm has been proposed to be appropriate.

3.2 Description of radiation quality

(81) The biological effectiveness of ionising radiation with respect to the induction of cancer or other tissue reactions in the human body and of hereditary effects depends on the type and energy of the radiation, on the tissue type exposed, on the dose and dose rate applied to the tissue and on the detriment considered. The induced effects differ also in the latency time between the exposure and the occurrence of the effects.

(82) In radiological protection the effectiveness at low doses and dose rates are mainly of interest. For these doses and dose rates the stochastic effects - cancer induction and hereditary effects - are important and the standard approach in radiological protection is that the shape of the dose-response relationship at low doses and dose rates is based on the model that the probability of a stochastic effect is proportional to the applied dose (linear-non-threshold model (LNT)) (ICRP, 2005).

(83) At higher doses, however, when non-stochastic effects (deterministic effects, tissue reactions) may occur, LNT is not an acceptable approximation. Tissue reactions occur always above a dose threshold. The threshold dose value depends on the type of the tissue reaction and is mostly above an applied absorbed dose of 0.5 - 2 Gy.

(84) In principle, for risk estimates from exposure by different types of ionising radiation, the absolute values of biological effectiveness of radiation with respect to the induced effect need to be known. The mostly used procedure of taking care of the differences in the biological effectiveness, however, is to use risk factors for a reference radiation (usually photons) and to consider the differences of other types of radiation by applying a factor *relative biological effectiveness* (RBE) which has already been introduced by Failla and Henshaw in 1931 (Failla et al., 1931) and is discussed in detail in ICRP Publication 92 (ICRP, 2003). While RBE-values always depend on the biological endpoint considered and on dose and dose rate applied, for the definition of quantities in radiological protection a single set of radiation weighting factors and radiation quality factors has been chosen (ICRP, 2007) based on data at low doses and dose rates. This is further discussed in the next sections.

3.2.1 Relative biological effectiveness

(85) In radiobiology the differences in the effectiveness of the different ionising radiations have led to the definition of the *relative biological effectiveness* (RBE). RBE values are given as the ratio of the absorbed doses of two types of radiation producing the

same specified biological effect under identical irradiation conditions (dose value of a reference radiation divided by the corresponding dose value of the considered radiation at the same level of the specified biological effect). RBE values depend on the conditions of exposure including the biological effect investigated, the tissue or cell type exposed, the dose and dose rate, and the dose fractionation scheme. Therefore, for a given type of radiation, experimental investigations often provide a large range of RBE values (ICRP, 2003). As the basis for selecting radiation weighting factors (see 3.2.2), RBE values with respect to stochastic effects (cancer induction and hereditary effects) are of main interest. Usually RBE-values increases with decreasing dose and dose rate and are believed to reach maximum values (RBE_M) at low doses and low dose rates. RBE_M-values are most relevant for radiological protection applications. In ICRP Publication 92 (2003), different methods are discussed to determine RBE_M at low doses and dose rates. The discussion includes various types of high-LET radiation, e.g. protons, neutrons and α-particles. For heavy ions, however, very limited data were available at that time.

(86) Generally, low-LET radiation is taken as reference radiation, mostly high-energy x-rays or γ-rays from ^{60}Co or ^{137}Cs. There are, however, substantial differences in the biological effectiveness of photons of different energy (Schmidt et al., 2002). Nevertheless, there exists no international recommendation on defining a specific photon source as a general reference radiation. This has the consequence that a broad range of experimental data with photons has been used as a basis for the definition of radiation weighting and quality factors (ICRP, 2003).

(87) While on the one hand RBE_M-values are the basis for the definition of radiation weighting factors and the $Q(L)$-function, on the other hand, RBE-values are used for the assessment of radiation risks from human exposures by different types end energies of radiation. A risk factor for the radiation and tissue of interest is obtained by multiplying the risk factor for the reference radiation, e.g. photons, by the corresponding RBE-value. An uncertainty for risk assessment, however, comes in, because RBE-values are often determined by investigating biological effects in single cells or small animals at higher doses, while radiation risks are assessed for stochastic effects, e.g. cancer induction and hereditary effects, in humans.

(88) The biological effectiveness of ionising radiation is known to be correlated with its energy deposition properties along the tracks of charged particles, especially with the ionisation density along their tracks. For applications in radiological protection, the complex structure of the charged particle tracks in tissue is characterized by a single parameter only, the unrestricted linear energy transfer, L_∞, (often denoted linear energy transfer, LET or L). Unrestricted linear energy transfer, L_∞ means that the transfer energy includes the energies of all emitted δ-electrons independent of their range, while restricted LET, L_Δ, means that only δ-electrons with energies of less than Δ are considered. In general, LET is not simply related to the biological effectiveness because, for example, ions of different Z show different effectiveness at the same LET-value (Cucinotta et al., 2000a).

(89) The study of the LET-dependence of RBE is concentrated on the study of radiation effects in single cells by irradiating thin cell samples with charged particles of various types and energies. In animal experiments, however, with long ranges of charged particles in the tissue, the LET-dependence of an effect, e.g. cancer induction, is more difficult to study.

(90) While for neutrons and alpha particles a broad range of experimental data to many different biological endpoints exists including data from animals (NCRP, 1990; ICRP, 2003), the situation for high-energy charged particles is more problematic. Epidemiological data on cancer induction in humans from exposure to high-energy particles and heavy ions are not

available and experimental data on cancer induction in animals are scarce (ICRP, 2003). Most RBE data for high-energy protons and heavy ions have been obtained by experiments with cells at high doses (> 1Gy) and high dose rates which are of particular interest for heavy-ion radiotherapy applications (Taucher-Scholz et al., 1999, George et al., 2003, Durante, 2002) with only a few studies of tumors in mice (Fry et al., 1985, Alpen et al., 1993, Weil et al., 2009).

(91) Experimental data of RBE versus LET have been obtained for various biological endpoints. The general shape of the RBE-LET relationship is always similar. At low LET-values there is an increase in RBE with increasing LET up to about 100 to 150 keV/μm and for higher LET-values, RBE decreases with increasing LET. Figures 3.2 to 3.4 show some typical examples of RBE-LET relationships obtained for different biological endpoints.

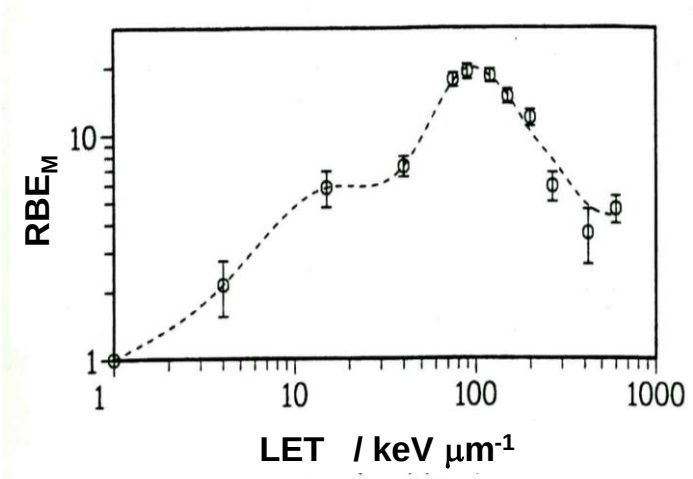

Fig. 3.2. RBE_M versus LET for oncogene transformations in C3H10T1/2 cells of embryos of mice (Brenner et al., 1992).

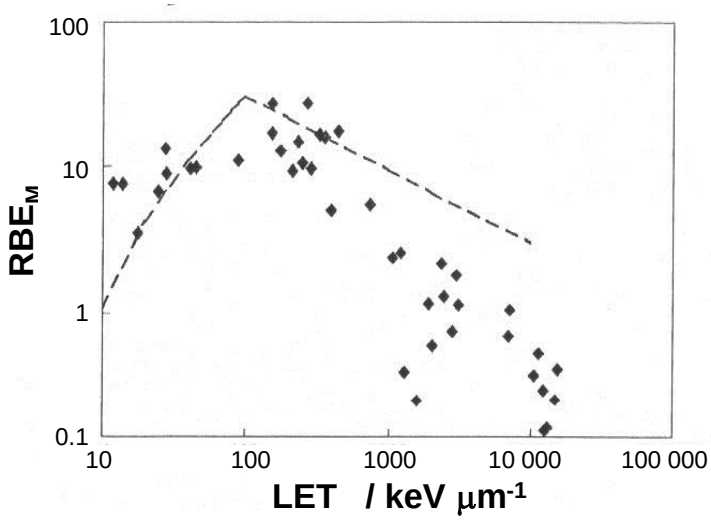

Fig. 3.3. RBE$_M$ versus LET for the induction of mutations at the hprt locus in Chinese hamster V79 cells. Data are from Kiefer et al. (1999, 2001). The dotted line shows the $Q(L)$ function as defined in ICRP Publication 60 (ICRP, 1991).

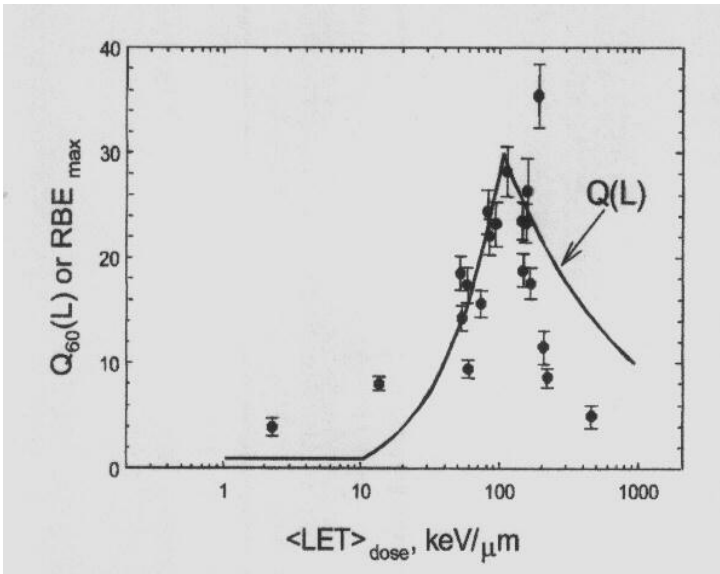

Fig. 3.4. RBE$_M$ versus LET for total chromosomal exchanges measured within the first cell cycle using the premature chromosome condensation (PCC) method (George et al., 2007, Cucinotta et al., 2008). The line shows the $Q(L)$ function as defined in ICRP Publication 60 (ICRP, 1991).

(92) In general, the biological effectiveness is not simply related to LET, especially for heavy ions with high LET-values. This is because the width of a particle track depends on the velocity of the particles. Particles of different Z show different effectiveness at the same LET-value (Cucinotta et al., 2011). The position of the peak RBE versus LET depends on particle charge number and does not occur at a fixed LET (see Figs. 3.5 and 3.6). The peak position changes from less than 100 keV/μm to more than 150 keV/μm as Z increases from protons with Z=1 to Fe with Z=26. RBE depends on charge Z and energy E of the particle,

and not on LET alone. At a fixed value of LET less than the peak position, particles with lower *Z* are more biologically effective. In addition, the slope of rise of RBE with LET is variable with the endpoint/system studied, and the slope of decrease of RBE at high LET-values is predicted to be proportional to LET^{-1} rather than $LET^{-1/2}$.

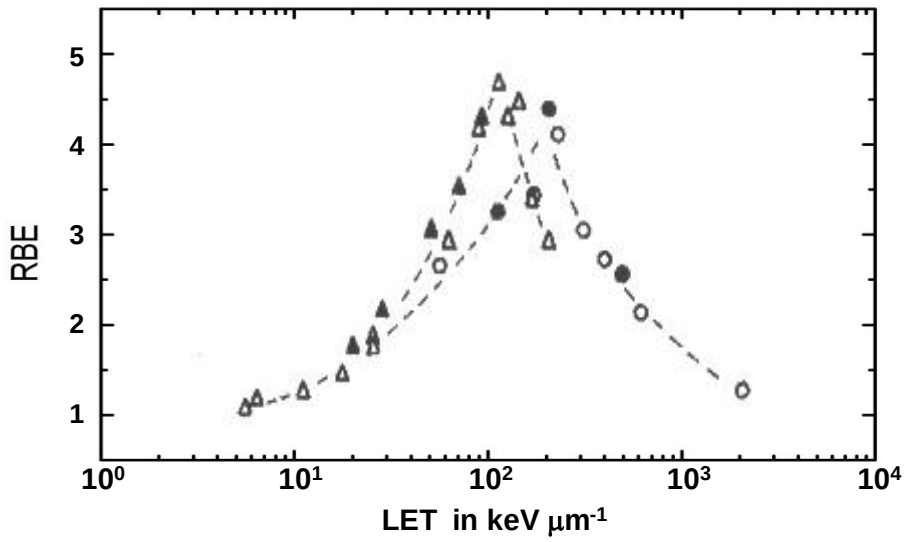

Fig 3.5. Relative biological effectiveness (RBE) for inactivation of V79 hamster cells (closed symbols) and T1 mammalian cells (open symbols) exposed to beams of accelerated heavy ions (▲, Δ deuterons and He-ions; •,○ heavier ions) versus LET (Thacker et al., 1979).

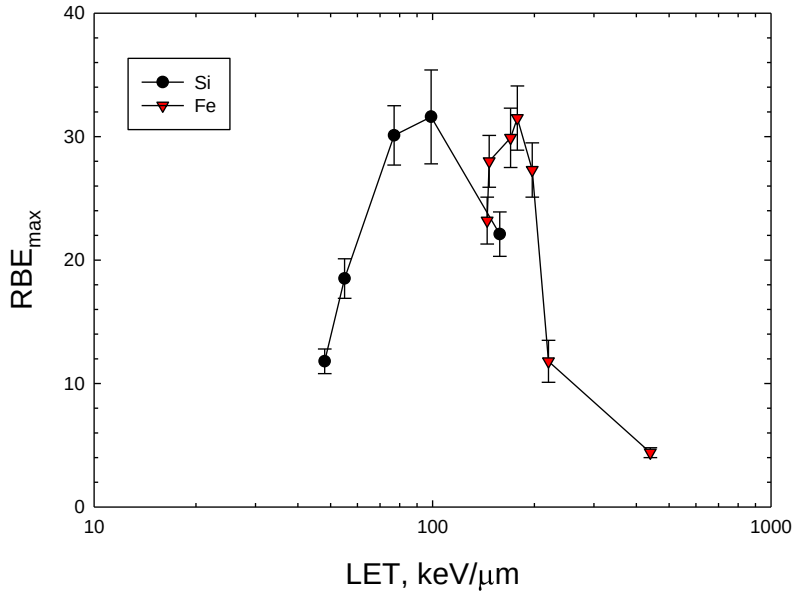

Fig. 3.6. RBE_{max} versus LET for chromosomal aberrations (total exchange) of human lymphocytes exposed to Si and Fe nuclei, relative to low-dose and dose-rate γ-rays (George et al., 2007).

.

(93) For the same LET-value the distribution of δ-rays strongly varies with the ion considered (see Fig 3.7). The approach of describing radiation quality in terms of LET assumes that the various ion tracks shown in Fig. 3.7 produce the same cancer risk, although

the initial physical-chemical stages are quite distinct. Hence, there is considerable support to relate RBE to a function better correlated to the track structure of the charged particles passing tissue (Cucinotta et al., 2011), especially to the spatial distribution of δ-rays along the tracks. Arguments from Katz (Katz, 1970; Katz et al., 1972) and observations by Goodhead et al. (Goodhead, 1980) supports the hypothesis that especially for heavy ions biological effects are strongly influenced by particle track structure including δ-ray effects rather than by the stopping power (LET) only.

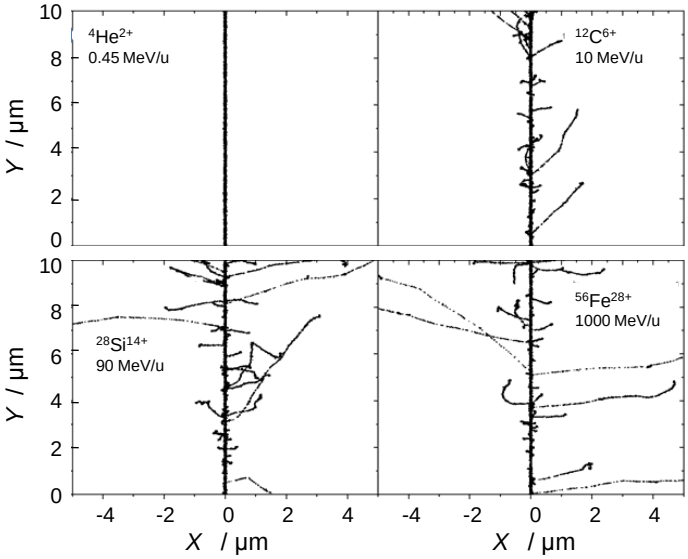

Fig. 3.7. **S**imulated tracks segments for the following ions in water: ^{4}He (0.45 MeV/u), ^{12}C (10 MeV/u), ^{28}Si (90 MeV/u), and ^{56}Fe (1 GeV/u). Shown are projections over the XY plane. Ions are generated at the origin along the Y axis in liquid water at 25°C under identical LET conditions (~150 keV µm^{-1}). Each dot represents a radiolytic species (Plante et al., 2008).

(94) A parameter Z^{*2}/β^2, where Z* is the effective charge number of the nuclei and β the velocity of the nuclei relative to the light velocity, has been proposed by Katz and others (Katz, 1970; Katz et al., 1972) to be a better descriptor of energy deposition in small volumes than LET, especially for heavy ions. This is based on the idea that a reaction cross section with respect to biological reactions in tissue should include the effect of δ-rays. A value of Z* can be obtained by using the following equation given by Barkas (Barkas, 1963):

$$Z^* = Z\,(1-\exp(-125\,\beta\,Z^{2/3})) \qquad (3.7)$$

where Z is the charge number of the nuclei considered. As an example Figure 3.8 shows calculations comparing the frequency of energy deposition above 300 eV in a volume of about the size of a nucleosome. Obviously the parameter Z^{*2}/β^2 provides an improved descriptor of energy deposition in small volumes compared to LET.

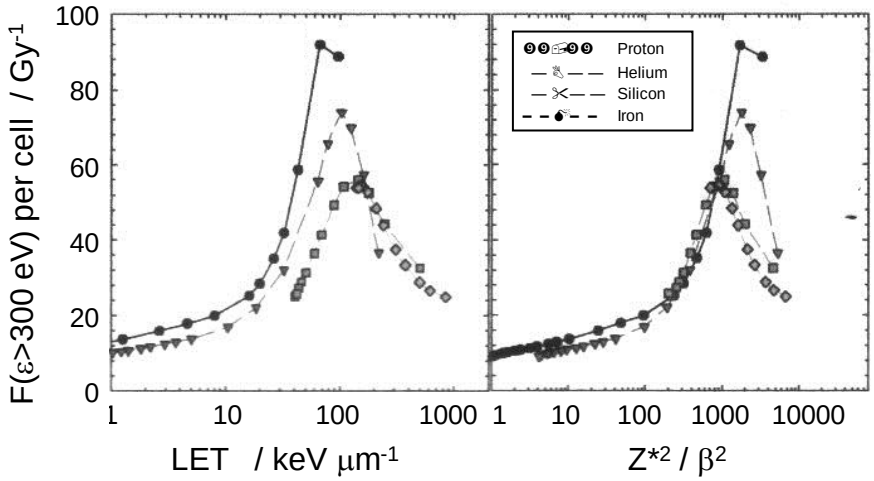

Fig. 3.8. Number of nucleosomes per cell receiving 300 eV or more as a function of LET (left) or Z^{*2}/β^2 (right). Calculated data are shown for H, He, Si, and Fe nuclei (Cucinotta, 2011).

(95) As a consequence, a RBE function has been derived and described to be dependent on two parameters of the particle, either given by E and Z, or alternatively by Z^{*2}/β^2 (Cucinotta et al., 2011). In Fig. 3.9 the same RBE data as shown in Fig. 3.5 are plotted against Z^{*2}/β^2 and this plot may be a better basis for defining a quality factor function than using the LET parameter.

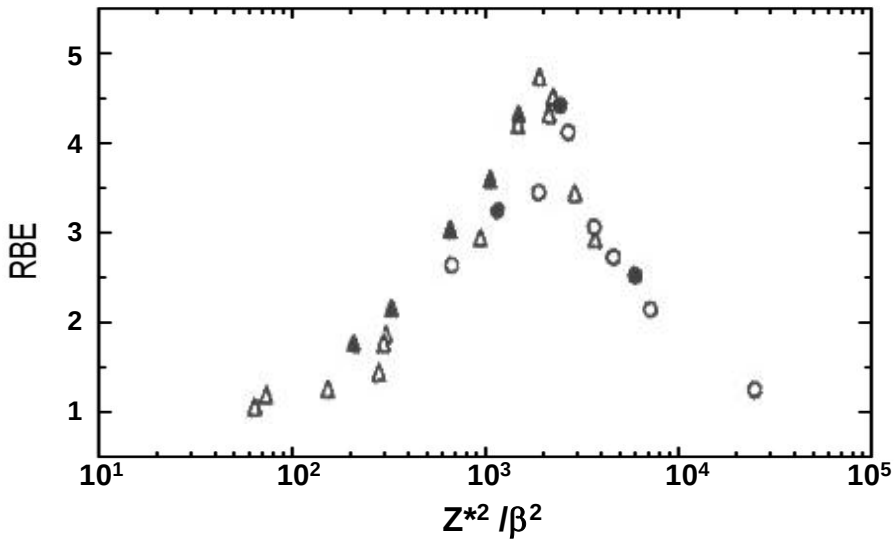

Fig 3.9. Relative biological effectiveness (RBE) for inactivation of V79 hamster cells (closed symbols) and T1 mammalian cells (open symbols) exposed to beams of accelerated heavy ions (▲, Δ deuterons and He-ions; •,○ heavier ions) versus $(Z^*/\beta)^2$ (Thacker et al., 1979).

3.2.2 Radiation weighting factor

(96) Radiation weighting factors, w_R, have been used in the definition of the protection quantity equivalent dose in an organ or tissue in ICRP Publication 60 (ICRP 1991) and numerically modified in Publication 103 (ICRP, 2007). Values of w_R are given for various

types of radiation either incident on the human body or emitted by radionuclides in the body. Data for w_R are given in Table 3.2. The same values of the radiation weighting factors are applied to all tissues and organs of the body independent of the degradation of the primary radiation and the production of secondary radiations of different radiation quality. It may be seen as a mean factor representing radiation quality averaged over the different tissues and organs of the body. The application of w_R-values is restricted to low doses and dose rates and should not be applied in cases of higher doses where tissue reactions may occur.

(97) Except for neutrons, all types of particles are given a single weighting factor value. This simplification is seen to provide sufficient precision for general applications in radiological protection, even if it is well known that radiation quality depends also on the energy of the particle involved. This is especially the case for heavy ions of high energies which, however, in most radiation fields at the Earth are less important of radiological protection.

Table 3.2. Radiation weighting factors[1], w_R (ICRP, 2007)

Radiation type	**Radiation weighting factor, w_R**
Photons	1
Electrons and muons	1
Protons and charged pions	2
Alpha particles, fission fragments, heavy ions	20
Neutrons	A continuous curve as a function of neutron energy (see equation 3.9 and Fig. 3.2)

(1) All values relate to the radiation incident on the body or, for internal sources, emitted from the source.

(98) For neutrons the following function is recommended for the calculation of radiation weighting factors (ICRP, 2007):

$$w_R = \begin{cases} 2.5 + 18.2\, e^{-[\ln(E_n)]^2/6} & , \quad E_n < 1\ \text{MeV} \\ 5.0 + 17.0\, e^{-[\ln(2E_n)]^2/6} & , \quad 1\ \text{MeV} \le E_n \le 50\ \text{MeV} \\ 2.5 + 3.25 e^{-[\ln(0.04E_n)]^2/6} & , \quad E_n > 50\ \text{MeV} \end{cases} \tag{3.8}$$

where the neutron energy, E_n, is given in MeV (see also Fig. 3.10).

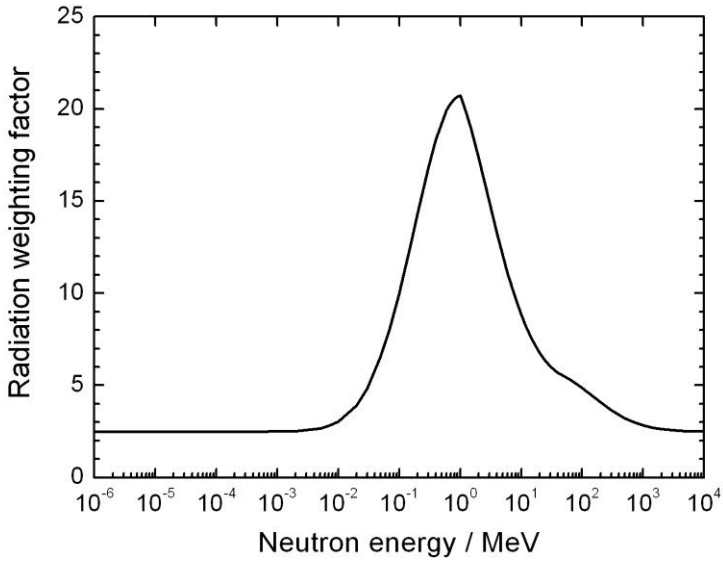

Fig. 3.10. Radiation weighting factor, w_R, for neutrons versus neutron energy (ICRP, 2007).

(99) For applications in space, where high-energy heavy ions significantly contribute to the total dose in the human body, a more realistic approach for radiation weighting should be chosen (ICRP, 2007). This could, for example, be based on the calculation of mean quality factors in the human body (see Section 3.2.3). Some other difficulties with the w_R-concept for application in high energy radiation fields have also been discussed by Pelliccioni (1998).

3.2.3 Quality factor

(100) Radiation quality is seen to be strongly correlated with its energy deposition properties along the tracks of charged particles, especially with the ionisation density along their tracks. For applications in radiological protection, the different biological effectiveness of radiation is considered by introducing the quality factor function, $Q(L)$. $Q(L)$ characterizes the biological effectiveness of a charged particle with a linear energy transfer L at a point of interest in tissue relative to the effectiveness of a reference radiation at this point. Q is defined by a function of L in water (not in tissue) as given in various publications of ICRP and ICRU (ICRP, 1963, 1977, 1991; ICRU, 1970, 1986). RBE-values provide the basis for the selection of a quality factor function used in the definition of the specific dose quantities in radiological protection (see Section 3.2). For this application, all photons and electrons (all low-LET radiation with L<10 keV/μm) are weighted by Q = 1. This is seen to be an approximation sufficient for usual radiation protection applications and greatly simplifies measurements and calculations.

(101) The actual quality factor function $Q(L)$ with L for charged particles in water was given in Publication 60 (ICRP, 1991):

$$Q(L) = \begin{cases} 1 & L < 10 \text{ keV/μm} \\ 0.32\,L - 2.2 & 10 \text{ keV/μm} \le L \le 100 \text{ keV/μm} \\ 300/\sqrt{L} & L > 100 \text{ keV/μm} \end{cases} \qquad (3.9)$$

(102) The $Q(L)$ function is the outcome of radiobiological investigations on cellular and molecular systems as well as on the results of animal experiments (see e. g. (ICRP, 2003)) and has not been changed since 1990. The function includes, however, also some judgments for simplifying radiological protection practice. $Q(L) = 1$ for $L < 10$ keV/µm, even it is well known that the RBE of photons increases with decreasing energy (ICRP, 2003).

(103) The quality factor Q at a point in tissue is then given by:

$$Q = \frac{1}{D}\int_{L=0}^{L=\infty} Q(L) D_L \mathrm{d}L \tag{3.10}$$

where D is the absorbed dose in tissue and $D_L = \mathrm{d}D/\mathrm{d}L$ the distribution of D in L (for charged particles in water) at the point of interest in tissue.

(104) For exposure of the human body by neutrons the radiation field is modified in the body by moderation of the incident neutrons and secondary radiation from neutron reactions. Therefore, for a given neutron exposure situation, the value of the quality factor depends on the position in the body and the mean radiation quality factor in organs and tissues of the body may differ. For each organ or tissue T, a tissue-mean radiation quality factor, Q_T , can be calculated using:

$$Q_\mathrm{T} = \frac{1}{m_\mathrm{T} D_\mathrm{T}} \int_{m_\mathrm{T}}\int_{\mathrm{L}} Q(L) D_L \mathrm{d}L \mathrm{d}m \tag{3.11}$$

where m_T is the mass of the organ or tissue T. A body-mean quality factor, Q_E, averaged over the human body by considering the mean organ absorbed doses, D_T, and the tissue weighting factors, w_T, is given by

$$Q_\mathrm{E} = \sum_\mathrm{T} w_\mathrm{T} Q_\mathrm{T} D_\mathrm{T} \,/\, \sum_\mathrm{T} \mathrm{w}_\mathrm{T} \mathrm{D}_\mathrm{T} \,. \tag{3.12}$$

(105) Figure 3.11 shows both the radiation weighting factor and the body-mean quality factor, $Q_{\mathrm{E,AP}}$, calculated for the adult male reference phantom, for monoenergetic neutrons (AP incidence) versus neutron energy. Values of Q_E are similar for other directions of neutron incidence (e.g. ISO). Obviously stronger differences between w_R and Q_E are only for neutron energies between 0.1 MeV and 10 MeV. For neutron energies above 10 MeV, the difference is negligible. Differences between Q_T for a single organ and w_R may be, however, much larger.

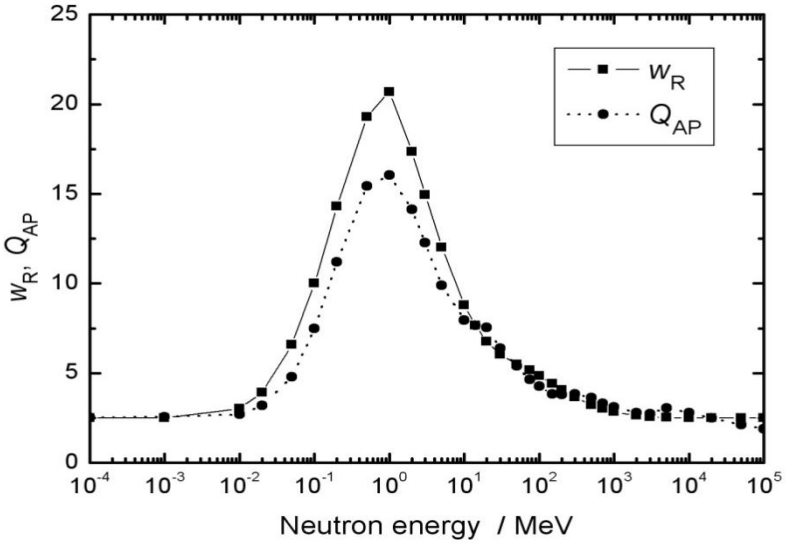

Fig. 3.11. Radiation weighting factor, w_R, and body-averaged mean quality factor, $Q_{E,AP}$, calculated for neutrons (AP incidence) versus neutron energy (Sato et al., 2009).

(106) Similar calculations have been performed for incident protons by Sato et al. (Sato, 2009) and these data are shown in Fig. 3.12.

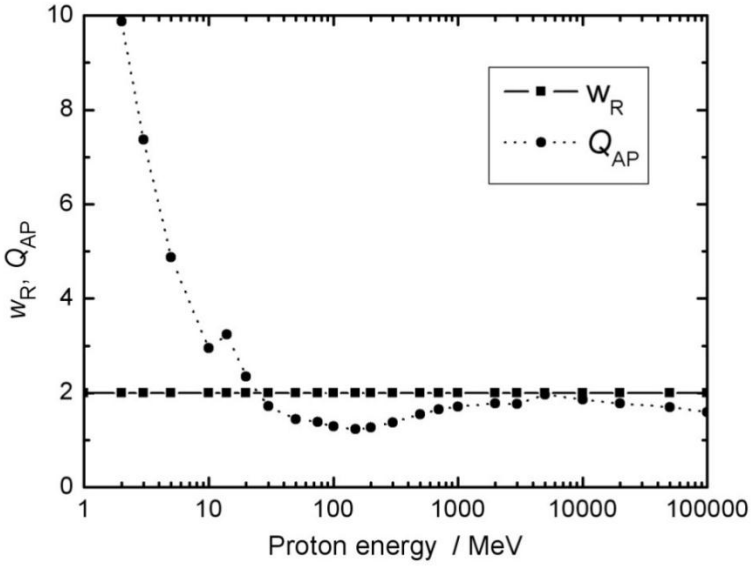

Fig. 3.12. Radiation weighting factor, w_R, and body-averaged mean quality factor, $Q_{E,AP}$, calculated for protons (AP incidence) versus proton energy (Sato et al., 2009).

(107) While for energies of incident protons below about 10 MeV there are large differences between the radiation weighting factor and the mean quality factor, they are much lower at higher proton energies and are less than 20% at proton energies above 1 GeV. Protons below about 10 MeV, however, are low-penetrating radiation which are mostly stopped already in the skin of exposed persons and hence contribute little to the effective dose in cosmic radiation fields with many protons of high energies. When exposure of the skin needs special attention, protons below about 10 MeV, however, need also to be

considered. In such cases, the absorbed dose to the skin, and not the effective dose is of prime interest.

(108) At proton energies above 20 MeV, the mean quality factor is always between 1 and 2. At these energies, protons can be seen to be low-LET particles. The increase of Q at energies above 150 MeV is due to proton reactions in tissue where secondary charged particles are produced.

(109) While for high-energy neutrons and protons the difference between w_R and the mean quality factor is relatively small, the situation is quite different for heavy ions.

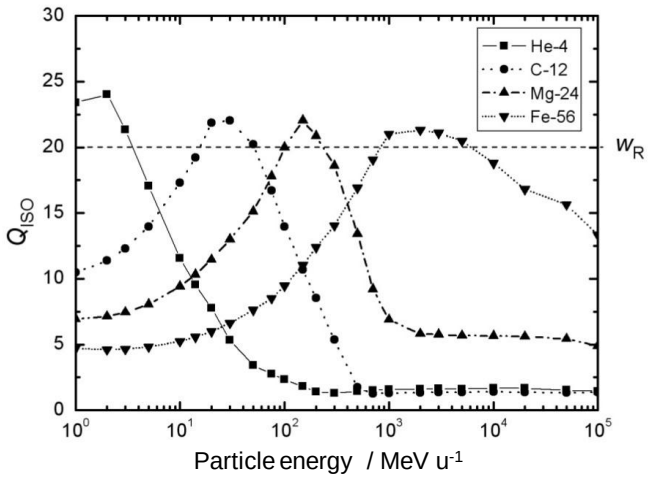

Fig. 3.13. Radiation weighting factor, w_R, and body-averaged quality factors, $Q_{E,ISO}$, for ^{4}He, ^{12}C, ^{24}Mg and ^{56}Fe (ISO incidence) versus particle energy (Sato et al., 2010).

(110) The body-mean quality factor is strongly varying with the type and energy of the ion (Sato et al., 2010), while the w_R-value has been fixed to 20 for all heavy ions and all energies. For example, Fig. 3.13 shows body-mean values of Q_E for ^{4}He, ^{12}C, ^{24}Mg and ^{56}Fe ions with isotropic radiation incidence to the body. The value varies between about 2 and 24 depending on the ion type and the energy. There are also stronger variations in Q_T depending on the position of the organ or tissue in the human body. This situation underlines the decision, not to select a single radiation weighting factor value for all heavy ions and all particle energies. The recommended concept of quantities for use in radiological protection of astronauts in space takes account of this fact (see Section 3.3.1).

(111) Similar to the dependence of RBE for high-energy ions, a different way of defining a quality factor function may be derived from the track structure of the charged particles rather than being only related to LET. Cucinotta et al. (Cucinotta, 2011a) have proposed a functional dependence of a quality factor on two parameters of the particle, Z and E or alternatively can be expressed in terms of Z^{*2} / β^2 and LET. Because the RBE values for an induction of leukaemia and of solid cancers are quite different, they proposed two different functions $Q(Z,E)$ for leukaemia and solid cancers (see Fig. 3.14).

(112) The general ideas discussed on track-structure models have been used to define a cross section function related to risk which may be written as

$$\Sigma(Z, E) = \Sigma_0 \, P(Z, E) + (\alpha_\gamma L / 6.24)\,(1 - P(Z, E)) \qquad (3.13)$$

with

$$P(Z, E) = (1 - \exp(-Z^{*2} / \kappa\beta^2))^m \qquad (3.14)$$

where Σ_0, m, and κ are parameters which should be based on fits to data from radiobiology experiments, and the low-LET slope, α_γ, estimated from epidemiological data for γ-radiations. The parameter β is the particle velocity relative to the velocity of light. Z* is the effective charge number which includes a velocity dependent correction to Z at low particle energies (Barkas, 1963) as defined in eq. (3.7).

Using the equations above, a quality factor function, $Q(Z,E)$ can then be defined by

$$Q(Z,E) = (1 - P(Z, E) + (6.25\ (\Sigma_0/(\alpha_\gamma\ L))\ P(Z, E) \qquad (3.15)$$

(113) Note that L is not an independent variable in addition to Z and E, but for a given Z and E, the L-value is fixed. Alternatively, one may write $Q(Z,L)$ or also $Q(E,Z^{*2}/\beta^2)$. At high particle energies, this function defines a $1/L$-dependence of Q different from the $1/L^{1/2}$-dependence given by the $Q(L)$ function of eq. (3.10). The interpretation of the parameters is quite general, and is not tied to a particular track structure models per se, but rather is an efficient parameterization of radiobiology data for particles. The parameters can be described as follows: Σ_0 is the maximum value of the cross section, which is related to RBE_{max} for the most biologically effective particle types, m is the slope of the cross section for increasing ionisation density, with values m>1 necessary to have RBE>1, and κ determines the saturation value of the cross section with increasing Z^{*2}/β^2, where the RBE begins to decline.

(114) High-energy protons of about 150 MeV have an LET similar to γ-radiation and their kinetic energy is below a value where nuclear reactions become important. Many experiments have shown a biological effectiveness for those protons to be very similar to γ-radiation. For proton of this energy, it is $P(Z,E) << 1$, and $Q \sim 1$.

(115) For solid cancer risks, radiobiology data are sparse. However, the largest RBE for HZE nuclei is in the range from 20 to 50 for solid tumors in rodents, and for chromosomal aberrations and mutations in human cells. A lower value is found for leukaemia. This assumes a linear dose response at low doses for charged particles, ignoring non-targeted-effects or other possible mechanisms which may lead to deviations from linearity. Thus, for example, if a peak RBE value of approximately 40 is assumed for Si at 100 keV/μm where $P(Z,E) \sim 1$, Σ_0/α_γ can be estimated as 40x100/6.24. A comparison of the quality factor based on LET and on both, L and Z is shown below (Fig. 3.14). The influence in the uncertainties in the values of these parameters, which describe the uncertainties in information on RBE_{max} and the peak position of the RBE_{max} with LET for different particles can be investigated using Monte-Carlo methods (Cucinotta et al., 2011).

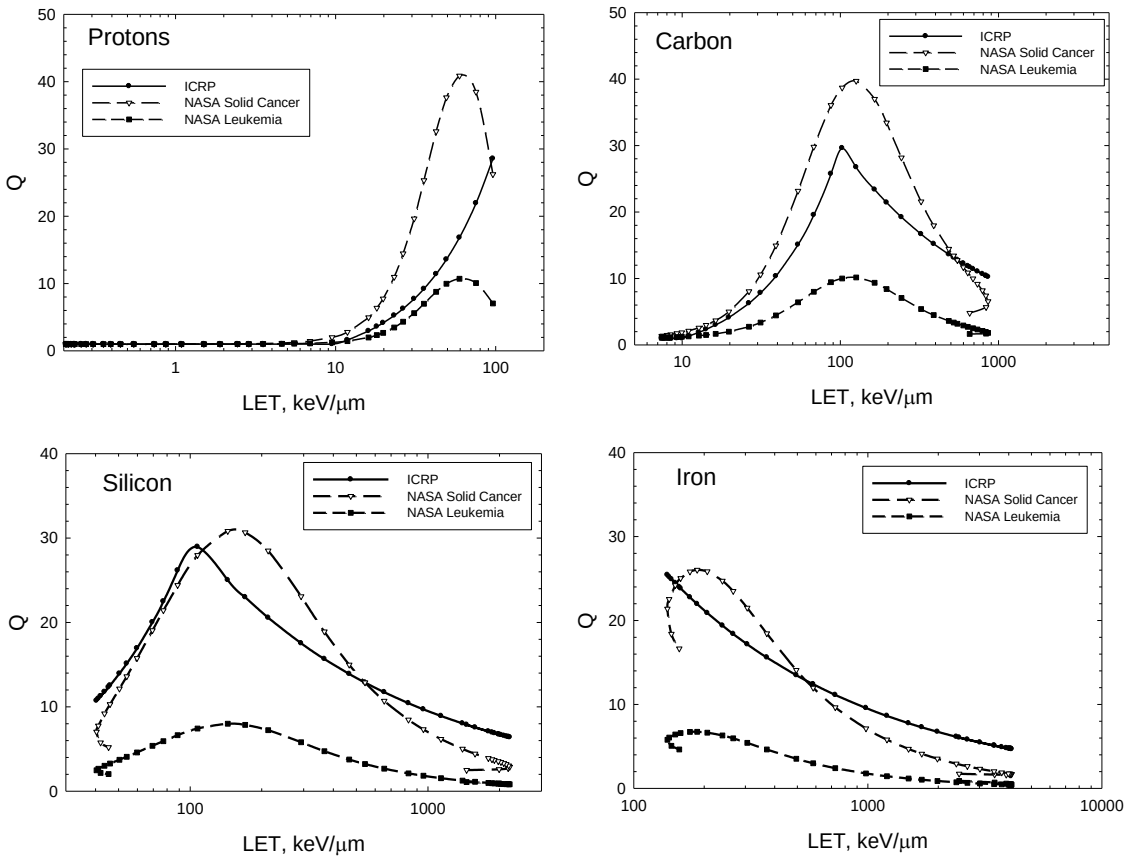

Fig. 3.14. LET dependence of the quality factor, *Q*, for H, C, Si, and Fe nuclei as defined by the Commission (ICRP, 1991) and as proposed by NASA (Cucinotta, 2011) differently defined for considering relative risks of either solid cancer or leukaemia .

3.3 Approach for space applications

(116) The situation in a space vehicle is characterized by the primary radiation field consisting of various high-energy charged particles from protons up to heavy ions such as Fe-56 or even higher Z values, and by radiation components of photons, electrons, neutrons and other reaction products from the interaction of primary particles with the materials of the spacecraft (see Chapter 2). This results in many different types of radiation together with broad energy distributions up to particle energies of many GeV/u.

(117) Individual doses are generally higher than in usual exposure situations on Earth. As a consequence, deterministic effects in specific organs, e.g. lens of the eye or skin, cannot be ignored. This needs specific consideration and will be further discussed in Sect. 3.3.3.

(118) The consequence of this specific situation is that some concepts of the quantities used in radiological protection on Earth have to be reconsidered for use in space. For example, the operational quantity for area monitoring of penetrating radiation which is based on the dose equivalent at 10 mm depth of the ICRU sphere has been mainly designed on the basis of photon and neutron data for control of effective dose and is limited in its application to radiation with energies where secondary charged particle equilibrium is achieved at about 10 mm depth in tissue. This is not the case for very high energy particles. For this situation computer modelling and simulation of exposure situations become very important in addition

to of measurements.

3.3.1 Protection quantities

(119) Radiation risk estimates are generally based on absorbed doses in the tissues and organs of the human body and the concept of the mean absorbed dose, D_T, in various organs and tissues of the body (see Section 3.1.1) has been assumed to be applicable also for astronauts in space. Limitation to this concept, however, may arise by the fact that fluence rates of heavy ions are very low. If only few particles pass an organ with a high energy transfer along each single particle track, averaging of the dose over an organ is a simplification which increases the uncertainty when risk estimates are considered. Another problem arises due to the large fraction of charged particles in the radiation field. Depending on their energy, they may be stopped in the human body and hence the depth dose distribution may not sufficiently homogenous over larger tissues or organs in the body to consider only an averaged value. Nevertheless, the mean absorbed dose in organs or tissues of the body is a very useful concept for radiological protection practice and for omni-directional (isotropic) exposure of an astronaut which can often be assumed in space, this problem is less important.

(120) D_T is a quantity which cannot be measured but is usually determined by applying calculated conversion coefficients which relate the mean dose in an organ or tissue to an external radiation field quantity (fluence for particles or air kerma for photons). They are, however, not calculated for any individual, but for adult male and female reference persons (ICRP, 2009) and are, therefore, restricted in the assessment of individual doses. The charged particles in the energy range of some GeV/u which are present in space, have very long ranges in tissue which results in a relatively homogeneous exposure of the human body and the variation of the mean organ doses is not very large, especially in case of isotropic exposure (see Section 6.3).

(121) Obviously, the general use of w_R = 20 for all heavy ions does not reflect the variation of RBE with type and energy of heavy ions and the Q-approach is better correlated with the assumption of a general dependence of RBE on LET and possibly on (Z^{*2}/β^2) (see Section 3.1.3). It is, therefore, endorsed to follow the approach already applied by space agencies and to use the term *dose equivalent in an organ or tissue* T, $H_{T,Q}$, defined by

$$H_{T,Q} = Q_T\, D_T \tag{3.16}$$

with the mean quality factor Q_T in an organ or tissue T for the given radiation field. When using the $Q(L)$ function, Q_T is calculated by

$$Q_T = \frac{1}{m_T D_T} \int_{m_T} \int_{L=0}^{L=\infty} Q(L) D_L \, \mathrm{d}L \mathrm{d}m \tag{3.17}$$

with the mass, m_T, of the organ or tissue considered.

(122) If a quality factor is defined by a function $Q(Z,E)$, a Q_T-value can be calculated by

$$Q_T = \frac{1}{m_T D_T} \int_{m_T} \left(\sum_Z \int_E Q(Z,E) D_E(Z,E) \mathrm{d}E\right) \mathrm{d}m \quad . \tag{3.18a}$$

or alternatively

$$Q_{\mathrm{T}} = \frac{1}{m_{\mathrm{T}} D_{\mathrm{T}}} \int_{m_{\mathrm{T}}} \left(\sum_{Z} \int_{L} Q(Z,L) D_L(Z,L) \mathrm{d}L \mathrm{d}m \right) \quad . \qquad (3.18b)$$

(123) Similar to equivalent dose in an organ or tissue, H_{T}, the value of dose equivalent in an organ or tissue is defined for organs and tissues in males and females by:

$$H_{\mathrm{T,Q}}^{\mathrm{M}} = Q_{\mathrm{T}}^{\mathrm{M}} D_{\mathrm{T}}^{\mathrm{M}} \quad \text{and} \quad H_{\mathrm{T,Q}}^{\mathrm{F}} = Q_{\mathrm{T}}^{\mathrm{F}} D_{\mathrm{T}}^{\mathrm{F}} \quad . \qquad (3.19)$$

(124) In most cases the difference of Q_{T} for males and females is small and a tissue-mean quality factor, Q_{T}, may be used for both sexes.

(125) Based on the definition of effective dose, E, the effective dose equivalent, H_{E}, can then be calculated by applying the tissue weighting factors, w_{T}, as given in ICRP Publication 103 (ICRP, 2007)

$$H_{\mathrm{E}} = \sum_{\mathrm{T}} w_{\mathrm{T}} H_{\mathrm{T,Q}} \qquad (3.20)$$

where for $H_{\mathrm{T,Q}}$ the mean value from doses for the male and female phantom is chosen. Note that this quantity has already been defined by the Commission in Publication 26 (ICRP, 1977) but with different tissue weighting factors and replaced by effective dose in Publication 60 (ICRP, 1991).

(126) An application of effective dose equivalent, however, is not recommended for the assessment of doses of individual or small groups of astronauts when these should become a basis for risk estimates. The recommended w_{T} values are single values for both sexes and also based on data for persons of all ages including children. They are not appropriate for a realistic risk assessment for male and female astronauts and hence risk estimates should be based on either absorbed dose or dose equivalent data for the organs and tissues of males or females respectively, and corresponding risk factors for these tissues for male and female adults (see e.g. Table A.4.19 in Annex B of ICRP Publication 103 (ICRP, 2007)). If necessary, also the age of the person considered may be taking into account. Even the quality factor may differ depending if leukaemia or solid cancer induction or mortality is considered (see Fig. 3.14).

(127) If, nevertheless, a value of effective dose equivalent is needed for recording, H_{E} should be calculated by:

$$H_E^{\mathrm{M}} = \sum_{\mathrm{T}} w_{\mathrm{T}} H_{\mathrm{T,Q}}^{\mathrm{M}} \quad \text{or} \quad H_E^{\mathrm{F}} = \sum_{\mathrm{T}} w_{\mathrm{T}} H_{\mathrm{T,Q}}^{\mathrm{F}} \qquad (3.21)$$

depending on the sex of the astronaut.

3.3.2 Operational quantities

(128) Radiation monitoring in a spacecraft and individual monitoring for each astronaut is a necessary measure for radiological protection in space and the assessment of mission doses of astronauts.

(129) On Earth, area monitoring in terms of the quantity ambient dose equivalent, $H^*(10)$, provides in fields of penetrating radiation the information which exposure in terms of effective dose a person would receive when staying for a given time at the position of the area monitor. In most external fields of strongly-penetrating radiation on Earth, only low-LET radiation, mostly x- and γ-radiation, partially also electrons, is present and in few cases only neutrons are also important for radiological protection. As a consequence, most area monitors used in radiological protection measure either photon or neutron doses and the total

ambient dose equivalent is then achieved by adding both dose components. Concentrating on photons, electrons and neutrons only has strongly influenced the idea of defining a special measurable dose quantity in an appropriate simple phantom (the ICRU sphere) for area monitoring and the assessment of effective dose.

(130) The consequence of the specific situation in space is that some concepts of the quantities used in radiological protection on Earth have to be revisited. For example, the operational quantity for area monitoring of penetrating radiation which is based on the dose equivalent at 10 mm depth of the ICRU sphere in aligned fields has been mainly designed on the basis of photon and neutron data for control of effective dose and is limited in its application to radiation with energies where secondary charged particle equilibrium can be achieved at about 10 mm depth in tissue. This is not the case for very high energy particles.

(131) In radiation fields in space with its large spectrum of different types of particles of very high energies the definition of $H^*(10)$ is inappropriate (ICRP, 2012) and it will be difficult to define a dose quantity independent from the human body with the same properties as ambient dose equivalent for photon and neutron radiation of conventional energy. In addition, monitoring and assessment of doses in the human body during missions of astronauts may not be restricted to effective dose equivalent and dose equivalent to the skin, the lens of the eye and the extremities, but should include other organs and tissues of the body, too. Hence no specific dose quantity for area monitoring in space has been defined up to now. The monitors used serve mainly as instruments for recording the environmental radiation outside or inside a spacecraft and for warning in cases of very intensive SPE´s. They measure particle fluence, LET-distributions or absorbed doses in detector materials (see Chapter 4). These data are used as input or validation data for calculations of doses in the human body.

(132) In individual monitoring, the situation is similar to area monitoring and a dosemeter calibrated in terms of $H_p(10)$ in photon or neutron radiation fields on Earth and worn on the body of an astronaut in space will not automatically provide an estimate of effective dose equivalent in complex space radiation fields.

(133) A specific operational dose quantity for individual monitoring in space has not been defined by ICRU or ICRP. Different quantities and procedures may be applied for an assessment of organ doses or effective dose equivalent (see Chapter 4). A combination of measurements of absorbed dose and LET-distributions at the surface of the body may become an appropriate way for individual dose assessment (see Sect. 4.3.3). Data from area monitoring within the spacecraft combined with calculated dose conversion coefficients can also be used to calculate organ dose equivalents or effective dose equivalents for persons present in that radiation field (see Chapter 6). This, however, needs the knowledge of the fluence and energy distribution of all components of the radiation field which in addition may vary with time. Furthermore application of methods of biological dosimetry may provide a comparative way of assessing mission doses of astronauts (see Sect. 4.3.4 and 6.4.2).

(134) Specific attention is needed for the measurement of doses from low-penetrating radiation, e.g. electrons or solar low-energy protons, which may contribute significantly to doses to the skin and the lens of the eye especially in situations when astronauts are working outside the spacecraft or during large solar flare events.

3.3.3 Quantities for high doses

(135) At high doses near to thresholds where deterministic effects (tissue reactions) may occur, organ dose equivalent and effective dose equivalent should generally not be used for

an assessment of radiation risks. While $H_{T,Q}$ and H_E may give an indication, if such dose range is reached, risk estimates should be based on mean absorbed doses in organs or tissues, maximum dose values in organs or tissues or on organ dose equivalent depending on the actual situation and the availability of risk factors for the different types of radiation and doses involved. Generally tissue reactions occur above a threshold dose in the range of 0.5 - 2 Gy.

(136) The mean absorbed dose in an organ or tissue, D_T, and the RBE weighted mean absorbed dose, RBE·D_T, when high-LET radiation is involved, is the appropriate quantity for assessing risks of deterministic effects at higher doses. The RBE-value to be chosen may depend on the organ or tissue considered and the specific dose and dose rate as well on the type and severity of the tissue reaction considered. In some cases of deterministic effects, however, not only the mean dose in an organ or tissue but also a local dose in that tissue may become important (e.g. local skin dose).

(137) The dose limits for tissue reaction are given in terms of the mean absorbed dose in an organ or tissue, D_T, and this value weighted by an appropriate RBE should be applied. The RBE values may be taken from ICRP Publication 58 (1989), where values of 6 (range 4 to 8) for neutrons of energy 1 MeV to 5 MeV, of 3.5 (2 to 5) for neutrons of energy 5 MeV to 50 MeV, of 2.5 (1 to 4) for heavy ions, and of 1.5 for protons are recommended.

(138) Measurements of particle fluence, LET-distributions or absorbed doses can be performed in any radiation field, even in strong radiation fields producing high doses, e. g. during solar particle events, where non-stochastic tissue reactions cannot be completely excluded. Measurements of $H_p(d)$ which is defined by using the fixed $Q(L)$ relationship may also be performed in such intense radiation fields for the purpose of dose recording. For risk assessment, however, it must be considered that the $Q(L)$ function has been defined based on RBE_{max} data at low doses and, therefore, its application in radiation is usually limited to the low-dose range.

4. METHODS OF MEASUREMENT OF RADIATION FLUENCES AND DOSES

(139) Radiation transport calculations, measurements, and interpretation of data are essential components for operational radiation safety. The measurements include an assessment of the environment at the exterior surface of the spacecraft or habitat; assessment of the interior environments in the spacecraft/habitat and EVA suit; the use of personal dosemeters; and the determination of the transmission of radiation to internal organs or tissues.

(140) Individual monitoring of occupationally exposed persons on Earth is mainly performed to ensure that the exposure is below legal dose limits which are generally set to limit exposure risks to an acceptable level. While the basic limits are given in terms of effective dose, it is generally accepted that at doses far below the limits the measured personal dose equivalent appropriately assesses effective dose in routine radiological protection applications (ICRP, 2007). The situation in space, however, is significantly different. Doses to astronauts in space may be much higher than annual dose limits for occupationally exposed persons on Earth, especially in long duration missions. It is, therefore, important to obtain more precise information about doses and exposure risks. For planning purposes and for operational radiation safety programs, risk assessment is seen to be as important as dose recording for astronauts in space. For any risk assessment, however, the knowledge of the radiation incident on the human body and/or the assessment of doses in the human body are basic preconditions.

(141) Calculations are essential to mission planning in that they provide pre-flight estimates of the doses that would be received by the astronauts during the different phases of a proposed mission. They are also an important part of the dose assessment process for determining the doses received by the astronauts during the mission.

4.1 Measurement quantities

(142) The objective of the adopted dose assessment approach in radiological protection is generally to determine the specific protection quantities defined for the low-dose range for limiting the probability of stochastic effects and for avoiding deterministic effects (tissue reactions) in the human body. For applications on Earth these quantities are the equivalent dose in an organ or tissue, H_T, and the effective dose, E (see Section 3.1). For the special situation of astronauts in space, the quantities mean absorbed dose in an organ or tissue, D_T, and dose equivalent in an organ or tissue, $H_{T,Q}$, are proposed for use instead (see Section 3.3). At higher doses when deterministic effects may occur, a differently weighted absorbed dose is required. In this case, a mean value of the relative biological effectiveness, RBE, needs to be determined from the information on the radiation field components and the specific RBE values of the different types of particles involved. There is an important role for biodosimetry. Individual biomarker measurements on astronauts can give consolidation for other dosimetric approaches.

(143) The radiation environment external to a spacecraft in low Earth orbit consists of electrons, positrons, neutrons, protons and all stable atomic nuclei (up to charge Z = 92). Particle energies range from a few eV for trapped electrons and from thermal neutrons to 10^{14} MeV for GCR (see Chapter 2). Most of the electrons will not penetrate the wall of the spacecraft, but could penetrate the space suits worn during extravehicular activity (EVA),

resulting in doses to the skin and lens of the eye. Nuclear interactions of neutrons, protons and heavier nuclei with spacecraft, space suits, the Earth's atmosphere and the human body produce secondary radiation, which add to the radiation field. The techniques of radiation monitoring vary according to particle type, energy, and the measurement location (inside or outside the spacecraft, inside EVA suits). The radiation environment can be classified on this basis:

- Trapped electrons – outside spacecraft and inside EVA suit;
- Trapped protons (< 10 MeV) – do not penetrate spacecraft or EVA suit;
- Protons and light charged particles (> 10 MeV) – outside and inside spacecraft, and inside EVA suit;
- GCR and secondary photons – outside and inside spacecraft, and inside EVA suit;
- Secondary charged-particles – inside spacecraft and inside EVA suit;
- Neutrons - outside and inside spacecraft, and inside EVA suit.

(144) In addition to variations of the primary external radiation field the relative contribution of each component (including the secondary radiation) to organ and tissue absorbed doses and dose equivalents at each location will also vary according to additional factors, including the mass distribution inside the spacecraft and the EVA suit construction.

(145) Mean absorbed doses and dose equivalent in organs and tissues of a human body are generally not directly measurable. An approach to the estimation of these quantities is given in Chapter 6. These include (1) calculations of particle type and energy and direction distributions of fluence in radiation fields at the location of an astronaut plus the application of organ absorbed dose and dose equivalent conversion coefficients; (2) direct assessment of organ absorbed doses and dose equivalents for an astronaut by radiation transport calculation using energy and direction distributions of fluence from outside of the spacecraft, or otherwise, at the astronaut's location; and (3) measurement of absorbed dose or dose equivalent near or on the astronaut and the use of results from calculations applying anthropomorphic phantoms.

(146) The main objectives of environmental measurements are the provision of radiation field data of particle types, fluences and microdosimetric quantities, absorbed doses and dose equivalents, using detectors in assemblies of various sizes, both integral and differential (with respect to time, or LET, or energy, or direction, as appropriate) and, in some cases, normalized to calculations of the radiation field components. For personal monitoring, the same quantities might be determined, but more importantly data are required for the determination of absorbed dose and dose equivalent. Absorbed dose and dose equivalent values measured by personal dosemeters worn on the body can be applied as estimates of D and H at a point in adjacent tissue, or can be used with prior data as estimates of absorbed dose or dose equivalent to specific organs and tissues at larger depth. Environmental monitoring can provide radiation field data as input for calculations which will yield estimates of doses in the human body or may even be used to directly assess individual risks. It may measure dose quantities such as absorbed dose, D, the distribution of D in L, $D(L)$, or dose equivalent, H. It can also provide measurements in support of in-flight dose management, dose recording, and ALARA actions.

(147) The radiation detectors determine a particular measurement quantity. These include (1) particle type and energy and direction distributions of fluence; (2) dose deposition in the detector material; and (3) other dosimetric quantities such as LET or lineal energy, y. In addition there are calibration data on detector response and normalization of detector response (for example normalized to equivalent water absorbed dose for a radiation type and

energy)

(148) Several types of instrumentation are available including both active and passive devices. Active instrumentation should have a time resolution sufficient to identify temporal variations in the radiation field. Alarm or warning capabilities of instruments can be used to support in-flight implementation of dose management and ALARA actions. Passive detectors provide an integration of the exposure information over long time intervals. They are usually very robust, small in their dimensions and need no power supply. Some devices also allow on-demand readout. For all instrumentation used for measurements in space the following must be established: (1) full response characterization and calibration; (2) measurement model; and (3) knowledge of uncertainties. Comparison of instrument responses is also useful. Many details of instrumentation for dosimetry in space have been published in review papers by Benton (2001), Badhwar (2002), and Caffrey and Hamby (2011). Further information has been presented by the HAMLET collaboration (HAMLET, 2011).

4.2 Purpose of measurements

(149) Measurements are performed for the purpose of determining individual exposures, monitoring changes of the radiation environment and performing ALARA. Instrumentation positioned inside or outside of a spacecraft or habitat can provide essential data for the characterization of the primary fields impinging on the spacecraft, such as galactic radiation, the trapped particle radiation field and the field caused by solar particle events. Such data from outside allow corrections to be made to the input data of transport codes to determine the field inside the spacecraft or habitat and so can reduce dose assessment uncertainties. Ion chambers or other active detectors with well-defined wall thickness can serve to monitor the short-term variations in the electron environment for EVA.

(150) Selectively located active and passive instrumentation allows radiation monitoring and further adjustments to the calculated internal environment. Particle spectrometers can provide data for the evaluation of transmission factors and of response functions of dosimetric devices and allow evaluation of calculated values and uncertainties of dosimetric quantities. Both active and passive devices are useful for determining absorbed dose, absorbed dose distribution over LET, absorbed dose distribution over lineal energy, and estimates of dose equivalent. Personal dosemeters worn by astronauts can determine some of these quantities at adjacent tissues.

(151) There are short-term and long-term variations depending on solar activity, which modify the environmental radiation field (components, particle fluences, energies and direction distributions), so that energy- and direction-sensitive instrumentation is mandatory. In addition, active instrumentation allows the time-resolution of trapped, solar, and GCR components.

4.3 Instrumentation for radiation spectrometry, area and personal monitoring

4.3.1 General

(152) No single device can determine the required dose quantities for all components of the radiation field. Since there are large variations in the relative contributions to total absorbed dose and dose equivalent from the different particle types, it is not generally possible to determine the absorbed dose or dose equivalent from just one component (or few components) and apply a correction factor to determine the absorbed dose or dose equivalent

for the entire radiation field.

(153) The dosimetry may be simplified by considering separately the radiation in terms of its energy deposition properties characterized by LET (or lineal energy). These include both low-LET charged particles (those of LET less than 10 keV/µm) and high-LET charged particles (those of LET equal to or greater than 10 keV/µm). High-LET particles may be separated into the high-energy heavy ions (Z >2) and their fragments, and the mainly high-LET particles produced by the strong-force interactions of neutrons and high-energy protons. Often separate dose measurements are performed for these categories, preferably minimizing any overlap of response to avoid "double counting". The choice of measurement devices is dictated by radiation response characteristics (dependence on particle type and energy and on the quantity to be determined), operational characteristics (direct determination of dose quantities, input to model calculations, desired accuracy, dose management and ALARA support), as well as practical issues such as reliability, robustness and availability. The addition of devices measuring y and L distributions of energy deposition in tissue from all particles has substantially improved the situation of dosimetry in space.

(154) Another important consideration is the time required for analysis of the measured data compared with the duration of the mission. It might be desirable for long duration missions that there are read-out facilities for passive devices on board.

(155) Additional passive personal dosemeters may be needed on the astronauts during EVA missions to take account of the spatial variations in the degree of shielding provided by the spacesuit and the spacecraft.

(156) The development of a set of coefficients that directly relate dose equivalent obtained with TLDs and NTDs at the surface of a body to mean organ absorbed dose or dose equivalent for the space radiation environment is desirable in principle. It is, however, a very difficult task due to the complexity of the radiation field in space. While it might be possible for the GCR component, it seems to be impossible for trapped radiation owing to its strong variation with time and location.

(157) Neutrons are indirectly ionising particles. They are generated by interactions of GCR and higher-energy protons with the atmosphere of Earth, or other body, the spacecraft or habitat, or within fellow astronauts. The energy distribution of those neutrons has several maxima due to reactions producing neutrons from the incident GCR nuclei or the target atoms in spacecraft materials or tissue. The lowest energy maximum occurs as about 1 MeV from neutrons produced from the nuclear evaporation process from target atoms in interaction with GCR. A second broader maximum occurs at about 100 MeV from knockout and cascade reactions leading to fast neutrons from emitted from target nuclei. At higher energies, there is an even broader maximum near about 1000 MeV due to neutrons produced from the GCR nuclei by either evaporation or knockout and cascade reactions. Various methods are applied for neutron monitoring in space (see e.g. Benton et al., 2001). To detect absorbed dose to tissue and dose equivalent from the high-LET secondary particles from neutrons, and for similar particles produced by strong-force interactions of higher energy protons, it is necessary to use detector materials and local shielding that closely matches tissue elemental composition.

4.3.2 Active devices

(158) Active devices record and display data in real time, or near-real time. This enables measurements of fluence or dose rates as well as time integrated values. Most active instruments can be turned on or off so as to operate in specific circumstances such as EVA

and during an SPE. Active detectors require electrical power that can be provided through connections with power supplies in the spacecraft or through batteries. During recent years a broad range of different types of active instruments has been used for radiation measurements on board of the ISS either for scientific investigations (see Table 4.1) or for operational area monitoring (see Table 4.2). In the following some types of instruments are described.

Table 4.1. Active radiation detectors applied on board the ISS for scientific applications during recent years, some of them in combination with the MATROSHKA phantom (Dettmann et al., 2007).

Instrument	Ref.	Heritage	Measured parameters
DOSMAP	(Reitz et al., 2005)	International collaboration	Various parameters
DOSTEL – Silicon Telescope	(Reitz et al., 2009)	Christian Albrechts University Kiel, German Aerospace Center, Cologne	LET distrib., absorbed dose, dose equivalent
SSD – Silicon Scintillator Device	(Reitz et al., 2009)	Christian Albrechts University Kiel, German Aerospace Center, Cologne	Absorbed dose, neutron dose, organ dose
LIULIN – Silicon Detectors	(Dachev et al., 2006)	Solar Terrestrial Influences Laboratory, Bulgaria	Absorbed dose, dose rate
ALTCRISS – Silicon strip detector	(Casolini et al., 2007)	INFN and University of Rome Tor Vergata, Rome, Italy	Particle energy distrib. up to Iron nuclei, LET distribution, dose equivalent
ALTEA – Silicon strip detector	(Fuglesang, 2007; Narici et al., 2004)		
BBND – Bonner Ball Neutron Detector	(Koshiishi et al., 2007)	Japan Aerospace Exploration Agency, JAXA, Japan	Neutron energy distrib. and neutron dose

Table 4.2. Active and semi-active radiation detectors used on board the ISS for area monitoring.

Instrument	Ref.	Heritage	Measured parameters
Tissue equivalent proportional counter (TEPC)	(Badhwar et al., 1994)	NASA Johnson Space Center, Houston	LET distribution, absorbed dose, dose equivalent
Charged particle detector system (IV-CPDS)	(Lee et al., 2007)		LET distribution, particle energy distribution, Nuclear abundances up to Oxygen
Charged particle detector system (EV-CPDS)			
Ionisation Chamber (R-16)	(Benghin et al., 2008)	Moscow State University, Moscow	Absorbed dose, dose rate
Silicon detector units (DB8)		Space Research Institute, Bulgaria	Absorbed dose, dose rate
TL – system (PILLE)	(Apáthy et al., 2002; 2007)	KFKI, Hungary	Absorbed dose, dose rate

Tissue equivalent proportional counters

(159) A tissue equivalent proportional counter (TEPC) is a low-pressure proportional counter with a wall of tissue-equivalent material especially designed for use in microdosimetry and radiological protection. The pressure of the gas in the detector is chosen to simulate a volume of tissue comparable to the dimensions of the nuclei of a mammalian cell. The charge produced by an ionising particle traversing the chamber volume is collected

and, by calibration of the detector, the electrical signal can be related to the energy loss of the crossing particle in that simulated tissue volume. Data are recorded on an event-by-event basis such that one can obtain a distribution of energy deposition events in a small element of tissue with a known covering material in terms of lineal energy, *y*, which can be correlated with LET, and therefore characterizes the ionisation density along tracks of particles and radiation quality. The lineal energy, *y*, is defined by the quotient $\varepsilon/\bar{l}$, where ε is the energy transferred to the chamber gas by ionisation by a crossing particle and $\bar{l}$ the mean path length of the charged particles in the chamber volume. Consideration should be given to factors which influence performance, such as wall effects.

(160) The response to photons and neutrons depends on the probability of the production of secondary charged particles in the wall passing the detector volume - and hence on the wall material. Mostly materials that are tissue-equivalent with respect to neutrons are chosen, for example A-150 plastic. For incident charged particles, each particle crossing the chamber volume produces a signal. Depending on the shape of the volume, even for incident monoenergetic charged particles a broad y-distribution is obtained. The y-distribution is further modified by straggling effects and secondary charged particles produced in the chamber wall (see Fig. 4.1).

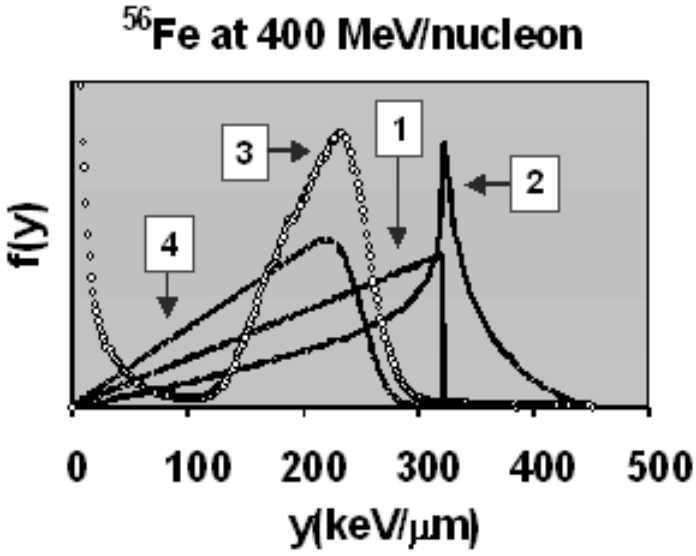

Fig. 4.1. Frequency distribution, f(*y*), of lineal energy in a TEPC for a uniform fluence of ^{56}Fe ions. Curves 1 and 2 are calculated by taking the chord length in a sphere (curve 1) and a cylinder (curve 2) times the LET of the Fe-ion. Data of Curve 3 are from measurements with a spherical detector and Curve 4 is the results of a calculation using restricted LET, L_{Δ}, and considering straggling (NCRP, 2002).

(161) The term $y \cdot f(y)$ as a function of *y* approximates the dose distribution in terms of LET and can be used to determine a mean quality factor for the absorbed dose to the detector configuration (Doke et al., 2001). When the data are integrated over the distribution of *y* or *L*, the TEPC can generate absorbed dose and absorbed dose rate. Data from a TEPC can be displayed continuously or stored for later transmission to mission control. Special TEPC systems have been designed for use in spacecraft (see e.g. Caffrey et al., 2011).

Semiconductor devices

(162) Semiconductor devices for the detection of charged particles are thin diodes, mostly Si-diodes (thickness of about 50 to 5000 µm), that record the energy deposited by a charged particle in the sensitive volume of the detector. For particles with normal incidence and fully traversing the sensitive detector volume, the ratio of the deposited energy to the thickness of the detector yields the approximate LET for the incident particle in that material. If charged particles from various directions pass the detector, a mean path length in the sensitive detector volume need to be determined for assessing an LET-distribution. Thus, a single detector can approximately provide an estimate of the charged particle fluence distribution in linear energy transfer and time. This distribution can be integrated to yield dose and dose rate for protons and heavier charged particles in the detector material, and by the use of conversion coefficients, determine dose to tissue. Often some detectors are used as a telescope which restricts the response to a smaller solid angle.

(163) Several multi-array solid-state detectors are combined to form a particle telescope that measures both energy deposition and flight direction. When these data are combined, the detector yields a more accurate estimate of LET in the detector material, and thus the distribution of fluence in LET, direction, and time. Using appropriate conversion coefficients, the data can also be used to obtain $D(L)$ distributions and Q-values for heavy charged particles, but with the restriction that the incident particles originate from a fixed direction depending on the orientation of the detector. Because of size limitations, this type of detector is only sensitive over a restricted solid angle.

(164) The energy lost in solid-state detectors of a telescope can also be used to identify the particle charge as well as the incident energy to ultimately obtain the distribution of fluence in energy, particle charge number and time. Several of these detectors can be combined to point in different directions to provide a more complete description of the radiation field either outside or inside a spacecraft.

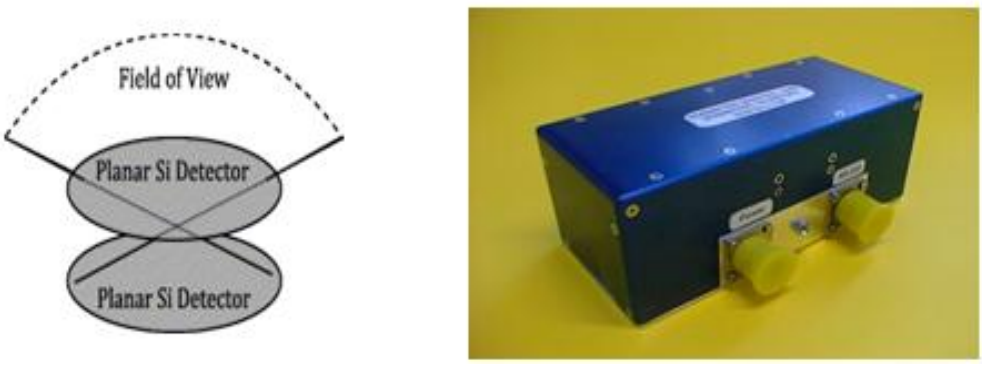

(a) (b)

Fig. 4.2. Charged particle spectrometer DOSTEL designed for space applications (Posner et al., 2005). Schematic view (a) and realized detector (b) (Beaujean et al., 2002).

Direct ion storage devices

(165) This device combines an ionisation chamber with a semiconductor device. Specifically, the direct ion storage dosemeter, DIS, is based on coupling a gas-filled ion chamber with a semiconductor non-volatile memory cell where the charges produced in the chamber volume are stored. These are compact integrating devices that can be read out periodically without deleting the information and are used to estimate accumulated doses

over periods of several hours to at least one year. The response of the DIS to charged particles incident on the detector and passing the chamber volume is approximately equal to the energy deposited, while the response to photons and neutrons incident on the DIS and producing secondary charged particles in the detector depends on the material and thickness of the chamber wall. The response to low-energy charged particles incident on the DIS depends also on the chamber wall thickness due to their energy loss in the wall.

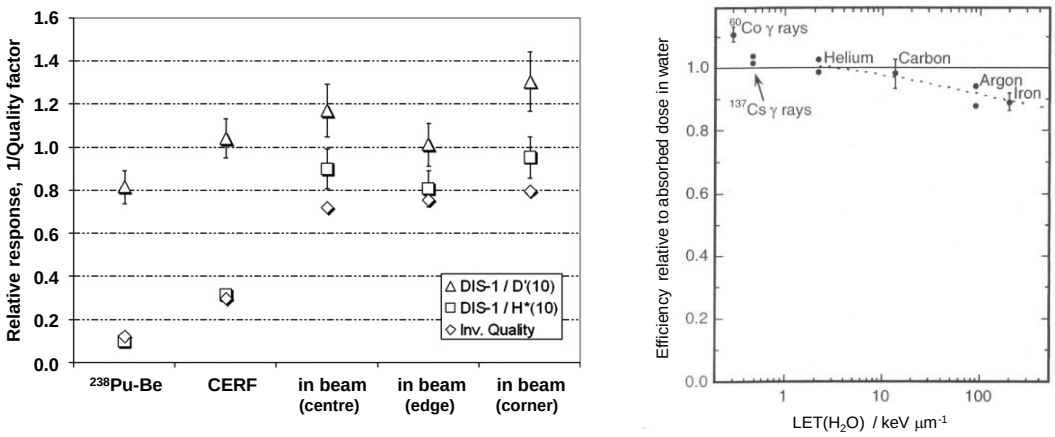

Fig. 4.3. Relative response of the DIS-1 dosemeter.
(a) Dosemeter reading in terms of personal dose equivalent, H_p(DIS), normalised to absorbed dose in 10 mm depth of tissue, D(10), (triangles), and ambient dose equivalent, H*(10) (squares). The inverse of the quality factor, 1/Q, is also indicated (diamonds) (Otto, 2010).
(b) Efficiencies of DIS-1 relative to absorbed dose in water as a function of LET(H_2O). Each point for ^{60}Co-γ radiation, carbon and iron ions represents an average value from six samples (1 s.d.). Two of the samples were irradiated with each of three doses (10 mGy, 25 mGy, and 50 mGy in water). Points for ^{137}Cs-γ radiation, helium ions and argon ions represent two samples irradiated with a dose of 10 mGy. (Yasuda, 2001).

Bonner sphere spectrometer

(166) In principle, a Bonner sphere spectrometer consisting of a set of Bonner spheres of different size is well suited for measuring neutron fluence and spectral distributions of neutrons. On ground, neutrons over a wide energy range are often monitored by such moderator-based survey instruments whose responses have also been extended to higher energies by introducing a layer of heavy metal in their moderator (see e.g. Wiegel et al., 2000). However, those instruments are not suitable for use in spacecraft because of their heavy weight as well as their high sensitivity to HZE particles. A Bonner Ball Neutron Detector (BBND) was used on Space Shuttle flight (Matsumoto et al., 2001) and on ISS (Koshiishi et al., 2007) for measuring the fluence of neutrons with energies below about 15 MeV. However, also high-energy neutrons are present in spacecraft (see par. 158). Thus, development of a new instrument having a light weight and less sensitivity to HZE particles is necessary for precisely monitoring neutron fluence or doses in spacecraft.

Electron detectors

(167) Active electron detectors need to be specially configured to measure low-LET radiations, in particular, electrons below about 1 MeV. Electrons of these energies are normally not an issue inside the spacecraft but could be of concern during EVA, since electrons above a few hundred keV can penetrate the spacesuits. Since the trapped electron

fluence rate can change by many orders of magnitude during and following a large magnetic storm, due to short-term perturbations of the geomagnetic field, it is recommended that an active detector sensitive to electrons be installed outside the spacecraft to serve as a monitor for fluctuations in the electron component of the space radiation environment to enable dose management during EVAs. Such a monitor could be a simple ionisation chamber or solid-state detector with a wall thickness sufficient to strongly attenuate very low energy electrons but thin enough to record electrons that could penetrate a spacesuit (Evans et al., 2008).

Active personal dosemeters

(168) Active personal dosemeters (APD) can give an instant indication of both accumulated dose and dose rate. Preset visual and audible alarms are also provided, so that these devices can be used simultaneously as an integrating dosemeter and as an alarm dosemeter. APD can be used as supplementary dosemeters to a passive dosemeter used for routine dosimetry. It is clear that for low-LET radiation the energy and directional response characteristics of APD are, in most cases, as good as passive dosemeters, able to measure doses in continuous radiation fields with acceptable accuracy.

(169) An ideal personal dosemeter would be active, store integrated dose data and dose rate time profiles, and respond to all field components allowing a sufficiently precise determination of absorbed dose rate and dose equivalent rate to adjacent tissues. Most available electronic personal dosemeters have been designed to measure absorbed dose to tissue under a defined covering layer from photon and beta radiation and their high-LET response characteristics are not well determined. Such dosemeters might be considered for the measurement of the low-LET component of the fields in spacecraft/habitat. However, even if used only to determine the low-LET component, a full characterization of their charged-particle and neutron response is necessary. Pixel-based detectors can be used as personal dosemeters. They can provide energy deposit distributions, energy and charge for all particles. They are based on a read out chip that embeds the electronics for each pixel within the pixel´s footprint. Careful calibration is necessary as for other devices.

(170) If active personal dosemeters are not used, then it may be necessary to develop on-board readout capabilities for passive dosemeters, especially on long-duration missions in space. Although on-board readout of nuclear etched track detectors is not feasible, on-board systems for readout of TL- and OSL-dosemeters already exist.

4.3.3 Passive devices

(171) Passive devices can be used for both area monitoring and personal monitoring. No single passive device is capable of dose measurement across the full energy and direction distribution of particles available in space. The instrumentation and detectors should be designed to have optimum performance in the types of particles noted above, namely: low-LET charged particles (*i.e.* L < 10 keV μm^{-1}), including such particle produced by non-ionising particles incident on the instrumentation; high-LET charged particles from neutrons and protons that undergo strong-force interactions; and high-LET heavy charged particles (HZE). While thermoluminescence detectors (TLD) radiophotoluminescence glasses (RPL), and optically stimulated luminescence dosemeters (OSLD) are used mostly for photon and electron dosimetry, as well as for neutron dosimetry, plastic nuclear etched track detectors (PNTD) are well suited for measurements in neutron and heavy charged particle fields. In space applications, measurement systems combining both detector types are often used in personal dosimetry.

Luminescence detectors

(172) Passive dosemeters currently in use are mostly thermoluminescence detectors (TLD). TLDs are small sintered chips or pellets of crystals which show luminescence after exposure to ionising radiation. By fast controlled heating of the crystal, the stored energy is released as light emitted. The function between the actual temperature and the intensity of the emitted light (the glow curve) shows various peaks, the heights of which are proportional to absorbed dose. Various crystal materials doped with different elements are in use for personal dosimetry.

(173) An alternative to TLD is the use of radiophotoluminescense glasses (RPL). Small glass elements respond as do TLDs to incident ionising radiation, storing energy in metastable electronic levels. The energy is released as light when the glass is exposed to ultra violet laser illumination.

(174) Optically stimulated luminescence dosemeters (OSLD) have also be proposed. In OSLD, the stored energy is released by optical laser stimulation. TLDs, RPL glasses, OSLD material, or similar types of dosemeters, will have to be fully characterized for the specific space environment.

(175) There might be a need for some passive elements to be read out frequently on board, and others that are read only on return to Earth. The mode of readout of the luminescence dosemeters should be carefully considered.

(176) TLDs, RPL glasses, and OSLDs measure absorbed dose in their material and are mostly calibrated in terms of absorbed dose in tissue or water in ^{137}Cs or ^{60}Co gamma radiation reference fields. The detector response, relative to the response to the reference radiation depends on the ionisation density around the track of a traversing particle. While for L < 10 keV/µm there is mostly only a small L-dependence of the response, TLDs, RPL glasses, and OLSDs show a strong LET-dependence above about 10 keV/µm, generally with decreasing response with increasing LET (see Fig. 4.4). This needs to be well known for dosimetry in space radiation fields. Fig 4.5 shows the relative variation of the response of some TLDs to cosmic radiation and ions with different LET-values in the detectors.

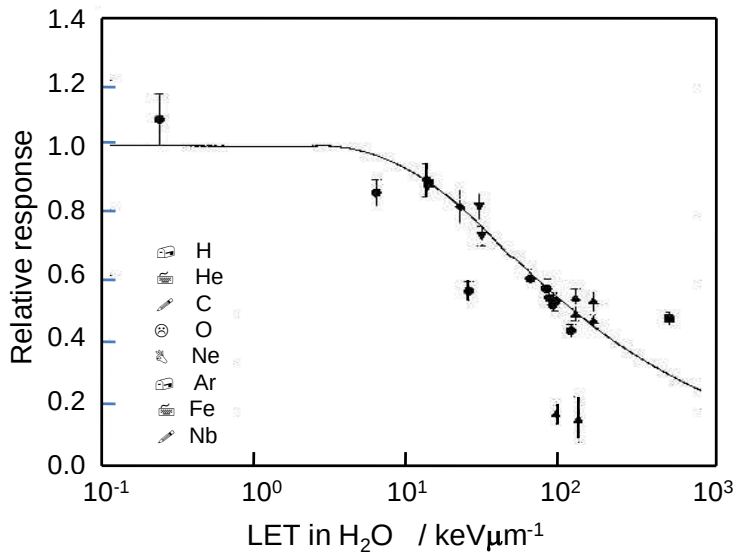

Fig. 4.4. Relative response of TLDs for various charged particles. The relative response (relative to ^{60}Co-γ rays) of peak 5 from TLD-600 and TLD-700 versus mean LET (in water) in the detector is shown (Benton et al., 2000; Berger et al., 2006).

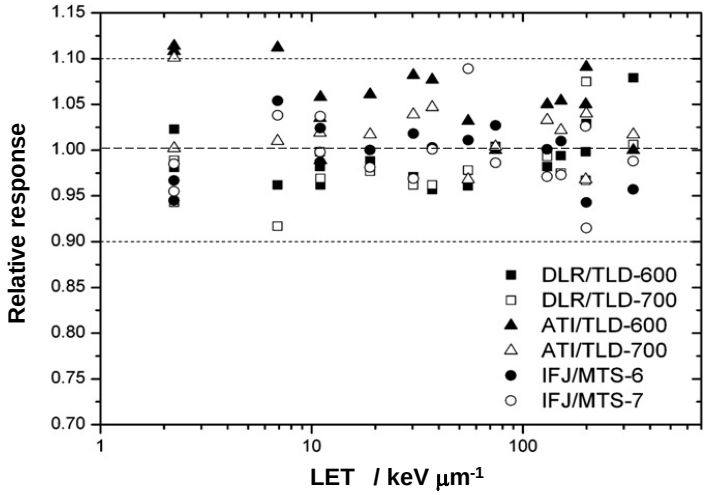

Fig. 4.5. Relative response of various TLDs (normalized to the mean value) to cosmic radiation and ion beams with different LET values in the detector; current results of the intercomparison of personal dosemeters (HAMLET) (Bilski et al, 2011).

Nuclear track detectors

(177) To detect the high-LET component of the radiation field, plastic nuclear etched track detectors (PNTD) and nuclear emulsions can be employed. Damage to the material is caused by the passage of a charged particle, and these particle tracks can be viewed microscopically, either before or after being realized by suitable chemical treatment. Etched track detectors are generally insensitive for radiation with an LET in water below about 10 keV µm^{-1} (depending on material) and may be employed in a method that provides *D*, *D*(*L*), or *D* averaged over certain ranges of *L*, and *H*. With suitable detector sets, etched track detectors and nuclear emulsions can determine the charged particle type and its direction in the detection medium, and can allow an analysis of the radiation field at the position of the detector. The analysis of the response of polyallyldiglycolcarbonate (PADC), commonly named CR-39, in terms of the dependence on LET allows the determination of absorbed dose and dose equivalent to a small element of tissue from all charged particles above about 10keVµm^{-1} (Zhou et.al., 2006). The detectors can separate the heavy charged particle and neutron contributions by looking at the particle ranges. A further separation procedure to detect the neutron dose component can be made using thin detectors and coincidence techniques or by using of a thin PADC detector and a combination of electrochemical and chemical etching. Stacks of PADC detectors can be used for spectrometry of HZE particles (see e.g. Gunther et al., 2002)

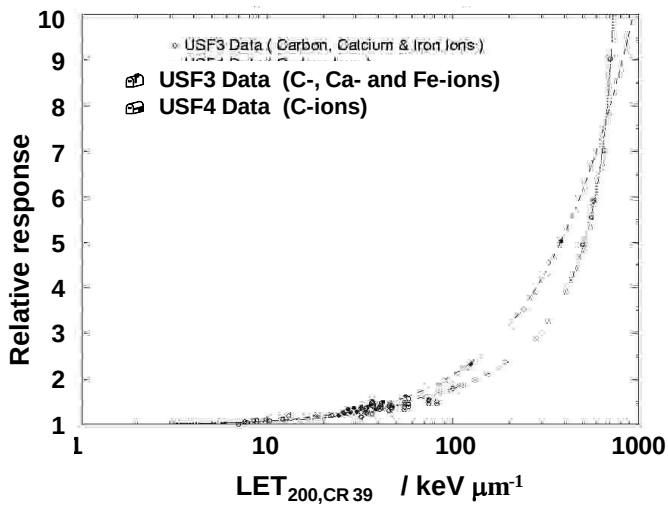

Fig. 4.6. Relative response of PADC detectors (CR-39) as a function of restricted LET, L_{200} (O´Sullivan et al., 1999; Zhou et al., 2008).

Superheated emulsions

(178) Superheated emulsion detectors, sometimes referred to as superheated drop or bubble detectors, are small droplets of a liquid above its normal boiling point suspended in a viscoelastic medium. The droplets remain in the liquid phase until a charged particle interacts inside or near the surface of the droplet. This transfers energy to the droplet and may cause local evaporation. If sufficient energy has been transferred and a critical radius is exceeded, all the liquid in the droplet will be vaporized and the bubble becomes visible. Superheated emulsion detectors respond to neutrons and to heavy-charged particles. A clear calibration procedure is required. Recent data on bubble detector responses are presented by Lewis et al. (Lewis et al, 2012).

Combined detector systems

(179) A combination of one detector for the measurement of the low-LET component and one for the high-LET component can allow the determination of dose equivalent in the complex radiation field in space. For passive dosimetry, with a package of TLD (or OSLD) and PNTD, the dose equivalent in adjacent tissue near the surface of the body is determined by:

$$H = D_{\mathrm{TLD}} - \int_{L>10\mathrm{keV}/\mu\mathrm{m}} \eta_{\mathrm{TLD}}(L) D_{\mathrm{TLD}}(L)\mathrm{d}L + \int_{L>10\mathrm{keV}/\mu\mathrm{m}} D_{\mathrm{ETD}}(L) Q(L)\mathrm{d}L - \int_{L<10\mathrm{keV}/\mu\mathrm{m}} \eta_{\mathrm{ETD}}(L) D_{\mathrm{ETD}}(L)\mathrm{d}L \qquad (4.1)$$

where D_{TLD} is the total absorbed dose recorded by the TLD (equivalent also for OSLD). $D_{\mathrm{PNTD}}(L)$ is the absorbed dose distribution in LET determined by the etched track detector in the high-LET range (L > 10 keV µm^{-1}) and for which Q is dependent upon L. The correction terms consider the non-zero response of the TLD. $\eta_{\mathrm{TLD}}(L)$ is the relative dose response in the region L > 10 keV/µm and $\eta_{\mathrm{ETD}}(L)$ that of the PNTD, respectively, in the region L< 10 keV/µm, so that intermediate LET components are not considered twice. It is recognized that this requires the verification of the LET-dependence of both the low-LET and high-LET detector system, and the elimination of parts from overlapping of responses.

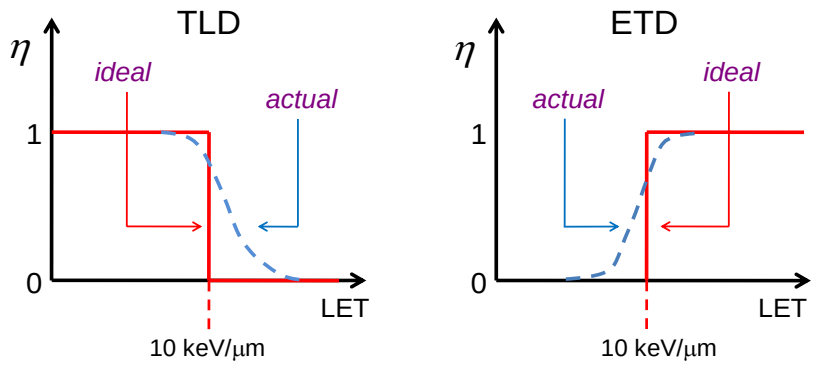

Fig. 4.7. Schematic relative dose responses of a TLD and a PNTD.

(180) An alternative method is to obtain data on the *y* or *L* distribution of energy deposition from a TEPC or a particle spectrometer used as a passive area dosemeter, and to apply this for correcting a measurement with a low-LET detector to obtain the full dose equivalent at the dosemeter's location. For such a correction the efficiency function, $\varepsilon(L)$, of the low-*y* or low-LET detector needs to be known, and an effective efficiency to be determined.

4.4 Biomarkers of exposure

(181) Biomarkers of health effects can be divided into 3 categories (Brooks, 1999): biodosimetry which is a measure of exposure, biomarkers of risk, and biomarkers of the presence of disease. The term biodosimetry in this context refers to a biological measurement to assess a biologically based dose equivalent. Because of the complex nature of the space environment, including nuclear and atomic processes occurring within tissues, and the large uncertainties in conversion of doses to risk, biodosimetry is routinely performed on the small population of astronauts involved in International Space Station (ISS) missions, and would likely be used in future space missions. There are also limitations in the size of devices that can be worn and practical obstacles to wearing a physical dosemeter at all times in space, which make biodosimetry an attractive supplement to physical dosimetry. To be useful as a biodosimetry method, the radiation quality dependence of the response of the assays should be similar to the $Q(L)$ relation from Eq. (3.10). Biodosimetry assays would likely be carried out on lymphocytes from a routine blood sample (see e.g. IAEA, 2011). Biomarker assays may require samples from other tissues including skin, swabs from the oral cavity to collect cells, urine or bone marrow. There are several biodosimetric methods that can be used for space travel which are summarized next.

Micronuclei

(182) Micronuclei result from loss of whole chromosomes or acentric chromosome fragments from daughter nuclei following cell division. They appear as small, membrane-bounded inclusions in the cytoplasm. Their assessment is relatively easy and rapid and by including cytochalasin B in the cell cultures analysis of cells is restricted to those in their 2nd post-exposure cycle. This has greatly increased the sensitivity of the assay. If individual pre-exposure levels of micronucleus frequency are available, absorbed doses as low as 50 mGy can be detected; without knowledge of the background frequency the detection level is

estimated to be 100 mGy. A modification of the assay uses a fluorescent pan-centromere probe to distinguish two types of micronuclei - those derived from either whole chromosomes or from chromosome fragments. By restricting analysis to the fragment type much of the background noise in the assay can be reduced (Vral et al., 1997).

(183) The frequency of micronuclei has been used for estimating exposures for a number of radiation accidents with reasonable agreement with physical dose estimates. The drawbacks are that few studies have been performed with high-LET exposures, and the assay is not reliable for partial body exposures. Micronuclei are unstable structures meaning that their frequency reduces with time due to the turnover of lymphocytes. This makes the assay unsuitable as a biodosimeter in astronauts exposed to space radiations over prolonged missions.

Acentric fragments in prematurely condensed chromosomes (PCC)

(184) Interphase chromosomes can be prematurely condensed to be observable microscopically either by fusion with mitotic cells or by treatment with a phosphatase inhibitor (calyculin A) (Blakely et al., 2003). Structural and numerical chromosomal alterations can be observed as an increase (or decrease) in centric chromosome number or from the presence of acentric fragments. The method has been used in a laboratory setting to assess exposure to x-rays and gamma radiation. The advantages are that non-dividing cells can be used for assay and the analysis is quite straightforward. The current drawback is that the assay has had no application as a true biodosimeter, and issues such as responsiveness to partial body exposures or chronic exposures have not been addressed. Further investigation appears warranted for assessing the value of PCC as a biodosimeter in the space environment.

(185) The fact that this PCC method has not been used in biodosimetry means that a lower detection level has not been established. A reasonable assumption is that it will be no more sensitive than other cytogenetic methods, given similar cell numbers analyzed. The advantage is a greater ease in obtaining large numbers of cells for analysis. As with micronuclei, this signal also is unstable with time due to the replacement of lymphocytes from the stem cell pool.

Chromosomal aberrations

(186) The method that has been most extensively used in biodosimetry is that of the analysis of structural chromosome aberrations. The incorporation of fluorescence in situ hybridization (FISH) techniques (Cornforth, 2001; Edwards, 2005) has enabled the assessment of symmetrical (transmissible) translocations. Unlike the assays described above, these are stable aberrations that pass successfully through cell division and are more suited to prolonged space missions. This allows for reliable dose estimation at long times after exposure. Chromosome aberration dosimetry has been successfully applied to radiation accident victims, A-bomb survivors and a wide range of occupationally and medically exposed persons including astronauts (George, et al., 2001; Cucinotta et al., 2008). These scenarios include chronic exposures and partial body exposures for which specific methods have been developed to aid in exposure estimation. The distribution of aberrations among cells is useful in this regard. Even with this strong record of success, the application of the method for dosimetry in astronauts in space has some drawbacks as evidenced by published studies (reviewed in Testard and Sabatier, 1999; and by Obe et al., 1999). One problem is the inter-individual variation in response which, however, can be overcome by individual calibration and determination of background in advance. The response is generally low due to the nature of the exposures by which only a small number of cells will actually be traversed.

This is especially the case for heavy charged particles. On the other hand, the effective area (or volume) of the blood system which is distributed over the whole body, is much larger than that of a passive dosemeter – biodosimetry sees the rare events better than a small physical dosemeter.

(187) Additional laboratory investigation is required in order to consider using cytogenetic analysis as a reliable dosemeter for space missions. Biodosimetry assays take skilled technicians to implement. The level of skill and time, however, to analyze data is no more demanding than physical dosimetry and the costs of biodosimetry are lower than physical dosimetry if the launch mass and crew time involved for physical dosimetry is considered.

(188) The detection of low doses using chromosomal aberrations is dependent upon the number of cells analyzed and whether an individual calibration curve is made prior to the exposure of interest. This point is addressed by Bauchinger (1995) who estimates that for 5,000 cells analyzed (using a generalized background frequency for dicentrics) a significant increase in dicentrics should be observed at about 100 mGy for a group of individuals. Twenty thousand cells would need to be analyzed to detect 50 mGy. Knowledge of the pre-exposure dicentric frequency can lower this detection level without increasing the number of cells analyzed.

(189) The study by Tucker et al. (1997) reports a lower detection level of about 500 mSv of effective dose for occupationally exposed individuals using FISH analysis of stable aberrations. The exposure was chronic in this case; a situation for which this type of translocation analysis is particularly applicable. Again, the sensitivity of the assay would be increased by having available the pre-exposure aberrations frequency. It might be further increased if the dose response to a reference radiation is determined using a blood sample obtained prior to space missions (George, et al. 2001). The number of painted chromosomes used also impacts the sensitivity of the assay. The older studies painted only one or two chromosomes. Newer studies involved a larger number of chromosome paints or painting the entire genome which increases the sensitivity. Tucker has recently reviewed the low-dose sensitivity of the FISH translocations assay (Tucker, 2008).

Other biomarker methods

(190) Several other assays as biomarker approaches have been proposed or recently developed. These include complementary DNA (cDNA) arrays to measure gene expression (Mezentsev et al., 2011), prolonged life span of erythrocytes bearing transferring receptors on their membrane (Gong et al., 1999), gene mutation assays, and electron paramagnetic resonance (EPR) spectroscopy. A review on EPR dosimetry with tooth enamel is given by Fattibene and Callens (Fattibene et al., 2010). For these methods to be applied to space biodosimetry, the dose, radiation quality and duration of the signal over many months will need to be understood. A more recent assay is the measurement of telomere length. Telomeres are the short repetitive DNA regions that cap the end of chromosomes protecting them from deterioration. Reduction in the average length of the telomere has been associated with several late effects including cancer, neurological disorders, and aging (Schoeftner et al., 2009). Measurement techniques include southern blot, Q-FISH (Williams et al., 2011), and flow cytometry. These latter two assays allow rapid analysis of many cells. However, the radiation quality and dose response of the assay to protons and heavy ions irradiation will have to be studied further before it can be considered for a deployable biodosimeter for space missions.

4.5 Instrument characterization and calibration

(191) For instrument characterization and calibration in a laboratory, it is necessary to clearly specify the relevant calibration conditions, including the characteristics of the reference radiation source, the irradiation facility, and the conversion coefficients used. Periodic, accurate calibrations are essential, as are meaningful instrument response comparisons. Calibration (ISO, 2007; JCGM, 2008a) covers a number of the procedures included in a type test. In the first step, a series of calibration factors (or calibration coefficients, see below) or responses may be determined for a set of reference conditions, usually a set of radiation energies and angles, to establish a matrix of calibration factors/coefficients or responses, or a calibration/response function. The second step, when used, applies these data to obtain the value of the desired quantity from the instrument indication.

(192) All instrumentation should be fully tested prior to use. This procedure is especially important for applications in space where an exchange of instruments during a mission is often not possible. Failure of any part of the test should be clearly detailed and reasons for the failure considered. Fully tested means the determination of the instrument performance characteristics, including detection limit; tests of influence quantities, including other particle field components; and tests of the reliability of the complete system, including system software.

(193) For a fully tested instrument, a reference calibration (determination of a single calibration factor or calibration coefficient for one set of reference conditions) is sufficient to ensure a traceable absolute dose measurement. The reference calibration of the instrument should be repeated at regular intervals. This may not be possible in space applications, but then there should be periodic checks on the performance which may be carried out using non-reference fields and a fixed procedure. In addition to the type test, some instrument should have a traceable individual normalization/calibration factor. For reusable dosemeters, this factor should be checked periodically and adjusted if necessary.

(194) The response characteristics of all the types of devices should be determined by a combination of calculation and measurements. By Monte Carlo or other simulations the response of an instrument is determined in terms of particle fluence, and its energy distribution. The energy dependence of the response should be simulated for the particle types and range of energies relevant to the radiation fields in space, plus the angle dependence of response of the instrument, if any. The simulated instrument response must be benchmarked in reference radiation fields. For the simulation of the response characteristics of personal dosemeters, some irradiations should be performed with the dosemeter positioned on either an anthropomorphic phantom or a surrogate.

(195) Where an instrument consists of more than one detector or more than one signal channel, the result of any algorithm to calculate the measured value is to be treated as the instrument indication in all determinations of calibration coefficient or factor or response.

(196) Experimental response data for the active and passive devices used should be determined for the following energy ranges as appropriate: protons from below 10 MeV to 1 GeV; helium from 10 MeV/u to 1 GeV/u; high-*Z*, high-energy ions (e.g. C, Si, Fe) from 50 MeV/u to 1 GeV/u; electrons from 0.5 MeV to 10 MeV; and neutrons from about 1 MeV to 400 MeV, monoenergetic or quasi-monoenergetic; plus response data for fields which replicate the field produced by the interactions of GCR with shielding material. All the radiation fields used must be well characterized and traceable to national standards (NMI) or related to NMIs via a traceability network (for example, quasi-monoenergetic neutron fields) or as part of an international comparison programme (for example, ICCHIBAN (Uchihori et

al., 2002; Yasuda et al., 2006)).

(197) There are a number of ISO standards for photon, beta and neutron radiation, covering radiation fields for most radiation protection situations on Earth. The situation for space applications is more complex. Well specified mixed radiation reference fields with very high energy particles and a large component of heavy ions do not exist on Earth. There are radiation fields available at very high energy accelerators (for example EG at GSI in Germany; HIMAC, TIARA, CYRIC, and RCNP in Japan: NASA Space Radiation Lab at BNL in the USA; TSL in Sweden; NPI in the Czech Republic; iThemba in South Africa; NFS in France, CERN in Switzerland) which include a broad range of secondary particles produced in the shielding surrounding a target. Such radiation fields replicate components of the radiation fields in space and have been used for testing and intercomparison measurements of various detector systems (Mitaroff et al., 2002). The precise specification of these radiation fields, however, can be a problem. Calculations are needed for the beam particle and secondary particles, fluence rate and its energy distribution, plus any scattered components. The specific detector response to heavy ions can also be determined using beams from heavy ion accelerators where the fluence rate of the heavy ion considered is well specified.

(198) Determination of the dosimetric characteristics of the instrument (device or combination of devices) and its reference calibration are closely interlinked. The result of a response characterization is the detailed description of the dosimetric properties of a given instrument. This includes the dependence of the response on particle type, energy, angle of radiation incidence, and on various influence quantities. A reference calibration without a prior dosimetric characterization can be misleading, as the calibration can be misinterpreted as applying to the radiation field in space without correction. An instrument dedicated to a specific type of radiation (e.g. to neutrons) can have a response also for other particle types. This needs also to be taken into account by calibrations.

(199) In modern instruments, the software has become of increasing importance for the generation of the measured value. Therefore, the final version of the software should be available at the beginning of the type test, as a great part of the software test is indirectly covered by the metrological test. The manufacturer should be aware of the fact that any change of the software may invalidate the type test. Dosimetry system software should be guided by the WELMEC software guide 7.2 (WELMEC, 2008).

4.6 Accuracy and uncertainties for measurements in spacecraft

(200) Astronauts are exposed to complex, multi-component fields that are difficult to determine routinely. Radiation quality-weighted organ absorbed doses can be significant, and a main objective is that the uncertainties in the fluence rate and its energy distribution and in the assessments of detector absorbed dose and radiation quality should be minimized. Nevertheless, one of the objectives should be to meet the general requirement that the total relative combined standard uncertainty of detector absorbed dose or dose equivalent should be minimized. The total relative uncertainty in a subsequent estimate of organ dose or dose equivalent will be greater.

(201) The uncertainty in measurement assesses the measurement accuracy or metrological quality of measurements or fitness for purpose of a measured quantity value. Measurement accuracy is an assessment of the uncertainty. Guidance is based on documents and recommendations prepared by the Joint Committee for Guides in Metrology (JCGM), which gives definitions and guidance for metrology in general. These are available from the website

of the Bureau International des Poids et Mesures: JCGM 200 (JCGM, 2008a), JCGM 100 (JCGM, 2008b), and JCGM 104 (JCGM, 2009). These definitions and guidance are published by the International Organization for Standards (ISO) and the International Electrochemical Committee (IEC) (ISO/IEC Guide 99, 2007; ISO/IEC Guide 98-3, 2005; ISO/IEC Guide 98-1, 2009).

(202) An essential aspect of quality assurance is assessing to what extent is it reasonable to believe that the reported number is a good estimate of the true dose value. The greater this belief, the confidence or probability that the measured value is within a certain defined range around the true value, or rather that the true value is within a certain range of the observed value, the better the quality of the measurement. In the evaluation of the uncertainty, all knowledge of the instrument and evaluating system both from experience and from type testing should be used possibly in combination with detailed information on the instrument assembly usage.

(203) In order to obtain dose data of which the quality is traceable and can be recognized it is recommended that the terms and definitions given in the documents issued by the JCGM and the ISO framework should be followed. In the formulation stage, all input/influence quantities that may contribute to the uncertainty should be identified, and must be considered in the measurement model; all model input/influence quantities should be characterized by a best estimate and either a probability density function (PDF) or a (combined) standard uncertainty. The shape of the PDF can be taken from measured data or from an assigned distribution. Results from a type test or other characterization of the response of a dosimetry system may be used as inputs to the uncertainty assessment; other parameters such as standard uncertainty and coverage intervals must be derived from the PDF of the output quantity.

(204) ICRP in Publication 75 (ICRP, 1997) recommends that "In practice, it is usually possible to achieve an accuracy of about 10 % at the 95 % confidence level for measurements of radiation fields in good laboratory conditions. In the workplace where the energy and directional distribution of the particles in the radiation field are generally not well known, the uncertainties of an assessment will be significantly greater. Non-uniformity and uncertain orientation of the radiation field will introduce errors in the use of standard models. The overall uncertainty at the 95% confidence level in the estimation of effective dose around the relevant dose limit may well be a factor of 1.5 in either direction for photons and may be substantially greater for neutrons of uncertain energy, and for electrons. Greater uncertainties are also inevitable at low levels of effective dose for all qualities of radiation." These statements of ICRP strictly apply to the assessment of E and H_T for occupational exposure at low doses on Earth. ICRU has published recommendations on the acceptable levels of total uncertainty for dose measurements in radiological protection in Reports 47 and 66 (ICRU, 1992, 2001) which are broadly consistent with ICRP statements. ICRU recommends for single measurements of the operational quantities that "....in most cases, an overall uncertainty of one standard deviation of 30% should be acceptable" and states "The error of instruments may substantially exceed this limit at some radiation energies and for certain angles of incidence, but conform to it when they occur in a radiation field with a broad energy spectrum and broad angular distribution".

(205) The statistical uncertainty of laboratory calibrations is commonly far less than the above uncertainties. However, the absorbed-dose and dose-equivalent response of devices are frequently appreciably energy- and angle-dependent. In order to minimize the total uncertainty in practical measurements, either determination of the response is required for the radiation field in which it is to be used, or a simulation of this field may be used to determine

and apply correction factors to the calibration factor of an instrument. It may also be possible to calculate the response in this field from the knowledge of the field and of the detailed energy- and angle-dependence of response of the device. Frequently, it is the direction distribution of the field which has the largest influence. For measurements in space, additional information on the particle type, energy and direction distributions, are available. Using these data, accuracies of better than a factor of 1.5 at the 95% confidence level (equivalent to a standard deviation for a normal distribution of about 0.25) should be achieved for the estimation of organ absorbed dose and organ dose equivalent.

(206) At doses approaching or exceeding mission risk limits, or career risk limits, the upper 95% coverage probability is used to include the measurement uncertainty for the assessment of the cancer risk projections from estimations of organ doses and radiation quality and tissue weighting factors (see Sect. 7.5). Obviously, reduction of measurement uncertainties is seen to be an important task for mission planning.

5. RADIATION FIELDS INSIDE SPACECRAFT AND ON PLANETARY SURFACES

(207) The radiation field inside or near spacecraft includes various components of the primary radiation field in space (see Chapter 2) partially absorbed in the walls of the spacecraft and secondary radiation which is produced by scattering and reactions of the primary radiation in the walls and other materials within the spacecraft. Due to both the variation of the primary radiation field with time and to the non-homogeneous distribution of materials within the spacecraft the internal radiation field depends on the position in the spacecraft and on time during the mission.

(208) The radiation field near planetary surfaces is determined by several factors, such as the existence and strength of a magnetic field, the thickness and composition of the atmosphere and the planetary material near to the surface. Important are the scattering, absorption and reactions in the planetary atmosphere and in the ground material.

5.1 General

(209) The physical description of the interaction of space radiation with matter requires knowledge of the energy and isotopic distribution of primary and secondary charge particles and neutrons produced in atomic and nuclear collision processes in the transport of radiation through matter. Computer codes describing proton, high-energy and charge (HZE) nuclei, and secondary radiation energy distributions and their transport through matter are used for shielding design of spacecraft and planetary habitats, and organ exposure assessments. The codes need to be benchmarked against space dosimetry results. The broad range of ion types and energies of the galactic cosmic radiation and solar particles, and the large number of materials of interest in spacecraft structures, planetary atmospheres, and tissues require a detailed description of the basic physical processes including the development of reliable computer models. Studies of potential risk mitigation including operational, shielding, and biomedical approaches must rely on theoretical models in the form of radiation transport codes to make projections and to support design studies of such mission.

(210) Dominant physical processes in the penetration of high-energy nuclei through matter are energy loss through atomic and molecular collisions and the absorption and particle production from nuclear interactions with spacecraft materials and tissue. For heavy ions with

high kinetic energies (> 100 MeV/u), nuclear absorption by fragmentation is the dominant reaction mode (Hufner, 1985, Townsend et al., 1996). The nuclear absorption cross section scales by the nuclear mass number to a power, $A^{1/3}$ and fragmentation of GCR nuclei is more efficient per unit mass for materials with light constituent atoms. At lower energies (<100 MeV/u), elastic scattering, compound nucleus formation or excitations of discrete nuclear levels that decay by gamma emission or particle emission are dominant interaction modes. However, the short-range and large stopping powers of heavy ions reduce the importance of nuclear reactions at lower energies except for neutrons. High-energy protons and neutrons interact through knockout and spallation reactions (Hufner, 1985). Such processes lead to a build-up of light particles ($Z \leq 2$) and the localized production near the primary track of heavy ion target fragments with large values of LET and short ranges (Wilson, *et al*., 1991, Cucinotta *et al*., 1996).

5.2 Physics of space radiation transport

5.2.1 Radiation transport

(211) The description of the passage of high-energy nuclei through matter can be made using the Boltzmann transport equations that treat the atomic and nuclear collisions. The equations may be solved by either numerical and analytic techniques - the straight ahead approximation, or as an alternative, by Monte-Carlo techniques which sample from interaction processes for individual primaries or their secondaries to develop histories of charged particle passage and energy deposition in materials. The Monte Carlo method is a widely used technique in particle physics and often applied in simulating radiation transport through matter and the calculation of dose distributions.

(212) The relevant Boltzmann transport equations are derived on the basis of conservation principles (Wilson *et al*., 2001) for the fluence rate $\varphi_j(x,\Omega,E)$ of type *j* particles as:

$$\Omega \cdot \nabla\varphi_j(\boldsymbol{x},\Omega,E) = \Sigma_k \iint \sigma_{jk}(\Omega,\Omega',E,E')\, \varphi_k(x,\Omega',E')\mathrm{d}E'\mathrm{d}\Omega' - \sigma_j(E)\, \varphi_j(\boldsymbol{x},\Omega,E) \qquad (5.1)$$

where $\sigma_j(E)$ and $\sigma_{jk}(\Omega,\Omega',E,E')$ are the media macroscopic cross sections. The $\sigma_{jk}(\Omega,\Omega',E,E')$ represent all those processes by which the particles of type k moving in direction Ω' with energy E' produce a particle of type j in direction Ω with energy E. The fluence rate $\varphi_j(x,\Omega,E)$ is the main physical quantity used to determine the physical or biological response by folding it with an appropriate response function for the physical or biological system under study.

(213) There may be several reactions, which produce a particular product, and the appropriate cross sections for Equation (5.1) are the inclusive ones. The total cross section $\sigma_j(E)$ with the medium for each particle type of energy E may be expanded as:

$$\sigma_j(E) = \sigma^{at}_j(E) + \sigma^{el}_j(E) + \sigma^{r}_j(E)\,, \qquad (5.2)$$

where the first term refers to collision with atomic electrons, the second term is for elastic nuclear scattering, and the third term describes nuclear reactions. The microscopic cross sections and average energy transfer are ordered as follows:

$$\sigma^{at}_j(E) \sim 10^{-16}\ \mathrm{cm}^2 \quad \text{with } \delta E_{at} \sim 10^2\ \mathrm{eV} \qquad (5.3)$$

$$\sigma^{el}_j(E) \sim 10^{-19}\ \mathrm{cm}^2 \quad \text{with } \delta E_{el} \sim 10^6\ \mathrm{eV} \qquad (5.4)$$

$$\sigma^{r}_j(E) \sim 10^{-24}\ \mathrm{cm}^2 \quad \text{with } \delta E_{r} \sim 10^8\ \mathrm{eV}\ . \qquad (5.5)$$

Over a distance of 1 g cm^{-2} of a material many atomic collisions (~ 10^6) occur, many less nuclear coulomb elastic collisions (~ 10^3) , while nuclear reactions are separated by up to many cm depending on energy and particle type. For neutrons, it is $\sigma^{at}{}_n(E)$ ~ 0 and the nuclear elastic process appears as the first-order perturbation. Mean free paths for elastic scattering of neutrons may become quite small, especially at low energies in the resonance region (ICRU, 2000).

(214) The solution of Equation (5.1) involves hundreds of multi-dimensional integro-differential equations which are coupled together by thousands of cross terms and must be solved self-consistently subject to boundary conditions that ultimately relate to the external environment and the geometry of the astronaut's body and/or a complex spacecraft. A series of approximate solutions can be studied and indicates a high level of accuracy for most applications (Wilson *et al*., 2001, Tweed *et al*., 2005). The mean energy loss can be introduced in a continuous slowing down approximation (csda), and straggling neglected for the broad energy spectra of the space radiation. The highly directional coulomb cross section for charged ions (Wong et al., 1990) and nuclear elastic scattering for neutrons generally dominate the second perturbation term. The angular dispersion and its effects on lateral beam spread and range straggling are important corrections in comparing to laboratory measurements. The nuclear elastic scattering is especially important to neutron fields and has been treated using Monte Carlo or multi-group methods (Hughes, et al., 1997). The third perturbation term consists of complex energy and angle functions. Results from Monte Carlo codes (Allsmiller *et al*., 1965) provided the basis for the generation of analytical techniques and the simplification of boundary conditions used in space shield code development (Wilson *et al.*, 1991).

5.2.2 Atomic processes.

(215) The transport coefficients describe the atomic/molecular and nuclear processes by which the particle fields are modified by the presence of material (Wilson *et al*., 2001). As such, basic atomic and nuclear theories provide the input to the transport code databases. The first order physical perturbation on the right side of Equation (5.1) is the atomic/molecular cross sections as noted in Equation (5.3) for which those terms in Equation (5.1) are expanded about the energy moments l as

$$S_n(E) = \Sigma_i \Sigma_l \ \varepsilon^n{}_i \sigma_i(E) \ , \tag{5.6}$$

where ε_i is based on the electronic excitation energy, and $\sigma_i(E)$ is the total atomic/molecular cross section for delivering ε_i energy to the orbital electrons (including discrete and continuum levels). The first moment (n=1) is the usual stopping power, and the usual continuous slowing down approximation (csda) is achieved by neglecting the higher-energy moments. The second moment represents the energy straggling (Payne, 1969) due to the stochastic distribution of energy loss.

(216) Stopping power data bases are derived semi-empirically as the Bethe reduction of Equation (6) in terms of mean excitation energies and shell corrections (Fano, 1963, Wilson *et al.*, 1991). The stopping power, *S*, is adequately described by the Bethe-Bloch formula for most ion energies (Bichsel, 1992):

$$S = \frac{4\pi Z_P{}^2 Z_T N_T e^4}{mv^2}\left\{\ln\left(\frac{2mc^2\beta^2\gamma^2}{I}\right) - \beta^2 - \frac{C(\beta)}{Z_T} + Z_P L_1(\beta) + Z_P{}^2 L_2(\beta) + L_3(\beta)\right\} \tag{5.7}$$

where e is the electronic charge, N_T is the density of target atoms, m is the mass of the electron, c is the speed of light, $\beta = v/c$, and I is the mean excitation energy. In Equation (5.7), the various terms are the shell correction $C(\beta)$, Barkas correction, $L_1(\beta)$, Bloch term, $L_2(\beta)$, and Mott and density corrections $L_1(\beta)$. The range of the ion is evaluated from the stopping power as

$$R(E) = \int_0^E \frac{dE'}{S(E')} \tag{5.8}$$

(217) The second energy moment is related to energy or range straggling and provides corrections to the ion slowing down spectrum (Fano, 1963, Payne, 1969). For broad-energy beams conditions of GCR or SPEs transport straggling effects are negligible, however they are important for laboratory studies with mono-energetic beams and for understanding radiation detector response. The next physical perturbation term is the Coulomb scattering by the atomic nucleus and is typically represented by Rutherford scattering modified by screening of the nuclear charge by the orbital electrons using the Thomas-Fermi distribution for the atomic orbits. The total nuclear Coulomb cross section found by integrating over the scattering directions is related to the radiation length. The differential cross section is highly peaked in the forward direction, and only after many scatterings is significant beam divergence seen. Numerical solutions to the Coulomb multiple-scattering problem have been investigated for many years (Fermi, 1940) and accurately describe experimental data with HZE (Wong *et al.*, 1990) or proton beams (Carlsson and Rosander, 1973).

5.2.3 Nuclear interactions

(218) The extent of the nuclear interaction cross section database required for the transport of cosmic radiation is for energies from 1 MeV/u to energies of tens of GeV/u, including a large number of projectile and target material combinations. The types of cross sections required for transport involve total yields and multiplicities and inclusive secondary energy spectra, inclusive double differential cross sections in angle and energy. The total absorption plays a critical role in ensuring a reasonable solution to the Boltzmann equation including the accuracy of particle conservation as a function of depth in the shield (Wilson et al., 1991). Similarly in Monte-Carlo approaches the absorption cross section plays the critical role of determining the probability of interaction events along the trajectory of a primary particle in the shielding. In addition, exclusive cross sections are used in some event generators in Monte-Carlo transport codes. The total cross section σ_{TOT} is found from the elastic amplitude in the forward direction as found in the optical theorem (Wilson et al., 1991) as the imaginary part of the elastic scattering amplitude (Im f):

$$\sigma_{TOT} = \frac{4\pi}{k} \operatorname{Im} f(q=0) \tag{5.9}$$

where q is the momentum transfer, and k the relative momentum of projectile and target nuclei.

(219) The total absorption (ABS) cross section is then also found from the elastic scattering amplitude by using:

$$\sigma_{TOT} = \sigma_{ABS} + \sigma_{EL} \tag{5.10}$$

where σ_{EL} is the total elastic cross section. Formula for these cross sections can be derived from microscopic theories of nuclear multiple scattering (Cucinotta et al., 1997). The absorption cross sections are accurately represented by energy dependent variants of the Bradt-Peters equation (Townsend et al., 1986a)

$$\sigma_{\mathrm{ABS}} = \pi r_0^2 c_1(E)(A_{\mathrm{p}}^{1/3} + A_{\mathrm{T}}^{1/3} - c_2(E))^2 \tag{5.11}$$

where r_0, $c_1(E)$ and $c_2(E)$ are parameters fit to experimental data. Absorption cross sections have been well studied both experimentally and theoretically and are known with a few percent uncertainties (Tripathi, 2001). The absorption cross section rises at low energy as reaction channels open and reaches a minimum at a few hundred MeV/u before rising again as meson production channels open.

(220) Table 5.1 shows reaction partners and secondaries of relevant reactions broken into distinct reaction types or mechanisms. Low energy evaporation products including heavy ion target fragments are high-LET events important in biological damage. Knockout products from proton or neutron reactions and projectile fragments from nuclei of GCR are typically of low to moderate LET, however, their large ranges leads to radiation build-up through further reactions. The abrasion-ablation models (Hufner *et al.*, 1975, Towsend *et al.*, 1986b, 1996, Wilson *et al.*, 1995b, Cucinotta, et al., 1997) are used to describe heavy ion fragmentation cross-sections. The description of nuclear reactions through abrasion (particle removal during ion-ion interaction) and ablation (nuclear de-excitation after the abrasion step) is illustrated in Fig. 5.1, which shows the roles of projectile overlap, fireball formation in central regions, and the decay of the pre-fragment spectators (NCRP, 2006). The individual steps of abrasion and ablation can be described in both semi-classical or quantum mechanical approaches (Cucinotta *et al.*, 1995; 2007). These different reaction processes have been described by quantum multiple scattering theories (QMST), semi-classical methods such as quantum molecular dynamics, or Monte-Carlo approaches to nuclear reactions using an intra-nuclear cascade model (see Durante and Cucinotta, 2011 and references therein for a review of nuclear reaction models).

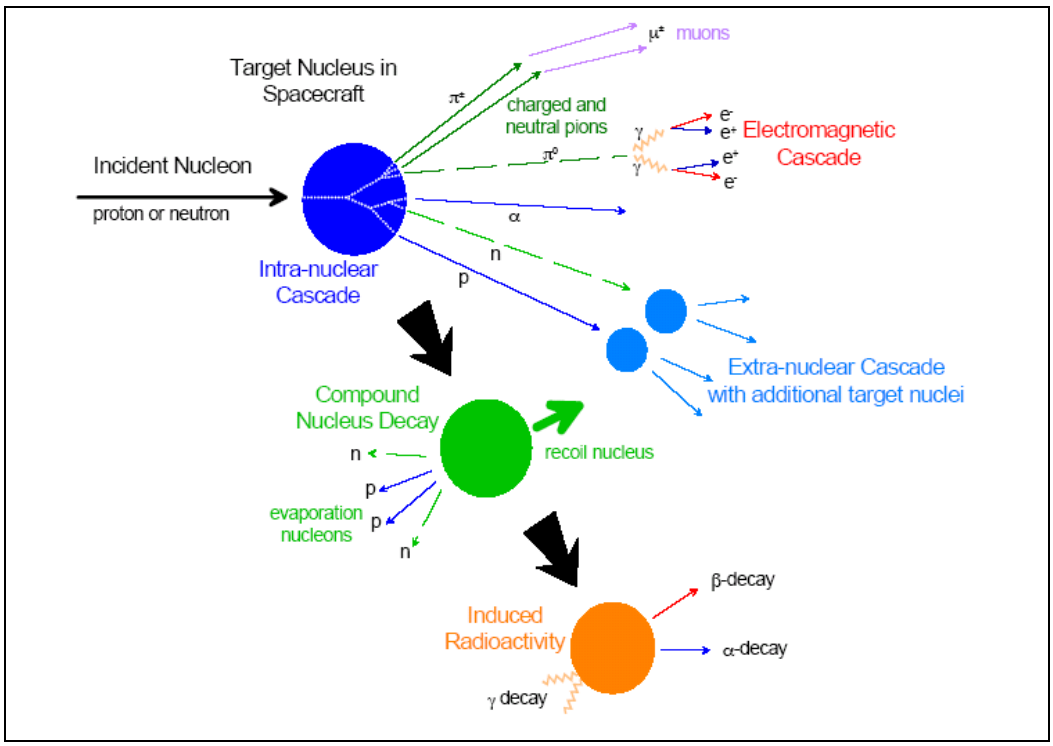

Fig. 5.1a. Schematic diagram of the reaction of an incident nucleon with a target nucleus at high energies (ICRU, 1978).

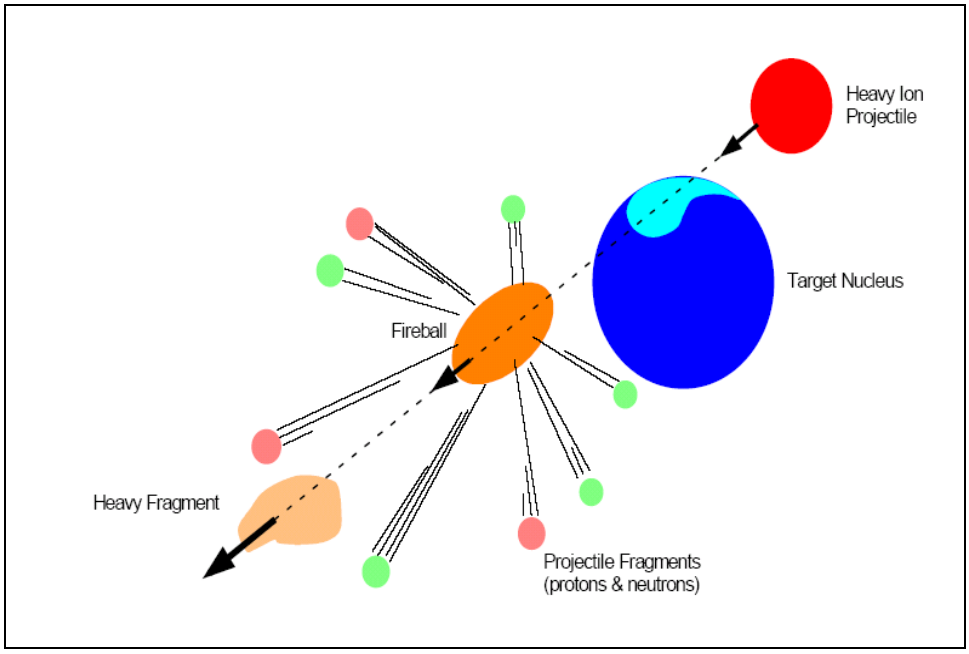

Fig. 5.1b. Schematic diagram of a relativistic heavy ion reaction with a target nucleus (Miller, 1997).

Table 5.1. Reaction products in nuclear reactions important to space radiation studies.

REACTION TYPE	SECONDARY	MECHANISM	COMMENT
Nucleon-Nucleus	Nucleon	Evaporation Knockout and elastic, quasi-elastic scattering	High LET, small range Large range
Nucleon-Nucleus	Light particle (d,t,h,α)	Evaporation Knockout, pickup	High LET, small range Large range
Nucleon-Nucleus	Heavy recoil	Elastic scattering Fragmentation or spallation	High LET, small range High LET, small range
Nucleus-Nucleus	Nucleon or light particle	Target or projectile Knockout or evaporation	Small LET, large range High LET, small range
Nucleus-Nucleus	Heavy ion	Projectile Fragment	Mod. LET, large range
Nucleus-Nucleus	Heavy ion	Target Fragment	High LET, small range
Nucleon or Nucleus-Nucleus	Pion, Kaon, anti-nucleon, gamma	Target reaction Proj. E > 500 MeV/u	Deep penetration (> 50 g/cm^2)

(221) Examples of fragmentation cross sections for Ar and Fe projectiles are shown in Fig.

5.2 in comparison to the quantum multiple scattering fragmentation (QMSFRG) model (Cucinotta, et al, 2002, 2006b, and 2007). Available fragmentation cross section data sets for target atoms of interest for space missions were reviewed by Durante and Cucinotta (2011) and NCRP (2006). One feature of the elemental distribution of the fragments is the strong even-odd effect in the charge number of the fragments observed. The effect appears to be largest for intermediate mass projectiles (A=20 to 40) and depends on the isospin of the projectile (Knott et al., 1996, 1997). Theoretical models provide a good representation of the odd-even effect if accurate nuclear de-excitation models are used (Cucinotta *et al*., 2002, 2006b, 2007). Figure 5.2 shows comparisons of fragmentation production cross sections of the QMSFRG model with experiments for several beam energies of ^{56}Fe interacting with a variety of target nuclei. Good agreement between experiments and the QMSFRG model within 25% for most fragment cross sections has been achieved as shown in Fig. 5.3. A larger data base for cross sections for proton and neutron induced reactions now exits with recent surveys of such data provided in ICRU Report 63 (ICRU, 2000). Above kinetics energies of a few 1000 MeV/u, multiple meson production processes are dominant and reactions models based on patron or quark-gluon models can be used to describe nuclear interaction cross sections (Fasso *et al*., 2005).

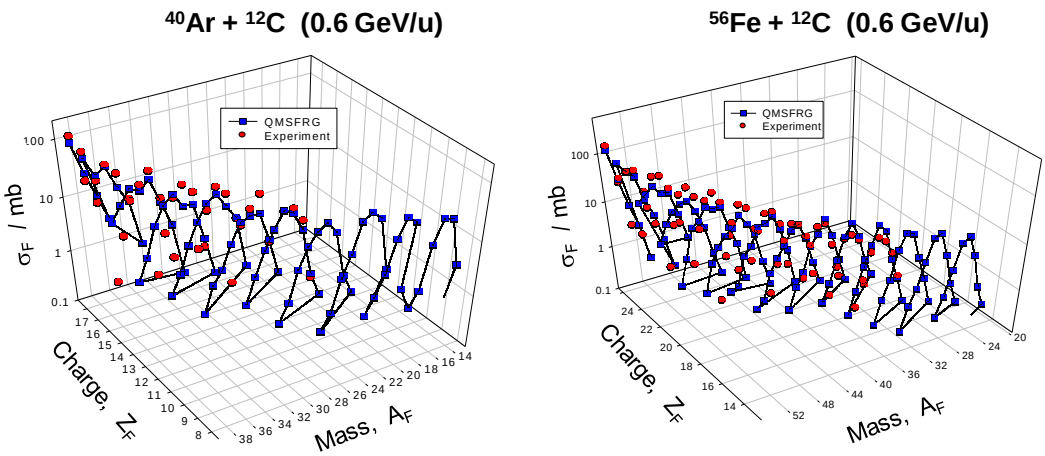

Fig. 5.2. Comparisons of the QMSFRG model (Cucinotta *et al*., 2006b) to experiment for isotopic distribution of fragments for ^{40}Ar on ^{12}C at 0.6 GeV/u (left panel) and ^{56}Fe on ^{12}C interactions at 0.6 GeV/u (right panel).

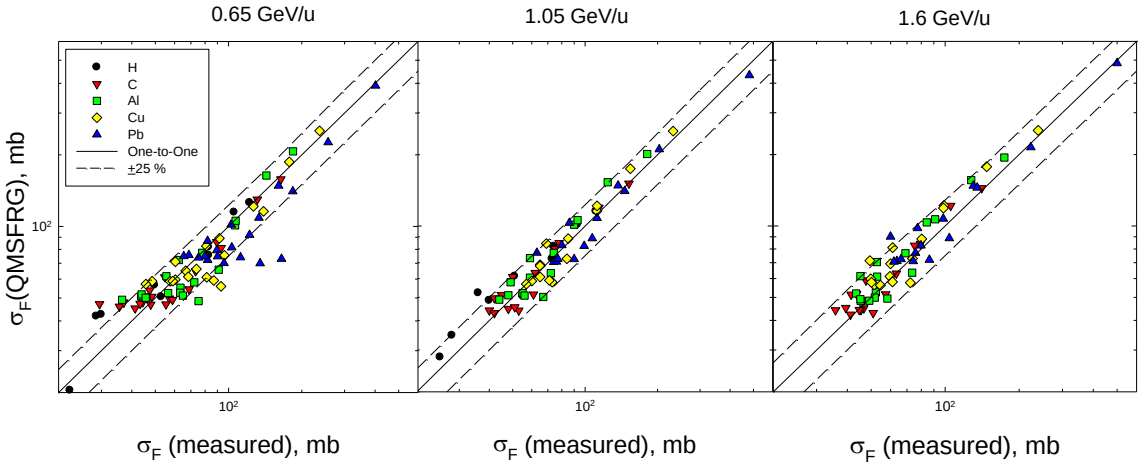

Fig. 5.3. Comparisons between experiments and the QMSFRG model for fragmentation cross sections for ^{56}Fe projectiles of different energies interacting with several target nuclei (Cucinotta et al., 2006b) where the dashed lines show ±25 % ranges of the experimental data.

(222) The momentum distribution of heavy projectile fragments is forward peaked and described as a Gaussian distribution in the projectile rest frame with a small downshift in the average momentum from the projectiles velocity. The longitudinal momentum width, σ_L, is well described by (Goldhaber, 1974):

$$\sigma_L = \sigma_0 \left[\frac{n(A_\mathrm{p} - n)}{A_\mathrm{p} - 1} \right]^{1/2} \tag{5.13}$$

where n is the number of nucleons removed from the projectile and σ_0 is approximately related to the Fermi-momentum of the projectile, p_F, by $\sigma_0 = p_\mathrm{F}/\sqrt{5}$. The transverse width is approximately the same as the longitudinal for heavier fragments. A small momentum downshift of the fragments relative to the projectile also occurs and is dependent on the fragment mass (Tull, 1990). Transformation of the Gaussian distribution to the laboratory rest frame reveals a narrow angular distribution for the projectile fragments that are strictly forward peaked in a narrow cone (<5°), which leads to the success of the straight-ahead approximation in transport models. For lighter fragments the longitudinal and traverse widths diverge and the Gaussian model breaks down. This is due to the multiple sources for light particle production including projectile abrasion, projectile ablation, target abrasion, and target ablation, as well as a possible intermediate source due to the formation of an intermediate rapidity fireball in central collisions.

5.3 Proton, neutron and heavy ion transport codes

(223) Several radiation transport codes have been developed for applications in radiotherapy, physical experiments at high-energy accelerators, detector simulations, and radiation protection in space. The different radiation transport codes utilize distinct nuclear data bases and methods including their treatment of nuclear interactions, secondary radiation, and shielding geometries. It is unlikely that space radiation problems can be handled with a one-size fits all approach and the specific application will drive the method to be used. Complex spacecraft and organ geometry are described using ray-tracing distributions, combinatorial geometry models of complex structures, or voxel based methods. Ray tracing methods are able to treat thousands of spacecraft parts accurately and can directly integrate

engineering designs in a CAD format. Ray tracing methods have only been developed for bi-directional (forward-backward scattering); however they have been shown to be quite accurate for the omni-directional radiation fields in space. Combinatorial geometry models, often used by Monte-Carlo codes, rely on approximations that paradoxically wash out the fine details of surface and angular effects that 3D-transport models are intended to describe.

(224) Models of the GCR, trapped radiation or SPE's are usually used as the boundary condition for transport codes. Several transport codes used in space applications are briefly summarized here:

FLUKA (FLUctuating KAscades)

(225) FLUKA is a general purpose Monte Carlo program for calculations of particle and photon transport (Fassò et al., 2005; Battistoni et al., 2006) which can simulate the interactions and propagation in matter of approximately 60 different particles, including heavy ions (http://www.fluka.org). The program can also describe the transport of polarised photons (e.g., synchrotron radiation) and optical photons. Photonuclear interactions can be simulated. Time evolution of the radioactive nuclei inventory and tracking of emitted radiation from unstable residual nuclei can be performed.

(226) Depending on the energies of the primary particles, hadronic interactions are simulated by different physical models. For higher energies, the Dual Parton Model is used. Below 3-5 GeV/c the PEANUT package includes a very detailed Generalised Intra-Nuclear Cascade (GINC) and a pre-equilibrium stage, while at high energies the Gribov-Glauber multiple collision mechanism is included in a less refined GINC. Nuclear interactions generated by ions are treated through interfaces to external event generators, except for the low energy (less than 150 MeV/u) range, for which a model based on the Boltzmann Master Equation (BME) has been implemented. The RQMD (Relativistic Quantum Molecular Dynamics) generator is invoked from 100 MeV/u to 5 GeV/u, and the DPMJET code is used for energies over 5 GeV/u.

(227) The transport of charged particles is described by applying a multiple scattering algorithm based on Moliere's theory of Coulomb scattering. The algorithm includes an accurate treatment of curved trajectories in magnetic fields. The energy loss is determined according to the Bethe-Bloch theory and from bremsstrahlung and pair production. Ionisation fluctuations are accounted for.

(228) For neutrons with energies lower than 20 MeV, FLUKA employs a multi-group transport algorithm, which uses a subdivision of the neutron energy range in 260 groups and is based on neutron cross section libraries containing more than 200 different materials, selected for their use in physics, dosimetry and accelerator engineering. Energy depositions for nuclei other than hydrogen are calculated by kerma coefficients.

(229) FLUKA can handle very complex geometries, using an improved version of the well-known Combinatorial Geometry (CG) package. Repetitive structures (lattices) and voxel geometries can be handled. Various visualisation and debugging tools are also available.

GEANT4

(230) The Monte-Carlo code Geant4 (Agostinelli, 2003 and Allison, 2006) states for GEometry ANd Tracking and is a software toolkit for simulating the passage of particles through matter. It has been developed and maintained by the Geant4 Collaboration which is a worldwide teamwork of physicists and software engineers (see: http://geant4.web.cern.ch/geant4). Geant4 and its predecessors were designed to utilise the

physics models, to handle complex geometries, and to enable its easy adaptation for optimal use in different sets of tasks. It has its applications in high energy, nuclear and accelerator physics as well as studies in radiation protection, medical and space science.

(231) The toolkit includes facilities for handling tracking, geometry, physics models, detector response, run management, visualisation and user interface. The software offers a large set of physical processes (e.g. electromagnetic, hadronic and optical model), different type of particles (leptons, bosons, mesons, baryons, etc) and databases with properties of matter and elements. Physics processes cover a wide range of energies which spans from 250 eV up to TeV depending on the case. Several of the modules contained in Geant4 are re-creations of physics in other codes including e. g. HZETRN, HETC. Spacecraft geometry models are available including multi-layered shielding simulation Software (MULASSIS) (Bernabeu and Casanova, 2007).

(232) The toolkit is implemented in C++ programming language making use of object oriented technique. This approach allows users effectively to manage complexity and limit dependencies by defining a uniform interfaces and common organisational principles in order to create an application for solving a specific problem.

HETC-HEDS (High Energy Transport Code-Human Exploration)

(233) HETC is a high energy Monte Carlo radiation transport code and was developed at Oak Ridge National Laboratory (Townsend et al., 2002). The code was originally developed for transport calculations with incident high-energy protons, neutrons, $\square^{+}$, $\square^{-}$, $\square^{+}$ or $\square^{-}$ only. Lateron Townsend et al. (Townsend et al., 2005) have extended the model especially for space radiation shielding applications. The code, now called HETC-HEDS, has been modified to include the transport of heavier nuclei (Charara et al., 2008).

(234) HETC-HEDS includes nucleus-nucleus cross sections, range-energy tables scaled from the proton data, and a nuclear collision module for heavy ion interactions. Nonelastic nucleon collisions and charged-pion collisions with hydrogen at energies above 3.5 GeV and 2.5 GeV, respectively, are treated by using calculational methods that utilize experimental data for the total non-elastic n-p, p-p, $\square^{+}$-p and $\square^{-}$-p cross sections and analytic fits to experimental data. The intra-nuclear-cascade evaporation concept of particle-nucleus interaction is used to determine the effect of particle-nucleus collisions below 3.5 GeV for nucleons and 2.5 GeV for charged pions. Following the intranuclear-cascade, the excitation energy left in the nucleus is treated using an evaporation model. The particles allowed during evaporation include protons, neutrons, d, ^{3}H, ^{3}He, and ^{4}He.

(235) HETC-HEDS used the combinatorial geometry package so virtually arbitrary geometries are allowed. Each particle in the cascade is followed until it eventually disappears by escaping from the geometric boundaries of the system, undergoes nuclear collision or absorption, comes to rest due to energy losses from ionisation and excitation of atomic electrons, or decays in the case of pions and muons.

HZETRN (High charge (Z) and Energy Transport code)

(236) HZETRN was developed by Wilson et al. (1991, 2004) at NASA. It solves the Boltzmann equation using numerical methods. The early version used the straight-ahead approximation but more recent versions use bi-directional transport or 3D transport for laboratory studies (Wilson, et al., 2009). Recently ray tracing representations of voxel models of human geometries have been developed (Slaba et al., 2009). Nuclear interactions are treated by the NUCFRG2 Model (Wilson et al., 1994a) or QMSFRG model (Cucinotta *et al.*,

2007) with proton and neutron cross sections described by the Bertini and Ranft models. To treat complex radiation geometries ray tracing methods are utilized, which is powerful because spacecraft engineers can utilize their designs directly in the transport code evaluations. Computer runs on small computer workstations can be performed in less than one hour for complex spacecraft geometries with multi-layer materials and deep shielding conditions (>100 g/cm^2) combined with models of the organ shielding of the human body.

MCNPX (Monte-Carlo N-Particle eXtended)

(237) The Los Alamos Monte-Carlo code MCNPX (see: http://mcnpx.lanl.gov) and its predecessors are very widely distributed (Waters, 2002; Pelowitz, 2008).The code is capable of tracking many particle types (nucleons and light ions) and over 2000 heavy ions up to very high energies. It uses standard evaluated data libraries for neutrons, photons, electrons, protons and photonuclear interactions and uses physics models for other particle types and at energies for which tabular data are not available.

(238) Current physics modules include the Bertini and Isabel models taken from the LAHET Code system, CEM 03, and INCL4 (James et al., 2009). The incorporation of a heavy ion physics model has enabled the transport of recoil nuclei. This model automatically transports all residuals that are produced from any reaction even if the source particle is not a heavy ion. Current stopping powers for heavy ions have been adjusted in an *ad hoc* fashion (Pelowitz, 2008) so that they better match SRIM results (Ziegler et al., 2008). Charged particles are slowed down to a lower total energy limit of 5 MeV, at which point their remaining energy is locally deposited.

PHITS (Particle and Heavy-Ion Transport code System)

(239) The Monte-Carlo radiation transport code PHITS (see: http://phits.jaea.go.jp) was developed under collaboration with several institutes including JAEA, RIST, KEK and Chalmers University of Technology (Niita et al., 2010; Sihver et al., 2010a). Nuclear interactions are described by various models such as JAM and JQMD up to 100 GeV/u. The code can determine the energy of charged particles emitted from low-energy neutron-induced nuclear reactions, using the event generator mode (Iwamoto et al., 2007, Niita et al., 2007) in combination with nuclear data libraries. This feature enables the direct calculation of dose equivalent in organs or tissues which cannot be calculated by employing the conventional kerma approximation. The accuracy of the code for use in space dosimetry was well verified by calculating neutron spectra inside Space Shuttle (Sato et al., 2006) and doses inside anthropomorphic phantoms (Sato et al., 2011), using simplified geometries of spacecraft. The code is also used for the computational analyses of the MATROSHKA and MATROSHKA-R experiments in space (Sihver et al., 2010b and Koliskova et al., 2012).

5.3.1 Inter-comparison and validation of radiation transport codes

(240) An assessment of the accuracy of space radiation transport models for prediction of energy spectra of charged particles and neutrons after primary radiation has passed matter can be made by comparisons to laboratory experiments with proton and heavy ion beams or from measurements in spacecraft. Spaceflight measurements, however, involve many factors such that potential inadequacies in radiation transport models are difficult to isolate relative to possible inaccuracies in environmental or shielding models. Also, space validation is limited by the access to space and current spacecraft materials, and may not be representative of

model predictions for other material types such as those that occur on planetary surfaces or in advanced materials selection concepts. In this respect, laboratory validation is advantageous to validate radiation transport computer codes and associated data base models and to provide tests for studying material properties for reducing biological doses (Schimmerling *et al*., 1999). Nevertheless, spaceflight measurements provide important tests of predictive capability of several factors and are needed for final validation of transport codes.

(241) Recently an extensive benchmarking of the calculated projectile fragmentation cross-sections from the reactions of 300 - 1000 MeV/u Si-28, Ar-40, and Fe-56 ions on polyethylene, carbon, aluminum, and copper targets (relevant to space radiation protection) has been carried out using PHITS, FLUKA, HETC-HEDS, and MCNPX. Calculated results were compared with measurements (Sihver et al., 2008).

(242) An over-all "reasonable" agreement between calculations and measurements was found. However, a general trend of a slight underestimation of the calculated fragment production cross-sections (partial charge-changing cross-sections) has been observed. The code HETC-HEDS seems to underestimate these cross-sections more than the other codes included in this benchmarking. PHITS also seems to underestimate the total charge-changing cross-sections, which is in agreement with other observations (Sihver et al., 2007).

(243) A recent inter-comparison of transport codes for SPE and GCR test cases indicates fairly good agreement between the various codes (Wilson *et al*., 2009; Heinbockel *et al*., 2011). Fig. 5.4 shows comparisons of results of depth-dose distributions from different codes for a large SPE. Fig. 5.5 shows a comparison of energy spectra of secondary particles produced by protons and Helium ions of GCR at solar minimum calculated with various codes.

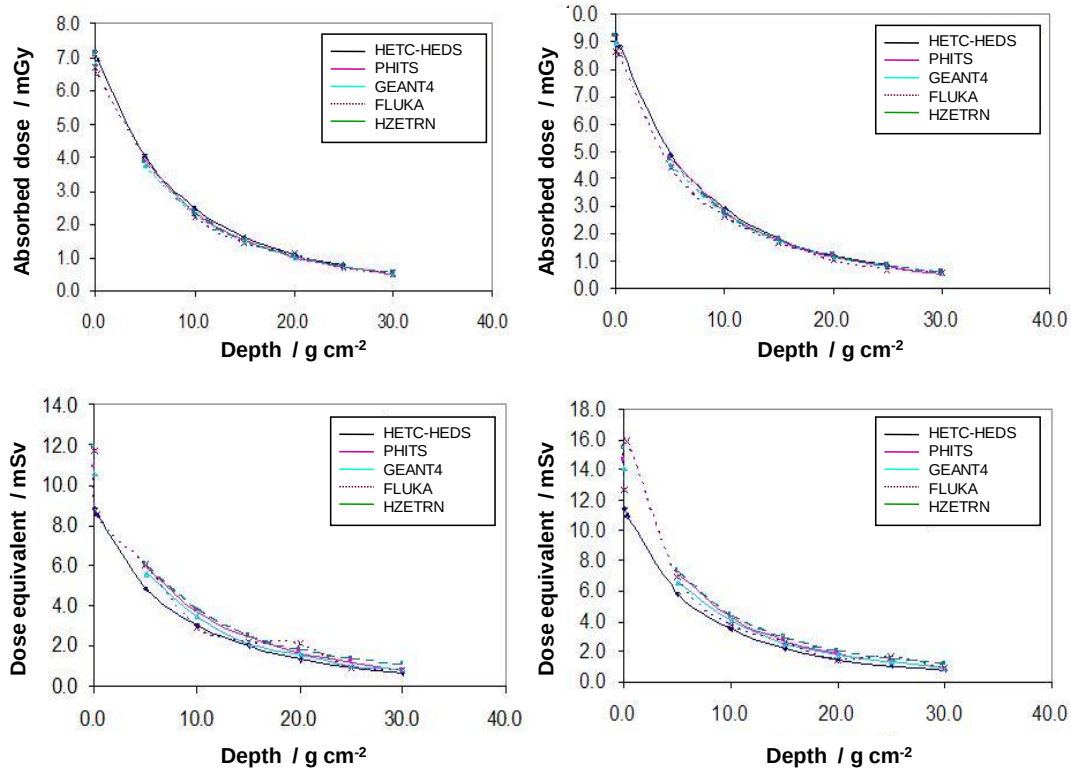

(a) Aluminum shielding **(b) Iron shielding**

Fig. 5.4. Inter-comparison of transport codes for depth-dose distributions of absorbed dose and dose equivalent from solar particle events in aluminum and iron shielding (Wilson et al., 2009).

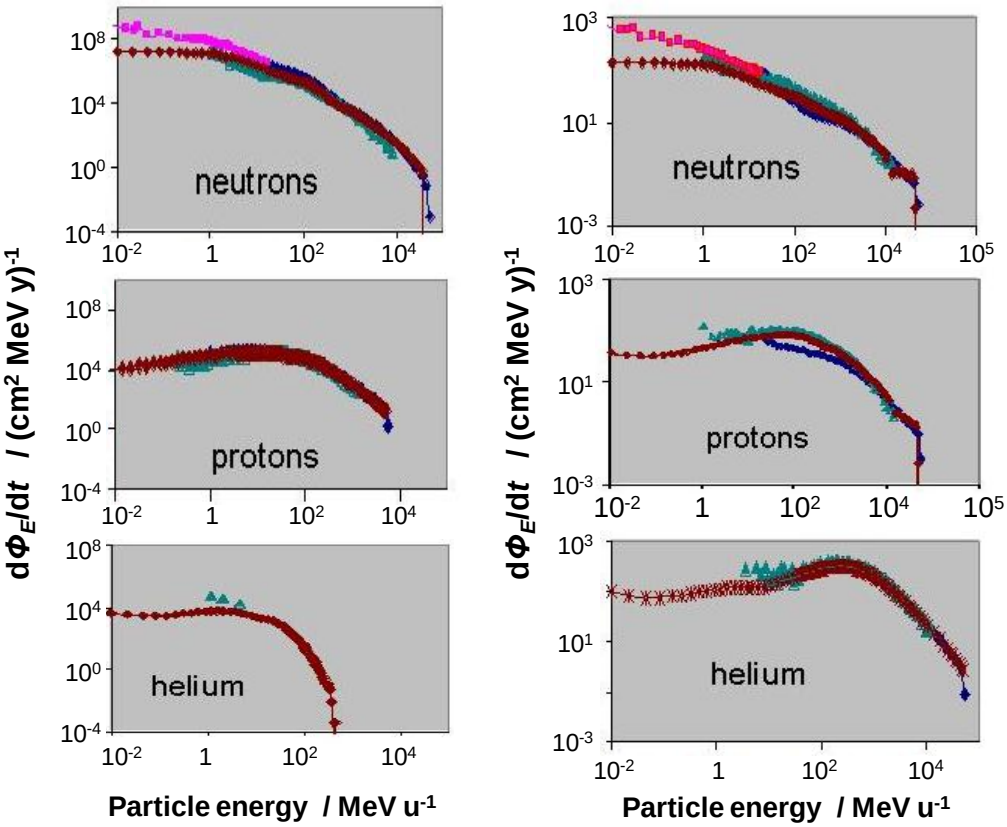

a) GCR protons b) GCR helium ions

Fig. 5.5. Inter-comparison of energy spectra (spectral fluence rate, $d\Phi_E/dt$) of light ions from GCR at solar minima calculated by different transport codes (Wilson et al, 2009).
♦ HETC-HEDS, ▲ Fluka, ♦, * HZETRAN2006

5.4 Radiation Fields inside spacecraft

(244) Radiation fields inside spacecraft are determined by the external radiation incident on the spacecraft and the secondary radiation produced by the interactions with the walls and the equipment inside and outside the spacecraft. The internal radiation field varies with time due to the variation of the external radiation (see Chapter 2) and with the location in the spacecraft due to the specific arrangement of the equipment and the shielding properties of the different walls and spacecraft components. Important effects are absorption, scattering, and degradation of the primary radiation, and production of secondary radiation. Hence the radiation field inside a spacecraft –and also in the outer region near to the spacecraft – includes projectile and target fragment, neutrons, photons, pions and muons in addition to the radiation components of the primary field. Assessment of the inner radiation field and its components can be performed either by measurements or by simulations using environmental models and radiation transport codes.

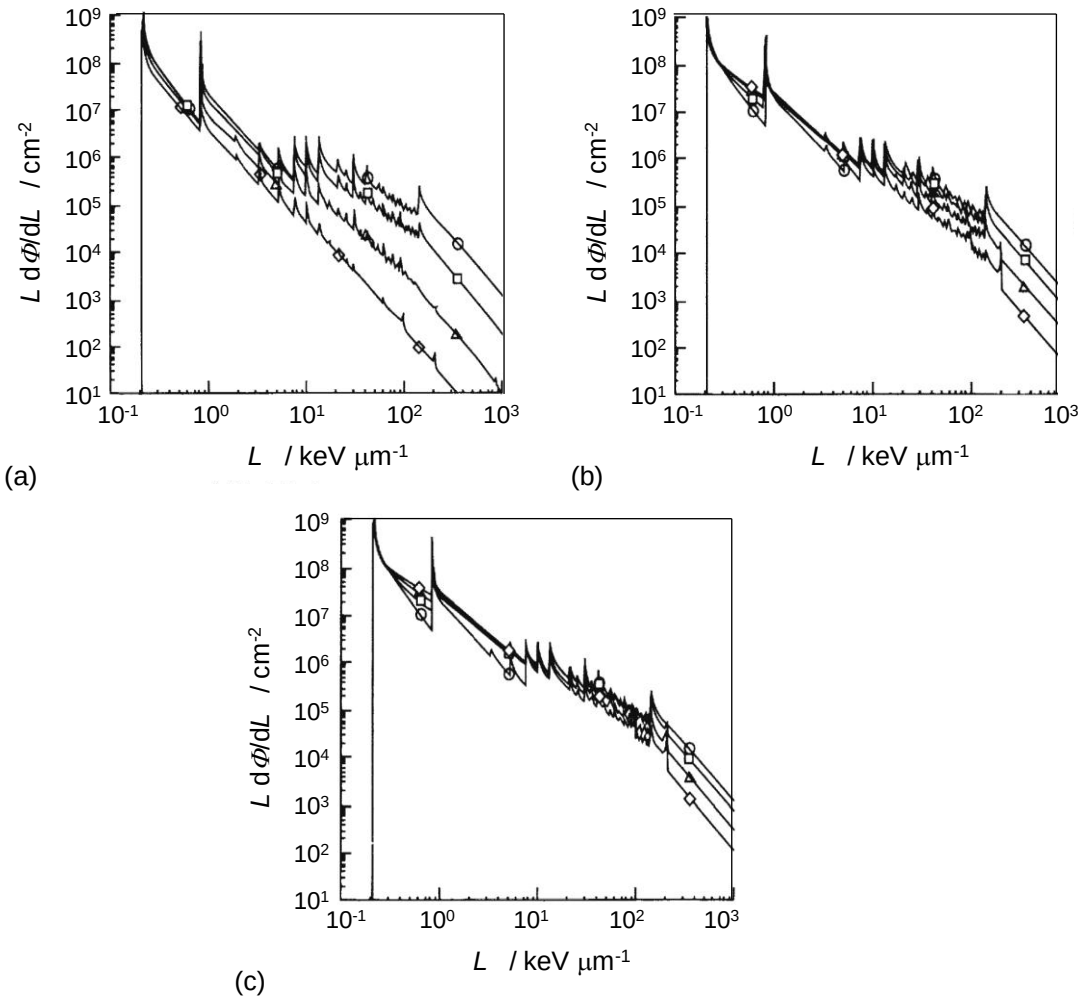

Fig. 5.6. LET distribution of particle fluence in space calculated using the HZETRN code for increasing amounts of liquid hydrogen, water, and aluminum shielding (Wilson et al., 1995c). ○ without shielding; with shielding thickness of □ 5 g cm^{-2}, Δ 15 g cm^{-2}, ◊ 30 g cm^{-2}.

(245) The exterior environment is modified by the types and amounts of radiation shielding. The LET distributions of particle fluence for increasing amounts of liquid hydrogen, water or aluminum shielding are shown in Fig. 5.6. The higher fluence at large values of LET (>50 keV/μm) for aluminum compared to the other materials is due to the contributions of secondary neutrons and charged particles produced in the shielding, which is reduced for materials containing hydrogen.

(246) The measurements on NASA space shuttle (STS) flights over many years and on the Russian space station MIR have allowed for a large number of comparisons of radiation transport calculations to flight measurements (Cucinotta et al., 2000b**)**. Passive measurements with nuclear etched track detectors (PADC) have limitations at both low LET (< 5 keV/μm) tracks and short-tracks from target fragments or stopping GCR ions of high-LET tracks. The use of active dosemeters on STS flights has allowed for separation of GCR contributions from that of trapped protons which is not possible with passive dosimetry (Badhwar and Cucinotta, 2000). Active detector measurements include tissue equivalent proportional counters, charged particle telescopes (Badhwar et al., 1995), and active Bonner spheres embedded with proportional counters (Koshiishi et al., 2007).

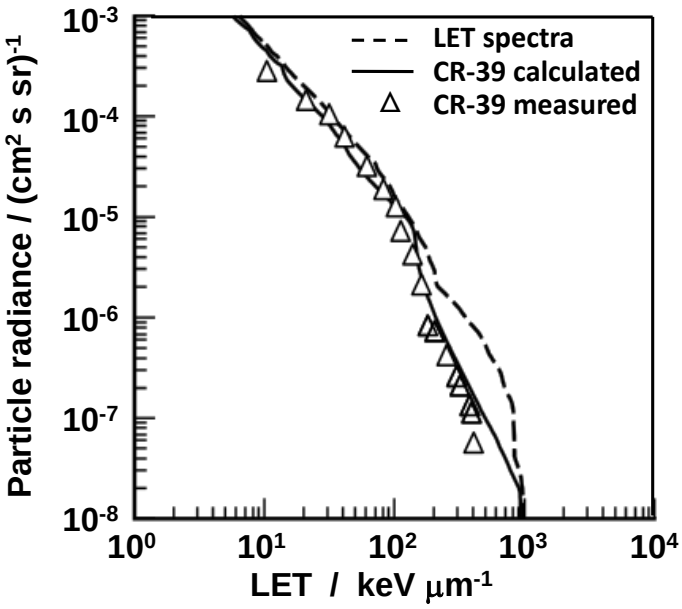

Fig. 5.7. Comparisons of LET distributions of particle radiance measured by nuclear etched track detectors (CR-39) to LET distributions and model calculations of LET distributions on Space shuttle mission (Wilson et al., 1994b, Shinn et al., 1998).

(247) Measurements on STS flights were performed by Badhwar et al. (2000) using a cylindrical tissue equivalent proportional counter (TEPC) with a length-to-diameter ratio of 1 simulating a 2 μm diameter site and covering a lineal energy range of 0.25 keV/μm to 1250 keV/μm. TEPC measurements on several missions in space have been compared to calculations using HZETRN for total dose and dose equivalent. The comparisons use the free space GCR model of Badhwar and O'Neill (1992) and representations of the STS or Mir shielding distribution around the detectors. The difference is found to be less than 15% for the majority of the comparisons. A comparison of LET distributions measured by PADC and calculated using the HZETRN code is shown in Fig. 5.7. They show a good agreement when the response of the PADC to short tracks is additionally considered (Wilson, et al., 1994b, Shinn et al., 1998).

(248) Particle energy distributions measured on STS-48 are shown in Fig. 5.8. Charged particle telescopes are used which provide measurements of the energy spectra of light particles from about 15 MeV to 400 MeV for protons and other Z=1 and Z=2 ions from 5 MeV to 70 MeV/u (see above). These measurements are strictly secondary radiation due to the Earth's geomagnetic cut-offs, which exclude particles below a few hundred MeV/u from entering the spacecraft orbit. Excellent agreement with the HZETRN code for protons is found. For deuteron spectra the agreement is satisfactory only when knockout deuterons from proton and neutron induced reactions are included. For ^{3}He and ^{4}He the agreement is less satisfactory, and may point to a deficiency in the evaporation cross sections of the FLUKA model used by HZETRN.

(249) Detailed simulations of the radiation environment in the ISS from trapped proton radiation have been performed by Wilson et al. (2007) using the HZETRN code and Ersmark et al. (2007) using the Geant4 code. The anisotropy of the radiation field due to variation in shielding has also been studied.

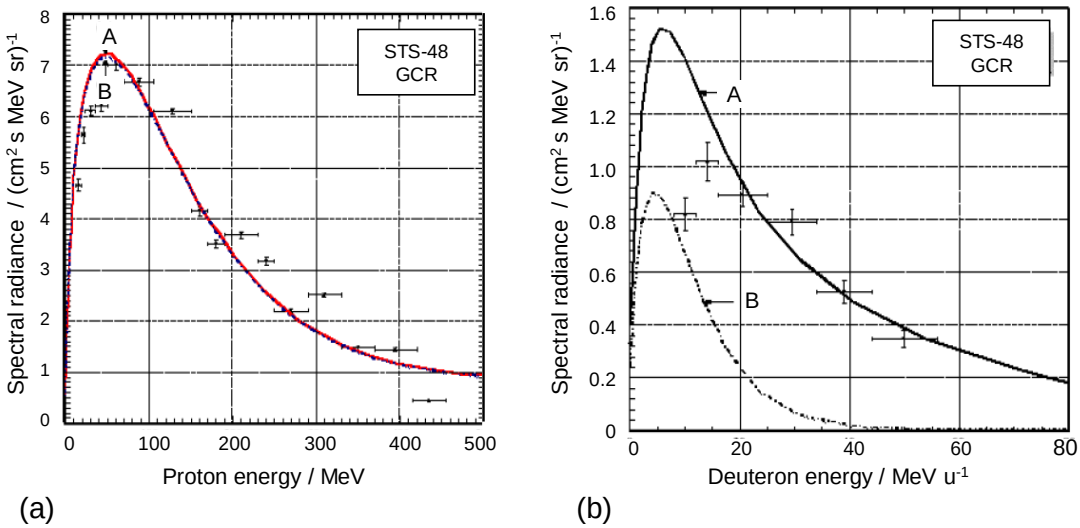

Fig. 5.8. Comparison of calculated (HZETRN code) and measured energy distributions of secondary protons (a) and deuterons (b) from GCR during STS-48 (Badhwar et al., 1995). Calculated proton and deuteron radiance (A) including knockout particles from proton and neutron induced reactions, (B) without those contributions.

5.5 Radiation Shielding

(250) Shielding models are applied for the spacecraft and spacesuits and allow evaluation of the interior environment to which the astronauts are exposed. The models describe the distribution of materials in the walls of and within the spacecraft and appropriate computational procedures are used to evaluate the interior field of transmitted particles. The internal environment, especially which based on protons from the SAA, shows a non-homogenous distribution with large spatial gradients and variations with time over both short-term and long-term temporal scales.

(251) With the exception of the absolute intensity of the trapped environment and possible solar particle events, the interior radiation environment can be well described using computational models. High-speed computational procedures allow rapid mapping of the interiors of the spacecraft.

(252) The interior environment of the spacecraft is also monitored by various instruments, which can be used to adjust the trapped-particle intensity, reduce the uncertainty in the model estimates, evaluate transmission factors, and evaluate calculated dosimetric quantities.

(253) Materials with light constituent atoms, such as hydrogen are most efficient per unit mass of material at slowing down ions, attenuating heavy ion projectiles through projectile fragmentation, and minimizing the build-up of neutrons and other target fragments produced directly from the shielding by nuclear interaction. Energy loss through ionisation is proportional to the number of electrons per atom (Z/A) where Z is the charge number and A the mass number, and the energy loss per unit mass is proportional to (Z/ρA) where ρ is the density of the material. For the GCR, materials such as aluminum (the most common spacecraft material) have relatively flat depth-dose equivalent responses due to the build-up of light particles in balance with the attenuation of heavy ions (Wilson *et al.*, 1995a). Materials, such as concrete or lead, have a response to the GCR that is predicted to increase the dose with shielding depth because of the large production of neutrons and target

fragments. Spacecraft materials are often deficient in hydrogen and therefore neutron spectra will change appreciably in the first few cm of tissue as low-energy neutrons (< 5 MeV) are produced more frequently compared to aluminum or other common spacecraft materials.

(254) For a given area density and a given incident charged particle, ionisation energy loss increases with the charge-to-mass ratio of the target nucleus (Z_T/A_T), while the fragmentation cross section per unit mass is proportional to $A_T^{-1/3}$. Hence, hydrogen is the most efficient material for shielding against heavy ions, and materials abundant in loosely bonded hydrogen atoms are excellent candidates for efficient radiation shielding.

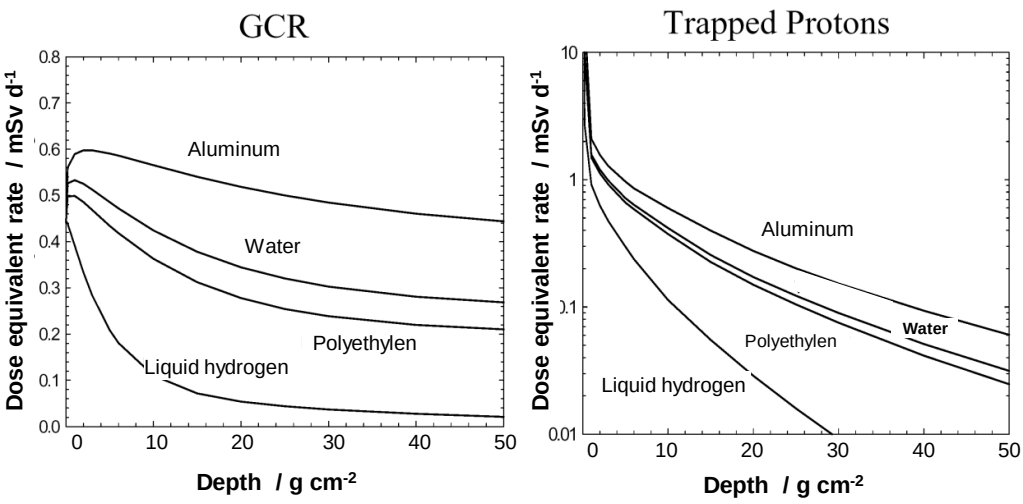

Fig. 5.9. Calculated dose equivalent rate in tissue versus shielding thickness for different shielding materials in the ISS orbit for GCR and trapped protons and solar minimum conditions (Cucinotta et al., 2000b)

(255) Having just one shielding material is an ideal case, which will in practice be very hard to realize. The final shielding effectiveness will therefore also depend on the geometry and the abundance of the various other materials used in the shielding. Ultimately, detailed simulations will always be mandatory in evaluating and designing a realistic spacecraft or habitat. Simulations suggest that shielding is effective against trapped protons in LEO, but its efficiency is poor against GCR penetration. This is demonstrated clearly in Fig. 5.9.

(256) In case of thicker shields, the neutrons, which as primary components of space radiation are negligible, can become a noticeable source of radiation exposure. This occurs not only in heavier shielded spacecraft but also on planetary or lunar surfaces which lack an atmosphere thick enough to attenuate the primary radiation source to a reasonably low level. On the surface of Mars and even more so of the Moon, these secondary “albedo” neutrons emerging from the ground contribute significantly to the overall exposure, in particular, since neutrons are high-LET radiation with a high radiobiological effectiveness.

(257) There is an immense body of work already done in developing shielding strategies for human space exploration missions. This activity resulted in numerous workshops and publications in this field (Wilson et al., 1995a; Durante and Cucinotta, 2011). As mentioned above, all calculations and measurements show that hydrogenous materials are the best candidates per unit mass basis. The next set of figures (Fig. 5.10) taken from Wilson et al. (2001) shows this clearly for cosmic ray spectra on Moon and Mars and a worst-case SPE.

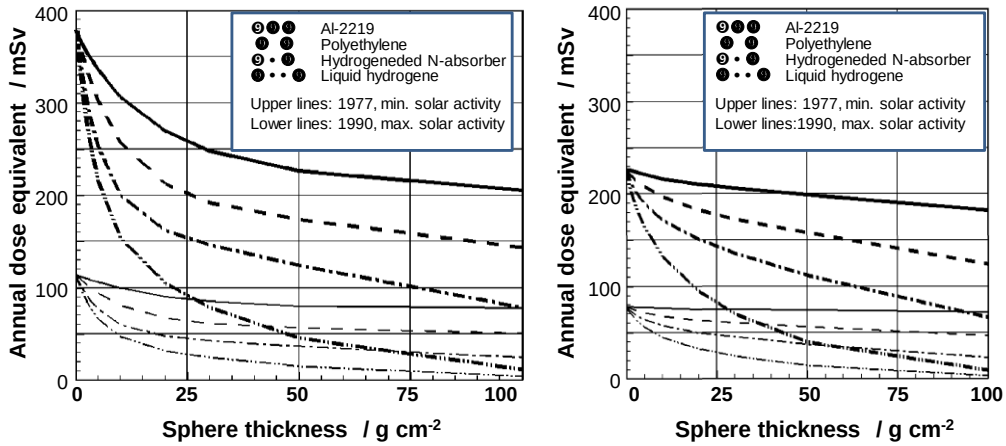

(a) GCR at the Moon (left) and Mars (right)

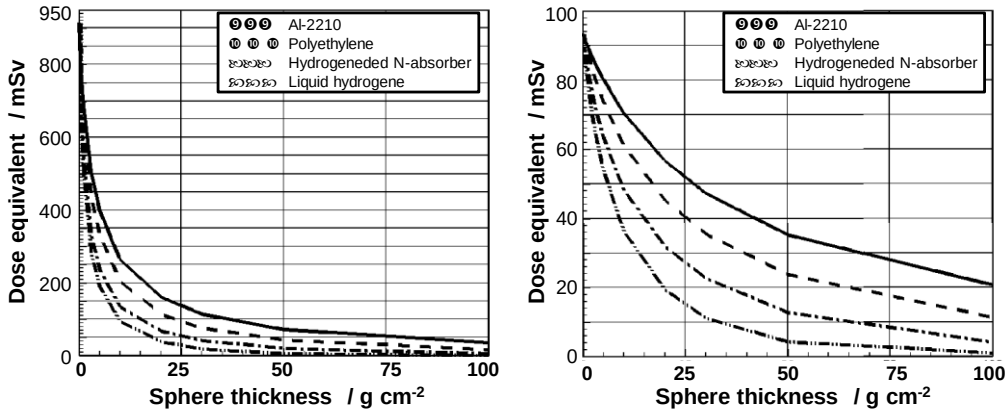

(b) Worst Case SPE at the Moon (left) and Mars (right)

Fig.5.10. Set of calculations showing dose equivalents for different shielding materials versus shielding thickness on the surface of Moon (left) and Mars (right) for GCR (a) and a worst-case SPE (4x the fluence of the SPE on Sept. 1989) (b) (Wilson et al., 2001)

(258) Much of the protection inside a spacecraft is provided by structural elements and the equipment present in it. For the structure of the spacecraft, a compromise between shielding efficiency and mechanical stability needs to be chosen, with multifunctional materials needed to optimize the process. For a shelter inside the spacecraft there are not such restrictions – if the material is acceptable for space application – and the efficiency per mass is the only important endpoint. Some recent studies were performed for different shielding materials as shown in Fig 5.11 for vertical incidence (Zeitlin et al., 2006). The effect of the incidence angle of the particles in producing secondary neutrons is complex and exhibits a strong interaction with the type of the shielding material. Such studies of course need to be extended.

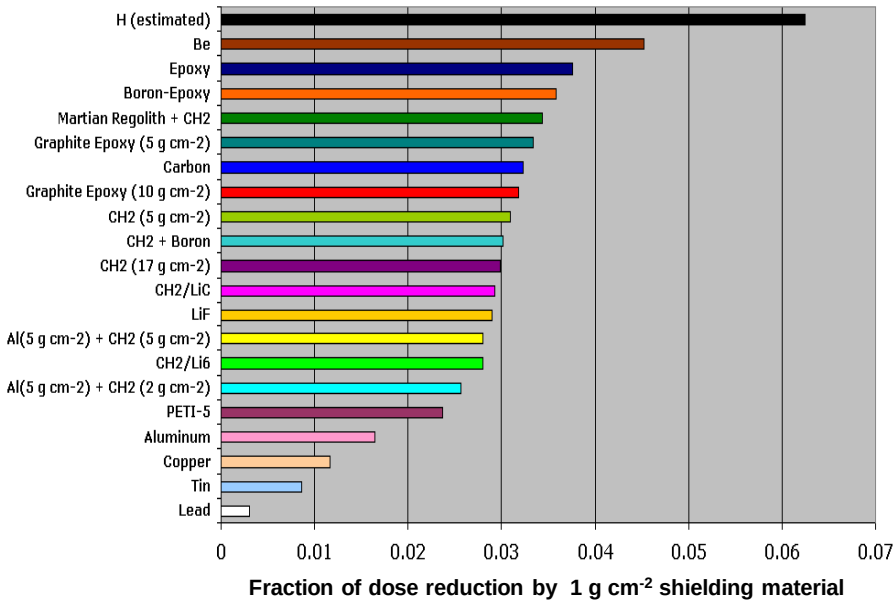

Fig 5.11. Fraction of dose reduction in a body by a 1 g cm^{-2} thick shielding for different shielding materials and incident Fe particles of 1067 MeV/u. (Zeitlin et al., 2006)

(259) Since the earliest attempts at in situ space radiation dosimetry, it has been known that - even for the most simple transport problems - satisfactory agreement between measurements and calculations would not be attainable unless the detailed thickness distribution around the point of interest were known, especially if areas of thinner shield were present. Therefore estimates of radiation exposures for 'homogeneous' 'isotropic' shields of an 'average' thickness can only serve for qualitative comparison of different configurations. For accurate quantitative assessments of radiation exposures, the knowledge of the distribution of the surrounding shield matter as a function of representative shield thickness is essential.

(260) Shielding to galactic cosmic radiation is generally limited. Nevertheless, with the selection of optimized shield material and an optimal inclusion of consumables in the shield design, a significant dose reduction of about 30 % can be achieved at solar minimum and to a lesser extent at solar maximum. For SPE's the reduction is highly dependent on the initial proton spectrum; however shielding can reduce effective doses by factors of 2 to more than 10. As a first step definition, procurement and characterisation of candidate flexible materials – to be used in future manned missions in LEO and beyond, for inhabited structures has to be done. Computer codes are the tool to make the characterisation of such materials. The next step is the improvement and validation of the models and tools for shielding analysis, by comparison with measurements from accelerator shielding studies and with flight measurements, correlation and tuning of models, with the objective of reducing the overall uncertainty.

5.6 Lunar and Mars Surface

(261) There are two effects strongly influencing the radiation environment on planetary or lunar surfaces compared to the GCR in free space. Because of the shielding of the ground, the cosmic radiation is incident on the surface only in 2π-geometry. In addition, from the surface of Mars or the Earth's Moon, albedo radiation occurs. Photons, neutrons or secondary

charged particles produced by neutrons will occur and will be dependent on the soil and atmospheric (on Mars) atomic composition including the presence of CO_2 or water frost and higher neutron fluence rate from lunar or Mars regolith (Clowdsley et al., 2000). Neutrons may be divided into a forward component produced by GCR interactions with the atmosphere and albedo components on planetary surfaces such as Mars. Albedo neutrons may be produced as deep as 1 meter into the soil and their flux will be influenced by the soil composition and seasonal variations in temperature as illustrated in Figure 5.12. Large dust storms on Mars could lead to additional scattering of neutrons and charged particles (Wilson et al., 1995a).

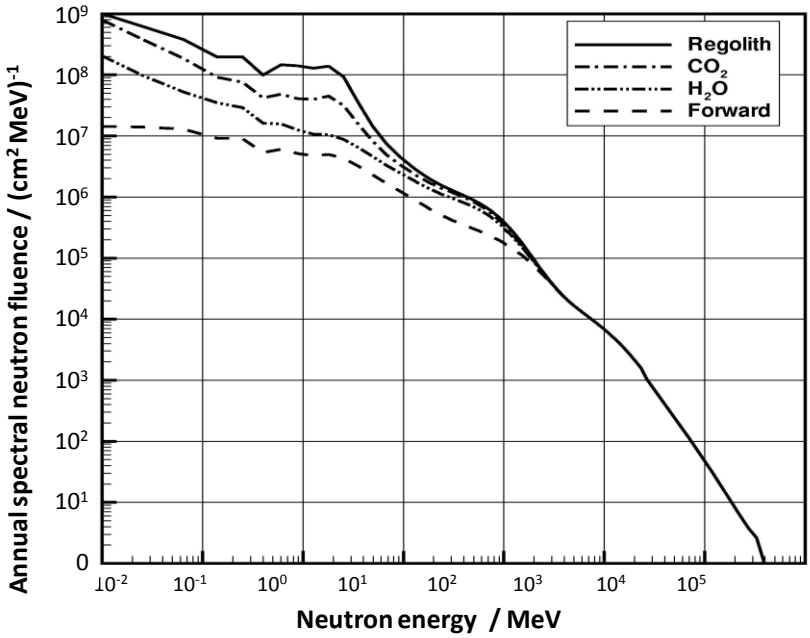

Fig. 5.12 Energy distribution of neutron fluence on the Mars surface calculated with HZETRN showing the annual contributions from the forward component produced by GCR in the Mars atmosphere and the albedo component that are dependent on the composition of the Mars surface (Wilson et al., 2004).

6. RADIATION FIELDS AND DOSES IN THE HUMAN BODY

(262) The radiation fields inside astronauts differ from those outside because of atomic and nuclear interactions in the human body. The analysis of particle transport inside the body is indispensable for the estimation of doses in astronauts and risks of both stochastic and deterministic effects due to cosmic radiation exposures. Various simulation codes (see 5.3) and computational phantoms, which represent the anatomy of human body or parts thereof, have been employed for this analysis. In radiological protection, the mean absorbed dose in an organ or tissue, D_T, is the basic quantity for a specification of doses in humans (see Chapter 3). In addition, appropriate weighting factors need to be applied to D_T for the assessment of risk of stochastic or deterministic detriments due to radiation exposure.

(263) Generally, two different procedures may be applied for the assessment of doses in

the human body, either by calculations or by measurements combined with calculations. Radiation field parameters, e. g. particle fluence, particle spectra and LET-distributions, outside or within a spacecraft may be determined either by measurements or calculations and then doses in organs and tissues of the human body may be calculated using particle transport codes. There are two possibilities in performing this task. One may either assess the radiation field parameters (e.g. energy distribution of fluence, $D(L)$-distributions etc.) (Section 5.3) near to an astronaut and then apply fluence-to-dose conversion coefficients for all types of particles involved for the assessment of organ doses (see Sect. 6.2) or one can generally calculate organ doses in a body using the radiation field data outside of the spacecraft and a code which combines radiation transport in the spacecraft and in the human body (see Sect. 6.3).

(264) Alternatively, absorbed dose or dose equivalent may be measured near to the body of the person of interest and these values may be directly correlated to doses in the human body. This is the usual procedure performed in individual dosimetry on the Earth, where the reading of an individual dosemeter for strongly-penetrating radiation is taken as a value of effective dose sufficiently precise for the purpose of usual radiological protection. In space, however, this method is a difficult task because of the very complex radiation field, which also shows variations with time and position within a spacecraft. As shown in Chapter 4, no single device will probably be able to fulfil this task, and a set of different detectors may be necessary for the assessment of dose equivalent in an organ or tissue or effective dose equivalent. The position and orientation of a person within the spacecraft can introduce variations in organ doses due to the anisotropic spacecraft shielding distributions, which can be important for solar protons and trapped radiation (Wilson et al., 1995c). In any case, particle transport calculations need to be used for testing if a system is appropriate for the foreseen task.

6.1 Phantoms

(265) The first computational phantom was developed at the Oak Ridge National Laboratory (Snyder et al., 1969) for the Medical Internal Radiation Dose (MIRD) Committee of the Society of Nuclear Medicine. The MIRD phantom designed as a hermaphrodite including organs and tissues of both sexes has been widely used in varieties of the radiation protection researches, in combination with various Monte Carlo codes. On the other hand, the Computerized Anatomical Man (CAM) (Billings and Yucker, 1973) and Computerized Anatomical Female (CAF) (Yucker and Huston, 1990) phantoms were developed in 1973 and 1990, respectively. They have a long history in space radiation research at NASA, in combination with the transport code HZETRN. These phantoms are based upon mathematical expressions representing planes, and cylindrical, conical, elliptical and spherical surfaces that describe the shape and position of idealized body organs.

(266) As an extension and improvement to these earlier models, various groups have developed a new type of anatomical phantom during the last two decades, called “tomographic” or “voxel” phantom. Voxel phantoms are anatomical models based on computed tomography, magnetic resonance, or other images obtained from high-resolution scans of a single individual and, thus, offer a more realistic replication of human anatomy. They consist of a large number of volume elements (voxels) and are the most detailed representation of human anatomy at the present time. However, being derived from a specific individual, these models do not represent the average Caucasian man or woman as defined by Publication 23 (ICRP, 1975) and Publication 89 (ICRP, 2002). To avoid this inconsistency,

the Commission introduced reference voxel phantoms representing the adult Reference Male and Reference Female defined in Publication 110 (ICRP, 2009), which were constructed based on medical image data of real persons, but their anatomical parameters were modified to be consistent with those given in Publication 89. These phantoms are used by the Commission in establishing radiation protection guidance and reference data, e.g. conversion coefficients for dosimetric quantities. NASA has used the voxel approach based on the MAX/FAX voxel model in a ray tracing approach appropriate for the HZETRN code (Slaba et al. 2010, Kim et al., 2010b)

(267) One limitation of the phantoms is that their resolutions are not high enough to reproduce the thin structure of a tissue or organ located at or near to the surface of human body, e.g. skin and lens of the eye. This causes both overestimation and underestimation of doses in such tissue and organ for the irradiation by low-energy particles such as trapped protons and electrons. Thus, special procedures are required to precisely calculate the dose in such tissues or organs, using the phantoms. A more detailed description on this issue is given in Publication 110 (ICRP, 2009).

(268) For realization of anthropomorphic phantoms, several materials such as water and tissue-equivalent plastics are used on ground. On the other hand, only solid plastic phantoms can be launched to space for practical reasons. The RANDO® phantoms of head and upper torso had been mounted on the Space Shuttle (Konradi et al., 1992, Yasuda et al., 2000, Badhwar et al., 2002) and the ISS (Cucinotta et al., 2008). The other RANDO®phantom had been exposed outside the ISS as a part of the MATROSHKA project (Reitz et al., 2009). A spherical phantom composed of tissue-equivalent plastic has also been mounted on the ISS as part of the MATROSHKA-R project (Shurshakov et al., 2004). A number of passive and active detectors were inserted in or attached on the phantoms. The data obtained from the detectors are useful in validating the accuracy of particle transport simulations performed using the computational phantoms.

6.2 Dose conversion coefficients

Mean absorbed dose in organs and tissues

(269) For a given organ T and radiation type R, the mean absorbed dose in the organ, $D_{\mathrm{T,R}}$, can be obtained folding the energy distribution of the fluence of particles incident on the human body with the fluence-to-absorbed dose conversion coefficients for that organ, $d_{\mathrm{T,R}}(E)$. It is:

$$D_{\mathrm{T,R}} = \int_0^\infty d_{\mathrm{T,R}}(E)\frac{\mathrm{d}\Phi_{\mathrm{R}}}{\mathrm{d}E}\mathrm{d}E \quad , \tag{6.1}$$

where Φ_{R} is the fluence of particles of type R incident on the body. Because conversion coefficients, $d_{\mathrm{T,R}}$, are mainly available for a homogeneous exposure of the human body, only, the application of this equation assumes always a uniform exposure of the body. In cases where this assumption is not approximately satisfied, further considerations are needed for the application of this approach.

(270) For assessing organ doses it is necessary to have conversion coefficients for all organs and tissues of the human body, for all particles and energies of interest and for the real geometry of irradiation.

(271) For the calculation of conversion coefficients, an exposure of a mathematical anthropomorphic phantom is simulated for the incidence of monoenergetic particles according to simple geometries, mostly homogeneous frontal incidence (AP), incidence from

the right or left side (RLAT, LLAT), from the back (PA) or rotational (ROT) and isotropic (ISO) exposure. The isotropic irradiation is usually assumed to appropriately describe the exposure of astronauts to cosmic radiation, mainly due to the isotropic fluence rate of the GCR and the movement of the astronauts in the spacecraft. Nevertheless, this assumption may not always represent the situation well (Wilson et al., 1995c).

(272) The absorbed dose in the various organs and tissues of the human body are estimated from the energies deposited in the regions assigned to each organ divided by their masses. In the case of the voxel phantoms the mean absorbed doses in the organs are estimated from the energies deposited in the voxels assigned to each organ divided by the organ mass. This method has been applied in most organs, including skin, for the calculations of the conversion coefficients adopted by the Commission. Exceptions are the red bone marrow and bone surface (endosteum), which are tissues not explicitly defined in the reference phantoms. According to Schlattl et al. (Schlatt et al., 2007), the mean absorbed dose in red bone marrow, D_{RBM}, and in endosteum, $D_{\mathrm{Endosteum}}$, are determined respectively by

$$D_{\mathrm{RBM}} = \sum_{\mathrm{i}} \frac{m_{\mathrm{RBM,i}}}{m_{\mathrm{RBM}}} D_{\mathrm{spongiosa,i}} \tag{6.2}$$

and

$$D_{\mathrm{Endosteum}} = \sum_{\mathrm{i}} \frac{m_{\mathrm{Endosteum,i}}}{m_{\mathrm{Endosteum}}} D_{\mathrm{spongiosa,i}} \tag{6.3}$$

where $m_{\mathrm{RBM,i}}$ is the mass of RBM in i-th spongiosa region, m_{RBM} the total mass of RBM, $D_{\mathrm{spongiosa,i}}$ the dose of i-th spongiosa region, $m_{\mathrm{Endosteum,i}}$ the mass of endosteum in i-th spongiosa region and $m_{\mathrm{Endosteum}}$ the total mass of endosteum.

(273) As an example, conversion coefficients for red bone marrow and gonads, respectively, published by the Commission for isotropic irradiation of the reference adult male and female phantoms are shown in Fig. 6.1 as a function of neutron energy (ICRP, 2012).

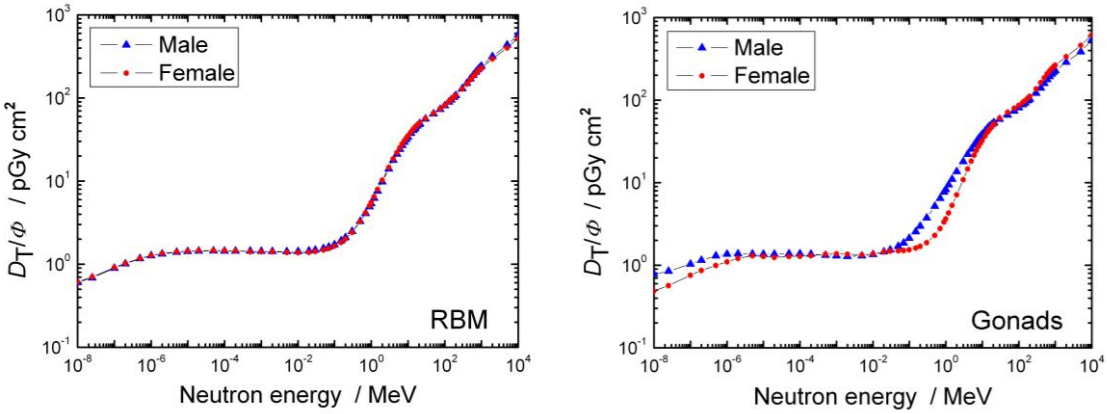

Fig. 6.1. Fluence to mean absorbed dose conversion coefficients for red bone marrow (left) and gonads (right) as a function of neutron energy for isotropic irradiation of the adult male and female reference phantoms (ICRP, 2012).

(274) Figure 6.2 shows similar conversion coefficients for red bone marrow and skin, respectively, as a function of energy for protons (ICRP, 2012). It should be noted that the gender dependence of the organ doses are significant only for few organs and varies with the type and energy of the radiation involved.

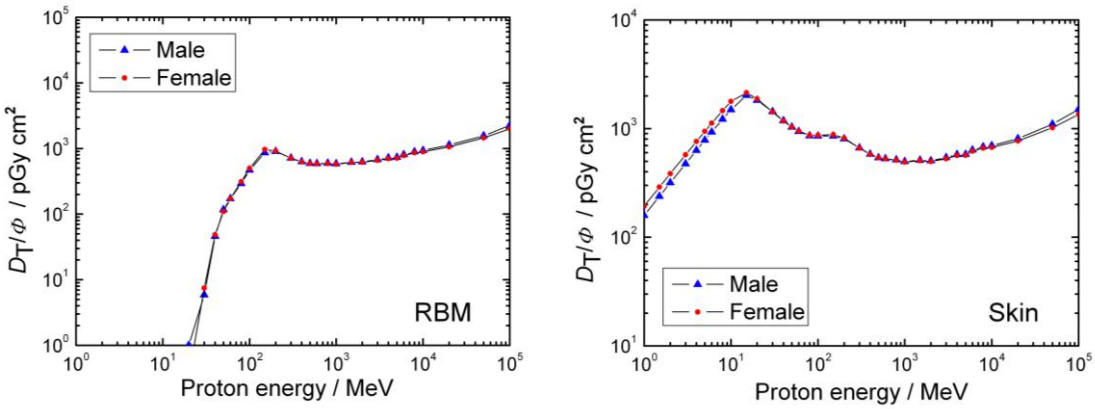

Fig. 6.2. Fluence to mean absorbed dose conversion coefficients for red bone marrow (left) and skin (right) as a function of proton energy for isotropic irradiation of the adult male and female reference phantoms (ICRP, 2012).

(275) The fluence to mean absorbed dose conversion coefficients for organs and tissues of the body have been systematically calculated for heavy ions with atomic numbers up to 28 and energies from 1 MeV/u to 100 GeV/u using the PHITS code coupled to the reference voxel phantoms (Sato et al., 2010), following the instruction given in Publication 103 (ICRP, 2007). A full set of data for male and female and isotropic exposure of the body is given in the Annex of this report.

(276) As an example, the data for red bone marrow (RBM), breast, stomach and skin are plotted in Figures 6.3 for isotropic (ISO) irradiation of the reference adult male phantom with ^{4}He and ^{28}Si ions, respectively.

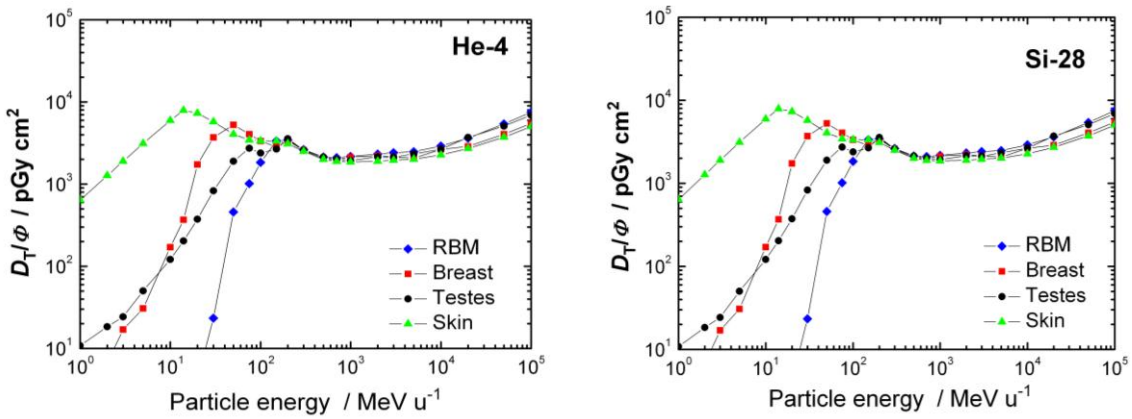

Fig. 6.3. Fluence to mean absorbed dose conversion coefficients for various tissues as a function of particle energy for isotropic irradiation of the reference adult male phantom by ^{4}He ions (left) and ^{28}Si (right).

(277) It can be seen from figure 6.3 that the dose conversion coefficients for the organs are very different for the energies below about 200 MeV, while they are very similar for high-energies. At low energies, the incident particles have short ranges in tissue and will generally stop in an organ or tissue near to the surface (i.e. skin). At high energies, on the other hand,

the incident particles have very long ranges and generally penetrate the human body without forming the Bragg peak. Thus, the doses are more uniformly distributed inside the human body in comparison to low-energy particle irradiations.

Organ and effective dose equivalent

(278) While fluence to mean absorbed dose conversion coefficients for organs and tissues, $d_{\mathrm{T,R}}$, are the basis for dose assessment in the human body, in mixed radiation fields with radiations of very different radiation quality fluence to dose equivalent conversion coefficients, $h_{\mathrm{T,Q,R}}$, for organs and tissues are often more appropriate for radiation protection applications and risk assessments in space environment. Most space organizations (e.g. NASA, ESA, etc.) have adopted these quantities and corresponding conversion coefficients since the late 1990s (NCRP, 2000).

(279) The calculation of the conversion coefficients for mean dose equivalents in organs and tissues and effective dose equivalent, are more complex than those for the absorbed doses, because the doses at the point of interest must be weighted by the quality factor as a function of LET. In this case, the charge and energy of ionizing particles depositing the energy at that point have to be determined. If kerma factors are used for determining the mean absorbed dose in tissues and organs (e.g. for neutrons below about 20 MeV) this does not allow the evaluation of a Q-value unless one includes further corrections.

(280) The dose equivalent in an organ or tissue T, $H_{\mathrm{T,Q}}$, is calculated by:

$$H_{\mathrm{T,Q}} = \sum_{\mathrm{R}} \int_{E} h_{\mathrm{T,Q,R}}(E) \frac{\mathrm{d}\Phi_E}{\mathrm{d}E} \mathrm{d}E = \sum_{\mathrm{R}} \int_{E} Q_{\mathrm{T,R}}(E) d_{\mathrm{T.R}}(E) \frac{\mathrm{d}\Phi_E}{\mathrm{d}E} \mathrm{d}E \tag{6.4}$$

with the mean quality factor $Q_{\mathrm{T,R}}$ based on $Q(L)$ as given in eq. (3.10).

(281) The mean quality factors, $Q_{\mathrm{T,R}}$, and the fluence to organ dose equivalent conversion coefficients, $h_{\mathrm{T,Q,R}}$ for organs and tissues have been systematically calculated for heavy ions with atomic numbers up to 28 and energies from 1 MeV/u to 100 GeV/u using the PHITS code coupled to the reference voxel phantoms (Sato et al., 2010). Data of mean quality factors for organs and tissues and isotropic exposure of the body are also given in the Annex to this report.

(282) The organ dose equivalent conversion coefficients obtained by PHITS for red bone marrow, breast, gonads (testes and ovaries, respectively) and skin of the adult male and female reference phantoms are depicted in Fig. 6.4 and 6.5 for ISO irradiation by ^{4}He and ^{56}Fe, respectively.

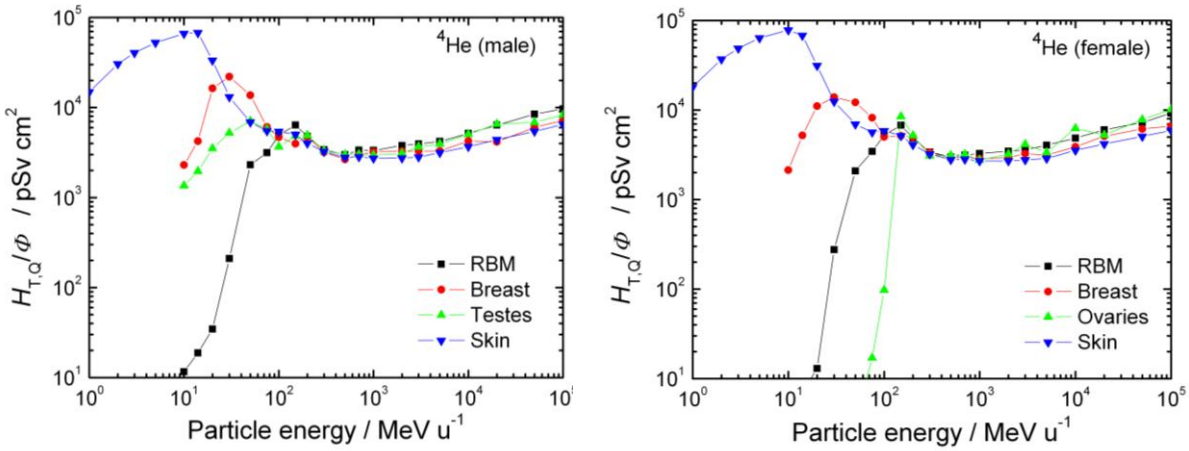

Fig, 6.4. Fluence to organ dose equivalent conversion coefficients for various tissues as a function of the particle energy for ^{4}He ions and isotropic irradiation of the adult male (left) and female (right) reference phantom.

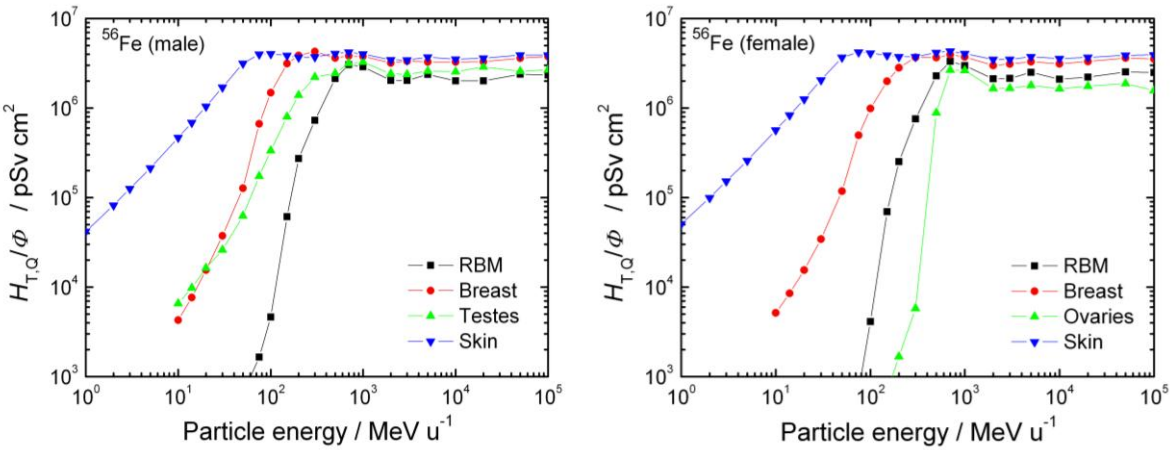

Fig. 6.5. Fluence to organ dose equivalent conversion coefficients for various tissues as a function of the particle energy for ^{56}Fe ions and isotropic irradiation of the adult male (left) and female (right) reference phantom.

(283) As far as fluence-to-effective dose equivalent conversion coefficients are concerned, the data for neutrons are very similar to those for effective dose. Larger differences between conversion coefficients for effective dose and effective dose equivalent exist for low energy protons, where the value of the mean quality factor is much higher than the value of 2 for the radiation weighting factor. In high-energy proton fields, however, this difference is not very important because of the small contribution of low-energy protons to effective dose and effective dose equivalent. Fig. 6.6 presents some data for several heavy ions.

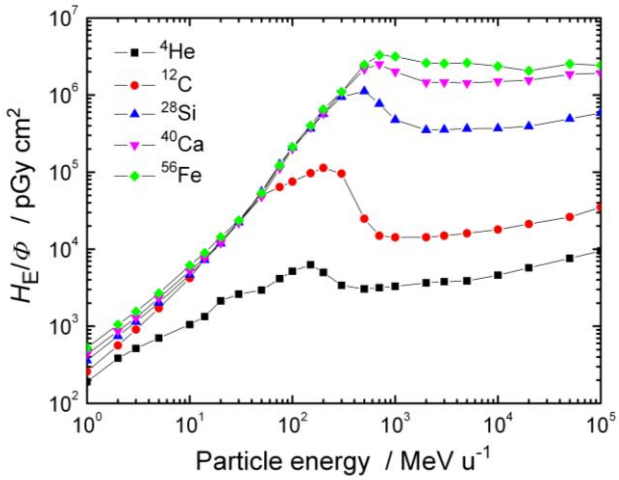

Fig. 6.6. Fluence to effective dose equivalent conversion coefficients for several particles as a function of the particle energy for isotropic irradiation of adult male reference phantom.

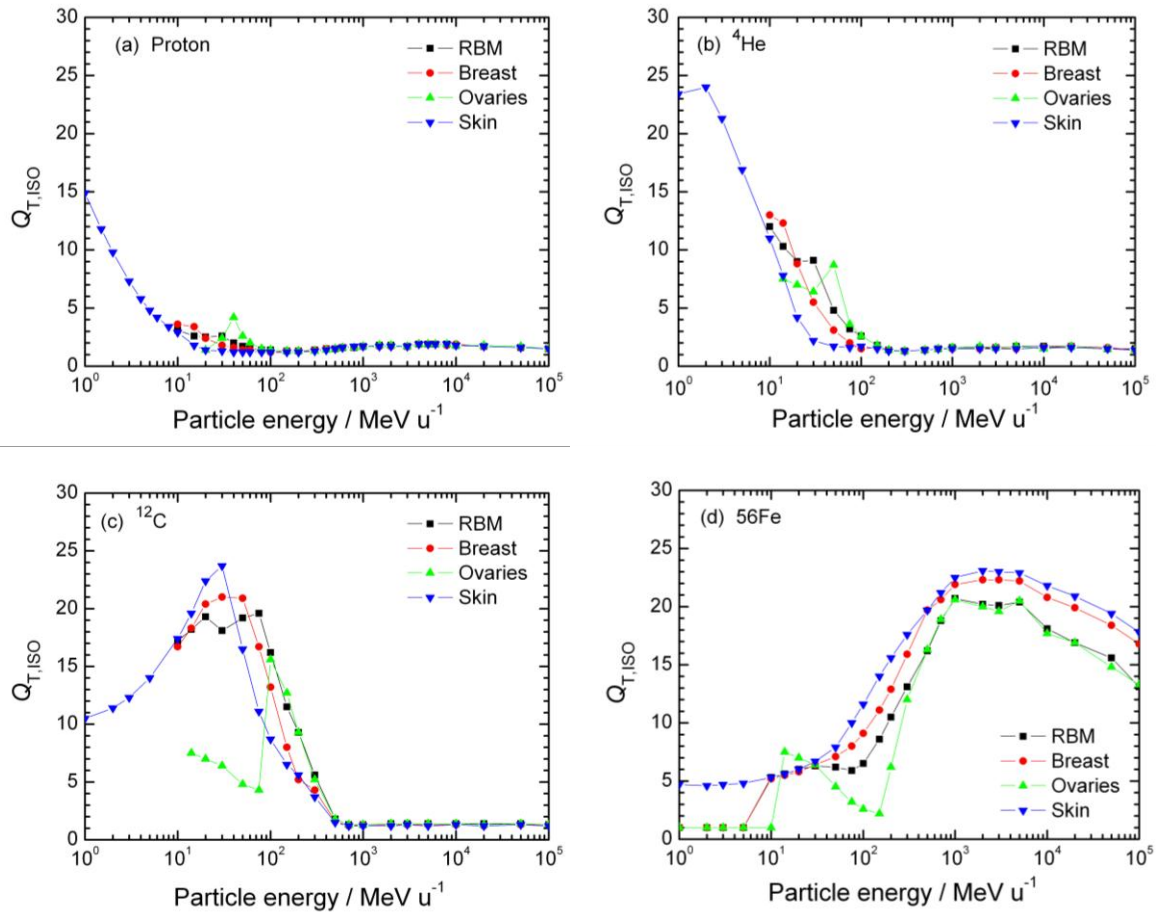

Fig. 6.7. Mean quality factors, $Q_{T,ISO}$, based on $Q(L)$ as defined in Publication 103, of some tissues as a function of particle energy for isotropic exposure of the adult female reference phantom by (a) p, (b) ^{4}He, (c) ^{12}C and (d) ^{56}Fe.

(284) The ratio of the mean dose equivalent in an organ to the mean absorbed dose in that

organ gives the mean quality factor for that organ. As an example, Figures 6.7 a-d shows the mean quality factors for red bone marrow, breast, stomach and skin for exposure of the adult female reference phantom by protons, ^{4}He-, ^{12}C- and ^{56}Fe-ions.

(285) As can be seen in Fig. 6.7, for isotropic exposure to a specific ion type the differences in Q_T of the different organs and tissues are relatively small. Therefore, a human-body averaged quality factor (performed by weighting the organs and tissues (see eq. (3.12)) using the tissue weighting factors given by the Commission (ICRP, 2007)) represents the radiation quality well in isotropic exposure situations.

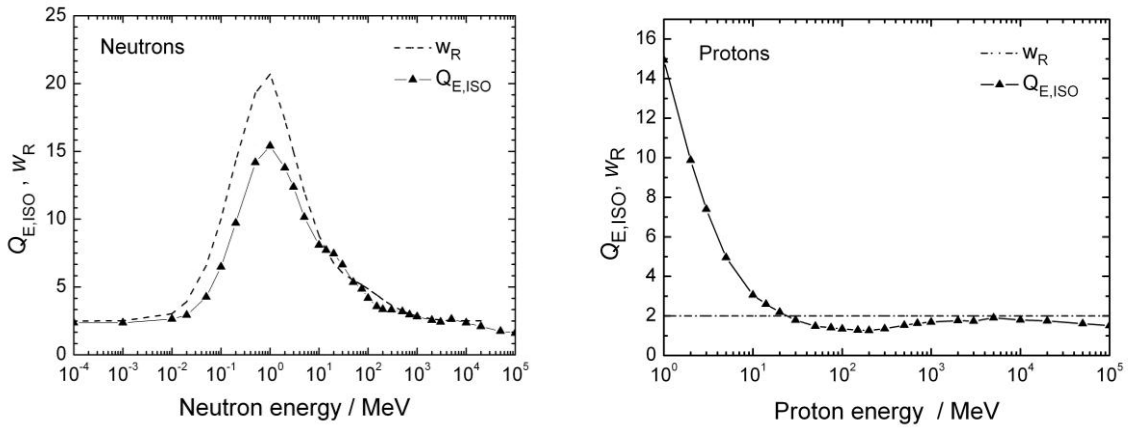

(a) (b)

Fig. 6.8. Phantom averaged quality factor, $Q_{E,ISO}$, as a function of neutron energy (a) and proton energy (b) for isotropic (ISO) exposure of the adult male reference phantom. The w_R-functions are additionally shown (dotted line).

(286) While for AP radiation incidence body averaged quality factors for neutrons and protons are shown in Figs. 3.3 and 3.4, for data for isotropic exposure are given in the Annex and presented in Fig. 6.8a,b. In Fig. 6.9a, b similar data are shown for various heavy ions.

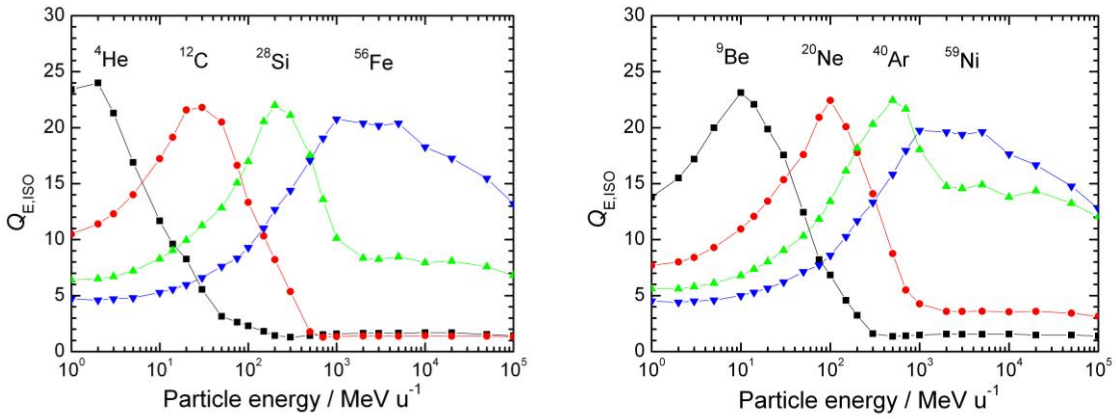

Fig. 6.9. Phantom averaged quality factor, $Q_{E,ISO}$, as function of particle energy for various particles and isotropic exposure of the adult male reference phantom.

(287) Mean quality factors for organs and tissues, $Q_{T,NASA}$, based on the Q-function as proposed by NASA for solid cancer (see Fig. 3.14), were also calculated using the PHITS code coupled to the reference voxel phantoms (Sato et al., 2012). As an example, figures 6.10

a-d show $Q_{T,NASA}$ of the red bone marrow, breast, stomach and skin for isotropic exposure by protons, ^{4}He, ^{12}C and ^{56}Fe ions. The values of red bone marrow were calculated using the NASA quality factor for leukaemia which is 1/4 of that for solid cancer.

(288) For proton and light ions, the values of $Q_{T,NASA}$ are generally larger than the corresponding data based on the $Q(L)$ function given in eq. (3.9) ICRP (Fig. 6.7), except for red bone marrow. For heavier ions, however, the values of $Q_{T,NASA}$ are generally smaller than the corresponding values based on the ICRP function especially for very low and very high particle energies. The smaller $Q_{T,NASA}$ observed at low energies is attributed to the strong decrease of $Q_{T,NASA}$ with increasing L in the high-LET region, while for high particle energies the consideration of the track structure in the NASA concept is important.

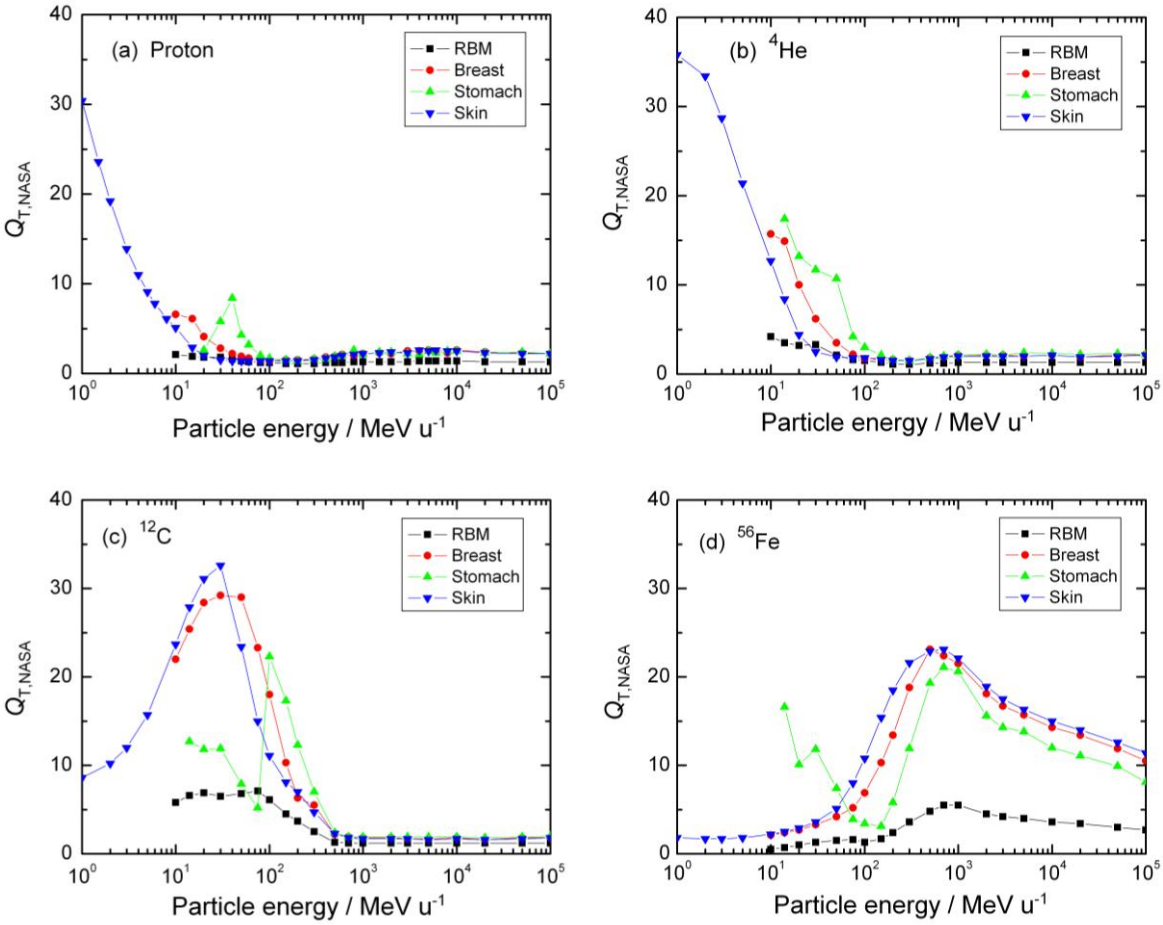

Fig. 6.10. Mean quality factors, $Q_{T,NASA}$, based on the Q-function proposed by NASA, of some organs as a function of particle energy for isotropic exposure of the adult female reference phantom by (a) protons, (b) ^{4}He, (c) ^{12}C and (d) ^{56}Fe.

(289) Figure 6.11 shows human body averaged quality factors based on $Q_{T,NASA}$ for isotropic exposure of the adult female reference phantom by various particles. The tissue weighting factor, w_T, as defined in Publication 103 (ICRP, 2007) were adopted in the calculation.

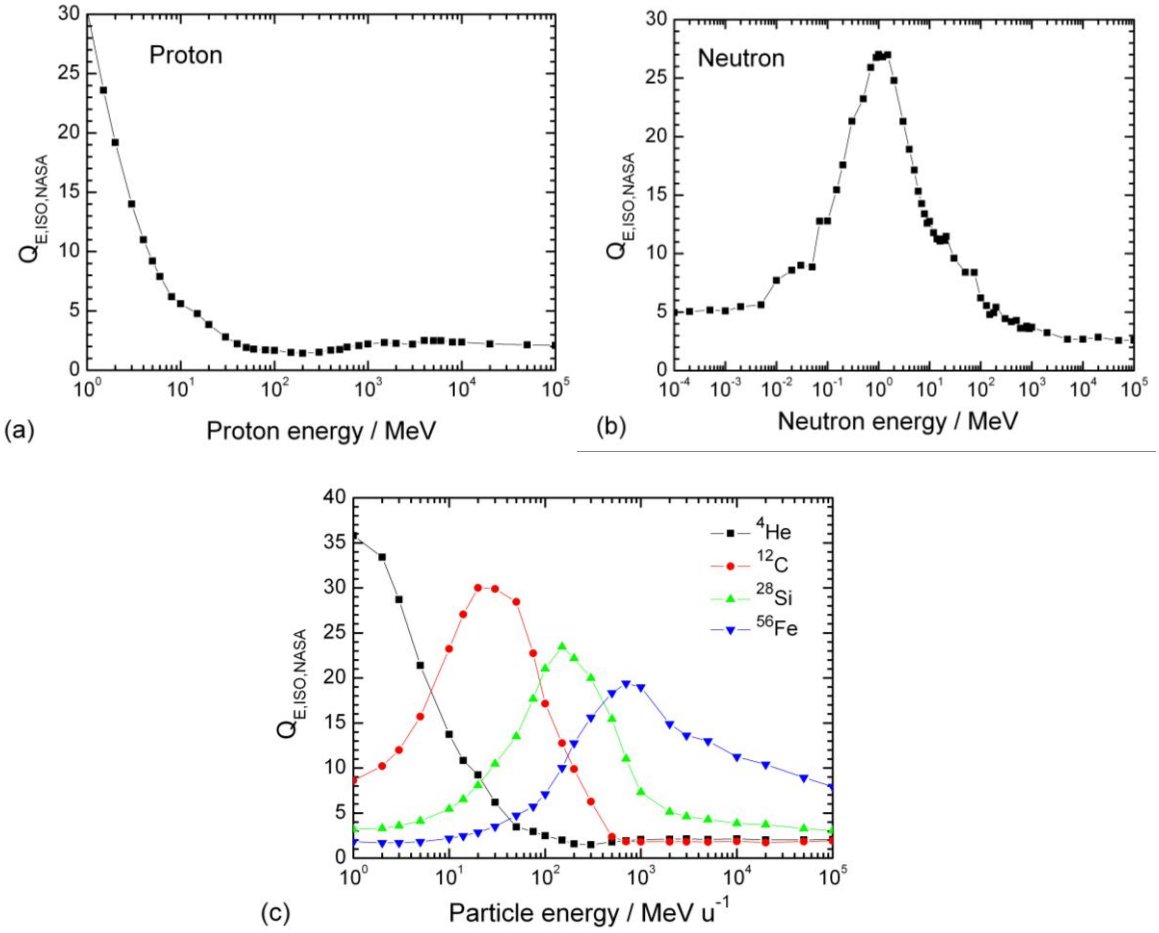

Fig. 6.11 Phantom averaged quality factor, $Q_{E,ISO,NASA}$, as function of particle energy for protons (a), neutrons (b) and various other ions (c) and isotropic exposure the adult male reference phantom.

6.3 Calculation of organ doses of astronauts within spacecraft

(290) Generally, organ doses in a body may be calculated using the radiation field parameters outside the spacecraft and a code which combines radiation transport in the spacecraft and in the human body. In principle, this procedure takes account of all inhomogeneities of the radiation field inside the spacecraft due to the variations in the spacecraft wall and the distribution of the material inside the spacecraft. The approach has been realized by NASA using the very fast radiation transport code HZETRN together with various human phantoms (see e.g. Wilson, et al., 1995c, Badhwar et al., 2002, Cucinotta et al., 2008). The external radiation field parameters to be known include the energy and directional distribution of the fluence of all types of radiation involved. Also the time dependence of some contributions needs to be known. This approach can be applied to the field for EVA and for astronauts in a habitat on the moon or planet.

(291) For checking this method, phantom torsos comprised of realistic distributions of human tissue equivalent materials have been flown on several space shuttle missions. Organ dose equivalents have been estimated by using a combined TLD and PNTD (CR-39) detector methodology (Badhwar et al., 2002; Yasuda et al., 2000). Table 6.1 shows a comparison of data calculated using the HZETRN/QMSFRG model (Cucinotta et al., 2008) to those from

measurements of Yasuda et al. (2000) on space shuttle mission STS-91, which flew in a 51.6 inclination orbit to the Mir station a similar orbit as flown by ISS. The corresponding data calculated by PHITS coupled with the dose conversion coefficients for isotropic irradiation are also given in the table (Sato et al., 2011).The comparison shows excellent agreement between measured and calculated data. The NASA phantom torso experiment that was flown on STS-91 (Badhwar et al., 2002), was re-flown on ISS Increment 2 in 2001. This experiment included several small active silicon detectors located at critical organ positions in the torso that provide time dependent dose data. The correlation of the time dependent data to the ISS trajectory allows for separation of the individual contributions from trapped protons and GCR to organ doses. Table 6.2 shows comparison of the HZETRN/QMSFRG results (without scaling) to the measurements indicating good agreement. The results show that the ratio of the GCR to trapped proton absorbed dose is about 2:1. Mean quality factors without tissue shielding for GCR (~3.5) are more than twice as high as that for the trapped protons (~1.5). These results support the assumption that organ dose equivalents for ISS missions and many space shuttle missions are predominantly from GCR.

Table 6.1. Comparison of measured organ dose equivalent for STS-91 mission using a combined PNTD/TLD method and data calculated using the HZETRN/QMSFRG model with random orientation in the spacecraft (Yasuda et al., 2000), as well as using PHITS coupled with the dose conversion coefficients(DCC) for isotropic irradiation (Sato et al., 2011).

Tissue	**Organ dose equivalent / mSv**				
	Measured	**HZETRN/ QMSFRG**	**Diff. %**	**PHITS/ DCC**	**Diff. %**
Skin	4.5 ±0.05	4.7	4.4	5.3	18.5
Thyroid	4.0 ±0.21	4.0	0	4.2	4.9
Bone surface	5.2 ±0.22	4.0	-23.1	4.3	-17.8
Esophagus	3.4 ±0.49	3.7	8.8	3.6	5.4
Lung	4.4 ±0.76	3.8	-13.6	3.9	-12.3
Stomach	4.3 ±0.94	3.6	-16.3	3.5	-17.5
Liver	4.0 ±0.51	3.7	-7.5	3.6	-10.7
Bone marrow	3.4 ±0.40	3.9	14.7	3.7	9.5
Colon	3.6 ±0.42	3.9	8.3	3.7	1.9
Bladder	3.6 ±0.24	3.5	-2.8	3.5	-2.3
Gonad	4.7 ±0.71	3.9	-17.0	4.2	-10.3
Breast	4.5 ±0.11	4.5	0	5.2	16.2
Remainder	4.0 ±0.57	4.0	0	3.7	-6.5
Effective dose equivalent	4.1 ±0.22	3.9	4.9	3.9	4.9

Table 6.2. Comparison of the organ absorbed dose rate measured by the ISS Increment-2 Phantom Torso experiment (July-August, 2001) with predictions obtained using the HZETRN/QMSFRG model at a fixed position in the spacecraft (Badhwar *et al.*, 2002).

Organ	**Absorbed dose rate trapped radiation mGy/d**		**Absorbed dose rate from GCR mGy/d**		**Total absorbed dose rate mGy/d**		**Difference (%)**
	Exp.	Model	Exp.	Model	Exp.	Model	
Brain	0.051	0.066	0.076	0.077	0.127	0.143	13.3

Thyroid	0.062	0.072	0.074	0.077	0.136	0.148	9.4
Heart	0.054	0.061	0.075	0.076	0.129	0.137	6.7
Stomach	0.050	0.057	0.076	0.077	0.126	0.133	5.5
Colon	0.055	0.056	0.073	0.076	0.128	0.131	2.5

(292) The doses received in interplanetary missions have been evaluated by the same approach by a number of authors (i.e. Badhwar et al., 1994; Cucinotta and Durante, 2006a, Hoff et al., 2004, Zapp et al., 2002, Ballarini et al., 2006, Trovati et al., 2006). The FLUKA code associated with a Golem voxel phantom (Zankl et al., 2001) was used for an estimate of the doses inside a capsule-like enclosure with variable Al-wall thickness (Ferrari, 2007). It was supposed that particles of GCR impinge uniformly and isotropically on the spacecraft. As an example, Figure 6.12 shows calculated results in terms of absorbed dose rate to red bone marrow (RBM) as a function of the thickness of the Al wall. The contribution of the primary particles to the total dose rates is also shown in Figure 6.12.

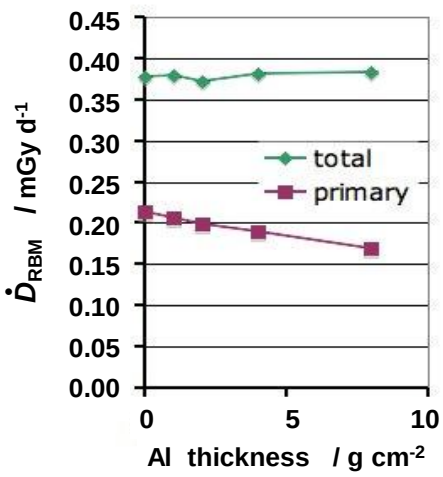

Fig.6.12. Absorbed dose rate to red bone marrow (RBM) of a voxel phantom exposed to galactic cosmic radiation inside a capsule as a function of the Al wall thickness of the capsule (Ferrari, 2007).

(293) The calculated absorbed dose rate behind 1 g cm^{-2} of Al resulted in 0.378 mGy/d, with 59% due to protons, 21% to alpha particles, 10% to ions of $2 < Z \leq 8$, 5% to ions of $8 < Z \leq 14$ and 5% to ions of $Z > 14$. The dose rate contributions of the various ion groups include those of primary ions and of all products generated in their interactions. The dose rate contribution of the uncollided particles was 0.206 mGy/d.

(294) Examples of direct evaluation of the organ dose equivalent rates from external radiation fluence rates of GCR without use of conversion coefficients are shown in Fig. 6.13. Similar to simulations already described above (see Fig. 6.12) the figure shows the dose equivalent rate to RBM as a function of the Al wall thickness of a capsule (Ferrari, 2007). It should be noted that for these data the tissue weighting factors recommended in the Publication 60 (ICRP, 1991) were applied.

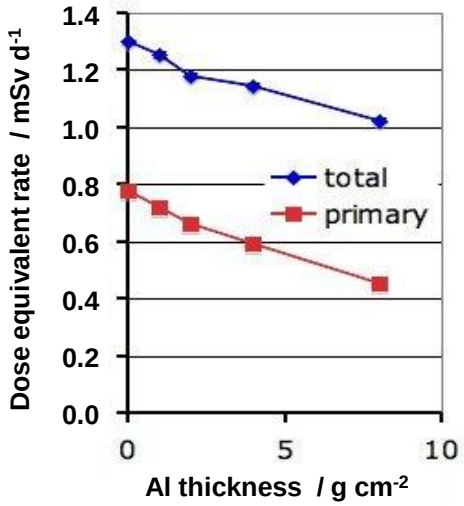

Fig 6.13. Dose equivalent rate to the RBM of a voxel phantom inside a capsule exposed to galactic cosmic radiation as a function of the Al wall thickness of the capsule (data from Ferrari, 2007).

(295) The calculated RBM dose equivalent rate behind 1 g cm^{-2} of Al is 1.26 mSv/d, where 31% are due to protons, 11% to alpha particles, 13% to ions of $2 < Z \leq 8$, 16% to ions of $8 < Z \leq 14$, 29% to ions of $Z > 14$. The contributions of the various ion groups include the primary ions contributions and those of all products generated in their interactions. The contribution of the uncollided particles was 0.72 mSv/d.

(296) Several other authors used the method described above in order to determine the organ dose equivalent and effective dose equivalent received by the astronauts, especially for studying the shielding effect of the wall thickness of the capsule. Slaba et al. (Slaba et al., 2010) computed the protection quantities under both a galactic cosmic radiation and solar particle event environment. The spherical shell of aluminum was supposed isotropically irradiated and various computational models (CAM, CAF, MAX, FAX) have been used. Ballarini et al. (2006) and Trovati et al. (2006) calculated the GCR and SPE organ doses in deep space with different shielding by Monte Carlo simulations using the FLUKA code coupled to a mathematical model and a voxel phantom.

(297) Furthermore, it is of interest to which extent the values of dose equivalent in these radiation fields depend on the different concepts of the quality factor. As function of Z of the primary incident particle with an energy distribution as given in the GCR field, Fig. 6.14 shows a comparison of body-averaged mean quality factors using the $Q(L)$ relationship and the recent NASA approach to quality factors based on particle track structure concepts and using different quality factor values for solid cancers and leukaemia. The calculations are made using the HZETRN code for solar minimum in the orbit of the International Space Station (ISS). Different calculations were carried out applying either a thin (5 g/cm^2) or a thick (20 g/cm^2) aluminum shielding. Differences between the different approaches occur mainly for low- and high-Z particles.

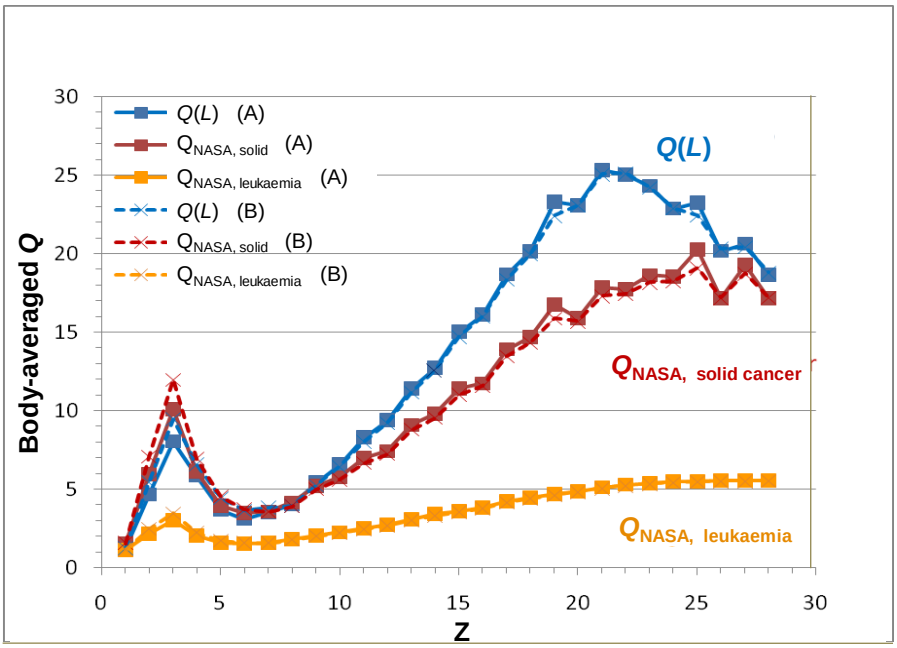

Figure 6.14. Comparison of body-averaged quality factor values as a function of primary incident particle of charge Z calculated by applying either the ICRP $Q(L)$ function or the NASA quality factors for solid cancers or leukaemia for thin or thick aluminum shielding conditions. (A) 5 g/cm^2 Al shielding; (B) 20 g/cm^2 Al shielding.

6.4 Assessment of doses in the body by measurements

(298) Specific operational quantities for an assessment of dose in the body of astronauts in space have never been defined. Some properties of the radiation field, however, may provide some help in the determination of effective dose equivalents of astronauts. Firstly, there is a major component of very high-energy particles with long ranges in tissue in the field which strongly contribute to doses in the body. Secondly, the radiation incidence on the body may be nearly isotropic considering the situation that the astronauts are usually moving around and are not fixed in a special position for long times. Therefore, isotropic exposure of astronauts has been assumed in calculations resulting in a relatively homogeneous dose distribution within the body from GCR exposure (see Fig. 6.12 and 6.13). This, however, is not the case for low-penetrating radiation which mainly contributes to doses of the skin and other tissues near to the surface.

(299) Any dose-measuring system, therefore, must have the ability to discriminate between strongly- and low-penetrating radiations. In addition, information about the distribution of absorbed dose in tissue in terms of lineal energy L, D_L, is necessary for the assessment of equivalent dose in the body.

(300) Measurement of dose distributions and organ doses in a human phantom in space have also be performed by the MATROSHKA collaboration (Reitz and Berger, 2005; Reitz et al., 2009) and exploited by members of the HAMLET collaboration (see www.fp7-hamlet.eu). A tissue-equivalent anthropomorphic phantom, called MATROSHKA, has been equipped with hundreds of dosemeters of different types, mostly TLD and NTD - and exposed in space during various ISS missions.

(301) The MATROSHKA experiments provide detailed depth dose distributions in a human phantom exposed outside the ISS (MTR-1 mission) and in two positions inside the ISS at different shielding locations (MTR-2A, MTR-2B missions). Figure 6.15a shows the measured dose rate distribution in the MATROSHKA phantom for the MTR-1 mission based on TLD readings at 1598 locations inside the phantom. For measurements with the phantom outside the ISS, the absorbed dose rates range from 0.1 mGy/d to 0.5 mGy/d, with the highest dose at the phantom surface. For other missions inside the ISS due to the spacecraft shielding the absorbed dose rates are mostly restricted to a range from 0.13 mGy/d to 0.23 mGy/d.

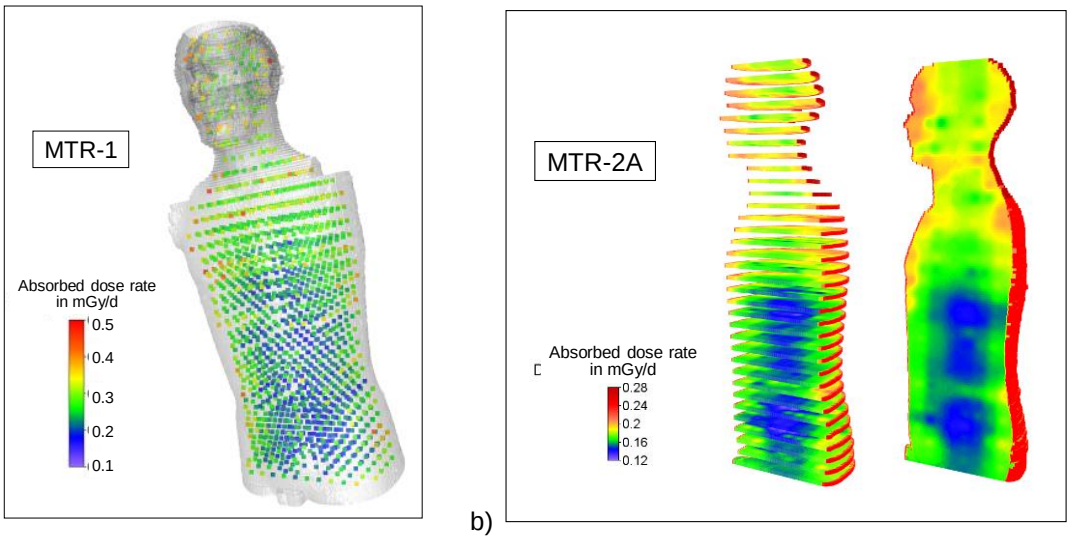

Fig. 15. (a) Measured absorbed dose rate distribution in the MATROSHKA phantom for the MTR-1 mission outside of the ISS based on TLD readings (Reitz, 2012).
(b) Absorbed dose rate distribution in the MATROSHKA phantom for the MTR-A2 mission inside the ISS obtained by interpolation of point doses over the whole phantom volume (Reitz, 2012).

(302) Computer tomography scans of the MATROSHKA phantom are taken in order to build up a voxel model called NUNDO (Numerical Rando). A computer program allows calculation of dose distributions by interpolation of point doses over the whole phantom volume (see Fig. 6.15b). For total absorbed dose and dose equivalent rate distributions and hence an assessment of mean absorbed dose rates and dose equivalent rates in organs and tissues, data measured by TLD and PNTD have been combined. The dose equivalent rate was calculated using quality factors as defined in ICRP Report 60 (ICRP, 1991).

(303) The high dose gradient near to the skin for the MTR-1 missions is due to the high contribution of electrons and protons at the South Atlantic Anomaly. Inside the ISS this contribution is strongly reduced due to the shielding by the spacecraft (see Fig. 6.16 and 6.17). The dose rates in the deeper lying organs are nearly constant due to the high energies and nearly isotropic fluence distribution of the GCR. For astronauts moving within the spacecraft, this is even more the case.

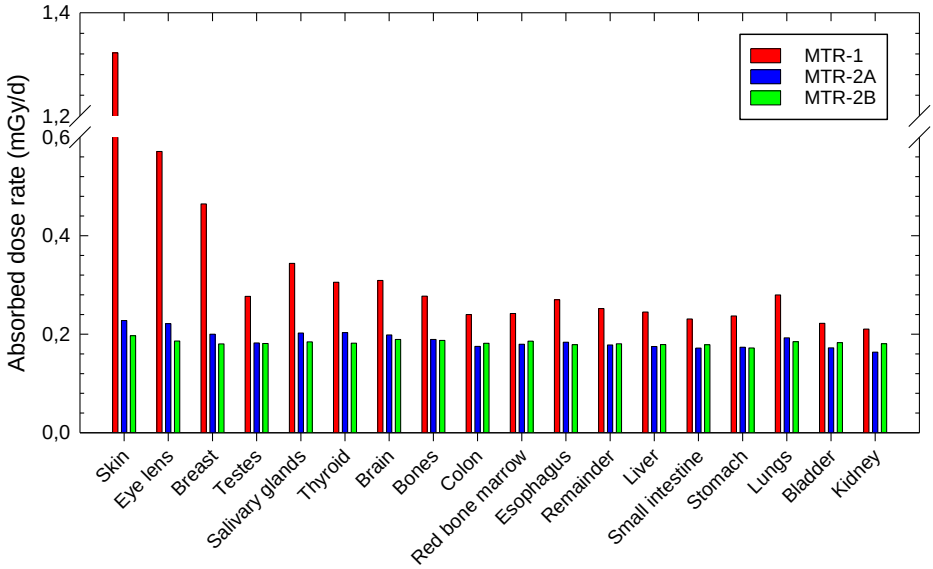

Fig. 6.16 Mean absorbed dose rates in organs and tissues of the MATROSHKA phantom during different space missions at the ISS determined from measurements using TLD and PNTD (Reitz, 2012).

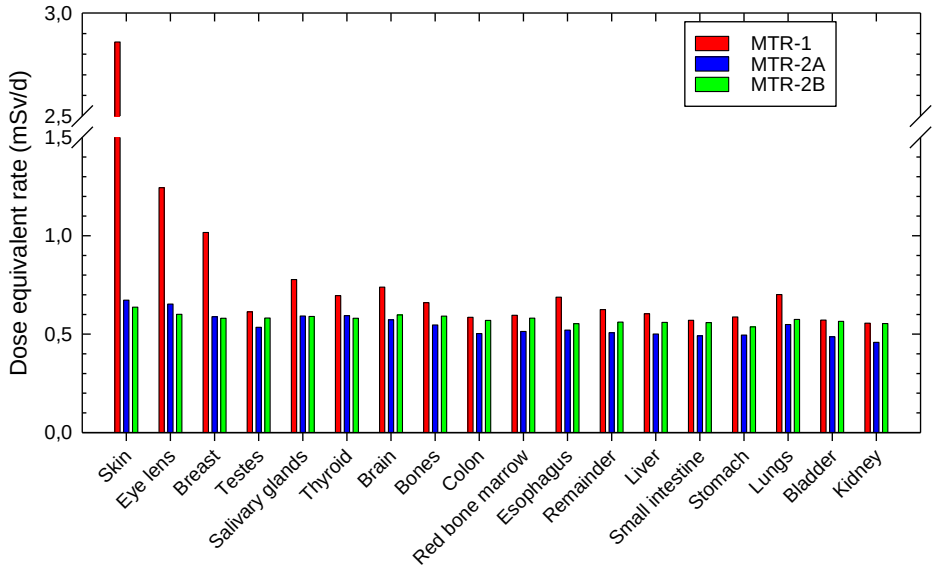

Fig. 6.17. Mean dose equivalent rates in organs and tissues of the MATROSHKA phantom during different space missions at the ISS determined from measurements using TLD and PNTD (Reitz, 2012).

(304) The measured organ absorbed dose data were compared with corresponding values obtained from dose conversion coefficients multiplied with cosmic-radiation fluxes in the spacecraft calculated by PHITS using a simplified geometry of the ISS (Sato et al 2011). The agreement was found quite satisfactory in spite of some discrepancies observed for some organs, taking account of the various approximations introduced, in primis the hypothesis of isotropic irradiation.

(305) Similar data have been calculated for comparison with organ absorbed doses measured by the MATROSHKA experiment outside the ISS. As shown in Table 6.3 an

acceptable agreement has been achieved.

Table 6.3. Organ absorbed dose rates measured by the MATROSHKA experiment outside ISS (Reitz et al., 2009) in comparison with corresponding calculated dose rates obtained from PHITS simulations (Sato et al., 2011).

Organ/Tissue	Measured absorbed dose rate mGy/d	Calculated absorbed dose rate mGy/d
Skin	0.944	1.814
Salivary glands	0.33	0.435
Breast	0.39	0.690
Lung	0.26	0.279
Oesophagus	0.24	0.250
Stomach	0.242	0.245

(306) The agreement is seen to be very good for the interior organs such as lung, oesophagus and stomach. The calculation, however, substantially overestimates the measured absorbed dose rates for the organs located near to the surface of the body, especially for the skin. That is probably due to the effect of a high yield of low-energy trapped protons and electrons encountered and also to some differences between phantoms and geometries of their surrounding environment employed in the calculation and experiment.

(307) The accuracy of heavy ion transport codes was discussed in Section 5.3.1. With respect to the different anthropomorphic voxel models used the differences in the values of absorbed dose and dose equivalent of single organs and tissues calculated using the NUNDO model (MATROSHKA) or the ICRP reference voxel phantom are quite small as shown in Fig. 6.18 (Matthiä, 2012).

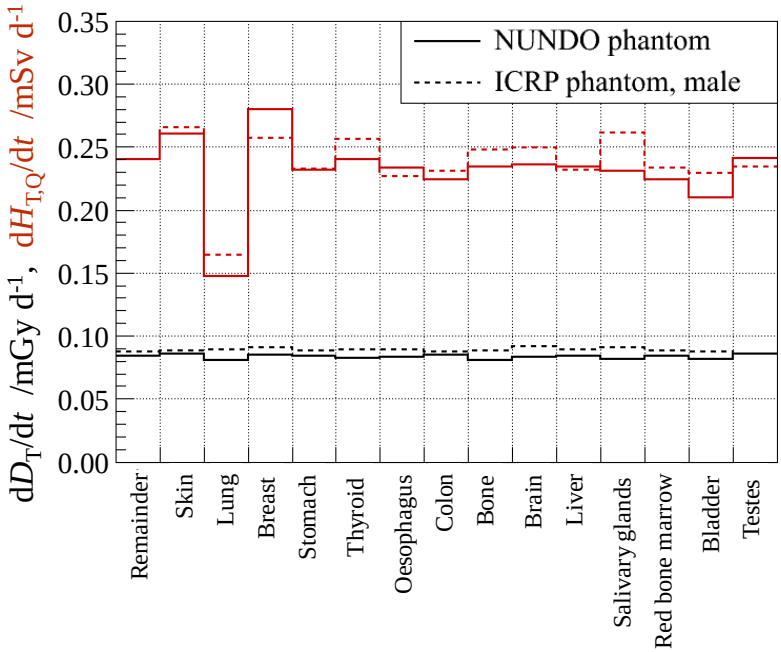

Fig. 6.18. Mean absorbed dose rate and dose equivalent rate in various organs and tissues calculated using the GEANT4 code and the NUNDO model and the ICRP reference phantom for galactic cosmic radiation (Matthä, 2012).

6. 5 Biodosimetric measurements

(308) Biodosimetric measurements offer an alternative to the measurement of individual doses external to the body of an astronaut for the assessment of effective dose equivalent, because of the very complex radiation field in the spacecraft which in addition is varying in intensity and composition with time. Lymphocytes in the human body are circulating and hence provide a target which is well distributed over the human body. In addition, the RBE-LET dependence for total chromosomal exchanges during the first cell cycle is similar to the Q(L) relationship defined by the Commission (see Fig. 3.4) when using the premature chromosome condensation method (Cucinotta et al., 2008).

(309) The method has already been applied for estimating doses of astronauts in space shuttle flights (George et al., 2001), at the MIR station (Yang et al., 1997, Fedorenko et al., 2001) and at the ISS (Cucinotta et al., 2008).

(310) In Table 6.4 doses obtained by physical and biological dosimetry for ISS missions are compared, where the comparison includes biomarker results based on an individual or population based calibration using gamma radiation (Cucinotta et al., 2008). Mission lengths of 4 to 7 months occur for the different results described. Biomarker results are given in terms of RBE·D (unit: mGy). This RBE-weighted dose value may be compared with values of dose equivalent to organs or tissues (here with the dose equivalent of the skin) and effective dose equivalent obtained from dosemeter readings and applying the $Q(L)$ relation as given by Publication 103 (ICRP, 2007). The overall agreement between the methods lends confidence that the complex environment in space has been adequately characterized.

Table 6.4. Data of mission doses of ISS astronauts obtained by biological dosimetry and by measurements with individual dosemeters (Cucinotta, 2008). The data of skin dose equivalent and effective dose equivalent are obtained by calculations adjusted to the individual's dosemeter readings.

Astro-naut	**RBE·*D* mGy**		**Individual dose-meter reading in mGy**	**Skin dose equivalent (calc.) mSv**	**Effective dose equivalent (calc.) mSv**
	Individual based calibr.	**Population based calibr.**			
1	94 ±12	128 ±25	31	89.9	77.6
2	127 ±57	84 ±41	30	86.5	73.7
3	78 ±16	81 ±19	33	96.4	82.1
4	60 ±24	87 ±20	32	93.8	79.9
5	36 ±15	54 ±26	29	85.1	72.5
6	59 ±19	61 ±21	32	90.8	80.0
7	41 ±19	72 ±27	29	83.3	70.6
8	83 ±29	40 ±21	31	88.3	74.7
9	113 ±17	130 ±25	40	115	98.6
10	-	75 ±26	31	88.3	74.5
11	74 ±32	55 ±26	22	64.5	54.7
12	128 ±40	71 ±24	23	65.4	55.7
13	134 ±45	88 ±29	22	64.7	59.8
14	66 ±21	59 ±15	26	78.0	66.3
15	83 ±27	125 ±52	30	88.6	75.2
16	10 ±24	15 ±35	20	56.8	47.5
17	147 ±48	134 ±66	36	103.0	86.3
18	113 ±26	109 ±34	30	83.7	76.9
19	119 ±32	69 ±23	24	70.1	59.5
Mean*	85 ±38	81 ±32	28.9 ±4.9	83.8±14.1	71.9 ±12.0

- Uncertainties listed are based on the data variation in the column and do not include measurement uncertainties.

7. OPERATIONAL RADIATION PROTECTION IN SPACE

(311) The guiding principles used for radiation protection on Earth including justification, dose and risk limitation and ALARA are essential also for radiation protection during space travel. Operational radiation protection for astronauts in space, however, differs significantly from those requirements for external radiation exposure on Earth (see for example EC, 2009). On Earth, doses are generally well below annual limits; if constraints are approached, better estimates of effective dose are made from the results of measurements of operational quantities. For astronauts, doses are mainly based on the environmental situation in space, being typically about 1 mSv per day. Radiation protection for missions includes a large range of different measures which should all have the aim of reducing the radiation exposure of astronauts to a level where the health risks are acceptable (NCRP, 1989). In contrast to many of the other flight risks, effects from radiation exposure can have long latency times, and cancer and other detriments may occur long after a space mission has ended. However, as noted by the NCRP (NCRP, 1989, 1997) and discussed by others (Schimmerling 2010; Cucinotta et al., 2011b), the acceptance of radiation risks in spaceflight should consider many factors both dependent and independent of other flight risks.

(312) The operational radiation protection for each mission is to assess the radiation exposure of astronauts in space. This is prospectively performed by calculating organ and tissue doses weighted for radiation quality and, if needed also effective dose equivalent considering tissue weighting, for comparison with mission dose or risk limits related to stochastic and tissue reactions. After the mission, all available data should be combined, including results from measurements of area and individual instruments, to assess the doses and the probability of a radiation induced event.

(313) There may be defined special dose levels or constraints for short term exposure, annual exposure, and for an astronaut's career. The dose levels should apply to the assessed total detriment, to the lens of the eye, and to the skin. The total detriment is related to a probability of cancer risk. The dose constraints for tissue reactions are to avoid the occurrence of impairment during or after a mission. The complex nature of the radiation field in space requires continuous analysis of the environment by calculation, area monitoring of the astronauts' environment, and, where possible, the analysis of the results of active personal dosemeters, in order to meet action levels and the dose limits.

7.1 Pre-flight mission design

(314) The flight mission design needs to be carried out with the aim of reducing radiation exposures in line with ALARA. The application of ALARA requires that the space radiation environment is well known – outside and inside a spacecraft. This requires knowledge of the external radiation environment with its various components (see Chapter 2), of the spacecraft/habitat construction, and of the results of transport calculations modelling the internal radiation environment.

(315) The design of the spacecraft/habitat requires the use of radiation transport codes to compute dose equivalents. As described in Chapter 5 the computer codes may be one- or three-dimensional, deterministic or based on Monte Carlo (MC) methods. The construction of a spacecraft/habitat should include areas where the dose rates are lower than elsewhere in the spacecraft. There should be area monitors with visual displays of dose rates.

(316) To reduce uncertainties (see 7.5) further improvements are needed in the models of

the galactic cosmic radiation, the solar energetic particles, and the trapped radiation to allow the accurate forecasting of the fully integrated model of the radiation environment incident on the spacecraft/ habitat. Models have been developed for each of the radiation components. These models suffer several shortcomings: (i) the GCR models inadequately characterize the solar cycle dependency and the scaling with heliocentric distance; (ii) the SPE models have an incomplete understanding of the acceleration mechanism of the transport through the heliosphere and a lack of prediction capability; (iii) the radiation belt models no longer reflect the current state of the Earth's magnetosphere and lack the ability to properly describe the dynamic behaviour of the trapped particles.

(317) The forecast models require an improved understanding of the physical processes on the Sun; the transport and acceleration of the solar wind through the heliosphere; the processes in the magnetosphere (wave-particle interactions, source and loss processes, and acceleration mechanisms). The space environment is highly variable on very different time scales as a result of the variability of the Sun.

(318) In general all aspects of the space environment are affected, but SPEs and CMEs are the most dramatic radiation events and may constitute for several missions a serious hazard. All the radiation components (including GCR and trapped) are also modulated by SPEs (Forbush decreases in the GCR fluences, for example). An accurate prediction of SPEs and CMEs would allow for a more effective approach in the shielding strategy. Forecasting through real time observation and propagation modelling should be improved.

(319) Astronauts are particularly vulnerable during EVAs, when they should be monitored with active dosemeters. Real-time space weather predictions and remote satellite and areas instrumentation will assist in EVA activity. The real-time measurements will provide guidance, and can suggest changes in mission scheduling to maintain the total risk below predefined limits.

(320) The development of shielding requirements and strategies is important for the achievement of ALARA. The reduction in exposure can be made by reducing the exposure time or by passive shielding. Passive shielding may cause an increased risk by increasing the dose equivalent from any generated secondary particles, projectile and target fragments (including neutrons). For shielding effectiveness, the use of a shielding material with a low mean atomic mass is generally better.

(321) Information about radiation transport codes (see Chapter 5) is important and the strengths and weaknesses of the codes should be investigated in detail via benchmarking procedures against experimental data, including data obtained with advanced anthropomorphic phantoms exposed at accelerators. The physics at the basis of the particle transport and cross sectional data tables must also be improved to further develop the codes.

7.2 Area monitoring

(322) Area monitors at well selected locations in the spacecraft can determine the environmental conditions and are appropriate for an immediate warning about changing exposure conditions.

(323) Instruments are required to determine the radiation environment in terms of particle type, fluence rate, energy, and direction distributions and, in some instances, dose quantities. Dose quantities used to assess doses to astronauts and to monitor radiation at a number of locations should give values of the dose rate. These data can be used to implement ALARA. Area monitors at well selected locations in the spacecraft can be appropriate for immediate warning about changing exposure conditions. This can be of importance before or during

SPEs, electron belt enhancements, and EVA. Real-time calibration of instruments should be explored.

(324) If appropriately designed and accurately calibrated instruments are used, it may be that a quantity measured in fixed position in a spacecraft can, along with appropriate occupancy data, provide the basis for an adequate assessment of doses to an astronaut or of doses to the local skin or the extremities. While in principle this procedure may be applicable to astronauts in space, the large variation of the radiation field in intensity and composition of radiation types inside a spacecraft, and its variation with time together with the flexibility of the astronaut´s position, has the consequence that area monitoring is not sufficient to completely substitute individual monitoring, especially considering the high individual doses to astronauts and the interest in providing a basis for individual risk estimates.

7.3 Individual monitoring

(325) The assessment of organ and tissue absorbed doses, together with radiation quality factors, of individual astronauts can be accomplished by calculations using anthropomorphic phantoms or by measurements using personal dosemeters (see Chapter 6).

(326) One method of calculation of organ and tissue absorbed doses and radiation quality factors does so directly for a standard male or female phantom for various locations in a spacecraft with appropriate shielding. The phantoms can be adjusted to approximate a particular astronaut. The results are normalized using readings of area monitors and personal dosemeters. Another method requires knowledge of particle fluence and applies conversion coefficients from particle type, energy and direction distribution of fluence to organ and tissue absorbed doses and corresponding radiation quality factors for uniform irradiation of an astronaut.

(327) Individual monitoring is mostly performed using personal dosemeters worn at the surface of the body. The personal dosemeter serves as the dosemeter of record. A single dosemeter system is, however, not sufficient to provide an assessment of the absorbed dose at the surface of the body weighted by radiation quality. The broad range of different types of particle requires at minimum two detectors, one sensitive to low-LET radiation and the other to high-LET radiation. Because of a possible anisotropy of the exposure in the spacecraft due to variations of shielding properties, it may be useful to wear more than one dosemeter. Also care needs to be taken regarding low-energy electrons and particles which are stopped in the skin and, therefore, contribute only marginally to organ doses other than the skin dose, but may induce a large signal in an external dosemeter.

(328) The use of adequate active personal radiation detectors would enable improved characterization (input energy, nuclear abundance, fluence rate, direction) of the radiation field both on the body of the astronaut as well as in the environment. The measurement of dose-rate can contribute directly to ALARA.

(329) The results of bio-marker measurements can be additionally used to estimate individual radiation exposure. The determinations can be collaborative and provide all the experimental radiation information and relative codes needed to achieve an efficient risk assessment, minimizing the uncertainties in the final risk estimates.

7.4 Dose recording

(330) Astronauts in space are exeptionally exposed and the assessment of their individual doses should be part of the radiation protection programme for space flights. Astronauts

should be informed of their doses and risk assessments as soon as possible. Their doses should be regularly registered and a long term registry for all missions should be maintained.

(331) The dose record is the formal statement of the crew member's exposure and should be kept as a confidential medical record. The record should contain the history of the exposure and all the calculation and experimental results, including all information on the particle type energy and direction distributions of fluence; computer codes; conversion coefficients and weighting factors; area monitor, personal dosemeter, and biomarker results

7.5 Consideration of uncertainties

(332) There are large uncertainties in projecting cancer risks and the risks of other late effects from ionising radiation on Earth. Space radiation carries additional considerations, which further increase uncertainties. As radiation workers approach a significant fraction of exposure limits, the calculations of uncertainty bounds is needed because exposures leading to acceptable levels of risks may no longer be confidently avoided when the uncertainties are considered.

(333) It is important to provide all the information needed to establish the uncertainties of the organ risk estimates. The overall uncertainty will be reduced by improvements in modelling of radiation sources and the transport of the field through the spacecraft or habitat; improved accuracy of radiation transport codes; improved accuracy of radiation monitoring; better estimation of dose and dose-rate effectiveness factor; better determination of radiation quality factors; better understanding of the statistics and dosimetry of epidemiological data.

(334) A full risk model may need to be developed using real time radiation readings, space weather forecasts, and risk assessments. This can allow changes to the mission, with an assessment of uncertainties, whilst maintaining the total risk below predefined limits.

(335) Uncertainties in estimates of exposures and the relationship between exposure and risk are a major concern for operational radiation protection in space due to the types of radiation, which includes heavy ions and neutrons, and the higher exposure levels, which may approach exposure and risk limits. Figure 7.1 illustrates schematically an operational approach where an evaluation of uncertainties is included in the radiation protection approach (Schimmerling, 2010). Obviously, "acceptable" levels of cumulative exposure depend on the uncertainty and hence reduction of uncertainties is seen to be an important task for mission planning. Methods to estimate uncertainties in exposure and risks are described elsewhere (Cucinotta et al., 2011; NCRP 2006)

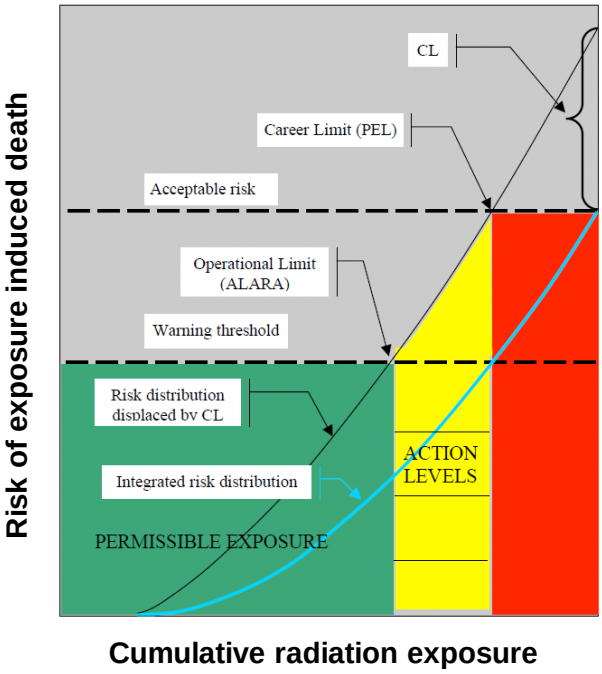

Fig. 7.1. Schematic view of risk management with ALARA and large uncertainties. The risk distribution function versus cumulative radiation exposure with and without considering uncertainties (based on 95% confidence limit (CL)) is displaced. ALARA practices and action levels for an "acceptable" level of risk and permissible exposure limit (PEL) are also shown (Schimmerling, 2010).

8. CONCLUSIONS

(336) Astronauts in space are living under extraordinarily different environmental conditions than on Earth. The radiation environment in space needs specific attention and considerations regarding the exposure of astronauts and the limitation of such exposures to a level where the health risks are comparable to other risks during space missions.

(337) The number of astronauts undergoing missions in space is very small compared to the number of occupationally exposed persons on Earth. In long-term missions, however, doses to the astronauts are generally higher than those at other working places on Earth. Hence a more individually based dose and risk assessment should be performed for astronauts in space compared to persons on Earth, where these exposures are usually much less than the limits defined for occupationally exposed persons.

(338) The following points are specifically mentioned:

- The primary radiation field in space is complex and includes electrons, protons, αparticles and heavy ions up to very high energies. Additional secondary radiation (e.g. γ-radiation, muons, neutrons and pions) is produced by interactions in the materials of a spacecraft, its equipment, and in the astronauts.
- The physics at the basis of the particle transport and cross sectional data tables must be improved to further develop the computational methods. There is a lack of experimental cross-section data for light fragments and neutrons. Codes need to be improved to treat all primary and secondary cascades including photons, protons, light ions, heavy ions, mesons and electromagnetic cascades. The nuclear interaction database needs to be updated, especially for neutrons and light ions.
- The simple concept of considering the differences in radiobiological effectiveness by radiation weighting factors, w_R, e.g. a constant radiation weighting factor of 20 for all heavy ions of all energies, is not appropriate for dosimetry in space and the quality factor (Q) is applied for the definition of the quantity dose equivalent in an organ or tissue of the human body.
- The basis for risk assessments for the astronauts are the dose equivalents in organs and tissues of adult males and females, $H_{T,Q}^{M}$ and $H_{T,Q}^{F}$, which are based on mean absorbed doses, D_T, and mean quality factors in the corresponding organs or tissues, Q_T.
- Conversion coefficients which relate particle fluence to mean absorbed doses in organs and tissues of the human body and corresponding mean quality factors for all types of radiation present in space, are an important data base for the assessment of the exposure of astronauts. For the estimation of radiation risks of astronauts based on mean absorbed doses in the body, an assessment of the uncertainty of D_T and Q_T would be very useful.
- The concept of operational dose quantities for area monitoring of external exposure and an assessment of effective dose is not applicable because many different types of particles are involved with very high energies. Instead the measurement and determination of particle fluence and its distribution in energy and direction is more important and provides a basis for an assessment of doses.
- A broad range of instrumentation has been specifically designed for fluence and dose measurements in space. Obviously a single instrument is not sufficient for a determination of all particle fluences and their energy distributions and for an

assessment of organ doses in the human body. Particle spectrometers, individual dosemeters and specific instruments measuring the low-penetrating radiation on the body of an astronaut are needed.

- While passive individual dosemeters are generally appropriate to measure mission doses integrated over the flight time, active detector systems allow the measurement of fluctuations in the exposure and also the inclusion of warning capabilities, e.g. in cases of a large SPE.
- The use of biomarkers of health effects is an attractive supplement to physical dosimetry. Biomarkers from blood samples from astronauts can be used to assess individual mission doses. In addition, biomarkers may serve for an individual risk assessment or an indication for the presence of a disease. Biodosimetry is routinely performed on the small population of astronauts involved in International Space Station (ISS) missions, and would likely be used in future space missions. To be useful as a biodosimetry method, the radiation quality dependence of the response of the specific assay need to be known.
- The exposure of astronauts in space is a special case of environmental exposure quite different from that on Earth. In space missions, especially in long-term interplanetary missions, their exposure will be higher than the annual limits recommended for exposure of workers on Earth. Although astronauts are exposed to ionizing radiation during their occupational activities they are usually not classified as being occupationally exposed in the sense of the ICRP system for radiation protection. Thus, for a specific mission planned, reference levels for risks or doses may be selected at appropriate levels and no dose limits may be applied for a given mission.

REFERENCES:

Azimi-Garakani, D., Wernli, C., 1991. Rsponse and background study of various PADC materials. Int. J. Radiat. Appl. Instr. Part D. Nucl. Tracks and Radiat. Meas. 19 (1-4)445-448

Agosteo, S., Colautti, P., Fazzi, A. et al., 2006. A solid state microdosimeter based on a monolithic silicon telescope. Radiat. Prot. Dosim. 122, 382-386

Agostinelli, S., Allison, J., Amako, K. et al., 2003. GEANT4 – a simulation toolkit. Nucl. Instr. Meth. in Phys. Res. A 506 (3), 250-303.

Allison J., Amako, K., Apostolakis, J. et al., 2006. Geant4 developments and applications. IEEE Transactions on Nucl. Sc. 53 (1), 270-278.

Allkofer, O.C., 1975. Introduction to Cosmic Radiation, Buchreihe der Atomenergie, Bd. 10, Verlag Karl Thiemig, München.

Alpen, E.L., Powers-Risius, P., Curtis, S.B., DeGuzman, R., 1993. Tumorigenic potential of high-Z, high-LET charged particle radiations. Radiat. Res. 88, 132-143.

Alsmiller, R.G., JR., Irving, D.C., Kinney, W.E., Moran H.S., 1965. The Validity of the Straightahead Approximation in Space Vehicle Shielding Design Studies. Second Symposium on Protection Against Radiations in Space, Arthur Reetz, Jr., ed., NASA SP-71, 177-181.

Andersen et al., 2004. The FLUKA code for space applications: recent developments. Adv. Space Res. 34 (6), 1302-1310.

Apáthy, I., Deme, S., Fehér, I. et al., 2002. Dose measurements in space by the Hungarian Pille TLD system. Radiat. Meas. 35, 381-391.

Apáthy, I., Akatov, Y.A., Arkhangelsky, V.V. et al., 2007. TL dose measurements on board the Russian segment of the ISS by the “Pille” system during Expedition-8, -9 and -10. Acta Astronaut. 60, 322-328.

Atwell, W., 1994. Anatomical models for space radiation application- An Overview. Adv. Space Res. 415-422.

Badhwar G. D., 1997. The radiation environment in low earth orbit. Radiat. Res. 148, S3-S10.

Badhwar, G. D., Atwell, W., Badavi, F. F. et al., 2002. Space radiation absorbed dose distribution in a human phantom. Radiat. Res. 157, 76–91.

Badhwar, G.D., Cucinotta, F.A., 2000. A Comparison on Depth Dependence of Dose and Linear Energy Transfer Spectra in Aluminum and Polyethylene. Radiat. Res. 153, 1-8.

Badhwar, G.D., Cucinotta, F.A., Braby, L.A., Konradi, A., 1994. Measurements on the Shuttle of the LET spectra of galactic cosmic radiation and comparison with the radiation transport model. Radiat. Res. 139, 344–351.

Badhwar, G.D, O’Neill, P.M., 1992. An Improved Model of GCR for Space Exploration Missions. Nucl. Tracks Radiat. Meas. 20, 403-410.

Badhwar, G.D., Patel, J. U., Cucinotta, F.A., Wilson, J.W., 1995. Measurements of Secondary Particle Energy Spectrum in the Space Shuttle. Radiat. Meas. 24, 129-138.

Badhwar, G.D., Atwell, W., Reitz, G., Beaujean, R., Heinrich, W., 2002. Radiation measurements on the Mir Orbital Station. Radiat. Meas. 35(5), 393-422.

Bahadori, A.A., Van Baalen, M., Shavers, M.R. et al., 2011. Effect of anatomical modeling on space radiation dose estimates: A comparison of doses for NASA phantoms and the 5th, 50th, and 95th percentile male and female astronauts. Phys Med Biol 56, 1671-1694.

Bahadori, A.A., Van Baalen, M., Shavers, M.R. et al., 2012. Dosimetric impacts of microgravity: an analysis of 5th, 50th, and 95th percentile male and female astronauts. Phys Med Biol. 57, 1047-1070.

Ballarini, F. et al., 2004. Nuclear models in FLUKA: present capabilities, open problems and future improvements. SLAC-PUB-10813, SLAC, Stanford, USA.

Ballarini, F., Battistoni, G., Cerutti, F. et al. 2006. GCR and SPE organ doses in deep space with different shielding: Monte Carlo simulations based on the FLUKA code coupled to anthropomorphic phantoms, Adv. Space Res. 37(9), 1791-1797.

Barkas, W.H., 1963. Nuclear Research Emulsions, Vol. I. Academic Press, New York.

Bartlett, D.T., Hager, L.G., Tanner, R.J., 2006. Results of measurements on shuttle missions to the ISS of the neutron component of the radiation field. Adv. Space Res. 37, 1668–1671.

Battistoni, Muraro, S., Sala, P.R., Cerutti, F., Ferrari, A., Roesler, S., Fasso, A., Ranft, J., 2007. The FLUKA code: Description and benchmarking" Proceedings of the Hadronic Shower Simulation Workshop 2006 at Fermilab, M. Albrow, R. Raja eds., AIP Conference Proceeding 896, 31-49, (2007).

Beaujean, R., Kopp, J., Burmeister, S. *et al.*, 2002. Dosimetry inside MIR station using a silicon detector telescope (DOSTEL), Radiat. Meas. 35, 433–438.

Benghin, V.V., 2008. On-board predicting algorithm of radiation exposure for the International Space Station radiation monitoring system. J. Atmos. Sol.-Terr. Phys. 70, 675-679

Benton, E.R., Benton, E.V., 2001. Space radiation dosimetry in low-Earth orbit and beyond. Nucl. Instr. Meth. B 184(1-2), 255-294.

Benton, E.V., Badhwar, G.D. (edt.), 2001. Prediction and measurements of secondary neutrons in space. Radiat. Measurem. 33 (3), 227-392

Benton, E.R., Frank, A.L., Benton, E.V., 2000. TLD efficiency of ^{7}LiF for doses deposited by high-LET particles. Radiat. Measurem. 32 (3), 211-214

Berger, T., Hajek, M., Fugger, M. et al., 2006. Efficiency corrected dose verification with thermoluminescence dosemeters in heavy ion beams, Radiat. Prot. Dosim. 120, 361–364.

Bernabeu, J., Casanova, I., 2007. Moon surface radiation environment analysis for February 1956 solar event conditions. Adv. Space Res. 42 (12), 1906-1912.

Bichsel, H., 1992. Stopping Power and Ranges of Fast Ions in Heavy Elements. Phys. Rev. A. 46, 5761-5773.

Bigbee, W.L., , W.,C. et al., 1998. Human in vivo somatic mutation measured at two loci: individuals with stable elevated background erythrocyte glycophorin A (*gpa*) variant frequencies exhibit normal T-lymphocyte *hprt* mutant frequencies. Mutation Research/ Fundamental and Molecular Mechanisms of Mutagenesis 397 (2), 119-136.

Billings, M.P., Yucker, W.R., 1973. The computerized anatomical man (CAM) model. Summary Final Report, MDC-G4655, McDonnell Douglas Company, Huntington Beach, CA.

Bilski, P. , Berger, T., Hajek, M., Reitz, G., (2011). Comparison of the response of various TLDs to cosmic radiation and ion beams: Current results of the HAMLET project. Radiat. Meas., doi:10.1016/j.radmeas.2011.03.023).

Blakely, W.F., Miller, A.C., Grace, M.B. et al., 2003. Radiation biodosimetry: Applications for spaceflight. Adv. Space Res. 31 (6), 1487-1493.

Boberg, P.R., Adams, J.H., Beaujean, N.L., et al., 1993. The mean charge state of solar energetic oxygen at 10 MeV/nucleon. In: Proceedings of 23th ICRC, Vol. 3, 396-399.

Boschung, M., Fiechtner, A., Mayer, S., Wernli, C., 2008. Field calibration and comparison of personal neutron dosemeter designs based on CR-39 for the use around high-energy accelerators. Radiat. Meas. 43 (2-6), 1081-1084.

Brandt, W., Ritchie, H.R., 1974. Primary Processes in the Physical Stage. Physical Mechanisms in Radiation Biology, R.D. Cooper, and R. Woods. Eds. Tech. Info. Center, US, Atomic Energy Commission, 20-29.

Braun, H., Christl, M., Rahmstorf, S. et al., 2005. Possible solar origin of the 1470 year glacial climate cycle demonstrated in a coupled model. Nature 438, 208-211.

Brechtmann, C., Heinrich, W., 1988. Fragmentation Cross Sections of ^{32}S at 0.7, 1.2, and 200 GeV/nucleon. Z.Phys. A331, 463-472.

Brenner, D.J., Hall, E.J., 1992. Commentary 2 to Cox and Little: radiation-induced oncogenic transformation: the interplay between dose, dose protraction, and radiation quality. Adv. Radiat. Biol. 16, 167-79.

Brooks, A.L., 1999. Biomarkers of exposure, sensitivity, and disease. Int. J. Radiat. Biol. **75**, 1481-1503.

Caffrey, J.A., Hamby, D.M., 2011. A review of instruments and methods for dosimetry in space. Adv. Space Res. 47 (4), 563-574.

Carlsson, J., Rosander, K., 1973. Effects of Multiple Scattering on Proton Beams in Radiotherapy. Phys. Med. Biol. 18, 633-640.

Casolino, M., Altamura, F., Minori, M. et al., 2007. The Altcriss project on board the International Space Station. Adv. Space Res. 40, 1746–1753.

Charara, Y.M., Townsend, L.W., Gabriel, T.A. et al., 2008. HETC-HEDS Code Validation Using Laboratory Beam Energy Loss Spectra Data. IEEE Trans. Nucl. Sci. 55 (6), 3164-3168

Chen, J., 2001. Physics of coronal mass ejections: a new paradigm of solar eruption. Space Science Reviews 95, 165-190.

Clowdsley, M.S., Wilson, J.W., Kim, M.Y. et al., 2000. Neutron Environment on the Martian Surface. Physica Medica XVII, 94-97.

Cornforth, M.N., 2001. Analyzing radiation-induced complex chromosome rearrangements by combinatorial painting. Radiat. Res. 155, 643–659.

Compton, A.H., 1936. Recent developments in cosmic rays. Rev. Sci. Instrum. 7, 71-82

Cucinotta, F.A., Durante, M., 2006a. Cancer risk from exposure to galactic cosmic rays: implications for space exploration by human beings. Lancet Oncol. 7(5) 431-5.

Cucinotta, F.A., Hu, S., Schwadron, N.A. et al., 2011b. Space radiation risk limits and Earth-Moon-Mars environmental models. Space Weather 8.

Cucinotta, F.A., Kim, M. Y., Chapell, L.J., 2011a. Space Radiation Cancer Risk Projections and Uncertainties – 2010. NASA/TP-2011-216155

Cucinotta, F.A., Kim, M.Y., Schneider, S.I., and Hassler, D.M., 2007. Description of light ion production cross sections and fluxes on the Mars surface using the QMSFRG model. Radiat. Environ. Biophys, 46, 101-106.

Cucinotta, F.A., Kim, M.Y., Willingham, V., George. K.A., 2008. Physical and biological organ dosimetry analysis for International Space Station Astronauts. Radiat. Res. 170 (1), 127–138.

Cucinotta, .F.A., Nikjoo, H., Goodhead, D.T., 2000. Model of the radial distribution of energy imparted in nanometer volumes from HZE particles. Radiat Res. 153, 459-468.

Cucinotta, F.A. et al., 1997. Computational Procedures and Data-Base Development. In: NASA Workshop on Shielding Strategies for Human Space Exploration. Eds.: Wilson J.W., Miller J., Konradi A., and Cucinotta F.A., NASA CP-3360.

Cucinotta, F.A., Schimmerling, W., Peterson, L.E. et al., 2001b. Space Radiation Cancer Risks and Uncertainties for Mars Missions. Radiat. Res. 156, 682-688.

Cucinotta, F. A., Schimmerling, W., Wilson, J. W., Peterson, L. E., Badhwar, G. D., Saganti, P. B., Dicello, J. F., 2001a. Space radiation cancer risk projections for explorative missions: uncertainty reduction and mitigation, NASA JSC Document (JSC-29295), NASA Washington DC.

Cucinotta, F.A., Townsend, L.W., Wilson, J.W. et al. 1995. Light Ion Component of the Galactic Cosmic Rays: Nuclear Interactions and Transport Theory. Adv. Space Res. 17, 77-86.

Cucinotta, F.A., Wilson, J.W., Saganti, P. et al., 2002. Physics of the Isotopic Dependence of GCR Fluence Behind Shielding. NASA TP-2003-210792.

Cucinotta, F.A., Wilson, J.W., Shinn, J.L. et al., 1996. Effects of Target Fragmentation on Evaluation of LET Spectra From Space Radiations: Implications for Space Radiation Protection Studies. Radiat. Meas. 26, 923-934.

Cucinotta, F.A., Wilson, J.W., Tripathi, R.K., Townsend, L.W., 1998. Microscopic Fragmentation Model for Galactic Cosmic Ray Studies. Adv. in Space Res. 22, 533-537.

Cucinotta, F.A., Wilson, J.W., Williams, J.R. et al., 2000b. Analysis of Mir-18 results for physical and biological dosimetry: Radiation shielding effectiveness in LEO. Radiat. Meas. 132, 181-191.

Cummings, J.R., Binns, W.R., Garrand, M.H. et al., 1990. Determination of the Cross Sections for the Production of Fragments with Relativistic Nucleus-Nucleus Interactions I. Measurements. Phys. Rev. C 42, 2508-2529.

Dachev, T., Atwell, W., Semones, E. Et al., 2006. B., Observations of the SAA radiation distribution by Liulin-E094 instrument on ISS. Adv. Space Res. 37, 1672-1677.

Dachev, T., Tomov, B., Matviichuk, Y. et al., 2002. Calibration results obtained with Liulin-4 type dosimeters. Adv. Space Res. 30 (4), 917-925.

Dettmann, J., Reitz, G., Gianfiglio, G., 2007.MATROSHKA—The first ESA external payload on the International Space Station. Acta Astronaut. 60, 17-23.

Doke, T., Hayashi, T., Kikuchi, J. et al., 2001. Measurements of LET-distribution, dose equivalent and quality factor with the RRMD-III on the Space Shuttle Missions STS-84, -89 and -91. Radiat Meas. 33(3), 373-87.

Durante, M., and Cucinotta, F.A., 2011. The physical basis for radiation protection in space. Rev. Mod. Phys. 83, 1245–1281.

EC, 2009. Technical Recommendations for Monitoring Individuals Occupationally Exposed to External Radiation. Report Radiation Protection 160 of the European Radiation Dosimetry Group, WG2. European Commission, Luxembourg.

Edwards, A.A. et al., 2005. Review of translocations detected by FISH for retrospective biological dosimetry applications. Radiat. Prot. Dosim. 113, 396-402.

Ersmark, T., Carlson, P., Daly, E. et al., 2007. Geant4 Monte Carlo simulations of the belt proton radiation environment on board the International Space Station/Columbus. IEEE Trans. Nucl. Sci. 54 (4), 1444-1453.

Evans, H.D.R., Bühler, P., Hajdas, W. et al., 2008. Results from the ESA SREM monitors and comparison with existing radiation belt models. Adv. Space Res. 42, 1527-1537

Facius, R., Reitz, G., 2007. Space weather impacts on space radiation protection. In: Space Weather Physics and Effects. Eds. Bothmer, V. and Daglis, I.A. Springer-Praxis Books in Environmental Sciences, ISBN:3-540-23907-3

Failla, G., Henshaw, P., 1931. The relative biological effectiveness of x rays and gamma-rays. Radiology 17, 1-43.

Fano, U., 1963. Penetration of Protons, Alpha Particles, and Mesons. Annual Review of Nucler Science, Vol. 13, Emilo Segre, ed. 1-66.

Fasso, A., Ferrari, A., Ranft, J., Sala, P.R., 2005. FLUKA: a multi-particle transport code. CERN-2005-10, INFN/TC_05/11, SLAC-R-773

Fattibene, P., Callens, F., 2010. EPR dosimetry with tooth enamel: A review. Appl. Radiat. Isot. 68(11), 2033-116.

Fedorenko, B., Druzhinin, S., Yudaeva, L. et al., 2001. Cytogenetic studies of blood lymphocytes from cosmonauts after long-term space flights on Mir station. Adv. Space Res. 27, 355-359

Fermi, E., 1940. Summer Lectures, University of Chicago.

Ferrari, A., 2007. Fragmentation in human tissue; from cancer terapy to space missions, paper presented at NUFRA2007, 26 September 2007.

Ferrari, A., Ranft, J., Sala, P.R., 2001.The FLUKA radiation transport code and its use for space. Proceedings of the 1st Intern. Workshop on Space Radiation Research and 11th Annual NASA Space Radiation Health Investigators' Workshop. Physica Medica 17 Suppl. 1, 1-295

Filius, R.W., 1965. Trapped protons of the inner radiation belt, Dissertation, Department of Physics and Astronomy, University of Iowa.

Flesch, F., Hirzebruch S.E., Hüntrup, G. et al., 1999. Fragmentation cross section measurements of iron projectiles using CR-39 plastic nuclear track detectors. Radiat. Meas. 31 (1-6), 533-536.

Flesch, F., Iancu, G., Heinrich, W., Yasuda, H., 2001. Projectile Fragmentation of Silicon Ions at 490 A MeV, Radiat. Meas. 34, 237 -240

Freden, S.C., Paulikas, G.A., 1964. Trapped protons at low altitudes in the South Atlantic magnetic anomaly. J. Geophys. Res. 69, 1259-1269.

Fry, R.J.M., Powers-Risius, P., Alpen, E.L. et al., 1985. High LET radiation carcinogenesis. Radiat. Res. 104, S188-S195.

Fuglesang, C., 2007. Using the human eye to image space radiation or the history and status of the light flash phenomena. Nucl. Instrum. Meth. A 580, 861–865.

George, K., Cucinotta, F.A., 2007. The influence of shielding on the biological effectiveness of accelerated particles for the induction of chromosome damage. Adv. Space Res. **39**, 1076–1081.

George, K., Durante, M., Wu, H., Willingham, V., Badhwar, G., Cucinotta, F.A., 2001. Chromosome aberrations in the blood lymphocytes of astronauts after space flight. Radiat. Res. **,** 731-738.

George, K., Durante, M., Willingham, V. et al., 2003. Biological effectiveness of accelerated particles for the induction of chromosome damage measured in metaphase and interphase human lymphocytes. Radiat. Res. 160, 425-435

Goldhaber, A.S., 1974. Statistical models of fragmentation processes. Phys. Lett. 53B, 306-309.

Goldhagen, P., Clem, J.M., J. W. Wilson, J.W., 2004. The energy spectrum of cosmic ray induced neutrons measured on an airplane over a wide range of altitude and latitude. Radiat. Prot. Dosim. 110(4), 387-392.

Gong, J.K., Glomski, C.A., Guo, Y., 1999. A lifelong, wide-range radiation biodosimeter: erythrocytes with transferrin receptors. Health Phys. 77(6), 713-718.

Goodhead, D.T., Munson, R.J., Thacker, J., Cox, R., 1980. Mutation and inactivation of cultured mammalian cells exposed to beams of accelerated heavy ions. IV. Biophysical interpretation. Int J Radiat Biol. 37, 135-167.

Gudowska, I., Sobolevsky, N., Andreo, P. et al., 2004 Ion beam transport in tissue-like media using the Monte Carlo code SHIELD-HIT Phys. Med. Biol. 49 (10), 1935–1958

Gunther, W., Leugner, D., Becker, E. et al., 2002. Energy spectrum of 50-250 MeV/nucleon iron nuclei inside the MIR space craft. Radiat. Meas. 35 (5), 511-514

HAMLET, 2011. Human model MATROSHKA for radiation exposure determination of astronauts. European Commission: Seventh Framework Programme (FP7) of the EU. www.fp7-hamlet.eu.

Hathaway, D.H., Wilson, R.M., Reichmann, E.J., 2002. Group sunspot numbers: Sunspot cycle characteristics. Solar Physics 211, 357-370.

Heinbockel, J.H., Slaba, T.C., Blattnig, S.R. et al., 2011. Comparison of the transport codes HZETRN, HETC and FLUKA for a solar particle event. Adv. Space Res. 47, 10791088.

Heinrich, W., Spill, A., 1979. Geomagnetic shielding of cosmic rays for different satellite orbits. J. Geophys. Res. 84, 4401.

Henkner, K., Sobolevsky, N., Jäkel, O., Paganetti, H., 2004. Test of the nuclear interaction model in SHIELD-HIT and comparison to energy distributions from GEANT4. Phys. Med. Biol. 54 (22), 509-517

Hoff, J.L., Townsend, L.W., Zapp, E.N. 2004. Interplanetary crew doses and dose equivalents: variations among different bone marrow and skin sites. Adv. Space Res. 34, 1347-1352.

Hufner, J., 1985. Heavy fragments produced in proton-nucleus and nucleus-nucleus collisions at relativistic energies. Phys. Rep. 125, 129-185.

Hufner, J., Schafer, K., Schurmann, B., 1975. Abrasion-ablation in reactions between relativistic heavy ions. Phys. Rev. C12, 1888-1898.

Hughes, H.G., Prael, R.E., Little, R.C., 1997. The LAHET/MCNP Code Merger. Los Alamos National Laboratory, LA-UR-97-4891. X-Division Research Note XTM-RN(U)97-012.

IAEA, 2011. Cytogenetic dosimetry applications in preparedness for and response to radiation emergencies. International Atomic Energy Agency (in press).

IAGA, 1992. The International Geomagnetic Reference Field (IGRF) 1991 Revision. International Association of Geomagnetism and Aeronomy, Division V, WG 8, EOS Trans. AGU 73, 182.

ICRP/ICRU, 1963. Report of the RBE Committee of the ICRP and ICRU. Health Physics 9, 357.

ICRP, 1977. Recommendations of the International Commission on Radiological Protection. ICRP Publication 26. Ann. ICRP 1 (3).

ICRP, 1989. RBE for deterministic effects. ICRP Publication 58. Ann. ICRP 20 (4).

ICRP, 1991. 1990 Recommendations of the International Commission on Radiological Protection. ICRP Publication 60. Ann. ICRP 21 (1-3).

ICRP, 1997. General Principles for the Radiation Protection of Workers. ICRP Publication 75. Ann. ICRP 27 (1).

ICRP, 2003. Relative biological effectiveness (RBE), quality factor (Q) and radiation weighting factor (w_R). ICRP Publication 92. Ann. ICRP 33 (4).

ICRP, 2005. Low-dose Extrapolation of Radiation-related Cancer Risk. ICRP Publication 99. Ann. ICRP 35 (4).

ICRP, 2007. The 2007 Recommendations of the International Commission on Radiological Protection. ICRP Publication 103. Ann. ICRP 37 (2-4).

ICRP, 2009. Adult reference computational phantoms, ICRP Publication 110, Annals of the ICRP 39 (2).

ICRP, 2012. Conversion Coefficients for Radiological Protection Quantities for External Radiation Exposures. ICRP Publication 116, Annals of the ICRP 40 (1).

ICRU, 1970. Linear Energy Transfer. ICRP Report 16. ICRU Publications: Bethesda, MD.

ICRU, 1978. Basic Aspects of High Energy Particle Interactions and Radiation Dosimetry. ICRU Report 28. ICRU Publications: Bethesda, MD.

ICRU, 1985. Determination of Dose Equivalents Resulting from External Radiation Sources. ICRU Report 39. ICRU Publications: Bethesda, MD.

ICRU, 1986. The quality factor in radiation protection. ICRU Report 40. ICRU Publications: Bethesda, MD.

ICRU, 1988. Determination of Dose Equivalents from External Radiation Sources – Part 2. ICRU Report 43. ICRU Publications: Bethesda, MD.

ICRU, 1992. Measurements of Dose Equivalents from External Photon and Electron Radiations. ICRU Report 47. ICRU Publications: Bethesda, MD.

ICRU, 1993. Quantities and Units in Radiation Protection Dosimetry. ICRU Report 51. ICRU Publications: Bethesda, MD.

ICRU, 2001. Determination of operational dose equivalent quantities for neutrons. ICRU Report 66. Journal of ICRU 1 (3).

ICRU, 2010. Reference data for the validation of doses from cosmic radiation exposure of aircraft crew. ICRU Report 84. Journal of ICRU 10 (2).

ICRU, 2011. Fundamental Quantities and Units for Ionising Radiation (*Revised*). ICRU Report 85a. Journal of ICRU 11 (1a).

ISO/IEC, 2005. Guide 98-3 Guide to the Expression of Uncertainty in Measurement (GUM). International Organization for Standardization, Geneva.

ISO/IEC, 2007. Guide 99 International vocabulary of basic and general terms in metrology(VIM). International Organization for Standardization, Geneva.

ISO/IEC, 2009. Guide 98-1 Uncertainty of Measurement – Part 1: Introduction to the Expression of Uncertainty in Measurement. International Organization for Standardization, Geneva.

Iwamoto, Y., Niita, K., Sakamoto, Y., Sato, T., Matsuda, N., 2007. Validation of the event generator mode in the PHITS code and its application International Conference on Nuclear Data for Science and Technology 2007 doi: 10.1051/ndata:07417

James, M.R., McKinney, G.W., Durkee, J.W. et al., 2009. MCMPX 2.7.X – New features being developed. IEEE/NSS, Orlando, http://mcnpx.lanl.gov/

JCGM - Joint Committee for Guides in Metrology, 2008b. Evaluation of measurement data - Guide to the expression of uncertainty in measurement. JCGM 100, ISO/IEC Guide 98-3.

JCGM - Joint Committee for Guides in Metrology, 2009. Evaluation of measurement data - An introduction to the "*Guide to the expression of uncertainty in measurement*". JCGM 104, ISO/IEC Guide 98-1.

JCGM - Joint Committee for Guides in Metrology, 2008a. International vocabulary of metrology - Basic and general concepts and associated terms (VIM). JCGM 200, ISO/IEC Guide 99:2007

Jones, M. R., 2000. ACS WFC CCD Radiation test: The Radiation Environment. ACS Institutional Science Report 00-09, Space Telescope Science Institue.

Katz, R., 1970. RBE, LET and z/β^{α}. Health Phys. 18, 175-???.

Katz, R., Sharma, S.C., Homayoonfar, M., 1972. The structure of particle tracks. In: Attix, F.H. Topics in Radiation Dosimetry. Supplement 1. 317-383. Academic Press, New York, London.

Kiefer, J., Schreiber, A., Gutermuth, F., Koch, S., Schmidt, P.,1999. Mutation induction by different types of radiation at the *Hprt* locus. Mutation Research/Fundamental and Molecular Mechanisms of Mutagenesis 431 (2), 429-448.

Kiefer, J., Schmidt, P., Koch, S., 2001. Mutations in Mammalian Cells Induced by Heavy Charged Particles: An Indicator for Risk Assessment in Space. Radiat. Res. 156, 607-611.

Kim, Y., Atwell, W., Tylka, A.J. et al., 2010a. Radiation dose assessments of solar particle events with spectral representation at high energies for the improvement of radiation protection. 38th COSPAR Scientific Assembly, paper number F24-0005-10.

Kim, Y., De Angelis, G., Cucinotta, F.A., 2011. Probalistic assessment of radiation risk of astronauts in space missions. Acta Astronautica 68, 747-759.

Kim, M.Y., Qualles, G.D., Slabba, T.C., Cucinotta, F.A., 2010b. Comparison of organ dose and dose equivalent for human phantoms of CAM vs. MAX. Adv. Space Res. 45, 850-857.

Knoll, G.F., 2000. Radiation detection and measurement, 3rd edition. New York: John Wiley & Sons.

Knott, C.N. et al., 1996. Interactions of Relativistic Neon to Nickel Projectiles in Hydrogen, Elemental Production Cross Sections. Phys. Rev. C 53, 347-357.

Knott, C.N. et al., 1997. Interactions of Relativistic ^{36}Ar and ^{40}Ar Nuclei in Hydrogen: Isotopic Production Cross Sections. Phys. Rev. C 56, 398-406.

Kolıskova, Z., Sihver, L., Ambrozova, I. et al., 2012. Simulations of absorbed dose on the phantom surface of MATROSHKA-R experiment at the ISS. Adv. Space Res. 49, 230-236.

Konradi, A., Atwell, W., Badhwar, G. D., Cast, B. L., Hardy, K. A., 1992. Low Earth orbit radiation dose distribution in a phantom head. Nucl. Tracks Radiat. Meas. 20, 49–54.

Koshiishi, H., Matsumoto, H., Chishiki, A. et al., 2007. Evaluation of the neutron radiation environment inside the International Space Station based on the Bonner Ball Neutron Detector experiment. Radiat. Meas. 42, 1510–1520.

Lee, K., Flanders, J., Semones, E. Et al., 2007. Simultaneous observation of the radiation environment inside and outside the ISS. Adv. Space Res. 40, 1558-1561.

Lenchek, A.M., Singer, S.F., 1962. Effects of the finite gyroradii of geomagnetically trapped protons. J. Geophys. Res. 67, 4073-4075.

Lewis, B.J., Smith, M.B., Ing, H. et al., 2012. Review of bubble detector response characteristics and results from space. Radiat Prot. Dosim. 150, 1-21

Lutz, G., 1999. Semiconductor radiation devices. Device Physics. Berlin: Springer Verlag.

Matsumoto, H., Goka, T., Koga, K. et al., 2001. Real-time measurement of low-energy-range neutron spectra on board the space shuttle STS-89 (S/MM-8). Radiat. Meas. 33, 321-333.

Matthiä, 2012. DLR Cologne, personal communication (to be published).

Menzel, H.G., Paretzke, H.G., Booz, J. (eds), 1989. Implementation of dose equivalent meters based on microdosimetric techniques in radiation protection. Radiat. Prot. Dosim.29 (1-2).

Mezentsev, A., Amundson, S.A., 2011. Global gene expression to low- or high-dose radiation in a human three-dimensional tissue model. Radiat. Res. 175(6), 677-688.

Miller, J., 1997. “Database development and laboratory validation“ in „Shielding Strategies for Human Space Exploration, Wilson, J.W., Miller, J., Konradi, A., Cucinotta, F.A. eds. NASA CP-3360, NASA Langley Research Center.

Mitaroff, A., Silari, M., 2002. The CERN-EU high-energy Reference Field (CERF) facility for dosimetry at commercial flight altitudes and in space. Radiat. Prot. Dosim. 102, 7- 22.

Narici, L., Belli, F., Bidoli, V. Et al., 2004. The ALTEA/ALTEINO projects: studying functional effects of microgravity and cosmic radiation. Adv. Space Res. 33, 1352-1357.

NCRP, 1989. Guidanc on Radiation Received in Space Activities. NCRP Report No. 98. National Council on Radiation Protection and Measurements. Bethesda, MD.

NCRP, 1990. The Relative Biological Effectiveness of Radiations of Different Quality. NCRP Report No. 104. National Council on Radiation Protection and Measurements. Bethesda, MD.

NCRP, 1997. Acceptability of Risk from Radiation- Application to Human Space Flight. NCRP Symposium Proceedings No. 3. National Council on Radiation Protection and Measurements. Bethesda, MD.

NCRP, 2000. Radiation Protection Guidance for Activities in Low-Earth Orbit. NCRP Report No. 132. National Council on Radiation Protection and Measurements. Bethesda, MD.

NCRP, 2002. Operational Radiation Safety Program for Astronauts in Low-Earth Orbit: A Basic Framework. NCRP Report No. 142. National Council on Radiation Protection and Measurements. Bethesda, MD.

NCRP, 2006. Information Needed to Make Radiation Protection Recommendations for Space Missions Beyond Low-Earth Orbit. NCRP Report No. 153. National Council on Radiation Protection and Measurements**,** Bethesda, MD.

Niita, K., Iwamoto, Y., Sato, T., Iwase, H., Matsuda, N., Sakamoto, Y., Nakashima, H., 2007. A new treatment of radiation behaviour beyond one-body observables International Conference on Nuclear Data for Science and Technology 2007 doi: 10.1051/ndata:07398

Niita, K., Matsuda, N., Iwamoto, Y. et al., 2010. PHITS: Particle and Heavy Ion Transport code System, Version 2.23. JAEA-Data/Code 2010-022.

Nikjoo, H., Uehara, S., Pinsky, L., Cucinotta, F.A., 2007. Modelling and calculations of the response of tissue equivalent proportional counter to charged particles. Radiat. Prot. Dosim. 126, 512-518

NMDB, 2011. Real time database for high resolution monitor measurements. Neutron Monitor Data Base. EU 7th research programme, http://www.nmdb.eu/?q=node/138

Nymnik, R.A., 1999. The problems of cosmic ray particle simulation for the near-Erth orbital and interplanetary flight conditions. Rad. Measurements 30, 669-677.

Obe, G., Facius, R., Reitz, G. et al., 199. Manned missions to Mars and chromosome damage. Int. J. Radiat. Biol. 75 (4), 429-433.

O'Sullivan, D., Zhou, D., Heinrich, W. et al., 1999. Cosmic rays and dosimetry at aviation altitudes. Radiat. Meas. 31 (1-6), 579-584.

Otto, Th., 2010. Response of the DIS-1 personal dosimeter to neutrons, protons and other hadrons. Radiat. Meas. 45, 1564-1567.

Payne, M.G., 1969. Energy straggling of heavy charged particles in thick absorbers. Phys Rev. 185, 611.

Pellicioni, M., 1998. Radiation weighting factors and high energy radiation. Radiat. Prot. Dosim. 80, 371-378.

Pellicioni, M., 2009. (Private information).

Pelowitz, D.B., 2008. MCNPX User's Manual, Version 2.6.0. LA-CP-07-1473 (Los Alamos: New Mexico)

Plante, I., Cucinotta, F.A., 2008. Ionization and excitation cross sections for the interaction of HZE particles in liquid water and application to Monte-Carlo simulation of radiation tracks. New J. Phys. 10, 125020 doi: 10.1088/1367-2630/10/12/125020.

Posner, A.; Hassler, D. M.; McComas, D. J., 2005. A high energy telescope for the solar orbiter Adv. Space Res. 36 (8), 1426-1431.

Prosser, J.S., Moquet,J.E., Lloyd, D.C., Edwards, A.A., 1988. Radiation induction of micronuclei in human lymphocytes. Mut.Res. Fundam. Molecular Mechan. of Mutag. 199(1) 37-45.

Reedy R. C., 1996. Constraints on solar particle events from comparisons of recent events and million-year averages. In: Solar Drivers of Interplanetary and Terrestrial Disturbances. (Balasubramaniam K S, Kiel S. L, Smartt R N, Eds.) p. 429-436, ASP Conf. Ser. Vol.95, Astronomical Society of the Pacific.

Reitz, G., Beaujean, R., Benton, E. et. al., 2005. Space radiation measurements on_board ISS – The DOSMAP experiment. Radiat. Prot. Dosim. 116, 374 – 379.

Reitz, G., Berger, T., 2006. The MATROSHKA facility—Dose determination during an EVA. Radiat. Prot. Dosim. 120 (1−4), 442−445.

Reitz, G., Berger, T., Bilski, P. et al., 2009. Astronaut's organ doses inferred from measurements in a human phantom outside the International Space Station. Radiat. Res. 171, 225-235.

Reitz, G., 2012. Private communication

Sampsonidis, D., Papanastassiou, E., Zamani, M. et al., 1995. Fragmentation cross sections of ^{16}O, ^{24}Mg, and ^{32}S projectiles at 3.65 GeV/nucleon. Phys. Rev. 51(6), 3304-3308

Sato T., Endo A. and Niita K., 2010. Fluence-to-dose conversion coefficients for heavy ions calculated using PHITS code and ICRP/ICRU Adult reference computational phantoms, Phys. Med. Biol. 55(8), 2235-2246.

Sato T., Endo A. and Niita K., 2011. Dose estimation for astronauts using dose conversion coefficients calculated by the PIHTS code and the ICRP/ICRU adult reference computationl phantoms. Radiat. Environ. Biophys. 50, 115-123

Sato T., Endo A., Zankl M., Petoussi-Henss N., Niita K., 2009. Fluence-to-dose conversion coefficients for neutrons and protons calculated using the PHITS code and ICRP/ICRU adult reference computational phantoms. Phys, Med. Biol. 54 (7), 1997-2014.

Sato, T., Endo, A., Niita, K., 2012. Comparison of mean quality factors proposed by ICRP, ICRU and NASA. COSPAR-2012 (to be published)

Sato T., Niita K., Iwase H., Nakashima H., Yamaguchi Y., Sihver L., 2006. Applicability of particle and heavy ion transport code PHITS to the shielding design of spacecrafts. Radiat. Meas. 41, 1142-1146

Sawyer, D. M., Vette, J.I., 1976. AP-8 Trapped Proton Environment for Solar Maximum and Solar Minimum, NSSDC/WDC-A-R&S 76-06

Schimmerling, W., Wilson, J.W., Cucinotta, F.A. et al., 1999. Requirements for simulating space radiations with particle accelerators. In: Risk evaluation of cosmic- ray exposure in long-term manned space mission (K. Fujitaka, H. Majima, K. Ando, H. Yasuda, and M. Susuki, Eds.). Kodansha Scientific Ltd., Tokyo, 1-16.

Schimmerling, W., 2010. Accepting space radiation risks. Radiat. Env. Biophys. 49, 325-329.

Schlatt H., Zankl M. and Petoussi-Henss N. (2007), Organ dose conversion coefficients for voxel models of the reference male and female from idealized photon exposures, Phys. Med. Bio. 53, 2123-2145.

Schmidt, E., Regulla, D., Kramer, H.M., 2002. The effect of 29 keV x-rays on the dose response of chromosome aberrations in human lymphocytes. Radiat. Res. 158, 771-777.

Schmitz,Th., Waker, A.J., Kliauga, P., Zoetelief, H. (eds), 1995. Design, construction and use of tissue-equivalent proportional counters – EURADOS report. Radiat. Prot. Dosim. 61 (4).

Schoeftner, S., Blanco, R., de Silanes, I.L. et al., 2009. Telomere shortening relaxes X chromosome inactivation and forces global transcriptome alterations. Proc. National. Acad. Sci. 106 (46), 19393-19398

Semkova, J., Koleva, R., Shurshakov, V. et al., 2007. Status and calibration results of Liulin-5 charged particle telescope designed for radiation measurements in a human phantom onboard the International Space Station. Adv. Space Res. 40 (11), 1586-1592

Shinn, J.L., Cucinotta, F.A., Simonsen, L.C. et al., 1998. Validation of a comprehensive space radiation transport code. IEEE Trans. Nucl. Sci. 45(6), 2711-2719

Shurshakov, V.A., Akatov Y.A., Petrov, V.M. et al., 2004. MATROSHKA-R experiment onboard the ISS: current status and preliminary results, 9th WRMISS meeting, Vienna, Sep.8-10.

Sihver L., Mancusi D., Niita K. et al., 2007. Recent developments and benchmarking of the PHITS code. Adv. Space Res. 40, 1320-1331.

Sihver L., Mancusi, D., Niita, K. et al., 2008. Benchmarking of calculated projectile fragmentation cross-sections using the 3-D, MC codes PHITS, FLUKA, HETC-HEDS, MCNPX_HI, and NUCFRG2. Acta Astronautica 63, 865-877.

Sihver, L., Sato, T., Gustafsson, K. et al. 2010a. An update about recent developments of the PHITS code. Adv. Space Res. 45, 892-899

Sihver, L., Sato, T., Puchalska, M., Reitz, G., 2010b. Simulations of MATROSHKA experiments at the international space station using PHITS. Radiat. Environ. Biophys. 49, 351-357.

Slaba, T.C., Qualls, G.D., Clowdsley, M.S. et al. 2010. Utilization of CAM, CAF, MAX, and FAX for

space radiation analyses using HZETRN, Adv. Space Res. 45(7), 866-883

Slaba, T.C., Kim, M.Y., 2009. ((Section 5.3, par (237) HZETRAN))

Smart, D.F., Shea, M.A., 2008. World grid of calculated cosmic ray vertical cutoff rigidities for Epoch 2000.0. Proc. 30th International Cosmic Ray Conference: Caballero, R., D'Olivo, J.C., Medina-Tanco, G., Nellen, L., Sánchez, F.A., Valdés-Galicia, J.F. (eds.).Universidad Nacional Autónoma de México, Mexico City, Mexico, Vol. 1, 737–740).

Snyder, W.S., Ford, M.R., Warner, G.G. et al., 1969. Estimates of absorbed fractions for monoenergetic photon sources uniformly distributed in various organs of a heterogeneous phantom. MIRD Pamphlet No. 5. J. Nucl. Med. 10(Suppl. 3) 46–51.

Sobolevsky, N.M. 2003. The SHIELD transport code for Monte Carlo simulation of interaction of hadrons and nuclei with complex extended targets. GSI

Spjeldvik, W.N., Rothwell, P.L., 1983. The Earth radiation belts, AFGL-TR-83-0240, Air Force Geophysics Laboratory, Hanscom AFB, Massachusetts.

Spurny, F. , Dachev, T. S., 2003. Long-term monitoring of the onboard aircraft exposure level with a Si-diode based spectrometer. Adv. Space Res. 32(1), 53–58.

Taucher-Scholz, G., Kraft, G., 1999. Influence of radiation quality on the yield of DANN strand breaks for SV40 DNA irradiated in solution. Radiat. Res. 151, 595-604.

Townsend, L.W., Cucinotta, F.A., 1996. Overview of nuclear fragmentation models and needs. Adv. Space Res. 17(2), 59-68.

Townsend, L.W., Miller, T.M., Gabriel, T.A., 2002. Modifications to the HETC Radiation Transport Code for Space Radiation Shielding Applications: A Status Report. 12th Biennial ANS Radiation Protection and Shielding Division Topical Meeting, Sante Fe, NM.

Townsend, L.W., Miller, T.M., Gabriel, T.A., 2005. HETC radiation transport code development for cosmic ray shielding applications in space. Radiat. Prot. Dosim. 116, 135-139.

Townsend, L.W., Wilson, J.W., 1986a. Energy-Dependent Parameterizations of Heavy-Ion Absorption Cross Sections. Radiat. Res. 106, 283-287.

Townsend, L.W., Wilson, J.W., Cucinotta, F.A., Norbury, J.W., 1986b. Comparison of Optical Model Differences in Heavy Ion Fragmentation: Optical Versus Geometric. Phys. Rev. C 34, 1491-1495.

Tripathi, R.K., Wilson, J.W, Cucinotta, F.A., 2001. Medium Modified Two-Body Scattering Amplitude from Proton-Nucleus Total Cross-Sections. Nucl. Instrum. Meth. Phys. Res B173, 391-396.

Trovati, S., Ballarini, F., Battistoni, G. et al., 2006. Human Exposure to Space Radiation: Role of Primary and Secondary Particles. Radiat Prot Dosim. 122, 362-366.

Tull, C.E., 1990. Relativistic Heavy Ion Fragmentation at HISS. LBL-29718. Univ. of Calif.

Tucker, J.D., Tawn, E.J., Holdsworth, D. et al, 1997. Biological dosimetry of radiation workers at the Sellafield nuclear facility. Radiat. Res. 148(3), 216-226

Tucker, J.D., 2008. Low-dose ionizing radiation and chromosome translocations: A review of the major considerations for human biological dosimetry. Mutation Research/Reviews in Mutation Research 659(3), 211-220

Tweed, J., Waker, S.A., Wilson, J.W. et al., 2005. Computational methods for the HZETRN code. Adv. Space Res. 35(2), 194-201.

Uchihori, Y., Fujitaka, K., Yasuda, N., Benton, E., 2002. Intercomparison of Radiation Instruments for Cosmic-ray with Heavy Ion Beams at NIRS (ICCHIBAN Project). J. of Radiat. Res. 43S (Space radiation research), S81-S85.

Vette, J. I., 1991. The AE-8 Trapped electron model environment, NSSDC/WDC-A-R&S 91-24.

Vral, A., Thierens, H., De Ridder, L., (1997). *In vitro* micronucleus-centromere assay to detect radiation damage induced by low doses in human lymphocytes. Int. J. Radiat. Biol. 71, 61–68.

Waker, A.J., 1995. Principles of experimental microdosimetry.Radiat. Prot. Dosim. 61, 271-308.

Waters, L.S. ed., 2002. MCNPX User's Manual, Version 2.3.0. Los Alamos National Laboratory Report LA-UR-02-2607.

Webber, W.R., Southoul, A., Ferrando P. Gupta, M. 1990a. The Source Charge and Isotropic Abundances of Cosmic Rays with Z=9-16: A Study Using New Fragmentation Cross-Sections.The Astrophys. J. **348**, 611-620 (1990a).

Webber, W.R., Kish, J.C., Schrier, D.A., 1990b. Individual Isotopic Fragmentation Cross-Sections of Relativistic Nuclei in Hydrogen, Helium and Carbon Targets. Phys. Rev. **C41**, 547.

Weil, M.M., Bedford, J.S., Bielefeldt-Ohmann, H. et al., 2009. Incidence of acute myeloid leukemia and hepatocellular carcinoma in mice irradiated with 1 GeV/nucleon ^{56}Fe ions. Radiat. Res. 172, 213-219.

WELMEC, 2008. Software Guide (Measuring Instruments Directive 2004/22/EC). WELMEC 7.2 Issue 4. WELMEC secretariat, Ljubljana, Slovenia.

Wernli, C., Fiechtner, A., Kahilainen, J., 1999. The Direct Ion Storage Dosemeter for the Measurement of Photon, Beta and Neutron Dose Equivalents. Radiat. Prot. Dosim. 84(1-4), 331-334

Wernli, C., Kahilainen, J., 2001. Direct ion storage dosimetry systems for photon, beta and neutron radiation with instant readout capabilities. Radiat. Prot. Dosim. 96(1-3), 255-259

Westfall, G.D., Wilson, L.W., Lindstrom, H.J. et al., 1979. Fragmentation of relativistic ^{56}Fe. Phys. Rev. C 19, 1309-1323.

Wiegel, B., Alevra, A.V., 2002. NEMUS - The PTB Neutron Multisphere Spectrometer: Bonner Spheres and More. Nucl. Instrum. Meth. A 476, 36-41.

Wilson, J.W., 1978. Environmental geophysics and SPS shielding. Lawrence Berkeley Laboratory Report LBL-8581, pp 33-116.

Wilson, J.W., Tweed, J., Nealy, J.E. et al., 1994b. Galactic cosmic ray transport methods: Past, present, and future.Adv. Space Res. 14, 841-852

Wilson, J.W., Tripathi, R.K., Qualls, G.D. et al., 2004. Space radiation transport method development. Adv. Space Res. 34(6), 1319-1327

Wilson, *et al.*, NUCFRG2, 1995b. An Evaluation of the Semiempirical Nuclear Fragmentation Database. NASA TP 3533.

Wilson, J.W., Cucinotta, F.A., Miller, J. et al., 2001. Approaches and Issues Related to Shield Material Design to Protect Astronauts from Space Radiation. Materials and Design 22, 541-554.

Wilson J. W., Cucinotta F. A., Shinn J. L., Simonson L. C., Dubey R. R., Jordan W. R., Jones T. D., Chang C. V., Kim M. Y., 1999. Shielding from solar particles events in space. Radiation Measurements 30(3).

Wilson, J.W., Kim, M.Y., L.W., Schimmerling, W. et al., 1995a. Issues in Space Radiation Protection. Health Physics 68, 50-58.

Wilson, J.W., Nealy, J.E., Dachev, Ts.P. et al., 2007. Time serial analysis of the induced LEO environment within the ISS 6A.. Adv. Space Res. 40, 1562-1570

Wilson, J.W., Nealy, J.E., Wood, J.S. et al., 1995c. Variations in astronaut radiation exposure due to anisotropic shield distribution. Health Phys. 69, 34-45.

Wilson, J.W., Shinn, J.L., Townsend, L.W., et al., 1994a. NUCFRG2: a semiempirical nuclear fragmentation model. Nucl. Instrum. Meth. Phys. Res. B 94, 95-102.

Wilson, J.W., Townsend, L.W., Schimmerling, W. et al., 1991. Transport Methods and Interactions for Space Radiations. NASA RP 1257.

Wissmann, F., Langner, F., Roth, J., Schrewe, U., 2004. A mobile TEPC-based system to measure the contributions to $H^*(10)$ at flight altitudes. Radiat. Prot. Dosim. 110, 347-349.

Wong, M., Schimmerling, W., Phillips, M.H. et al., 1990. The Multiple Scattering of Very Heavy Charged Particles. Med. Phys. 17, 163-171.

Yang, T.C., George, K.A., Johnson, A.S. et al., 1997. Biodosimetry results from space flight Mir-18. Radiat. Res. 148, 17-23.

Yasuda, H., Badhwar, G. D., Komiyama, T., Fujitaka, K., 2000. Effective dose equivalent on the ninth shuttle–Mir mission (STS-91). Radiat. Res. 154, 705–713.

Yasuda, H., 2001. Responses of a direct ion storage dosimeter (DIS-1) to heavy charged particles. Radiat. Res. 156 (6), 805-808.

Yasuda, N., Uchihori, Y., Benton, E.R. et al., 2006. The intercomparison of cosmic rays with heavy ion beams at NIRS (ICCHIBAN) project, Radiat. Prot. Dosim. 120(1-4), 414-420.

Zankl, M., Witmann, A., 2001. The adult male voxel model "Golem" segmented from whole-body CT patient data, Radiation and Environmental Biophysics, 40(2), 153-162.

Zapp, E.N., Townsend, L.W., Cucinotta, F.A., 2002. Solar particle event organ doses and dose equivalents for interplanetary crews: variations due to body size. Advances in Space Research, 30, 975-979.

Zeitlin, C., Fukumura, A., Heilbronn, L. et al., 2001. Fragmentation Cross Sections of 600 MeV/nucleon ^{20}Ne on Elemental Targets. Phys. Rev. C 64, 24902.

Zeitlin, C., Heilbronn, L., Miller, J. et al., 1997. Heavy Fragment Production Cross Sections from 1.05 GeV/nucleon ^{56}Fe in C, Al, Cu, Pb, and CH_2 Target. Phys. Rev. C 56, 388-3397.

Zeitlin, C., Heilbronn, L., Miller, J. et al., 2002. Charge-changing and fragment production cross sections of ^{28}Si on elemental targets from 400 MeV/nucleon to 1200 MeV/nucleon, LBNL-47655.

Zeitlin, C., Guetersloh, S.B., Heilbronn, L.H. et al., 2006. Measurements of materials shielding properties with 1 GeV/u ^{56}Fe. Nucl. Instr. Meth. Phys. Res. B 252, 308–318

Zhou, D., O'Sullivan, D., Semones, E., Heinrich, W., 2006. Radiation field of cosmic rays measured in low earth orbit by CR39 detectors. Adv. Space Res. 37, 1764-1769.

Zhou, D., O'Sullivan, D., Semones E., Zapp, N., Johnson, S., Weyland, M., 2008. Radiation dosimetry for high LET particles in low Earth orbit. Acta Astronautica 63 (7-10), 855-846

Ziegler, J.F., Biersack, J.P., Ziegler, M.D., 2008. SRIM - The Stopping and Range of Ions in Matter. SRIM Co. ISBN 0-9654207-1-X.

ANNEX

Conversion coefficients and mean quality factors for protons, neutrons, alpha particles and heavy ions (2 < Z ≤ 28).

(1) Conversion coefficients for mean absorbed doses in organs and tissues for males and females based on the reference voxel phantoms (ICRP, 2009) are given for heavy ions (2<Z≤28) with energies from 10 MeV/u to 100 GeV/u. For the skin data are given for the energy range from 1 MeV/u to 100 GeV/u. The exposure geometry is always isotropic (ISO) radiation incidence. The data were evaluated based on their calculated values using the PHITS code (Sato et al., 2010).

(2) Based on the $Q(L)$ function (ICRP, 1991), also mean quality factors for organs and tissues of the adult male and female reference phantom are given for the heavy ions and energies mentioned above (Sato et al., 2010).

(3) In addition to the mean quality factors based on $Q(L)$, data are presented for mean quality factors for organs and tissues of the adult male and female reference phantom based on the Q-concept developed by Cucinotta et al. (Cucinotta et al., 2011a) (see 3.2.3). The data were also evaluated based on their calculated values using the PHITS code (Sato et al., 2012).The quality factors are related to RBE for solid cancer, and those for leukaemia are one-fourth of the corresponding data for solid cancer.

(4) Furthermore, conversion coefficients from ICRP Publication 116 (ICRP, 2012) for isotropic (ISO) exposure and mean quality factors are given for protons, neutrons, and alpha particles. The mean quality factors were evaluated based on their calculated values using the PHITS code (Sato et al. 2009, 2010 and 2012). The energy range considered for these particles are the same as in ICRP Publication 116.